MECHANISM OF THE STABILITY OF SLOPES COMPOSED OF GRANULAR MATERIALS

- Laboratory Experiments and Modeling -

by

Yuichi ONDA

A dissertation
submitted to the Institute of Geoscience
University of Tsukuba
in partial satisfaction of the
requirements for the degree of Doctor of Science

1990

TABLE OF CONTENTS

LIST OF TABLES

TABLE PAGE

TABLE PAGE

LIST OF FIGURES

FIGURE PAGE

FIGURE PAGE

FIGURE PAGE

FIGURE PAGE

FIGURE PAGE

FIGURE PAGE

ACKNOWLEDGEMENTS

Associate Professor Yukinori Matsukura, Institute of Geoscience, University of Tsukuba, has ardently guided and greatly encouraged me in accomplishment of this study. Professor Sunamura, Institute of Geoscience, University of Tsukuba, reviewed the manuscript and gave useful suggestions. Professor Hajime Matsuoka, Faculty of Engineering, Nagoya Institute of Technology, for advice on using aluminum rods and gave variable suggestions. Thanks are also due to Kenichi Ueno, Hiroaki Oh-hashi, Takashi Hirose, Hironori Maeda, Yoshinori Kodama, Shin Watanabe, Keiji Mizuno, Naomi Yoneyama, Toshiaki Iga, Hiromi Ohgawara, for help the laboratory experiment and the modeling.

ABSTRACT

It has long been believed in the stability of slopes made of granular materials such as sand and gravel that the angle of repose is apparently equal to the angle of internal friction. This relationship is widely accepted, although only a few studies have cast a doubt on this relationship (Taylor, 1945; Metcalf, 1966). Mechanisms for the angle of internal friction have been considerably elucidated by a number of studies (*e.g.*, Roscoe *et al.,* 1958; Rowe, 1962), whereas mechanisms for the angle of repose have not been fully understood. Consequently, exact relationship between the two angles still remains veiled. The present study tackled this problem through (1) laboratory experiments such as tilting-box experiments and direct shear tests using an assembly of aluminum rods and (2) numerical modeling using computers.

Some confusion present as to the term, *angle of repose.* The angle of slope at which an avalanche commences on a slope composed of granular materials is called the *critical angle of repose,* α_c; this is different from the angle at which the avalanche ceases, *i.e.,* the *repose angle after avalanching,* α_R. The former angle is usually thought to be equal to the angle of internal friction for the state of loose packing of slope material.

According to the textbook by Lambe and Whitman (1969), the safety

factor (Fs) for an infinite slope is derived from the slope stability analysis:

$$Fs = \tan \phi'_p \; / \; \tan i \qquad (1)$$

where ϕ'_p is the peak angle of internal friction and i is the maximum angle of the slope. For the critical condition for avalanche occurrence, *i.e.*, Fs=1, we have

$$\phi'_p = i \qquad (2)$$

Since the value of α_c corresponds to the maximum angle of a slope composed of material packed in the loosest state, the angle of slope, i, is equivalent to α_c. Thus, the critical angle of repose is thought to be equal to the angle of internal friction, *i.e.*, $\phi'_p = \alpha_c$.

Little knowledge on avalanching of granular materials has been obtained. This is because the shape of avalanches of granular materials is 3-dimensional, and the cross section of the avalanche cannot be directly observed. The method is required to observe the cross section of the avalanche to know what is responsible for this phenomenon.

The behavior of an assembly of rods, piled up to form a slope, piled perpendicular to the slope direction, can be treated as a 2-dimensional phenomenon, which is easily observable from a side of the slope when an avalanche occurs. Rods were first used in Schnebeeli's experiment (1956); since then an assembly of rods have been often used to examine the shearing behavior of sand mass in the field of soil mechanics (*e.g.*, Dantu, 1957; Murayama and Matsuoka, 1970).

Observations and measurements of 2-dimensional avalanches clearly indicated that the mechanism for the avalanching is not the sliding but *rotation* of rods. It was also found that (1) the depth of the avalanche is approximately 8 times as deep as the mean diameter of rods (d_m), (2) the value for α_c is considerably high in the case of uniform rods with regular packing, and (3) α_c-value for the case of horizontal packing is larger than that of vertical packing.

Direct shear tests of the aluminum rods were performed to obtain the peak value of angle of internal friction, ϕ'_p. A comparison between α_c and ϕ'_p indicates that the previous theory does not hold. Mechanisms for the angle of internal friction and the angle of repose are found to be essentially different.

A statical and numerical model to describe the stability of 2-dimensional assembly was constructed with BASIC language by using a personal computer and a main flame. The program was named GSM (*Granular material Stability Model*). The first part of the program is for packing of an assembly of the rods, and the second part of the program is the main program. The first scheme of the main program is to calculate the static equilibrium of each particle individually, and the second procedure is to find unstable particles by following equation.

$$F = \mu \cdot DF + W \sin \theta + \rho \cdot N \qquad (3)$$

where F is the total force of the particle i, θ is a contact angle between the particles i and j, W is the weight of the particle i, μ is the sliding friction between two aluminum rods DF is the confining force between the particle i and k, and ρ is the non-dimensional coefficient of rolling friction of the aluminum rods. The second term of the right hand side, $\mu \cdot DF$ is the sliding friction at the particle contact between the particles i and j.

This model can explain that the shape of the uniform-diameter material with regular packing is likely to have a greater value of α_c compared with that made of mixed-diameter materials.

Based on the above discussion, mechanism of an avalanche is summarized as follows: An avalanche of rods is caused by instability of total forces and a depth of avalanche is determined by the transmitted forces at about the depth corresponding to 8-particle depth. An avalanche occurred by *rotation* of a marginal rod.

To apply the result of these 2-dimensional studies to the 3-dimensional environment, the parameter, $\rho \cdot C$, the product of the angle of rolling friction (ρ) and the volume concentration (C) was proposed. The plot of $\rho \cdot C$ against α_c indicates marked proportional relationship. The value for the regression coefficient for the case of $\rho \cdot C$ against α_c is considerably larger than the plot of ϕ'_p against α_c. This suggests that the result obtained by the present 2-dimensional analysis can be applied to 3-dimensional problems.

CHAPTER 1

INTRODUCTION

1.1 Previous Studies

Discrete mineral particles, such as sand and gravel, are the essential ingredient of earth surfaces. These materials are called granular materials, which have no cementing matter at points of particle contact. A granular medium is composed of distinct particles which displace independently from one another and interact only at contact points (Cundall and Strack, 1979). Points of particle contact of the granular materials are few; the coordination number, in the case of randomly-packed equal spheres, is smaller than 12 (Bernal and Mason, 1960; Oda, 1977). These discrete character of the medium results in a complex behavior (Cundall and Strack, 1979).

Many landforms are composed of granular materials, such as talus slopes, sand dunes, cinder cones, the foreset of deltas and river banks cut in loose materials. Most of these slope angles occur which masses of loose granular material can maintain under given conditions. There has been widespread acceptance among geomorphologists that the angle of this kind of steep straight slope coincides with the *angle of repose* of granular materials (*e.g.*, Van Burkalow, 1945; Hough, 1957; Allen, 1969; Carson, 1977).

The mechanisms controlling the angle of repose or the stability of the slope composed of granular materials have been considered by many workers as summarized in Table 1. Only two papers (Kirkby and Statham, 1975; Statham, 1976) assumed that the talus slope is formed by rockfalls. Yet, there seems to be a general agreement as to the stability of granular materials which is controlled by a sort of avalanche. This has been supported by the observation of processes acting on talus slopes (*e.g.*, Chandler, 1973; Machida *et al.*, 1975) or aeolian dunes (*e.g.*, Bagnold, 1966; Matsukura, 1975; Warren, 1979) in the field.

A number of terminology present for the avalanche of granular materials (Table 1); *i.e.*, *fragment slides* (Ward, 1945), *slumping* (Van Burkalow, 1945), *avalanching* (*e.g.*, Allen, 1969) and *dry fragment flow* (*e.g.*, Machida *et al.*, 1975). The present author use the term, "*avalanche*" or "*avalanching*", since most of the previous workers favor the simple terminology.

Some confusion exists as to the precise meaning of the term "angle of repose". Often this term has frequently been used without clear definition and different workers frequently apply various definitions to the same phenomenon (Table 2). This is probably because of the presence of *two* kinds of the angle of repose.

The first definition of the angle of repose is the "*critical angle of repose* (α_c)" (Allen, 1969; Carrigy, 1970; Matsukura and Onda, 1989), defined as the maximum stable angle of slope relative to the horizontal surface underlain by loose granular materials in the gravity field (Allen, 1969). The second definition of the angle of repose is "*repose angle after avalanching* (α_R)" (Allen, 1969; Carrigy, 1970; Matsukura and Onda, 1989). The present author would like to use both α_c and α_R for the angle of repose, although they should be clearly discriminated.

There has also been a number of experimental studies as to the stability of the slope composed of granular materials or the angle of repose by means of various experimental methods. The methods which previous workers have applied were compiled by Carrigy (1970) and Matsukura and Onda (1989).

The angle of repose can be duplicated by one of several procedures as illustrated in Fig. 1. The procedures are divided into three categories: (1) the pouring method (Nos. 1 to 3), (2) the discharge method (Nos. 4 to 9), and (3) the tilting method (Nos. 10 to 12). The most serious disadvantages of these methods are to measure only *repose angle after avalanching* (α_R) of the two angle of reposes. Only the tilting method is available to measure precisely both the *critical angle of repose* (α_C) and the *repose angle after avalanching* (α_R) (Carson, 1977; Matsukura and Onda, 1989).

There are two methods in the tilting method: *i.e.*, *tilting-box method* (Nos. 10 and 11) and the *rotating-drum method* (No. 12). According to Carson (1977), the tilting-box method is superior to the rotating-drum method as follows:

The advantage of the tilting-box method is that it provides a free runout of particles after avalanching, as exists in nature. An additional advantage of the apparatus is that facilitates measurement of angle on interior slopes, away from the effects of the side walls.

A comparison of data obtained by using both a rotating-drum and a tilting-box indicates that data obtained by the tilting-box method have smaller value of scattering of α_c (Matsukura and Onda, 1989). The tilting-box method is thus judged to be the best method to obtain both values of α_C and α_R.

The previous experimental and theoretical studies on the stability of slopes composed of granular materials are summarized in Table 3. The knowledge of both values of α_C and α_R for several materials have been developed by using a rotating drum or a tilting-box (Allen, 1970; Carrigy, 1970; Carson, 1977; Onda *et al.*, 1988; Matsukura *et al.*, 1989). Our knowledge of avalanching and what controls it, however, remains still qualitative.

1.2 The Angle of Repose and the Angle of Internal Friction

A friction angle of granular materials is defined as the *angle of internal friction* or the *angle of shearing resistance* obtained by using shear tests (Terzaghi, 1925). Some confusion may result from the a number of definition of different angles of friction. They are each related to a different condition of the sediment or a different type of test procedure, which are summarized in Table 4.

Figure 2 shows the relationship between friction angle ϕ'_p and the volume concentration, *C*, (defined as 1-porosity) for a medium fine sand (Rowe, 1962). Obviously, the relationship will vary from sand to sand, but the trend of higher ϕ'_p for denser soil is always the same (Lambe and Whitman, 1969). The lowest value of ϕ'_p is the ultimate friction angle (ϕ'_{cv}). It is thought to be obtained by using the loose sand, with which it reaches its maximum after considerable strain at a value equal to without passing the previous peak. However, Roscoe *et al.* (1958) proved that assemblies of particles attain a final single porosity for a given normal pressure, the value of which may depend on particle shape and grading, and this ultimate condition is associated with ϕ'_{cv}, which reached whatever the initial porosity of the sample is.

It is generally thought that the maximum angle of the stable slope corresponds to the peak angle of internal friction, ϕ'_p, obtained by shear tests (Hough, 1957; Lambe and Whitman, 1969). According to the textbook by Lambe and Whitman (1969), the safety factor (Fs) for an infinite slope is derived from the slope stability analysis:

$$Fs = \tan \phi'_p \; / \; \tan i \qquad (1)$$

where tan i is the maximum inclination of the slope. For the critical condition of avalanche occurrence, *i.e.*, $Fs = 1$, we have

$$\phi'_p = i \qquad (2)$$

The result has been applied to studies on the *angle of repose*. In the oldest and simplest procedure for obtaining the friction angle of dry and granular soil, the angle of repose of a small pile of the material was observed (Taylor, 1948). It has been recognized that the angle of repose is approximately equal to the angle of internal friction of granular materials in the loosest state of packing. Terzaghi (1943, p8) states as follows:

Early investigators of soil problems generally assumed that angle of internal friction of sand is identical with the angle of repose. However, laboratory experiments have shown that the angle of internal friction of sand depends to a large extent on the initial density. In contrast to the angle of internal friction, the angle of repose of a dry sand has a fairly constant value. It is always approximately equal to the angle of internal friction of the sand in the loosest state.

Since the value of α_c corresponds to the maximum inclination of slope composed of the loosest material, inclination of slope, *i*, is equivalent to α_c. The critical angle of repose is thus thought to be equal to the angle of internal friction, *i.e.*, $\phi'_p = \alpha_c$.

The presence of no consensus for the precise meaning of the term "angle of repose" makes some confusion as to the relationship between the angle of repose and the angle of internal friction. The previous studies dealing with the angle of repose and angle of internal friction are summarized in table 5. Some author stated that ϕ'_{cv} is identical with α_R (*e.g.*, Carson and Kirkby, 1972), while others suggested that ϕ'_{cv} is identical with α_C (*e.g.*, Bagnold, 1966). The latter view is more acceptable than the former one, because the latter theory is based on the stability analysis, which is already described in *Eqs.* (1) and (2). In a rather controversial paper, Metcarf (1966) attempted to argue against that the angle of repose is equal to the angle of internal friction, and certainly the issue is open to debate, although his data and method are thought to be unreliable.

1.3 Problems

A number of previous studies have treated that avalanching of slopes made of granular materials is directly analogous to the sliding of a solid body on a frictional surface (*e.g.*, Seed and Goodman, 1964), because ϕ'_p of granular materials is thought to be decided by the sliding of rough surfaces; *i.e.*, summation of particle-to-particle sliding friction angle and interlocking angle (Rowe, 1962).

The actual mechanism of controlling the angle of repose is already suggested by Van Burkalow (1945):

> The angle of repose represents a condition of balance between intergrain friction, tending to keep the fragments from moving, and the pull of gravity upon them, tending to pull them a lower position.

Taylor (1948) has pointed out as to the relationship between the angle of repose and the angle of internal friction:

Actually, the angle of repose is the friction angle under a pressure of practically zero, but it tends to differ from the angle of internal friction under ordinary pressures for several reasons. A pile of the material cannot be in equilibrium unless the least stable grains at its surface are in equilibrium; thus the angle of repose is determined by the least stable grains.

Little knowledge as to the actual condition of the instability of granular materials has been obtained. This is because the shape of avalanches of granular materials is three-dimensional (Carson, 1977), and the cross section of the avalanche cannot be directly observed. The method is required to observe the longitudinal cross section of the avalanche to know what controls this phenomenon.

The behavior of an assembly of the rods, in the case where they were piled up perpendicular to the slope direction, can be treated as a two-dimensional phenomenon. The advantages of using such materials are to be able to observe the cross section of an avalanche, to make several types of packing, and to make the same packing in a tilting box and a shear box. These rods were first used by Schnebeeli (1956), and an assembly of the rods has been often used to examine the shearing behavior of sand mass in the field of soil mechanics (Dantu, 1957; Rowe, 1962; Lambe and Whitman, 1969; Drescher and Jong, 1972;

Matsuoka, 1974; Oda and Konishi, 1974; Umeya *et al.*, 1975).

Previous experiments by using rods have been performed to study the mechanism of both slow-moving and rapid-moving behavior of granular materials. An example of the slow-moving behavior of granular materials is a slow-speed shearing processes (*e.g.*, Murayama and Matsuoka, 1970). Examples to model the rapid-moving behavior of granular materials are the particle-movement by lowering floor experiment (Matsuoka, 1973; Fig. 3) and a rapid collapse of a braced excavation (Lambe and Whitman, 1969).

1.4 The Purpose of This Study

In this study, two purposes are pursued. One purpose of the present study is to outline a theoretical and experimental study on the avalanching of granular materials by means of aluminum rods. By using cylindrical and ellipsoidal rods, the present study tackles the actual mechanism of the avalanching of granular materials. An advantage of the 2-dimensional assembly is to have the reproducibility of packing between a tilting-box experiment and a direct shear test. Results obtained through tilting-box experiments and shear tests can be compared, because the data were gained under the same situation of packing. An additional advantage of the 2-dimensional assembly is to be construct an extreme case of packing. Moreover, the most important advantage of the 2-dimensional experiment is that we can observe the cross section of the avalanche, although we had never observed them before. The result of the present tilting-box experiment and direct shear test will be described in Chapter 2.

An additional purpose of this study is to construct a model based on statics and tribology of the materials to investigate the mechanism of avalanching, which will described in Chapter 3. The discussion of this problem will follow, which is in Chapter 4. The conclusion will be stated in Chapter 5.

CHAPTER 2

LABORATORY EXPERIMENTS

2.1 Material Used in the Experiments

Assemblies of rods were used for the tilting-box experiment to observe the cross-section of avalanches and shear processes. The behavior of an assembly of rods, when they were piled up to form a slope, lying perpendicular to the slope direction, can be treated as a 2-dimensional phenomenon, which is easily observable from a side of the slope.

Some of the previous workers have used optically-sensitive materials (*e.g.*, Dantu, 1957; Drescher and Jong, 1972) made of a kind of plastic for a 2-dimensional assembly of granular materials. An advantage of this material is to be able to observe the stress state in the rods. However, it has two disadvantages: (1) the stress state in the assembly should be homogeneous (Drescher and Jong, 1972) and (2) the material having high sensitivity which can observe forces applied by its own weight, is considerably soft, like gelatin (Tsuji *et al.*, 1965).

Another workers have used aluminum rods (*e.g.*, Lambe and

Whitman, 1969; Matsuoka, 1974), because the specific gravity of aluminum is 2.69, which is almost the same as that of sand particles, and they are not soft as gelatin. The behavior of the aluminum rods is therefore similar to the sand particles, better than optical sensitive materials, since they are free from the problem owing to the different specific-gravity and different hardness. The author thus is going to use aluminum rods.

Eleven kinds of aluminum rods all 50mm in length were used for the experiment (Figs. 4 and 5). They are cylindrical aluminum rods, ellipsoidal rods, oval rods, quadrangular rods, and hexagonal rods. The diameters of cylindrical rods are 1.6mm, 3mm, 5mm, 9mm, 25mm, and 45mm. The ellipsoidal rods and oval rods were made by pressing the cylindrical rods with 5mm and 8mm in diameter: the dimensions of the ellipsoidal rods were a long axis (*a*-axis) of 5.7mm and a short axis (*b*-axis) of 4.2mm, and a = 9.1mm and b = 6.4mm, respectively. The dimension of oval rods which have *a*-axis is 5.6mm and *b*-axis is 3.9mm, and a = 8.7mm and b = 6.6mm, respectively. The ellipsoidal rods and oval rods (Fig. 5a) are similar in shape. Square rods with a side of 5mm (Fig. 5a-c), rectangular rods with a side of 6mm and 9mm, and octagonal rods with a diameter of 8mm were also used (Fig. 5b).

2.2 Two-Dimensional Tilting-Box Experiment

2.2.1 Experimental apparatus and packing

For measuring the critical angle of repose was used a tilting-box (Fig. 6), made of iron frames with a width of 3cm. The main part of the apparatus is a triangular-prism like box, which has a length of 40cm, a height of 25cm and a width of 40cm. The bottom and the backboard are made of plastic plates, on which the same rods to be used for the experiment were glued in a single layer. The box is suspended from one end of a wire which is attached to one end to a motor passing over a pulley at the top of a tower. The surface of an assembly of the rods will tilt, if the wire is drawn by the motor.

The motor having a power of 15W is a speed-control type with a brake (Oriental Motor Co. Ltd. ; 3RK15RGN-AM). Using this driving system, the uplifting speed of the tilting-box between 0.02' arc $second^{-1}$ (minimum) and 1.2' arc $second^{-1}$ (maximum) could be obtained with a gear ratio of 1:1,000. A 35-mm still camera and a video-camera (Sony Co. Ltd.; CCD-V90 or CCD-V900) was installed respectively on two bars stretching outwards from the both sides of the box (*see* Fig. 6); therefore, the pictures or images could be taken from the moving position with the test box.

Four kinds of rod arrangement were constructed to study the effect of packing on the critical angle of repose: (1) *regular packing* using cylindrical rods, (2) *random packing* using a mixture of two kinds of cylindrical rods, (3) *horizontal packing* using ellipsoidal (Fig. 7-1) or oval rods, and (4) *vertical packing* using ellipsoidal (Fig. 7-2) or oval rods. The rod arrangement of horizontal and vertical packing were performed to study the effect of structure. To make these structures, the rods were piled up by hand (Fig. 8). The horizontal packing is defined as the packing that the direction of a long axis is parallel to the surface (Fig. 7-1). The definition of the vertical packing is that the direction of a long axis is not parallel to the plumb line but vertical to the *bottom* of the box, because the technique of the packing is very difficult for this test condition (Fig. 7-2).

The tilting-box was filled with the aluminum rods and then the surface of the assembly was made level. The assembly of rods were slashed from the both sides to get the structure out, which was formed through piling the rods. After that, the box was set to pull up (Fig. 9) at a slow constant speed (0.1° to 0.2° arc $second^{-1}$) until an avalanche occurred. The definition of the avalanche is that a number of the rods are moving altogether. The value of the *critical angle of repose* (α_c), which is defined in this study as the angle just prior to avalanching, could be determined precisely from the value of a digital clinometer (Soar Co. Ltd., model 1700 having a resolution of

0.01°) on the video-taped images. The procedure was repeated several times in each case and an average value for α_c was calculated.

2.2.2 Statics of an aluminum rod

i) *Sliding friction and rolling friction of a rod*

The experiments to determine the value for the rolling friction and the sliding friction of an aluminum rod were performed by means of the tilting method (Fig. 10), using the tilting-box in which an aluminum plate was placed. The value of the *angle of the sliding friction* (μ) is defined as the angle at which an aluminum rod, 9mm in diameter, just starts to slide when the rod was aligned parallel to the slope (Fig. 10a). The procedure is repeated 100 times and the histogram of the result is shown in Fig. 11. Average value for the sliding friction was 19.8° .

The value for the angle of rolling friction is also defined as the angle at which an aluminum rod placed perpendicular to the slope just starts to rotate. The values for the rolling friction were usually expressed as the dimension of rolling moment $[M \cdot L^2 \cdot T^{-2}]$ (Matsubara, 1981). The balance of the forces in the critical condition for the rolling is expressed as:

$$F \cdot r = M \tag{3}$$

where F is the force supplying the rod and r is the diameter of the rod, which is equivalent to the length of the arm of the moment, and M is the rolling moment resisting to the rotation of the rod. The resisting moment, M, usually expressed as the rolling friction, can be rewritten in the case of the tilting experiment:

$$M = W \cdot r \cdot \tan \rho \qquad (4)$$

where W is the weight of the rod and ρ is the angle at which the rod just starts to rolling, which is defined as the *angle of rolling friction* in this study. The procedure of the experiment was performed for four diameter of the cylindrical rods, repeated 50 to 100 times in each case and the average value for ρ was obtained. The quantity ρ is a non-dimensional constant, expressed with the unit of degree. The method to measure the value of rolling friction is shown in Fig. 12.

The histogram of rolling friction is shown in Figs. 13 and 14. The values for rolling friction are much smaller than that for the sliding friction: the mean value is 1.37' in the case of 9-mm diameter rods. Scattering of data is considerably large: The range of the value of rolling friction is as much as 7 degrees in the case of 5-mm rods. The mean value for the rolling friction decreases in proportional to its diameter.

ii) *Pivoting angle for individual rod*

The first series of tilting-box experiments was carried out to test the simplest case of avalanching, performed by piling one layer of the rods. This experiment was conduced by piling one layer of 5-mm diameter rods on a plate, in which one layer of 5-mm diameter rods underlain were glued perpendicular to the slope. The tilting-box was drawn up until a particle began to move.

The result, listed in Table 6, indicates the particle was moved at the angle of slope between 27.3° and 29.4°, which are almost the same as the angle between the center of a moving rod and the center of the contact rod glued on the plate, *i.e.*, 30°. This kind of experiment was already performed (Li and Komar, 1986) by using 3-dimensional grains (Fig. 15). This angle is called the *pivoting angle*, which is identical with the angle between the center of gravity and a contact point located at the nearest place to the slope. For the case of one- or two-layer piling, the rods are likely to move approximately at the pivoting angle between the rods.

2.2.3 Avalanche of assemblies of the rods

i) *Nature of avalanching of assemblies of the rods*

The cross section of an avalanche occurred on a slope made of the oval rods with the vertical packing is shown in Fig. 16. The motion of rods decreased with increasing depth from the avalanche surface. No marked sliding surface was formed. Most of the rods were *rotating* during the avalanche. This indicates that the behavior of avalanche is not analogous to the sliding of a solid body. For example, the particle indicated by an arrow in Fig. 17 clearly shows rotation during an avalanche. Even for the case in which the oval rods or ellipsoidal rods were piled with the horizontal packing, the rods were not sliding but rotating during avalanche. As the slope angle became steeper, the rods, which were placed parallel to the slope in the surface layer at the initial stage, started to erect, and finally rotated resulting in avalanche.

The schematic diagram of the avalanche of the aluminum rods is illustrated in Fig. 18. As the slope become steeper, some unstable rods is start to rolling (Stage 2), and after that an avalanche occurs involving all of the rods located near the surface of the slope (Stage 3). In comparison with the avalanche and particle movement of the sand and gravels (Onda *et al.*, 1988; Matsukura *et al.*, 1989), the behavior of the 2-dimensional rods is similar to the behavior of 3-dimensional materials.

To check the reproducibility of the experiment, the tilting box experiment, using the mixture of ϕ 5mm and ϕ 9mm rods, was performed for 20 times. The result is shown in Fig. 19. The value of the α_c ranges from 23° to 29°, having the bi-modal distribution.

The result of all experiments was listed in Appendix 1. The value for porosity, slope length and α_c was also tabulated.

ii) *Effect of slope length on the critical angle of repose*

The first series of experiments has been carried out to test the *effect of slope length* (l) (Ishii, 1978; Matsukura and Onda, 1989b), by changing the number of rods. The number of rods was changed from 106 to 2976. The material used was 3-mm diameter rods and 5-mm diameter rods, and the mixture ratio of these materials was 3 : 2 by weight. The mean diameter (d_m) of this mixture was calculated at 3.8mm.

Notwithstanding no marked sliding surface, the longitudinal profiles of the avalanches can be recognized. They are defined as the boundary between the zone of moving and still rods, obtained by tracing movement of rods moving on the video-taped images. The shapes of an avalanche for various slope lengths are shown in Fig. 20. It is seen that the shape is slightly different with the slope length: the profiles become flatter with increasing the value for the *relative slope length* (l/d_m).

The test result is summarized in Table 7. The plot of l/d_m against the *maximum depth* (D), which is the maximum depth of avalanche measured perpendicular to the slope surface of the avalanche, indicates that D increases with increasing the value for l/d_m within a range of small l/d_m -value. However, the value for D gradually becomes constant (Fig. 21). This constant value is about 3 cm, which corresponds to 7.9 times as large as the value for d_m (D/d_m), when l/d_m -value is approximately greater than 60. The value for the critical angle of repose (α_c) is valid with $60 \leq l/d_m \leq 110$ (Onda and Matsukura, 1989b) in the case of the aluminum rods. The following tilting-box experiments were thus performed to satisfy the condition of $60 \leq l/d_m \leq 110$.

To test the constancy of D/d_m -value, an additional experiments using an assembly of the different diameter of rods were performed. The rod-diameter and the mixture ratio are as follows: (1) ϕ 5mm:ϕ 9mm = 3 : 2, (2) ϕ 1.6mm :ϕ 3mm = 3 : 2. Basement profiles of the avalanche indicate that they have a similar shape as shown in Fig. 22. The plot of d_m against D shows a linear relationship (Fig. 23a), and the following equation can be written:

$$D = 7.9 \cdot d_m \tag{5}$$

or,

$$D/d_m = 7.9 \quad (6)$$

This plot of D/d_m against d_m is shown in Fig. 23b. This equation means that the depth of avalanche depends on the mean diameter, *not* on any other factor.

iii) *Effect of the mixture ratio on the critical angle of repose*

The second series of experiments were carried out to examine the effect of the mixture ratio. The tests were conducted by changing the mixture ratio of 5-mm-diameter rods and 9-mm-diameter rods as 1 : 0 (Fig. 24A; uniform rods), 20 : 1, 10 : 1 (Fig. 24B), 8 : 2, 7 : 3 (Fig. 24C), 5 : 5 (Fig. 24D), 3 : 7, 2 : 8, 1:10 (Fig. 24E), and 0 : 1 (Fig. 24F; uniform rods). The results of this experiment are tabulated in Table 8. The value for the critical angle of repose (α_c) is not considerably different with the mixture ratio, ranging from 26° to 30°, except for the case of uniform rods. The values for the two cases of uniform rods with regular packing are large; being 56.5° and 52.5°, respectively.

iv) *Effect of the shape and fabric to the critical angle of repose*

The third series of experiments was carried out to test the effect of the rod shape and piling structures, conduced by using cylindrical, ellipsoidal and oval rods. The result of the experiment is summarized in Table 9. The result clearly indicate that the value for the critical angle of repose (α_c) in the case of the vertical packing of ellipsoidal rods and oval rods had lower than that of the horizontal packing. The value of α_c in the case of vertical open packing (shown in Fig. 25a) is 24.2°, whereas α_c-value of vertical close packing (in Fig. 25b) is 45.3°. The result for the case of uniform-diameter ellipsoidal rods illustrates that the value for α_c is only controlled by the *pivoting angle* of the surface rods.

The result for the case of *octagonal, square, rectangle* rods also have similar tendency to the case of uniform-diameter oval rods; that is to say, the value for α_c is controlled by the pivoting angle. However, α_c-value for the case of the horizontal packing of the rectangle rods is slightly higher in spite of the same pivoting angle.

v) *Effect of the porosity on the critical angle of repose*

The last series of experiments was carried out to test the effect of the porosity. The test was conduced as follows: First, the rods were piled up to make an assembly through the usual procedure (porosity = 21.2%), and a number of rods were decreased from the interior of the assembly to the surface by pushing using another rods, then the specimen having larger value (porosity = 25.7%) of porosity could be made. The picture and the results of tilting-box experiment, shown in Fig. 26, indicates that α_c-value slightly decreased for the case of the large porosity, although the difference of value is not so large enough.

2.3 Two-Dimensional Direct Shear Test

2.3.1 Apparatus and materials

Values for the angle of internal friction were obtained by direct shear tests. Two rectangular-shape shear boxes were used: One is 15cm long, 10cm wide and 10cm deep (15cm shear box), which is owned by Laboratory of Soil Mechanics, Nagoya Institute of Technology. The other shear box is 18cm long, 10cm wide and 10cm deep (18cm shear box), which is owned by Institute of Geoscience, University of Tsukuba. The aluminum rods were piled up in these shear boxes perpendicular to the shearing direction up to 10cm in height. Applying a normal stress ranging from 0.43kgf/cm^2 to 3.0 kgf/cm^2 (46kPa to 300kPa), an assembly of rods was sheared with a speed of 1mm/min. The peak values of the shear resistance were recorded and were divided by the normal stresses, the values for the *peak angle of internal friction* (ϕ'_p) were obtained.

The apparatus and the recording system for the 18-cm shear-box experiment are shown in Fig. 27. The normal force and the shear force were recorded through pressure transducers. The 15-cm shear-box test is not equipped with the electrical measuring system. Photographs taken during the shear test using the cylindrical rods and ellipsoidal rods are shown in Fig. 28.

The ratio, the least dimension of the specimen (D_s) to the maximum particle size (d_{max}) is called D_s/d_{max}-value (Chandler, 1973). The value for ϕ'_p is valid, providing the D_s/d_{max}-value is large enough (Chandler, 1973; Garga, 1988; Matsukura *et al.*, 1988). The critical value which sustains the validity of ϕ'_p is 10 to 12 (Chandler; 1973), 15 to 20 for pebble and 30 to 40 for sand (Matsukura *et al.*, 1988). Consequently, D_s/d_{max}-value should be larger to measure an exact angle of internal friction. For example, the D_s/d_{max}-value using the 9-mm rods in the 15-cm shear-box was 16.7 and 20 in the case of the 18-cm shear-box. Therefore, the data obtained by the 18cm shear box test is likely to show more reasonable values than those obtained by the 15-cm shear box.

The shear tests were also recorded by a video-camera or a 35-mm still camera. The behavior of the rods could be easily recognized by observing the straight line marked on each rod.

2.3.2 Experimental results

The behavior of the rods close to the shear zone, which were observed through the video-taped images, clearly shows that the rods were *sliding*, not *rolling*. The photos taken during shear tests are shown in Fig. 28. The observation for the experiment supports the previous view that the rods during shear test are sliding (Umeya *et al.*, 1975). The behavior of rods close to the shear zone can also been appreciated with this picture.

The stress-strain relationship for these experiment are shown in Fig. 29. For the case of the vertical packing, shear stress had a marked peak value (Fig. 29a), and a positive vertical displacement was measured. In contrast, no marked peak was measured in the case of the horizontal packing with small vertical displacement (Fig. 29b).

An example of the relationship between shear strengths, τ, and effective normal stresses, σ, is shown in Fig. 30. Since no value of cohesion is seen in this figure, this material is thought to be non cohesive material. Therefore, the value for the angle of internal friction, ϕ'_p , can be determined even only by one datum point.

The result of the experiment as to the effect of the mixture ratio is summarized in Table 10. The value for ϕ'_p has a general tendency to become larger with increasing value of mean diameter.

Because the tendency, however, may be influenced by the size of the shear box, it is not clear whether the relationship is substantial or not.

The effect of the packing or fabric on ϕ'_p-value is listed in Table 11. The ϕ'_p-value for the case of the vertical packing is larger than that for the horizontal packing. These relationship has already been reported by Oda (1972), Oda *et al.*(1983) and Takeda *et al.* (1983). The value of ϕ'_p for the uniform-diameter case is very low (21.9°), which fact suggest that the smooth sliding exists between the rods.

2.4 Comparison between critical angle of repose and angle of internal friction

Figure 31, plotting the relationship between the critical angle of repose and the angle of internal friction (summarized in Table 12), clearly shows that the previous view, $\alpha_c = \phi'_p$, does not hold. An assembly of larger oval rods with the horizontal packing has the lowest ϕ'_p-value due to low- and regular-interlocking angle (data point numbered 6). The vertical packing case, a mixture of two kinds of ellipsoidal rods (data No.1) and that of oval rods (data No.3) take on larger ϕ'_p-values due to higher angles of interlocking among the rods. Thus, the previous view (*e.g.*, Rowe, 1962) that the value for ϕ'_p can be affected by the interlocking angle seems reasonable.

For the horizontal packing cases, a mixture of two kinds of ellipsoidal rods (data No.2) and that of oval rods (data No.5) take on higher α_c-value compared with the cases of the vertical packing (data No.1 and No.3). Values for α_c of data No.6, No.7 (vertical packing with larger oval rods only), and No.8 (smaller cylindrical rods only) indicate much higher value than those of other data of mixed-rod cases.

Figure 32 indicates the influence of mixture ratio on both α_c and ϕ'_p. The difference in values for ϕ'_p and α_c are considerably large for the case of the uniform rods for which the value of α_c is greater than 50°, whereas ϕ'_p-value is approximately 30°. This fact also suggests that the angle of internal friction is not equal to the critical angle of repose.

CHAPTER 3

MODELING

3.1 The Outline of the GSM (Granular material Stability Model)

3.1.1 Programs and systems

The two-dimensional tilting-box experiments and the direct shear test, described in Chapter 2, present the result that the previous theory that the angle of repose equal to the angle of internal friction does not hold. A model which will describe the actual mechanism controlling the angle of repose for granular material would be required. The most powerful way of modeling for explain the stability of an assembly of rods is by numerical methods (Cundall and Strack, 1979), because they are more flexible in application than analytical modeling.

Here the author will propose a new 2-dimensional numerical simulation model, *Granular material Stability Model* (GSM), on the stability of the granular material, based on the static equilibrium among particles. By using GSM the confining force is numerically calculated, and the instability of particles is judged. The GSM is a 2-dimensional statical model, not like dynamic- and black-box-typed models as DEM (Distinct Element Method; constructed by Cundall and Strack, 1979).

The GSM is composed of three programs. The first part of the program is for packing of an assembly of particles (*PACK1000*). The second part of the program is the main program (*GSM1000*) in which the transmission of forces is calculated contact by contact. The first scheme of the main program which calculates the equilibrium of each particle individually, and the second scheme is to find unstable particles. The third program is an output program (*GSMPRT*), to output the result of the calculation to a printer or plotter.

These programs are written by BASIC language on a personal computer, NEC-PC9801 and a main flame FACOM M780/20. The flow charts of these programs are shown in Fig. 33. Although the present edition of the GSM model is a 2-dimemsional model, the model can be expanded to a 3-dimensional model, as have been expanded for DEM (Iwashita, 1988).

i) *Random packing program*

The random packing program (*PACK1000*) was executed with FACOM M780/20. The time for executing one case was as much as 30 minutes in CPU-time even using the FACOM for the case of 1000-particle packing. This CPU-time was identical to approximately two months, the time necessary for execution if NEC PC9801 was used. Many kinds of algorithm were proposed as to the packing method (Hakuno and Hirao, 1973). The scheme used in the program, *PACK1000* is based on the *intrusion method* (Round and Newton, 1963). A schematic diagram of the method for packing is illustrated in Fig. 34.

The scheme is as follows: the lowest place among the particles is searched (Fig. 34b) and then new particle is filled into the point to have at least two contact points. The x-coordinate value of center of gravity for a given particle is defined as x and x_i and x_j are the x-coordinate value for the contact points. The value of x_j is larger than that of x_i. The following equation must be satisfied to stable the particles (as like number 34 particle in Fig. 34c):

$$x_i < x < x_j \qquad (7)$$

Sometimes the contact points does not satisfy the Equation (7) as shown in Fig. 34d-3, or a particle is crossing to anther particles (Fig. 34d-2). In such cases, the next lowest place was searched, and this scheme was repeated again to satisfy the condition as shown in Fig. 34d-1.

This procedure is executed until the number of particles which have been planed ahead are piled up. The surface of the slope is not always flat when the piling is finished (Fig. 35a). Figure 35b shows the case which the surface is smoothed by removing projecting particles.

The mixture ratios can be changed to test the effect of mixing. The number of the particles vary from 35 to 1009. All the data of the packing are transmitted to the personal computer, NEC PC-9801.

ii) *Main program*

The second program is the main program, *GSM1000*, the numerical calculation in this program is close approximation, yet it is based on the statics and tribology. The calculation time of the GSM is as much as 24 hours on NEC PC9801 for the case of 1,000 particles. Main program had more than 1,000 lines.

The flow chart of the main program is illustrated in Fig. 36. The method of calculation using this main program is shown in Fig. 37: The vector representing the *total force* (the sum of the weight of its particle and the confining force of a particle derived from surrounding particles) of a particle is splitted into the two components. These components give forces to the two particles which are situated nearest both side positions from the direction of this total force. Here, the components of the force, as shown in Fig. 37b, can be obtained by solving the following simultaneous equations:

$$\begin{cases} |f_{ij}|\cdot\sin\theta_{ij} + |f_{ik}|\cdot\sin\theta_{ik} = 0 & (8) \\ |f_{ij}|\cdot\cos\theta_{ij} + |f_{ik}|\cdot\cos\theta_{ik} = |F_i| & (9) \end{cases}$$

where F_i is the total force of particle i, f_{ij} and f_{ik} are the confining forces between the particle i and j, and i and k, respectively, θ_{ij} and θ_{ik} are contact angles between particle i and j, and i and k, respectively. The scheme is executed from the upper particle to the lower particle and is repeated until all the forces for particles are calculated. Sometimes the value for $|f_{ij}|$ or $|f_{ik}|$ is calculated to be negative; this means that the vector of force, F_i, cannot be splitted between the particle j and k. For this case, another contact point of the particle i is selected and all the procedure is re-caluculated from the beginning. The numerical modeling of this algorithm is largely based on the procedure proposed by Murayama and Matsuoka (1970). In this scheme, the influence of particle-to-particle friction is ignored.

A particle sometimes have no contact points satisfying the Equations. (8) and (9). In this case, the stability of the particle is supported by only one particle contact: it is defined as a *marginal particle*. An example of a marginal particle is shown in Fig. 37a for a particle marked "M". For a few cases, a scheme falls into an infinity-loop because of a problem of the program. For this case, the particle contact, which is caused a infinity-loop, is neglected.

The next scheme is the judgement whether the marginal particles are stable or unstable. The critical conditions for the particle motion are illustrated in Fig. 38. Two critical conditions could be given. One condition is based on the sliding friction of two rigid bodies. This is written as:

$$F = W \sin\theta + \mu \cdot N \tag{10}$$

where θ is a contact angle between the particles i and j, F is the total force of the particle i parallel to the contact angle, W is the weight of the particle i, μ is the sliding friction between two aluminum rods, which is described in Chapter 2, and N is the normal force applied to the particle j. In most cases, because the particle i is confined by the particle j, slipping at the contact points should be taken into considertation. This equation can be re-written as follows:

$$F = \mu \cdot DF + \frac{W \cdot (\sin\theta + \mu\cos\theta)}{1 + (\sin\theta + \mu\cos\theta)\cdot\sin\theta} \tag{11}$$

where *DF* is the confining force between i and k. From the standpoint of the particle i, this *DF* force is defined as a *transmitted force.* The first term of the right hand side, $\mu \cdot DF$ is the sliding friction at the particle contact between the particles i and k.

The other condition is to describe the rolling of rods which must occur in nature. The moment of rotation around the rod i (M) is defined as:

$$M = F \cdot r \tag{12}$$

where r is the radius of the rod i. When the particle starts to roll on the rod j, sliding should occur at the boundary between the particles i and k, and as a result, the moment of rotation decreases. In addition, adding the force required to climb the slope θ, the following critical condition can be obtained:

$$M/r - \mu \cdot DF - W \sin \theta = \rho \cdot N \tag{13}$$

where ρ is the non-dimensional coefficient of rolling friction of the aluminum rods. This equation is re-written as follows:

$$F = \mu \cdot DF + W \sin \theta + \rho \cdot W \cdot \cos \theta \tag{14}$$

Equations (11) and (14) are the critical conditions for the motion of the rods by sliding and rolling, respectively.

All of these program lists are shown in Appendix 3. The program, *PACK1000*, was written with FACOM OS IV BASIC (Copyright by Fujitsu, Co. Ltd.). The programs *GSM1000* and *GSMPRT* are written with MS-DOS N88BASIC (Version 4.0). N88BASIC COMPILER (Version 4.0; Copyright by Microsoft Co. Ltd.) was used in executing the programs.

3.1.2 Parameters

The parameters used for the GSM program are the angle of rolling friction, and the angle of sliding friction. These parameters are listed in Table 13. The measuring method and the data are described in Chapter 2. The data of sliding friction is obtained from the experiments for the only case of the ϕ9mm. The value of sliding friction for the case of other diameters are considered as the same value as the ϕ9mm case.

3.2 The Results of the GSM

3.2.1 The comparison between the model and experiments

The tilting-box experiment was carried out to test the applicability of the GSM. Two kinds of large aluminum cylinders with the same length, 50mm, but with different diameters, 25mm and 45mm, were used for this purpose. In this experiment, thirty five cylinders were piled (Fig. 39) just the same as the packing generated with the program, *PACK1000*. Next, the tilting-box experiment was performed and the angle of slope at which first movement occurred was recorded. In addition, which particle moved first was also recorded. The tilting-box experiment using thirty five cylinders was performed for three times and an average critical angle was calculated.

The GSM calculations were performed for just the same packing as the tilting-box experiment. The calculation was executed with a step of 1°. The angle of slope at which a particle was judged to move was thus assumed as the average value between the angle just prior to the critical condition and the angle just attaining the critical condition. After all of the calculations and the experiments were performed, the comparison between both results was carried out.

The result of the experiment and calculation is listed in Table 14. Figure 40 shows that the plot of the calculated value against the observed value defines an equal relationship for the case of the critical condition for the rolling friction except for a few data points. This figure also illustrates that the calculated values using the critical condition for the sliding friction are likely to overestimate the observed values for many cases.

In addition, the GSM can predict which particle moves first. This fact suggests that the actual phenomena can be analysed sufficiently and accurately with the GSM taking the critical condition for rolling into account.

It should be noted that this comparison is very difficult. In experiment, the value for each parameter has certain amount of range; a parameter rolling friction is as much as 2.5° (*see* Fig. 14) for the particle of 25-mm-diameter cylinder. In addition, errors of the size to the accurate values of the cylinders and tilting-box were unavoidable. In contrast, only accurate and precise values are used in modeling. Figure 40 was made in this situation.

A few of data indicating the deviation from the relationship may be due to the restriction of numerical method of the present edition of the GSM.

3.2.2 The result of the GSM calculation

The calculation of the GSM for the case of the uniform material is shown in Fig. 41. All the particles are stable when the angle is 40° (Fig. 41a). Direction of total force for every particles indicates the same direction because the packing is regular. It is 61° when the marginal particle became unstable (Fig. 41b). This result is close to the observed value of 56.5' (Table 7) obtained thorough the tilting-box experiment. The angle of internal friction for that case of packing is 30.4' (Table 10), which is considerably different value compared with this observed value for α_c, 56.5'.

The GSM calculation for the case of mixed materials with small number particles with different-diameter is illustrated in Fig. 42. This result is substantially different as comparing with the uniform ones (Fig. 41), because of the mixture of a quite small number of different-diameter particles. Vectors have the different direction in each other. Many marginal particles on the slope are judged as unstable, due to the transmitted force caused by the inequality of direction of forces.

The calculation for the case of the mixed material (mixing ratio = 3:2) with random packing was shown in Fig. 43. Each direction of total force indicates different direction in each other. Many marginal particles are judged as unstable particles (arrow marked particles in Fig. 43), an avalanche therefore is likely to occur at an angle of 33'. Since the GSM is the statical model, it is impossible to predict a precise angle of slope at which a large avalanche occurs. However, it can be pointed out that the directions of many resultant vectors are parallel to the slope surface within the depth corresponding to the length of six to eight particles, this depth being similar to the depth observed in the tilting-box experiment.

The transmitted force probably exists along the "sliding surface" before avalanching of granular material.

The GSM was executed for various number of particles to study the effect of slope length. The result of the calculation for several slope lengths is shown in Figs. 44 through 49; they are the result of GSM calculation with an angle of slope at 14' for the case of 35 particles, and 33' for the case of 100 particles, 301 particles, 500 particles, 700 particles, and 1009 particles, respectively.

The structure of the transmission of the force within several-particle depth, as described above, is the most distinct for the case of 301 particles (Fig. 46), and this kind of structure cannot be observed for the case of 35 particles (Fig. 44). A number of the arc-like transmission of forces are observed for the cases of the 700 particles (Fig. 48) and 1009 particles (Fig. 49).

The change in resultant vector of each particle with changing slope angles is shown in Fig. 50 as an example of 200-particle case. Most of the vectors are of vertical direction for the case of that the slope angle is at 10' . It is seen that, as the slope angle increases, the direction of the vectors gradually change. The arc-like transmitted force can be observed when the slope is 33' .

CHAPTER 4

DISCUSSION

4.1 Mechanism for the Avalanche of an Assembly of Two-Dimensional Materials

4.1.1 Mechanism for the commencement of the avalanche

To investigate the mechanism for avalanching of the two-dimensional rods, the photographs or video-taped images are available. The cross section of an avalanche occurred on a slope made of the oval rods with the vertical packing is already shown in Figs. 16 and 17. No marked sliding surface was formed, and most of the rods were *rotating* during avalanche. This indicates that the behavior of avalanche is not analogous to the sliding of a solid body. Figure 51 shows the case of ellipsoidal rods with horizontal packing. Even for the case in which the oval rods or ellipsoidal rods were piled with the horizontal packing, the rods were not sliding but rotating during avalanche. As the slope angle became steeper, the rods, which were placed parallel to the slope in the surface layer at the initial stage (Fig. 51-1), started to erect at an angle of 29° to 30.5° (Figs. 51-2 and 51-3), and finally rotated at 35° resulting in avalanche (Fig. 51-4).

In the same manner, an avalanche of the square rods with regular packing is shown in Fig. 52, which is composed of these photographs sequentially taken by a 35-mm camera placed one side of the slope: *before the avalanche* (Fig. 52-1), *during the avalanche* (Fig. 52-2), and *after the avalanche* (Fig. 52-3). In this case, the images were also recorded by the video-camera placed at the opposite side of the slope. These images (Fig. 53) also clearly show that no marked sliding occurred at the boundary between moving rods and still rods and that the rods are rotating.

A more marked example using octagonal rods with regular packing during the avalanche (Fig. 54) indicates the occurrence of no sliding during avalanche; it occurs only due to a collapsing of pillar-like structures (Figs. 54-3 and 54-4).

An avalanche for the case of the mixed shaped materials of rectangular, square, and octagonal rods occurs by rotation of these rods as shown in Fig. 55. The avalanche occurs by the rotation of the arrow-marked rod, due to the transmitted force through a rod marked "A" (Fig. 55b), which is originally induced by a rod "B". Figure 56 is an image during the same avalanche as shown in Fig. 55. In this figure, the boundary between the regions showing moving and still rods is depicted by a white line. Movement of the rods is easily seen from blur of the picture in the upper half region. It is, therefore, tentatively suggested that the avalanche of rods does not commence by *sliding* but by *rotation* of the rods, which is caused by transmitted forces.

Previous studies considered that avalanching of slopes made of granular materials is analogous to sliding of a solid body on a frictional surface (Seed and Goodman, 1964), because the angle of internal friction for granular materials can be explained (*e.g.*, Rowe, 1962) by the summation of the *true angle of friction between mineral surfaces of the particles* (ϕ_μ) and the *dilatancy angles* (β):

$$\phi'_p = \phi_\mu + \beta \tag{15}$$

The schematic diagram of this equation is shown in Fig. 57. Rowe's model is thought to be accepted by many workers (*e.g.*, Lambe and Whitman, 1969; Matsuoka, 1978). Obviously, what we call the *angle of internal friction* has a general conception as a kind of *sliding friction* among particles under a confining pressure.

The present experiments show that the motion of rods during avalanching is completely different from the behavior of a sliding block on a frictional surface, as illustrated above using Figs. 51 through 56. In addition, the comparison of the data between the critical angle of repose and the angle of internal friction (Fig. 31), clearly shows that the previous view, $\alpha_c = \phi'_p$, is not supported. The ϕ'_p-value is thought to be determined by the interlocking angle and sliding friction, while the α_c-value is determined by the angle at which rods forming the surface layer lose their balance.

Almost the data indicate the relation of $\alpha_c \neq \phi'_p$, but some data such as No.4 (mixed rods) and No.5 (mixed ellipsoidal rods) in Fig. 31 and mixed-rod cases in Fig. 32 indicate $\alpha_c \simeq \phi'_p$. This suggests that in the case of the mixed material with random packing ϕ'_p and α_c are likely to have similar values, although the mechanisms controlling the both values is substantially different. Materials existing in nature are usually mixed in size and shape, and randomly packed. It seems that using such materials led to the conclusion of $\alpha_c = \phi'_p$ in previous studies (*e.g.*, Hough, 1957). The data of the present study shown in Fig. 58 support the above discussion.

These discussions and results obtained through tilting-box experiments and direct shear tests clearly suggest that the critical angle of repose is not equal to the angle of internal friction, because the mechanisms controlling these two values are completely different. A schematic diagram illustrating the mechanism of avalanching of 2-dimensional assembly is shown in Fig. 59. The avalanche does not commences by *sliding* but by *rotation* of the particle denoted as *A*, because the rolling friction is much smaller than the sliding friction. The movement of a marginal particle *A* causes the movement of the other particles (particle *B*, *C*, and *D*), because these particles are supported by the marginal particle *A*.

4.1.2 Mechanisms for avalanching

i) *Effect of angle of slope on instability processes*

The confining force (transmitted force) among particles can be transmitted only through the points of the particle contacts which have a small in number: they are less than 12 in each particle in the case of the equal-diameter spheres (Bernal and Mason, 1960). Instability of slopes made of granular materials should occur by these transmitted forces.

A schematic diagram of the GSM calculation as to the change of two contact points at which confining forces can transmitted is shown in Fig. 60. The particle named *B* gives forces, indicated by dotted lines in Fig. 60, to the particles *A* and *E* in the case of 5°. The contact points of particle *B* in which confining force can be transmitted change from particle *A* and *E* to the particles *E* and *F* when the slope angle is 20°. In this case, the direction of the total force of the particle *F*, indicated by a solid line, is perpendicular to the slope at a slope angle of 5°. This direction is changes to the parallel to the slope at 20°, because one of transmitted forces is given directly by particle *B* to the particle *F* through its particle contact. In this way, the direction of total forces gradually tend to become the slope direction and instability increases as the angle of slope becomes steeper.

ii) *Effect of porosity on instability process*

The effect of the porosity on the critical stable angle can be also analysed by the GSM method. The idealized diagram (Fig. 61) indicates the effect of the number of particle contact on the critical angle of repose. As the angle of slope becomes steeper, the position of particle contacts through which transmitted forces are given will change. The direction of a new particle contact would not change so much, if there were a number of particle contacts, *i.e.*, a dense state (Fig. 61a). In contrast to this, if there were a small number of particle contacts, the direction of a transmitted force would considerably changed (Fig. 61b).

It has been already known that the number of particle contact will increase as the porosity decreases in granular materials (Oda, 1977). The effect of the porosity on the critical angle of repose, thus, must be due to the number of particle contact at which internal forces can be transmitted. No well-illustrated effect of porosity on the critical angle of repose presents in the case of 2-dimensional rods (Fig. 26). However, a marked influence occurs for the case of 3-dimensional materials such as sand or gravel (*see* Appendix 3). This is probably because of the difference in the variance of a system of packing (Oda, 1977).

iii) *Shape and depth of an avalanche*

As already described in Chapter 3, the GSM calculation indicates that the directions of many vectors are parallel to the surface within the depths corresponding to the length of six to eight particles (Fig. 43). The boundary between moving rods and still rods exists prior to avalanching. The depth of the avalanche estimated by the GSM model is approximately identical to the depth observed in the tilting-box experiments.

The 35-rod experiment will offer some suggestions to the problem about the shape and depth of an avalanche. Figure 62 shows the result of the GSM calculation for the 35-rods case and that of tilting-box experiment conducted with the same piling condition as in the for GSM calculation. The bold line in this figure indicates the boundary between the moving rods and still rods which is observed from the tilting-box experiment. The angle of slope at which the initiation of the movement is predicted to be 13.5° by the simulation of GSM. Tilting-box experiment shows that the avalanche occurred at a slope angle of 13.8°. The prediction of the angle is justified in this case. In addition, which particle moved first is also predicted in this case. The particle No.33 became unstable under the condition of rolling. The particle No.33 first rotated, although the contact angle, defined as tangent angle in this study, between the particle Nos. 33 and 29 is very steep.

The boundary of the movement in the tilting-box experiment is approximately equal to the boundary between the particles having the vectors of unstable direction and the particles having the vectors of stable direction in the GSM calculation. The movement of the marginal particle (No.33) causes the movement of other particles which are supported by the marginal particles, and the boundary of movement is defined by the difference in direction of the total forces. The lower limit of rods, total forces of which show unstable directions, can determine the base of an avalanche zone.

Figure 63 shows an example of the distribution of force directions classified by the criterion shown in this figure. This figure indicates that forces with stable directions are mainly found at the deeper zone (a), forces with slightly unstable directions are found at the upper part of the slope (b), and forces with considerably unstable directions (c) are found at the shallow and lower zone of the slope.

To analyze quantitatively the tendency found in Fig. 63, Fig. 64

is drawn. Figures 64a and 64b show the frequency distribution, classified by 10 degrees. The former shows the number in direction of the vectors and the latter shows the summation of their absolute value of the vectors. The average values are indicated at the upper part of these rose diagrams. The pattern of the both distributions changes between 2-3cm and 3-4cm in depth. This depth is approximately equal to the observed depth in the tilting-box experiment. The changing pattern of Fig. 63b is more clear than that in Fig. 63a.

Figure 65 shows the direction of the resultant force calculated from the total forces of several particles existing in the grid system of 4cm × 1cm. This case is the same as shown in Fig. 63. The boundary (bold line) between the zone of stable direction and that of unstable direction is drawn. This boundary line is quite resemble in the shape of avalanche (Figs. 21-2 or 21-3) observed in the tilting-box experiment.

The same analysis as applied to construct Fig. 65 is carried out six times in the case of 300 particles, twice in 500 particles, three times in 700 particles, and 3 times in 1000 particles at the slope angle of 27°. Figure 66 shows the result of these calculations. Comparing this figure with Figs. 21 and 23 indicates that the boundary between the area of stable direction and that of unstable direction obtained from the calculations is quite similar to the basement of avalanching found in the experiments.

Based on the above discussion, a schematic diagram is shown in Fig. 67 to illustrate (1) *occurrence of the instability* at the upper part of the slope, (2) formation of the force direction at the middle part of the slope, and (3) *critical condition of avalanche occurrence* at the terminal part of the slope. An avalanche of rods is caused by instability of total forces (Fig. 67-1) and a depth of avalanche is determined by the magnitude of transmitted forces at about 8-particle depth (Fig. 67-2). An avalanche is triggered by *rotation* of a marginal rod (Fig. 67-3).

4.2 The Role of Rolling Friction in the Critical Angle of Repose

4.2.1 The rolling friction and the critical angle of repose

The mechanism of avalanche is discussed in Chapter 4.1. The important point is that the initiation of the avalanche of 2-dimensional rods does not commence due to *sliding* but to *rotation* of the rods. The rolling friction should, therefore, be a controlling factor for occurrence of the avalanche.

The angle of rolling frictions for an oval or an ellipsoidal rods, the long axis of which is perpendicular to the surface of the slope is 0 degree, because single rod cannot stand by itself. In contrast, an oval or an ellipsoidal rods, the long axis of which is parallel to the slope, the angles of rolling friction are 26.6° for an oval rod and 26.7° for an ellipsoidal rod (Table 15).

The α_c-values for an assembly of oval or ellipsoidal rods with the vertical packing are lower than the case of the horizontal packing; This fact cannot be explained by the previous view. Such an α_c-fabric correspondence is in good agreement with a similar correspondence found for the angle of rolling friction in the case of a single rod, as just mentioned. Low α_c-values for the case of the vertical packing using oval or ellipsoidal rods can be explained by low angles of rolling friction of piled single rods with vertical direction.

4.2.2 Rolling friction and critical angle of repose for 3-dimensional materials

The movement of materials such as sand or gravel begins with rolling as well as sliding when the slope failure occurs. Nevertheless, previous geomorphological and soil mechanical studies have overlooked the importance of the role of rolling friction. The angle of the rolling friction is defined in the case of the complicated-shaped (3-dimensional) material as the angle between the center of gravity for a particle and a fulcrum (Fig. 68). This definition of the rod is similar to the pivoting angle defined by Li and Komar (1986). The angles of the rolling friction of such materials as *coarse sand, beach shingle, glass beads, and crushed stone* (Fig. 69), were measured by the tilting method. The detail of the method of experiment and the result are shown in Appendix 2.

The values for the angle of rolling friction, critical angle of repose, the angle of internal friction, and *volume concentration* are listed in Table 16. Various values for the angle of rolling friction were gained. A plot of the critical angle of repose against the angle of rolling friction, ρ, (Fig. 70) shows a proportional relationship between the both angles as follows:

$$\alpha_c = 0.64\ \rho + 23.9 \qquad (16)$$

A little scattering of data points is seen.

In this figure, two values present for a certain angle of rolling friction. A parameter controlling α_c-values is the porosity, which is discussed in Chapter 4.1. The critical angle of repose will increase as the volume concentration, C, decreases, which is defined as 1 - porosity (Allen, 1969). It is already studied by Oda (1977) that the number of contact points increases as the volume concentration increases. Hence, the value of volume concentration is judged to be a function of the number of contact points. Volume concentration, C, and angle of rolling friction, ρ, are judged to be the essential parameters for controlling the critical angle of repose. Therefore, a new parameter, $\rho \cdot C$, is proposed. Figure 71 is the relationship between this parameter and the critical angle of repose, and this figure shows a good proportional relationship between the two:

$$\alpha_c = 1.15 \, \rho \cdot C + 23.7 \tag{17}$$

The value for correlation coefficient, r, is estimated as 0.968. It is strongly suggests that the critical angle of repose in the case of sand and gravel can be sufficiently analysed by using the parameter, $\rho \cdot C$.

Incidentally, a plot of the angle of internal friction against the critical angle of repose (Fig. 72) shows a poor correlation between both angles as correspond with Fig. 71.

CHAPTER 5

CONCLUSIONS

Tilting-box experiments using an assembly of aluminum rods were performed to gain an insight into what was the mechanism of the critical angle of repose (α_c). Observations and measurements of 2-dimensional avalanches clearly indicated that the mechanism for the commencement for the avalanching is not the sliding but *rotation* of rods. It was also found that (1) the depth of the avalanche is approximately 8 times as deep as the mean diameter of rods (d_m), (2) the value for α_c is considerably high in the case of uniform rods with regular packing, and (3) α_c-value for the case of horizontal packing is larger than that of vertical packing.

Direct shear tests of the aluminum rods were performed to obtain the peak value of angle of internal friction, ϕ'_p. A comparison between α_c and ϕ'_p indicates that the previous theory does not hold. Mechanisms for the angle of internal friction and the angle of repose are found to be essentially different. That is the former angle is controlled by sliding friction and the latter angle is controlled by rolling friction.

A statical and numerical model to describe the stability of 2-

dimensional assembly was constructed with BASIC language by using a personal computer and a main flame. The program was named GSM (*Granular material Stability Model*). The first part of the program is for packing of an assembly of the rods, and the second part of the program is the main program. The main program is to calculate the static equilibrium of each particle individually, and to find unstable particles. This model can explain that the shape of the uniform-diameter material with regular packing is likely to have a greater value of α_c compared with that made of mixed-diameter materials. The basement shape of avalanching also can by analysed by the GSM.

Based on the above discussion, mechanism of an avalanche is summarized as follows: An avalanche of rods is caused by instability of total forces and a depth of avalanche is determined by the transmitted forces at about 8-particle depth. An avalanche occurred by *rotation* of a marginal rod.

To apply the result of these 2-dimensional studies to the 3-dimensional environment, the parameter, $\rho \cdot C$, the product of the angle of rolling friction (ρ) and the volume concentration (C) was proposed. The plot of $\rho \cdot C$ against α_c indicates marked proportional relationship. The value for the regression coefficient for the case of $\rho \cdot C$ against α_c is considerably larger than the plot of ϕ'_p against α_c. This suggests that the result obtained by the present 2-dimensional analysis can be applied to 3-dimensional problems.

References

Allen, J.R.L. (1969): The maximum slope-angle attainable by surfaces underlain by bulked equal spheroids with variable dimensional ordering. *Bull. Geol. Soc. Am.*, **80**, 1923-1930.

Allen, J.R.L. (1970): The avalanching of granular solids on dune and similar slopes. *J. Geol.*, **78**, 326-351.

Allen, J.R.L. (1975): *Principle of Physical Sedimentology.* 35-38, George Allen & Unwin, New York, 272pp.

Bagnold, F.R.S. (1954): Experiment on a gravity-free dispersion of large solid spheres in a Newtonian fluid under shear. *Proc. Roy. Soc. A*, **225**, 49-63.

Bagnold, F.R.S. (1966): The shearing and dilatation of dry sand and the 'singing' mechanism. *Proc. Roy. Soc. A*, **295**, 219-232.

Bernal, J.D. and Mason, J. (1960): Co-ordination of randomly packed spheres. *Nature*, **188**, 910-911.

Burkalow, A.V. (1945): Angle of repose and angle of sliding friction: and experimental study, *Bull. Geol. Soc. Am.*, **56**, 669-708.

Bruce, I.G., Cruden, D.M. and Eaton, T.M. (1989): Use of a tilting table to determine the basic friction angle of hard rock samples. *Can. Geotech. J.*, **26**, 474-479.

Carrigy, M.A. (1970): Experiments on the angles of repose of granular materials. *Sedimentology*, **14**, 147-158.

Carson, M.A. (1977): Angles of repose, angles of shearing resistance and angles of talus slopes. *Earth Surface Processes*, 2, 363-380.

Carson, M.A. and Kirkby, M.J. (1972): *Hillslope Form and Processes*. 62-98, Cambridge Univ. Press, London, 475pp.

Chandler, R.J. (1973): The inclination of talus, arctic talus terraces, and other slopes composed of granular materials. *J. Geol.* 81, 1-14.

Cundall, P.A. and Strack, O.D.L. (1979): A discrete numerical model for granular assemblies. *Gêotechnique*, 29, 47-65.

Dantu, P. (1957): A contribution to the mechanical and Geometrical study of non-cohesive masses. *Proc. 4th ICSMFE*, 144-148. (*in French with English abstract*).

Drescher, A. (1976): An experimental investigation of flow rules for granular materials using optical sensitive glass particles, *Gêotechnique*, 26, 591-601.

Drescher, A. and Jong, G.J. (1972): Photoelastic verification of a mechanical model for the flow of a granular material. *J. Mech. Phys. Solids* 20, 337-351.

Franklin and Johanson (1955): Flow of granular material through a circular orifice. *Chem. Eng. Sci.*, 4, 119-129.

Garga, V. K. (1988): Effect of sample size on shear strength of basaltic residual soils. *Can. Geotech. J.*, 25, 478-487.

Hakuno, M. and Hirao, H. (1973): One example of two dimensional random packing of sand particles. *Proc. Japan. Soc. Civil Eng.*, 219, 55-63. *(in Japanese)*

Hayashi, S. (1970): Studies on the measurement of the angle of repose. *J. Soc. Powder Tech. Japan*, 7, 530-533. (*in Japanese*)

Hough, B.K. (1957): *Basic Soil Engineering*. The Ronald Press Company, New York, 513pp.

Ishii, T. (1978): Influences of the grain size of rock fragment and the slope length on the development of talus slope. *Geogr. Rep. Osaka Kyoiku Univ.*, 17, 35-46.

Ishii, T. (1981): Roles of grain size on scree slope. *Trans. Japan. Geomorph. Union*, 2, 19-24. (*in Japanese with English abstract*)

Ishii, T. (1988): Dry fragment flow and talus slope. *Geogr. Rep. Osaka Kyoiku Univ.*, 26, 1-14. (*in Japanese with English abstract*)

Iwashita, K. (1988): Dynamic fracture analysis of ground by granular assembly simulation . *Bull. Earthq. Res. Inst. Univ. Tokyo*, 63, 201-235. (*in Japanese with English abstract*)

Kirkby, M.J. and Statham, I. (1975): Surface stone movement and scree formation. *J. Geol.* 83, 349-362.

Lambe, T.W. and Whitman, R.V. (1969): *Soil Mechanics*. John Wiley & Sons, New York, 553pp.

Li, Z. and Komar, P. (1986): Laboratory measurements of pivoting angles for applications to selective entrainment of gravel in a current. *Sedimentology*, 33, 413-423.

Machida, T., Matsumoto, E. and Ishii, T. (1975): Formation processes of a talus cone in the Ashio waste land. *Geogr. Rev. Japan*, 48, 768-784. (*in Japanese with English abstract*)

Matsubara, Y. (1981): *Tribology.* Sangyo-Tosho, Tokyo, 279pp. *(in Japanese)*

Matsukura, Y. (1975): Relation of the amount of sand drift to the wind-velocity profile over the aeolian dunes on Enshunada beach, Shizuoka Prefecture. *Sand Dune Res.*, 21, 29-40. (*in Japanese with English abstract*)

Matsukura, Y. and Onda, Y. (1989): Angle of repose: a matter of semantics and a variety of the measuring methods. *Bull. Environm. Res. Center, Univ. Tsukuba*, 13, 27-35. (*in Japanese*)

Matsukura, Y., Okuyama, T., and Onda, Y. (1988): Preliminary study using large-sized direct shear apparatus on relation between debris-size and dimension of shear box. *Bull. Environm. Res. Center, Univ. Tsukuba*, 12, 43-48. *(in Japanese)*

Matsuoka, H. (1973): Deformation characteristics of soil. Doctor thesis of Kyoto University, 233pp.

Matsuoka, H. (1974): A macroscopic study on shear mechanism of granular materials. *Soils and Foundations*, 14(1), 29-43.

Matsuoka, H. (1978): Constitutive equations of soils 5. Approach as granular materials. *Soils and Foundations*, 18(3), 97-104.

Metcalf, J.R. (1966): Angle of repose and internal friction. *Int. J.*

Rock. Mech. Min. Sci. 3, 155-161.

Murayama, S. and Matsuoka, H. (1970): A microscopic consideration on the shearing behavior of granular materials using the two-dimensional models. *Annuals, Disast. Prev. Res. Inst., Kyoto Univ.* 13B, 505-523. (*in Japanese with English abstract*)

Oda, M. (1972): Initial fabrics and their relations to mechanical properties of granular material. *Soils and Foundations*, 12(1), 1-18.

Oda, M. (1974): A mechanical and statistical model of granular material. *Soils and Foundations*, 14(1), 13-27.

Oda, M. (1977): Co-ordination number and its relation to shear strength of granular material. *Soils and Foundations*, 17(2), 29-42.

Oda, M. and Konishi, J. (1974): Microscopic deformation mechanism of granular material in simple shear. *Soils and Foundations*, 14(4), 25-38.

Oda, M, Konishi, J. and Nemat-Nasser, S. (1983): Experimental micromechanical evaluation of the strength of granular materials: effect of particle rolling. *in* Jenkins, J.T. and Satake, M. eds. *Mechanics of Granular Materials*, 21-30, Elsevier, Amsterdam.

Onda, Y. and Matsukura, Y. (1989a): A preliminary experiment of angle of repose by an assembly of aluminum rods. *Bull. Environm. Res. Center, Univ. Tsukuba*, 13, 141-146. *(in Japanese)*

Onda, Y. and Matsukura, Y. (1989b) The influence of slope length on critical angle of repose: tilting-box tests using an assembly of aluminum rods. *Ann. Rep. Inst. Geosci. Univ. Tsukuba*, **15**, (in press)

Onda, Y., Matsukura, Y., Iseki, H. and Okuyama, T. (1988): Preliminary study on angle of initial yield and angle of rest by tilting-box tests. *Bull. Environm. Res. Center, Univ. Tsukuba*, **12**, 49-55.

Onda, Y., Matsukura, Y. Matsuoka, H., Oh-hashi, H. (1989): A preliminary study on failure mechanism of slope composed of two-dimensional granular materials. *Proc. 22th Japan. Conf. Soil. Mech. & Found. Eng.*, 1605-1606. *(in Japanese)*

Round, G.F. and Newton, R. (1963): Random packing of equal spheres on a plane surface. *Nature*, **198**, 747-749.

Roscoe, K.W., Schofield, A.N. and Wroth, C.P. (1958): On the yielding of soils. *Géotechnique*, **8**(1), 22-53.

Rowe, P.W. (1962): The stress-dilatancy relation for static equilibrium of an assembly of particles in contact. *Proc. Roy. Soc. A.*, **269**, 500-527.

Sarkar, A.D. (1980): *Friction and Wear*. Academic Press, London, 423pp.

Schneebeli, M. (1956): Mecanique des soils - Une analogie mecanique pour les terres sans cohesion. *C. r. Hebt. Seanc. Acad. Sci.*, **243**, 125-126. *(in French)*

Seed, B. and Goodman, R.E. (1964): Earthquake stability of slopes of cohesionless soils. *Proc. ASCE*, **90**, SM6, 43-73.

Soda, N. (1971): *Introduction to Tribology (Masatsu no Hanashi).* Iwanami, Tokyo, 214pp. *(in Japanese)*

Statham, I. (1974): The relationship of porosity and angle of repose to mixture proportions in assemblages of different sized materials. *Sedimentology*, 21, 149-162.

Statham, I. (1976): A scree slope rockfall model. *Earth Surface Processes*, 1, 43-62.

Statham, I. (1977): *Earth Surface Sediment Transport.* 46-49, Oxford Univ. Press, Oxford, 184pp.

Takeda, K., Tada, M. and Mori, M. (1983): Shear behavior of granular materials with anisotropic structures. *Proc. 18th Japan. Conf. Soil. Mech. & Found. Eng.*, 285-288. *(in Japanese)*

Takeuchi, K. and Miwa, S. (1970): Measurement of angle of repose of flowing surface in the vacuum and various gases, *J. Soc. Powder Tech. Japan*, 7, 41-45. (*in Japanese*)

Tanaka, K. (1985): *Basic Tribology (Masatsu no Ohanashi).* Nihon Kikaku Kyokai, Tokyo, 249pp. *(in Japanese)*

Taylor, L.D.W. (1948): *Fundamentals of Soil Mechanics.* John Wiley & Sons, New York, 700pp.

Terzaghi, C. (1925): Principles of soil mechanics (2): Friction in sand and clay. *Eng. News-Record*, 95, 1026-1029.

Terzaghi, K. (1943): *Theoretical Soil Mechanics.* John Wiley & Sons, New York, 510pp.

Tsuji, J., Nishida, M. and Kawada, K. (1965): *Experimental Method of the Photo Elastic Materials (Kohdansei Jikken Hou).* Nikkan Kogyo Shibun-Sha, Tokyo, 532pp. *(in Japanese)*

Umeya, K., Hara, R. Kikuta, J. (1975): On two-dimensional shear tests by model powders, *J. Chem. Eng. Japan*, **8**, 56-62 (1975).

Ward, W.H. (1945): The stability of natural slopes. *Geogr. J.*, **105**, 170-190.

Warren, A. (1979): Aeolian Processes. in Embleton, C. and Thornes, J. eds. "*Process in Geomorphology*", 325-351, Edward Arnold, London.

Table 1 Terminology for mechanisms controlling the stability of slope composed of granular materials

Author(s)	Year	Mechanism
Sharp	(1938)	*debris slide* (m: talus slope)
Ward	(1945)	*fragment slide* (m: talus slope)
Burkalow	(1945)	*slumping* (experiment)
Bagnold	(1966)	*avalanche / avalanche flow* (m: dune)
Allen	(1969)	*avalanche / avalanching* (experiment)
Carrigy	(1970)	*avalanching / slumping* (experiment)
Chandler	(1973)	*shallow landslide* (m: talus slope)
Statham	(1974)	*slide* (experiment)
Kirkby & Statham	(1975)	*rockfall* (m: talus slope)
Machida *et al.*	(1975)	*dry fragment flow, rockfall, debris flow* (m: talus slope)
Matsukura	(1975)	*avalanche* (m: aeolian dune)
Statham	(1976)	*rockfall* (m: talus slope)
Carson	(1977)	*avalanche* (experiment)
Ishii	(1978)	*dry fragment flow* (experiment)
Warren	(1979)	*slide* (m: aeolian dune)
This study	**(1990)**	***avalanche / avalanching***

m: measurement

Table 2. Terminology and symbols concerning to the *angle of repose*. The underlined terms are used as the *angle of repose*.

Author(s)	(Year)	Upper angle	Lower angle
Van Burkalow	(1945)	*angle of sliding friction*	<u>*angle of repose*</u>
Metcalf	(1966)	<u>*angle of repose*</u>	
Allen	(1969)	<u>*angle of initial yield*</u> (ϕ_i)	<u>*residual angle after shearing*</u> (ϕ_r)
Carrigy	(1970)	<u>*critical angle*</u> (α_C)	<u>*angle of rest*</u> (α_R)
Carson & Kirkby	(1972)	*angle of maximum slope*	<u>*angle of repose*</u>
Carson	(1977)		<u>*angle of rest after avalanching*</u> (ϕ_{rep})
Matsukura & Onda	(1989a)	<u>*critical angle of repose*</u> (α_C)	<u>*repose angle after avalanching*</u> (α_R)
This study	**(1990)**	<u>***critical angle of repose***</u> **(α_C)**	<u>***repose angle after avalanching***</u> **(α_R)**

Table 3 Summary of previous papers of experimental and theoretical approach to the angle of repose and stability of slopes made of granular materials.

Author(s)	(Year)	Angle of repose	Experimental apparatus (Fig.1)	Purposes
Van Burkalow	(1945)	α_R	④, ⑥	*size , mixture, density, shape, surface texture*
Allen	(1969)	α_C	(Theoretical)	*model of* α_C
Allen	(1970)	α_C , α_R	rotating drum ⑫	*deposit rate & avalanche*
Carrigy	(1970)	α_C , α_R	rotating drum ⑫	*shape, surface textures, size, in water & in air*
Hayashi	(1970)	α_R	②, ③	*various powder, diameter of base ring.*
Takeuchi & Miwa	(1970)	α_R	⑫, ②	*in air & vacuum*
Statham	(1974)	α_C , α_R	rotating drum ⑫	*size, mixture,* α_C *;constant,* α_R *;variability*
Kirkby & Statham	(1974)	ϕ'_{ud}	stock piling ①	*height of fall, discrete particle rockfall model*
Carson	(1977)	α_C , α_R	tilting-box ⑩ stock piling ①	*compare among methods* *size effect*
Ishii	(1978)	α_C , α_R	stock piling ①	*slope-length effect*
Onda *et al.*	(1988)	α_C , α_R	tilting-box ⑪	*size & density effect*
Matsukura *et al.*	(1988)	α_C , α_R	tilting-box ⑪	*slope-length effect*
Matsukura & Onda	(1989a)	α_C , α_R	①, ⑪, ⑫	*compare among methods*

Table 4.1 Definition of angle of shearing resistance and angle of repose

Symbol	Definition	Comments
$\phi_{\mu s}$	Static angle of plane sliding friction	*Angle of slope of an inclined plane at which an object resisting on the plane will first begin to slide because of its own weight.* (Van Burkalow, 1945)
$\phi_{\mu d}$	Dynamic angle of plane sliding friction	*The slope angle at which a moving particle will just come to rest.* (Statham, 1976).
ϕ_{μ}	True physical angle of friction	*The true angle of friction between the mineral surfaces of the particles* (Rowe, 1962)
β	Dilatancy angle	*Deviation of the tangent at the contact points.* (Rowe, 1962)

Table 4.2 Definition of angle of shearing resistance and angle of repose

Symbol	Definition	Comments
ϕ'_{cv}	Angle of internal shearing resistance (constant volume)	*Ultimate state of a sample at which any arbitrary further increment of shear distortion will not result in any change of voids ratio.* (Roscoe *et. al*, 1958)
ϕ'_{r}	Residual angle of internal shearing resistance	*Angle of internal shearing resistance for a material which has undergone considerable shear. approximately constant for a given material.* (Statham, 1977)
ϕ'_{p}	Peak angle of internal shearing resistance	*This angle is not a material property but depends strongly on the void ratio that existed prior to the application of a deviation stress.* (Lambe and Whitman, 1969)
α_{C}	Critical angle of repose	*Angle at which cohesionless aggregate begins to avalanching.* (Statham, 1977)
α_{R}	Repose angle after avalanching	*Angle at which cohesionless aggregate comes to rest after avalanching.* (Statham, 1977)

Table 5 Previous studies on the relationship between angle of repose and angle of internal friction.

Author(s)(Year)		Equation
Terzaghi	(1943)	*Angle of repose is approximately equal to the angle of shearing resistance in the loosest states*
Skempton	(1945)	$\phi'_{cv} = \alpha_R$
Taylor	(1948)	*The angle of repose is at best a crude approximation of the angle of internal friction, and in truly cohesionless soils it generally is appreciably smaller than the friction angle.*
Bagnold	(1966)	$\phi'_r = \alpha_C$
Metcalf	(1966)	*The angle of repose is not equal to angle of internal friction at loosest packing. Angle of repose approximates the angle of solid friction of the material* ($\phi_{\mu s} = \alpha_C$).
Lambe & Whitman	(1969)	*Angle of repose is about equal to the angle of internal friction for the loosest state* ($\phi'_{cv} = \alpha_C$).
Carson & Kirkby	(1972)	$\phi'_{cv} = \alpha_R$
Chandler	(1973)	$\phi'_{cv} = \alpha_C$
Statham	(1974)	$\phi'_{cv} \neq \alpha_R$
Statham	(1977)	*It seems reasonable to assume* α_C *is roughly equivalent to* ϕ'_p . ($\phi'_p = \alpha_C$)
Carson	(1977)	α_R *is approximately equal to the angle of shearing resistance in a loose state of packing.*

Table 6 Results of the tilting-box experiment for pivoting angle

Run No.	Experimental condition	Pivoting angle (degrees)
2	ϕ 5mm; 1-layer	28.0
4	*ditto*	28.0
5	*ditto*	29.5
6	*ditto*	29.4
7	*ditto*	27.1
(2.4.5.6.7 average)		[28.3]
8	ϕ 5mm; 3 rods	28.5
9	*ditto*	26.9
10	*ditto*	27.3
(8.9.10 average)		[27.6]

Table 7 Effect of the slope length on the critical angle of repose (α_c) and depth of avalanche

Weight (gf)	Number of rods*	Slope length (l, cm)	Porosity (%)	Depth of avalanche (D, cm)	Length of avalanche (l', cm)	l'/D (−)	l/d_m (−)	α_c (*degrees*)
134.8	106	9.0	13.8	1.50	5.94	3.96	23.7	31.3
303.3	237	13.0	14.9	2.08	9.70	4.66	34.2	30.8
537.9	421	18.0	17.1	2.19	11.56	5.28	47.4	29.5
842.8	661	22.0	18.2	2.43	14.73	6.06	57.9	27.5
1209	947	26.4	19.7	3.16	19.19	6.07	69.5	26.9
1646	1290	30.4	21.2	2.73	21.22	7.77	80.0	27.2
2151	1684	34.0	17.5	3.12	21.35	6.84	89.5	26.0
3363	2633	42.0	18.2	2.56	21.67	8.46	110.5	24.9
3800	2975	43.0	18.1	2.84	28.20	9.93	113.1	23.4
3333*	2609	44.1	19.2	3.54	29.68	8.38	116.1	22.6
3800**	2975	47.7	21.0	3.15	29.68	9.42	125.5	22.6

* Mixed ratio ϕ3mm:ϕ5mm=3:2 (weight ratio)

** In spite of the same volume of the rods as Nos. 10 and 11, respectively, the slope becomes longer because of a raised bottom.

Table 8 Mixture ratio, porosity and critical angle of repose

Mixture ratio (Weight ratio) φ 5mm: φ 9mm	Porosity n (%)	Critical angle of repose α_c (*degrees*)
φ 5mm uniform	9.5	56.5
20 : 1	13.7	29.1
10 : 1	13.7	30.0
8 : 2	15.8	26.3
7 : 3	18.0	26.4
5 : 5	17.2	28.6
3 : 7	17.9	27.6
2 : 8	16.6	27.6
1 : 10	14.3	27.4
1 : 20	16.6	26.4
φ 9mm uniform	12.2	52.5

Table 9.1 Effect of rod shape and packing condition on critical angle of repose

Shape	Packing	Porosity (%)	α_c (*degrees*)	Run No.
ellipsoidal *mixed*	horizontal	11.2	27.4	35,36
oval *mixed*	horizontal	13.9	29.3	171-173
ellipsoidal *mixed*	vertical	12.2	25.3	28,29,34
oval *mixed*	vertical	18.8	25.9	168-170
ellipsoidal *larger*	horizontal	23.7	23.7	38
oval *larger*	horizontal	17.0	27.8	158-160
ellipsoidal *larger*	horizontal, dense	2.6	48.0	39
oval *larger*	horizontal, dense	6.7	43.3	157,161
ellipsoidal *larger*	vertical	11.8	24.3	37
oval *larger*	vertical	7.9	24.2	162,163,167
oval *larger*	vertical, dense	1.1	45.3	164-166

Table 9.2 Effect of rod shape and packing condition on critical angle of repose

Shape		Packing	Porosity (%)	α_c (*degrees*)	Run No.
octagonal *larger*	(*A*)	dense	0.0	55.9	131-135
square side=5mm	(*B*)	regular	0.0	29.8	136-138
rectangle 6*9mm	(*C*)	horizontal	0.0	32.8	141,142,145
rectangle 6*9mm	(*C*)	vertical	0.0	31.9	146-148
A,B,C mixed 1:1:1		random	14.9	32.5	151,152,156

Table 10 Effect of mixing ratio of rods on peak angle of shearing resistance

Material and packing		Normal stress (kgf/cm^2)	Porosity (%)	ϕ'_p (degrees)	Run No.
ϕ5mm	regular	1.05-3.00	12.6	30.8	T1 - T3
ϕ5mm:ϕ9mm=10:1	random	2.06	15.3	28.4	T4
ϕ5mm:ϕ9mm=3:2	*ditto*	2.08-2.23	20.1	33.8	T5 - T6
ϕ5mm:ϕ9mm=5:5	*ditto*	1.80-1.90	20.5	31.9	T7 - T8
ϕ5mm:ϕ9mm=2:3	*ditto*	1.92-2.09	21.1	32.4	T9 - T10
ϕ5mm:ϕ9mm=1:10	*ditto*	1.83-2.24	20.4	36.5	T11- T12
ϕ9mm	regular	2.12-2.26	13.0	34.5	T13- T14

Length of the shear box is 18cm

Table 11 Effect of shape of rods and packing condition on peak angle of shearing resistance

shear box size	material and packing		normal stress (kgf/cm²)	porosity (%)	ϕ'_p (degrees)	Run No.
15	ellipsoidal *mixed*	vertical	0.47	14.2	41.6	N 4
18	oval *mixed*	vertical	2.00-2.03	16.4	36.0	T17-T18
15	ellipsoidal *mixed*	horizontal	0.47	14.2	31.9	N 5
18	oval *mixed*	horizontal	2.06-2.12	15.9	29.1	T15-T16
18	oval *larger*	horizontal	2.10-2.13	18.2	21.9	T19-T20
18	oval *larger*	vertical	1.10-2.48	15.2	32.7	T21-T22

Table 12 Comparison of peak angle of shearing resistance and critical angle of repose

material and packing		porosity (%)	ϕ'_p (*degrees*)	porosity (%)	α_c (*degrees*)
ϕ5mm	regular	12.6	30.4	9.5	56.5
ϕ5mm:ϕ9mm=10:1	random	15.3	28.4	13.7	29.1
ϕ5mm:ϕ9mm=3:2	*ditto*	20.1	33.8	21.2	26.6
ϕ5mm:ϕ9mm=5:5	*ditto*	20.5	31.9	17.2	28.6
ϕ5mm:ϕ9mm=2:3	*ditto*	21.1	32.4		
ϕ5mm:ϕ9mm=1:10	*ditto*	20.4	36.5	14.3	27.4
ϕ9mm	regular	13.0	34.5	12.2	52.5
ellipsoidal *mixed*	vertical	14.2	41.6	12.2	25.3
oval *mixed*	vertical	16.4	36.0	18.8	25.9
ellipsoidal *mixed*	horizontal	14.2	31.9	11.2	27.4
oval *mixed*	horizontal	15.9	29.1	13.9	29.3
oval *larger*	horizontal	18.2	21.9	17.0	27.8
oval *larger*	vertical	15.2	32.7	7.9	24.2

Table 13 Parameters used for the GSM calculation.

	Sliding friction	Rolling friction
ϕ5mm	19.8°	2.21°
ϕ9mm	19.8°	1.37°
ϕ25mm	19.8°	0.92°
ϕ45mm	19.8°	0.50°

Table 14 Comparison between the results obtained from the tilting-box experiments and the GSM calculation (35-particle experiment)

Run NO.	GSM calculation *rolling**	*sliding**	experimental result*	number of moving particles at avalanche	Comments
20	23.5	30.5	23.7	17	
21	6.5	11.5	9.0	4	
22	5.5	5.5	9.9	8	
23	6.5	14.5	7.4	1	
24	11.5	19.5	10.5	1	
25	12.5	14.5	13.8	11	
27	13.5	20.5	14.7	9	
28	13.5	16.5	13.7	6	
29	4.5	8.5	7.4	3	
30	10.5	16.5	8.1	4	
32	24.5	30.5	20.9	9	
34	10.5	12.5	13.5	31	
35	9.5	9.5	5.1	3	Restriction of the GSM
36	1.5	5.5	8.0	7	
38	8.5	18.5	2.8	3	

*Unit: *degrees*

Table 15 Rolling friction and critical angle of repose on rods

Shape and packing		ρ (*degrees*) *individual*	α_c (*degrees*) *uniform*	α_c (*degrees*) *mixed*
Oval	*vertical*	$\simeq$ 0	24.3	25.9
	horizontal	26.6	48.0	29.3
Ellipsoidal	*vertical*	$\simeq$ 0	24.2	25.3
	horizontal	26.7	43.3	27.4

Table 16 Experimental results using the three-dimensional materials

Materials	rolling friction ρ (*degrees*)	C^* (%)	$\rho \cdot C$	α_c (*degrees*)	ϕ'_p (*degrees*)	C^* (%)
Grass ballotini	6.22	58.5	3.64	27.4	35.5	57.8
Beach shingle	22.7	57.4	13.0	37.2	44.5	60.5
		63.0	14.3	37.9		
Coarse sand	27.8	50.0	13.9	37.0	36.9	58.7
		52.5	14.6	38.6		
Crushed stone #6	28.7	54.8	15.7	43.9	44.0	57.0
		60.4	17.3	46.2		
Crushed stone #7	29.4	51.1	15.0	42.9	38.2	60.0
		61.1	18.0	44.9		
Aluminum rods	1.87	73.8	1.38	25.7	33.8	79.9
ϕ5mm:ϕ9mm=3:2		78.8	1.47	26.6		

・ C^*: volume concentration (1 - porosity)

Table 17 Rolling friction and length of side of a polygon (l_s)

diameter (mm)	rolling friction ρ (*degrees*)	number of the sides	l_s (mm)
5	2.21	81.4	0.193
9	1.39	129.5	0.218
25	0.92	195.6	0.401
45	0.50	360	0.393

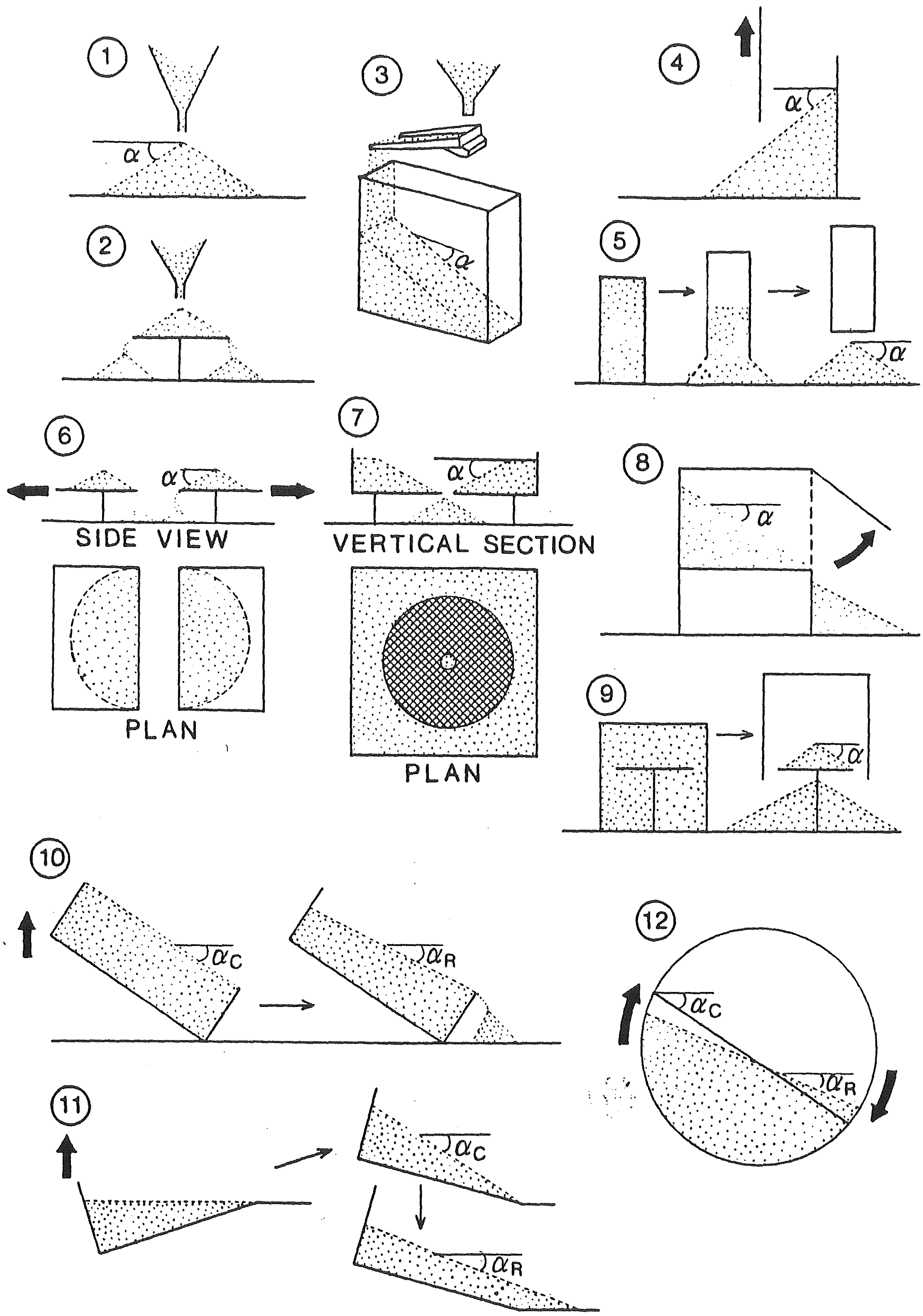

After Matsukura & Onda (1989)

Fig.1 Various methods of measurement for the angle of repose in granular materials

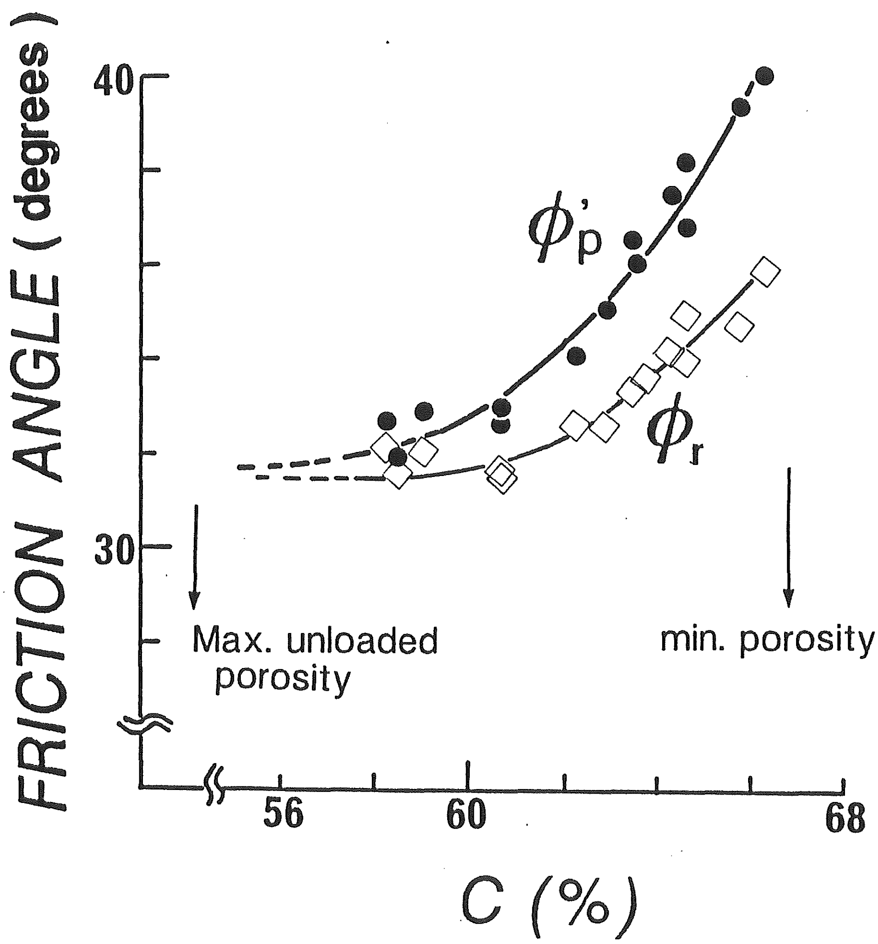

After Röwe (1962)

Fig.2 The relationship between volume concentration, *C*, and friction angles (after Röwe, 1962)

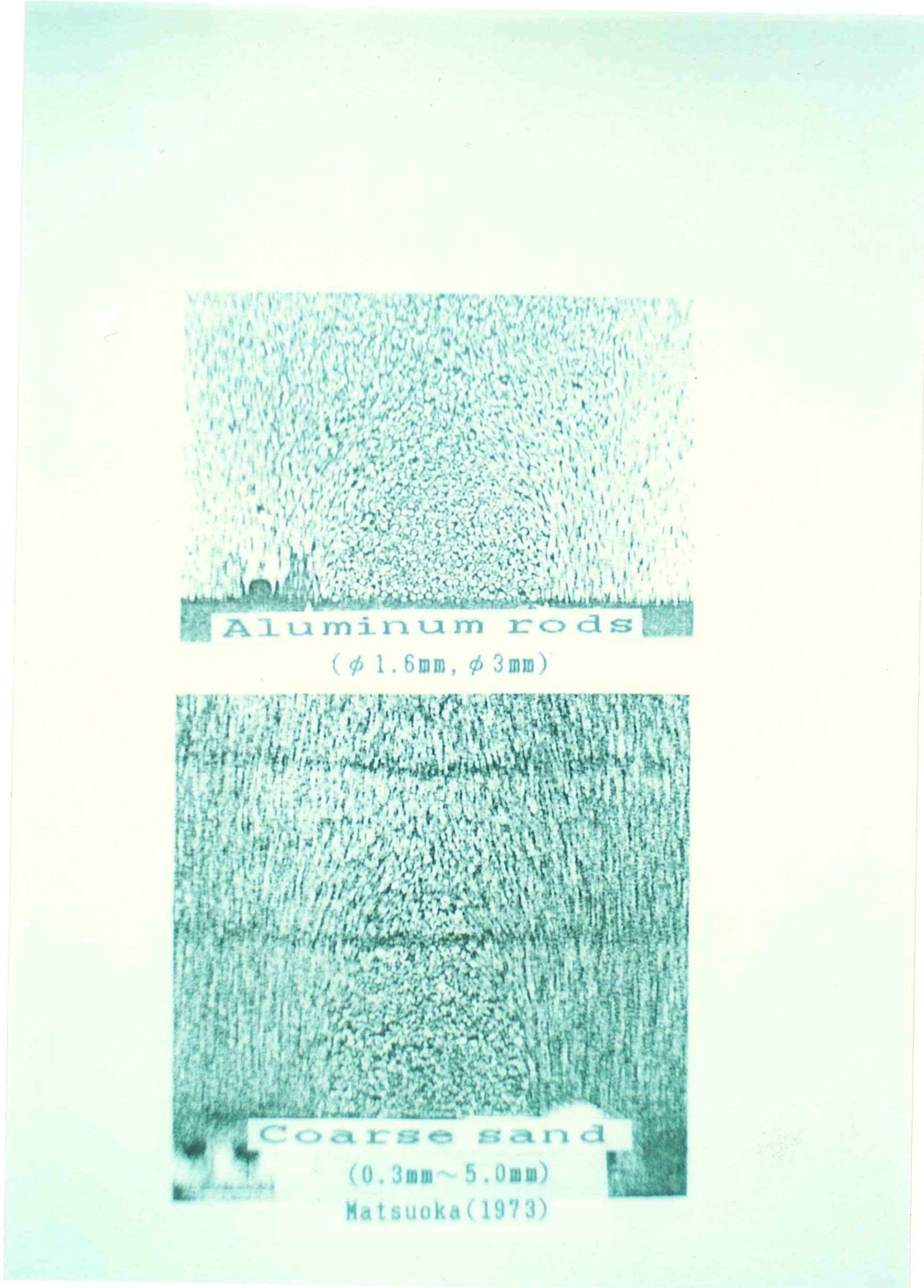

Fig.3 The behavior of aluminum rods and sand in the lowering floor experiment (after Matsuoka, 1973)

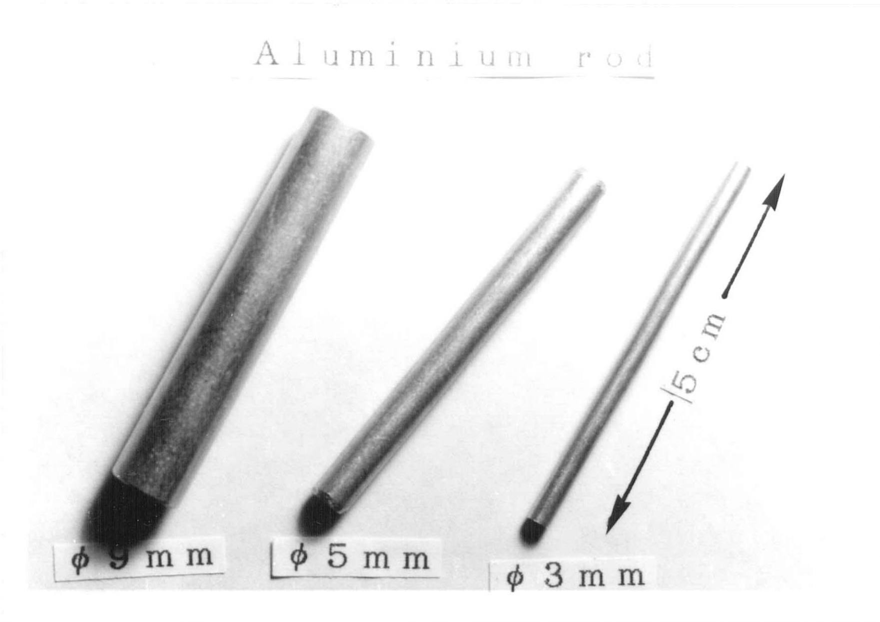

Fig.4 The cylindrical aluminum rods used for the experiment

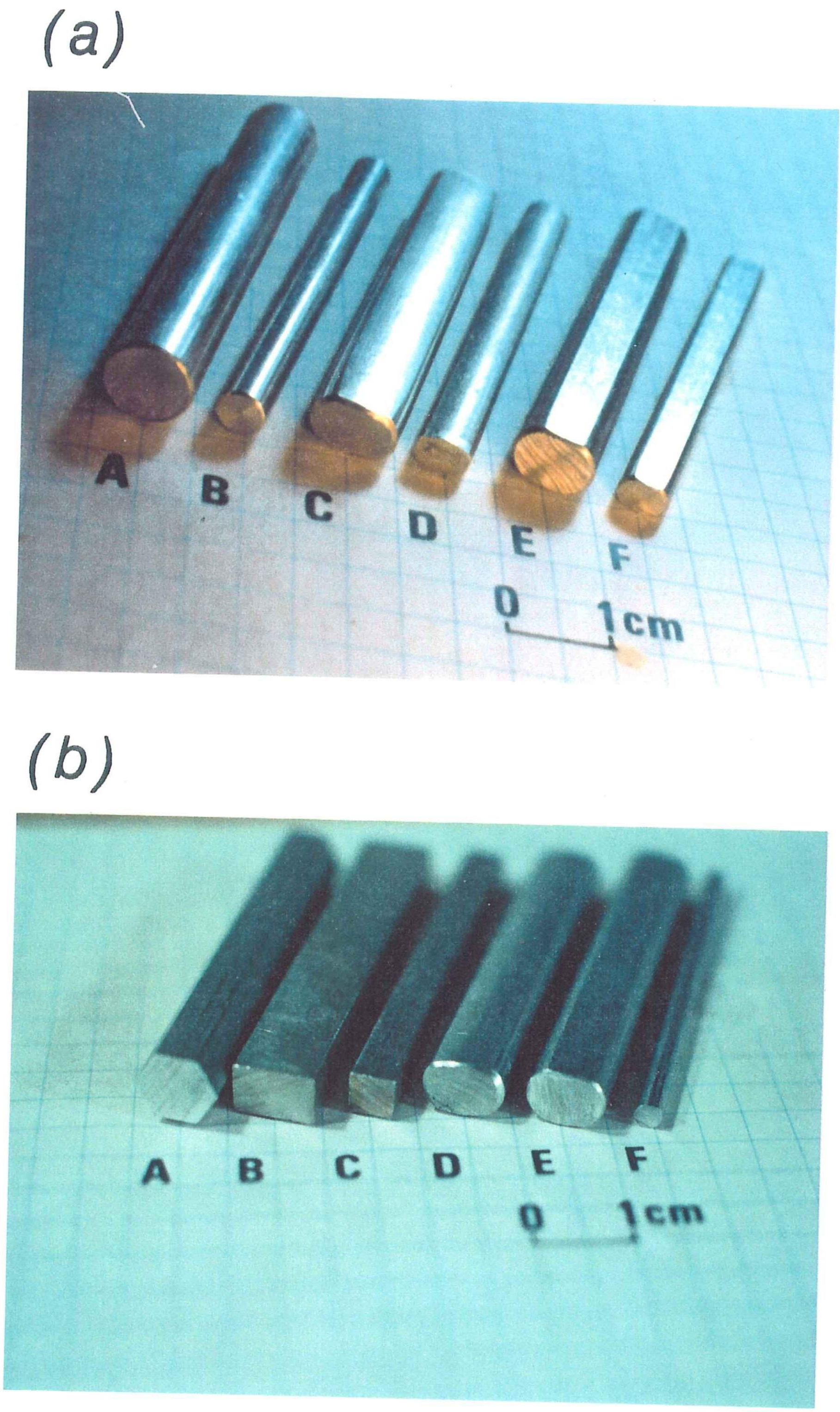

Fig.5 The cylindrical aluminum rods and ellipsoidal aluminum rods (a), and the square rods (b) used for the experiments

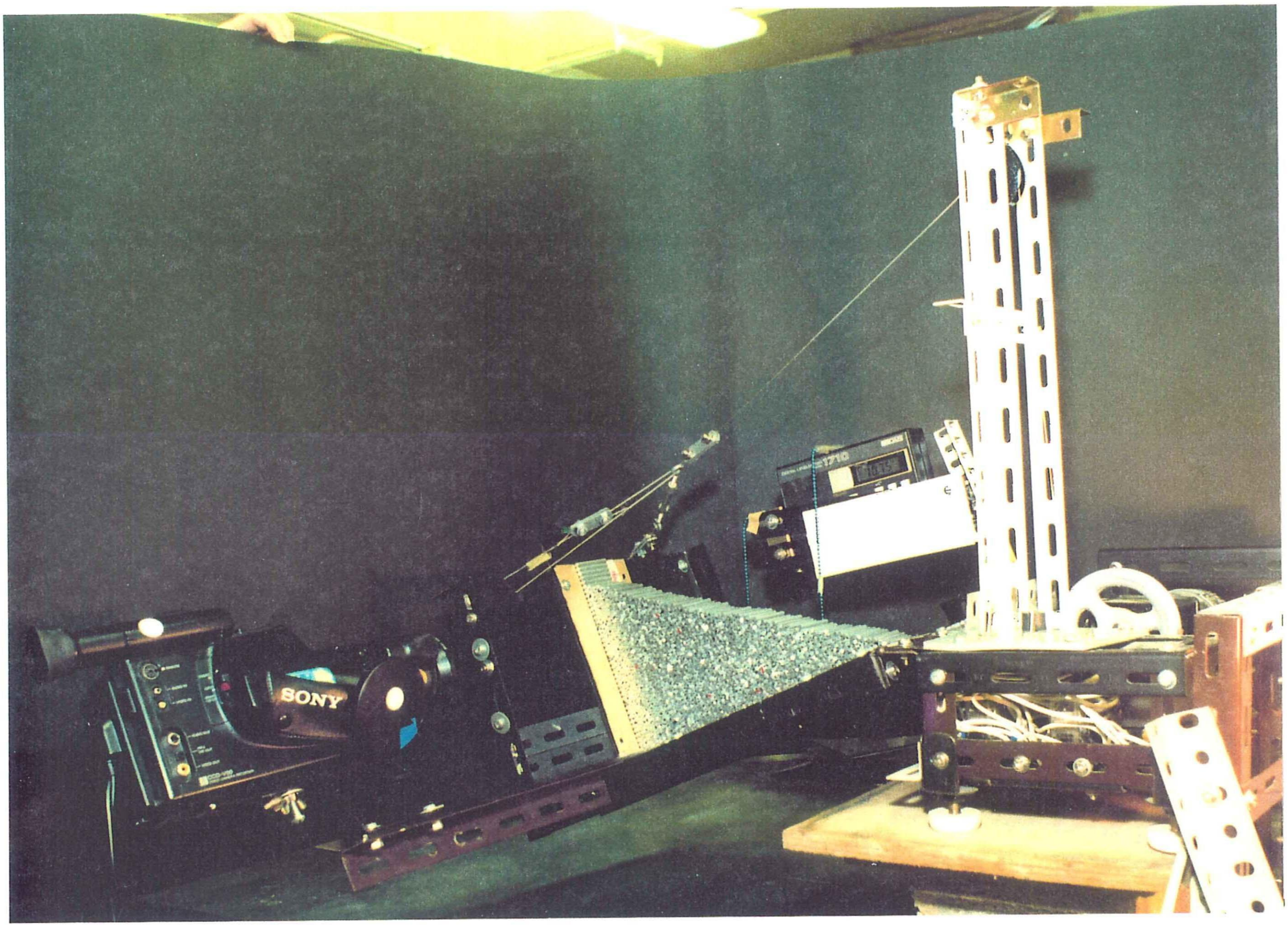

Fig.6 Tilting-box test apparatus

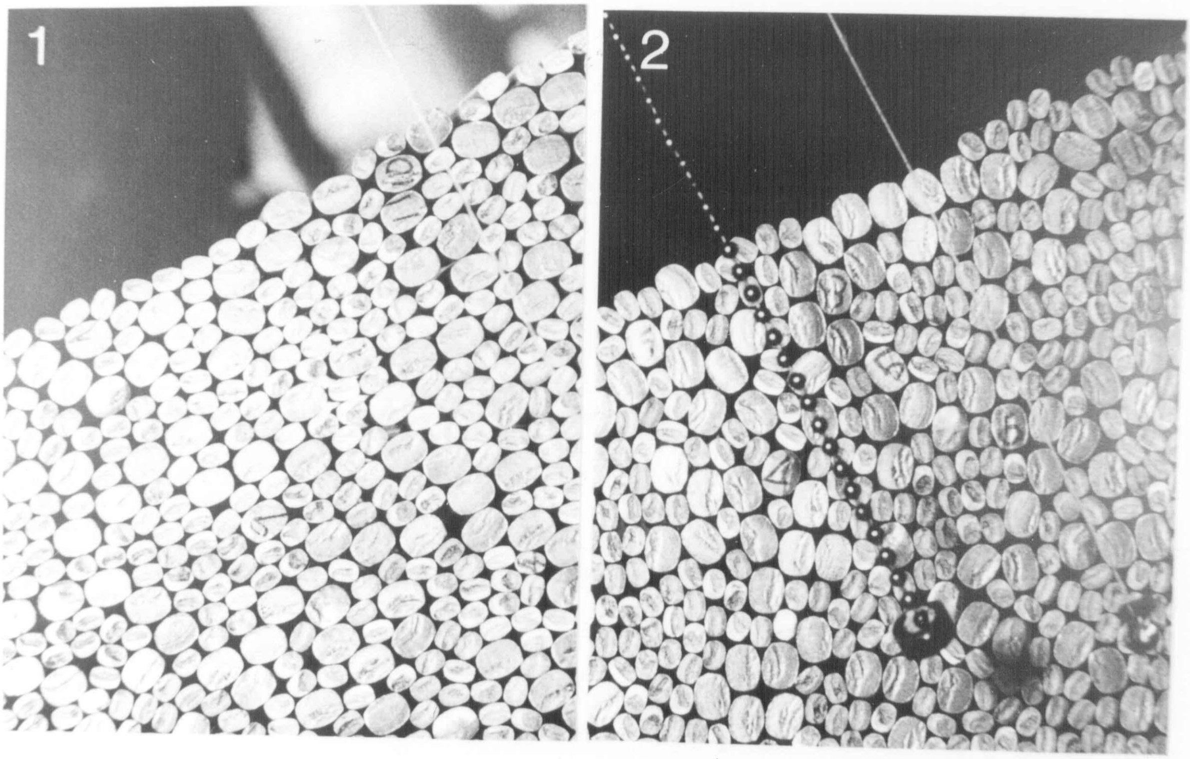

Fig.7 The horizontal packing (1) and the vertical packing (2) of mixed ellipsoidal aluminum rods

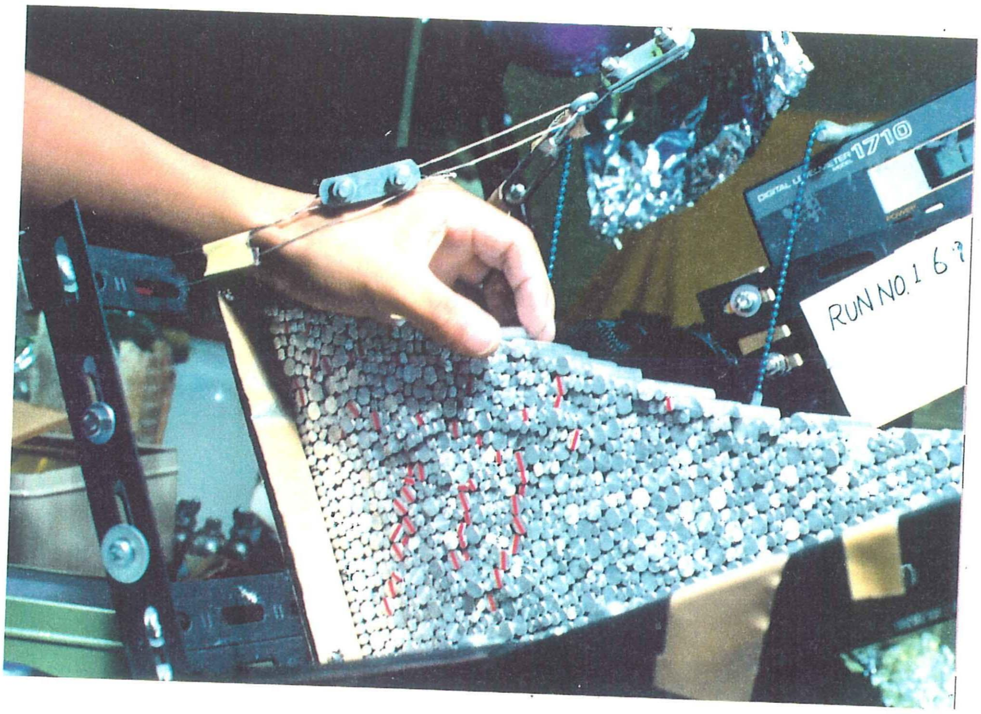

Fig.8 Technical method for making a horizontal packing

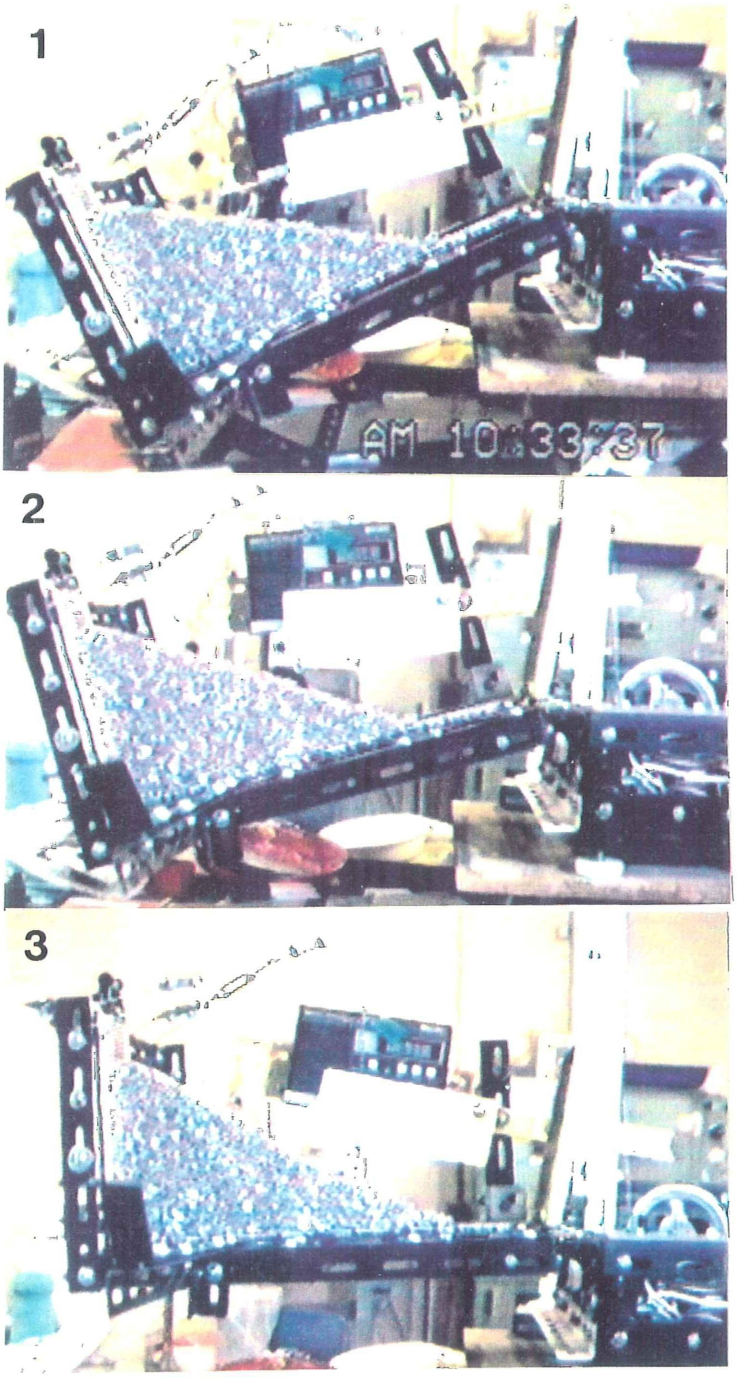

Fig.9 Procedure of the tilting-box experiment

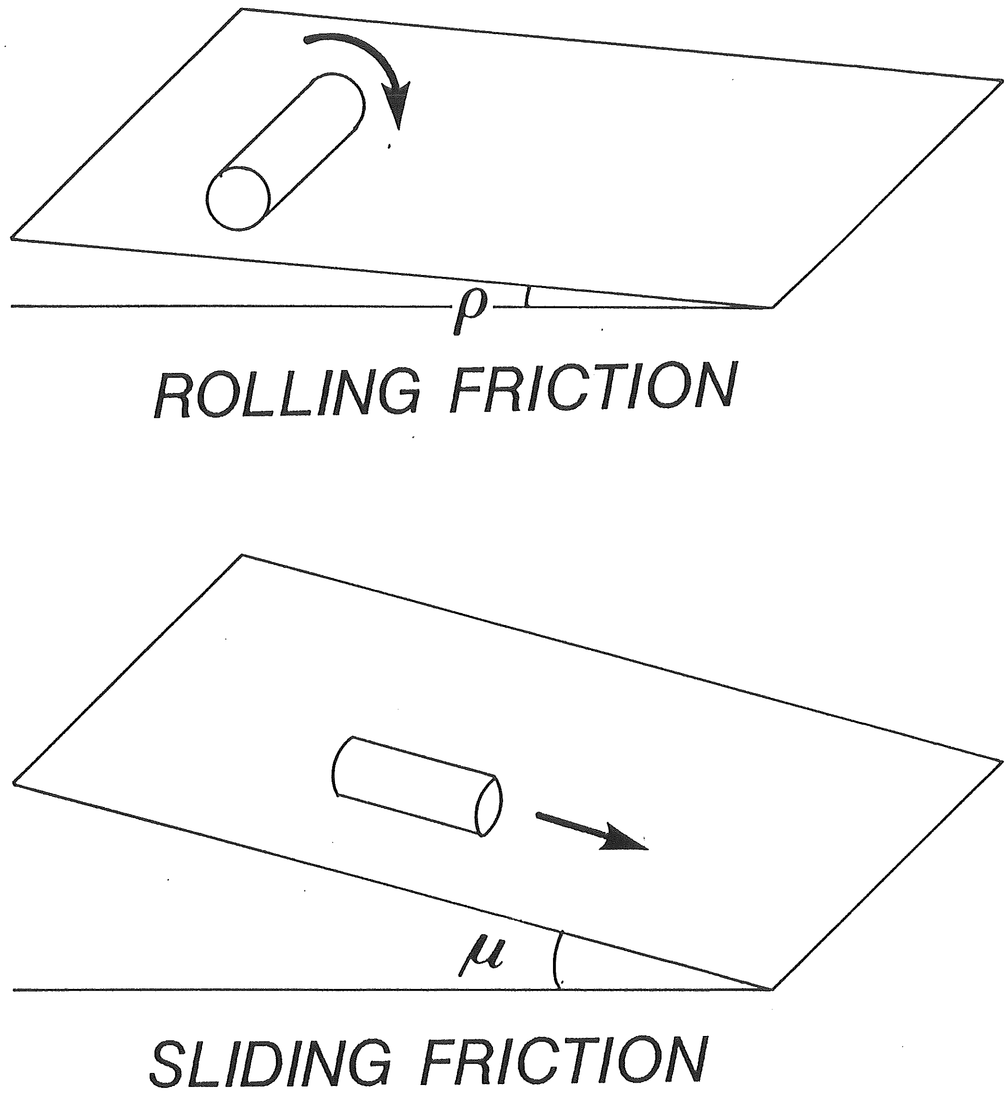

Fig.10 Measuring method for rolling friction and sliding friction

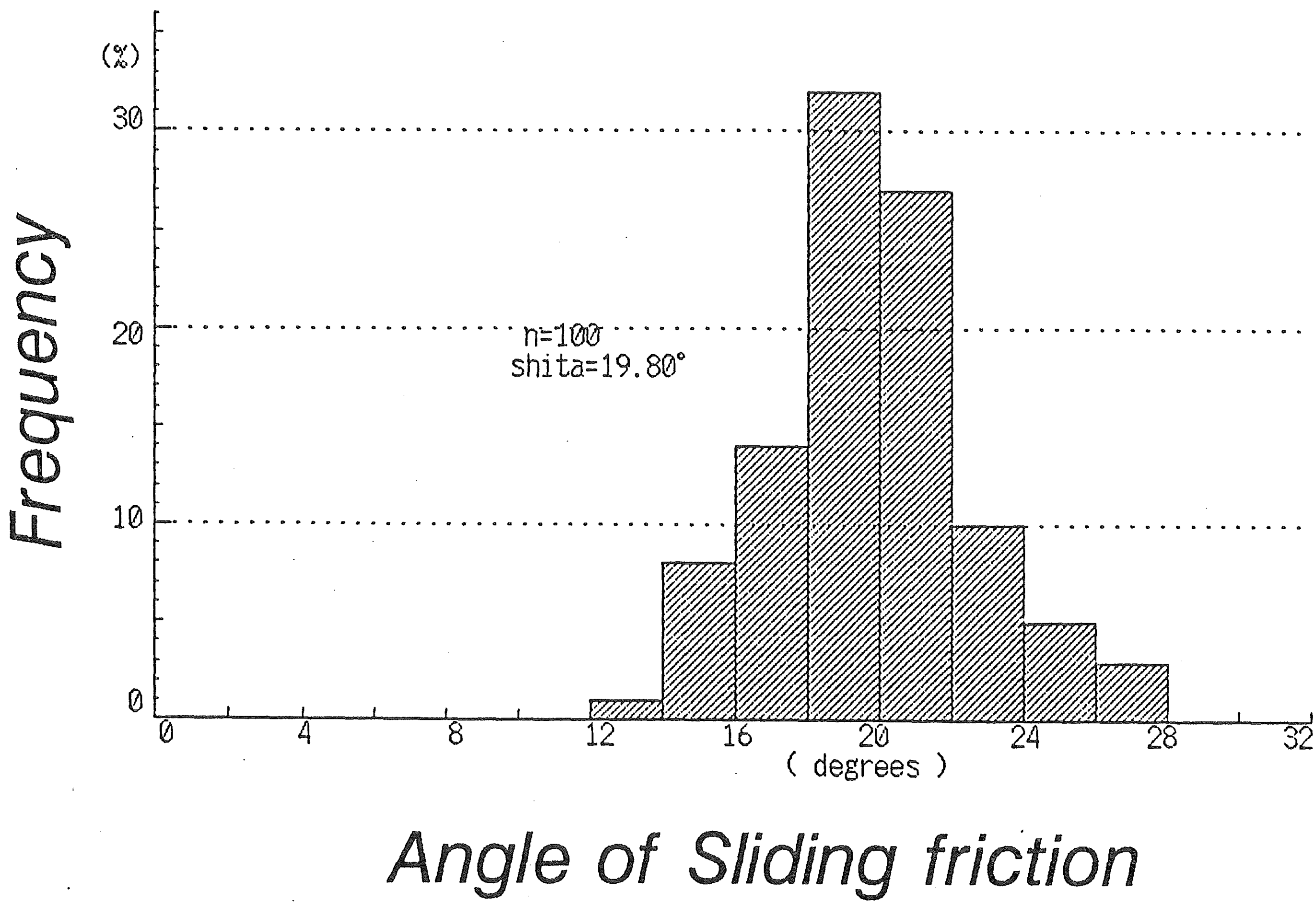

Fig.11 Histogram of the values for angle of sliding friction of 9-mm rods on aluminum plate

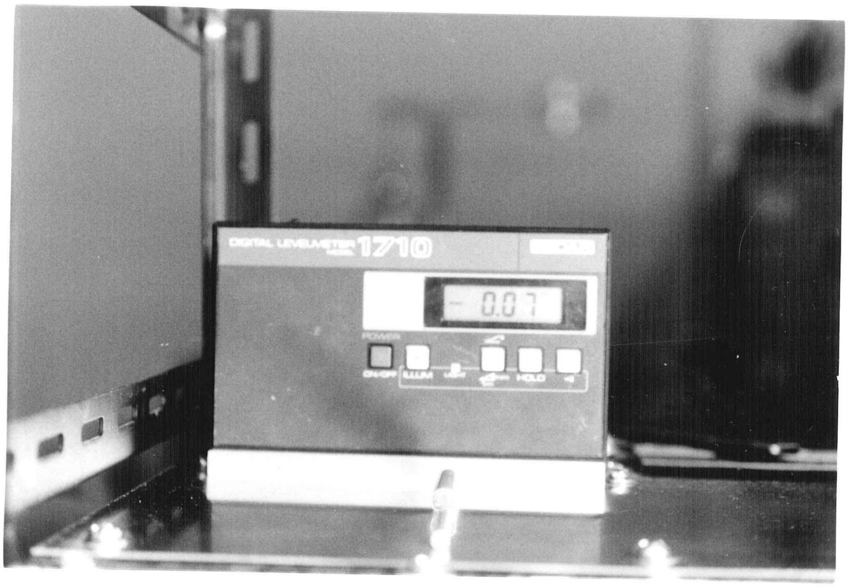

Fig.12 Measuring method for rolling friction

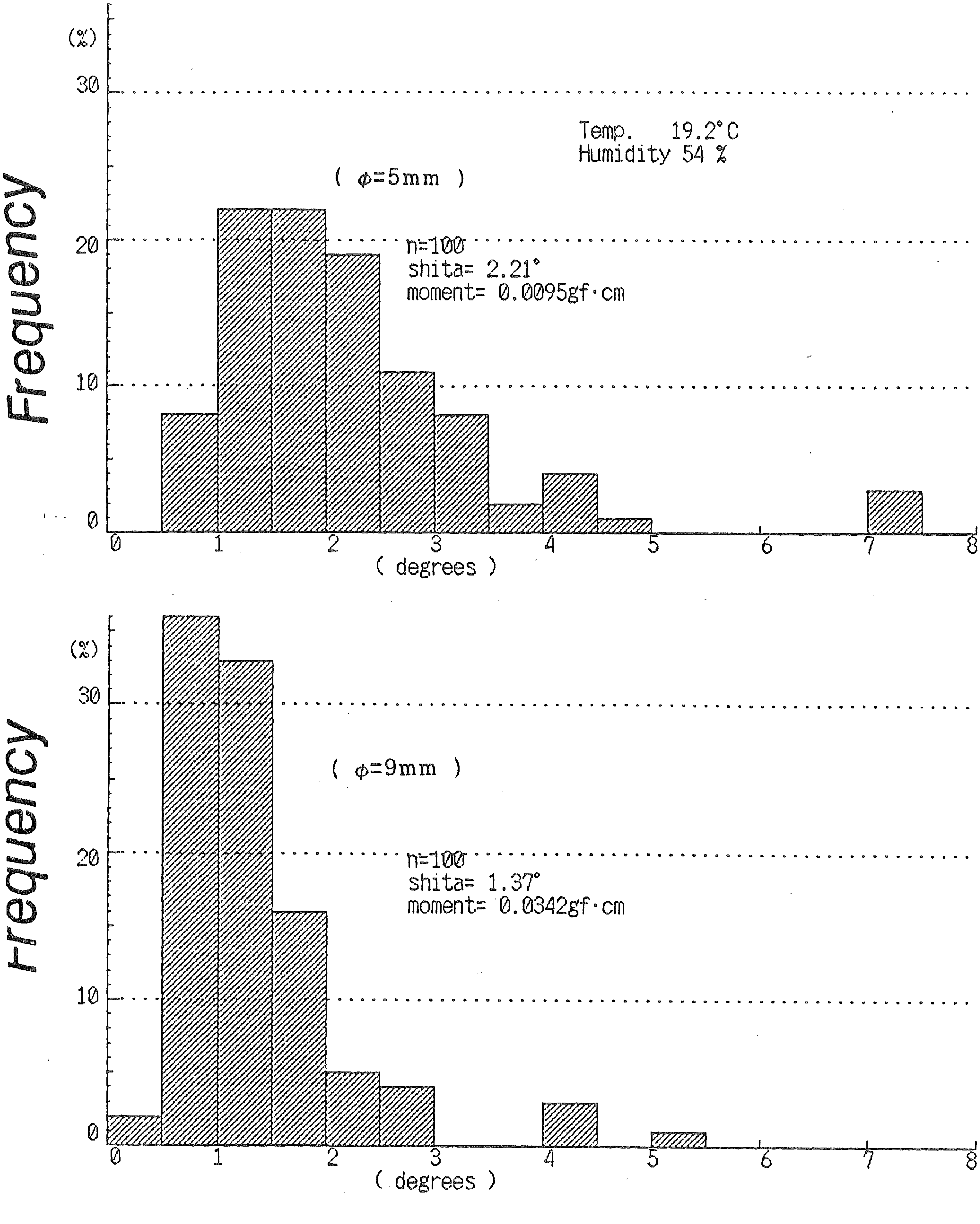

Fig.13 The result of the measurement for rolling friction of the aluminum rods (upper; ϕ = 5mm, lower; ϕ = 9mm)

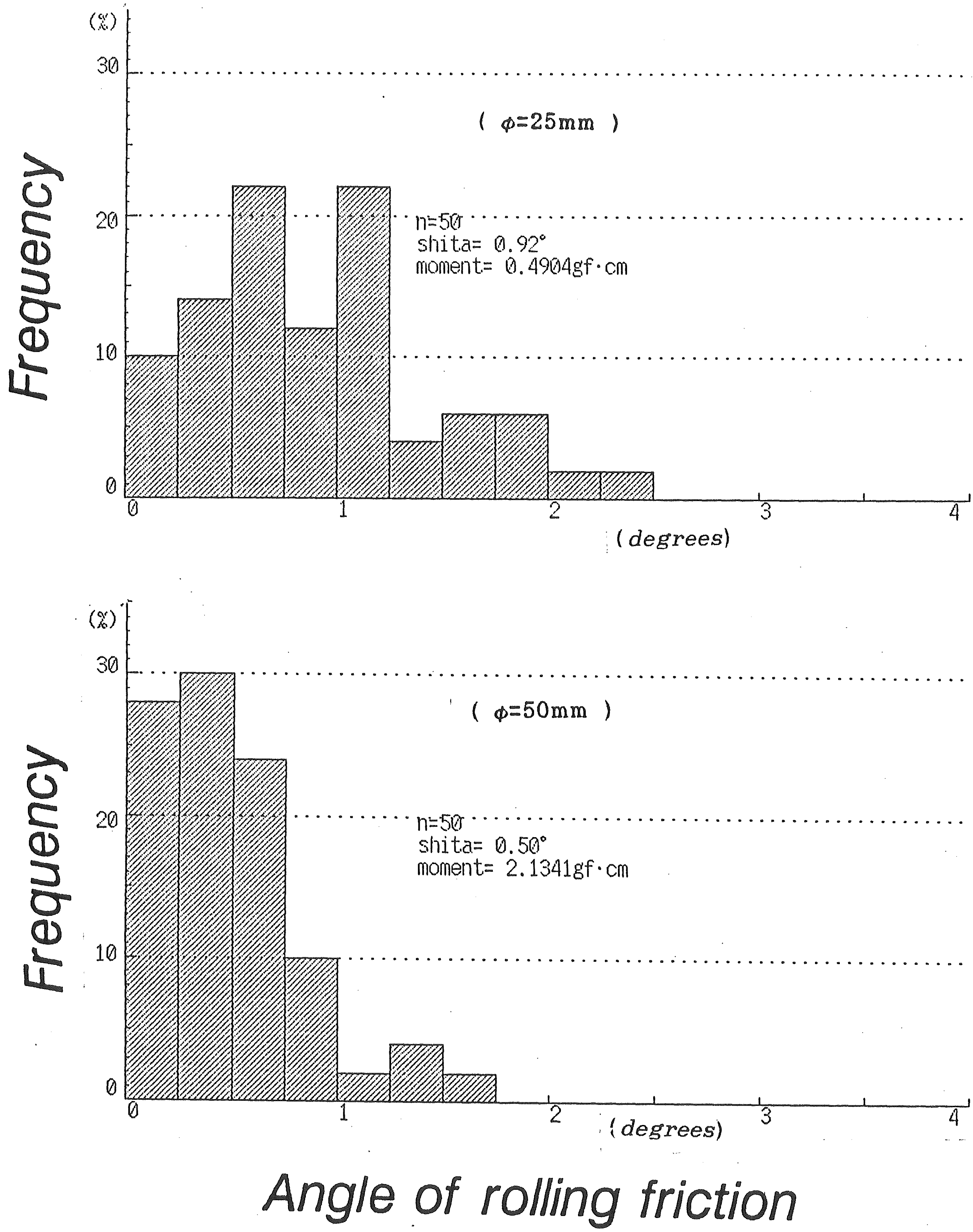

Fig.14 The result of the measurement for rolling friction of the aluminum rods (upper; ϕ = 25mm, lower; ϕ = 50mm)

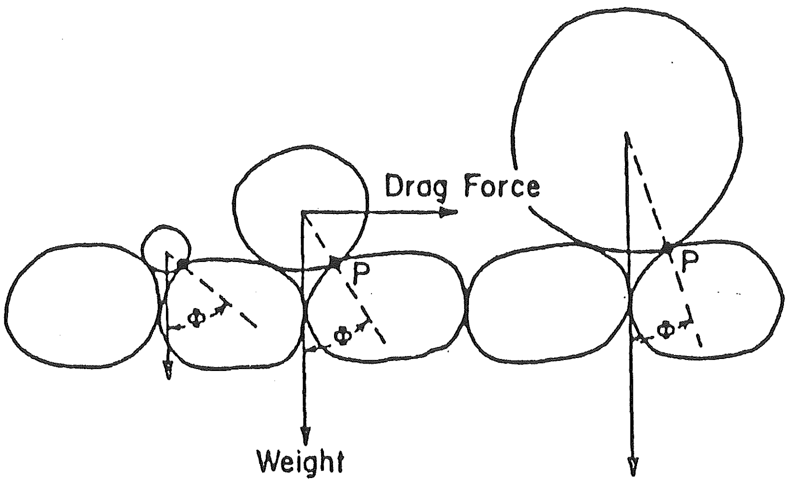

The pivoting angle Φ about the grain's contact point P, important to its entrainment by a flowing fluid. The size of Φ is seen to depend on the ratio of the diameter of the grain to be moved to that it rests upon.

Fig.15 The pivoting angle (Φ) defined by Li and Komar (1986)

(a)

(b)

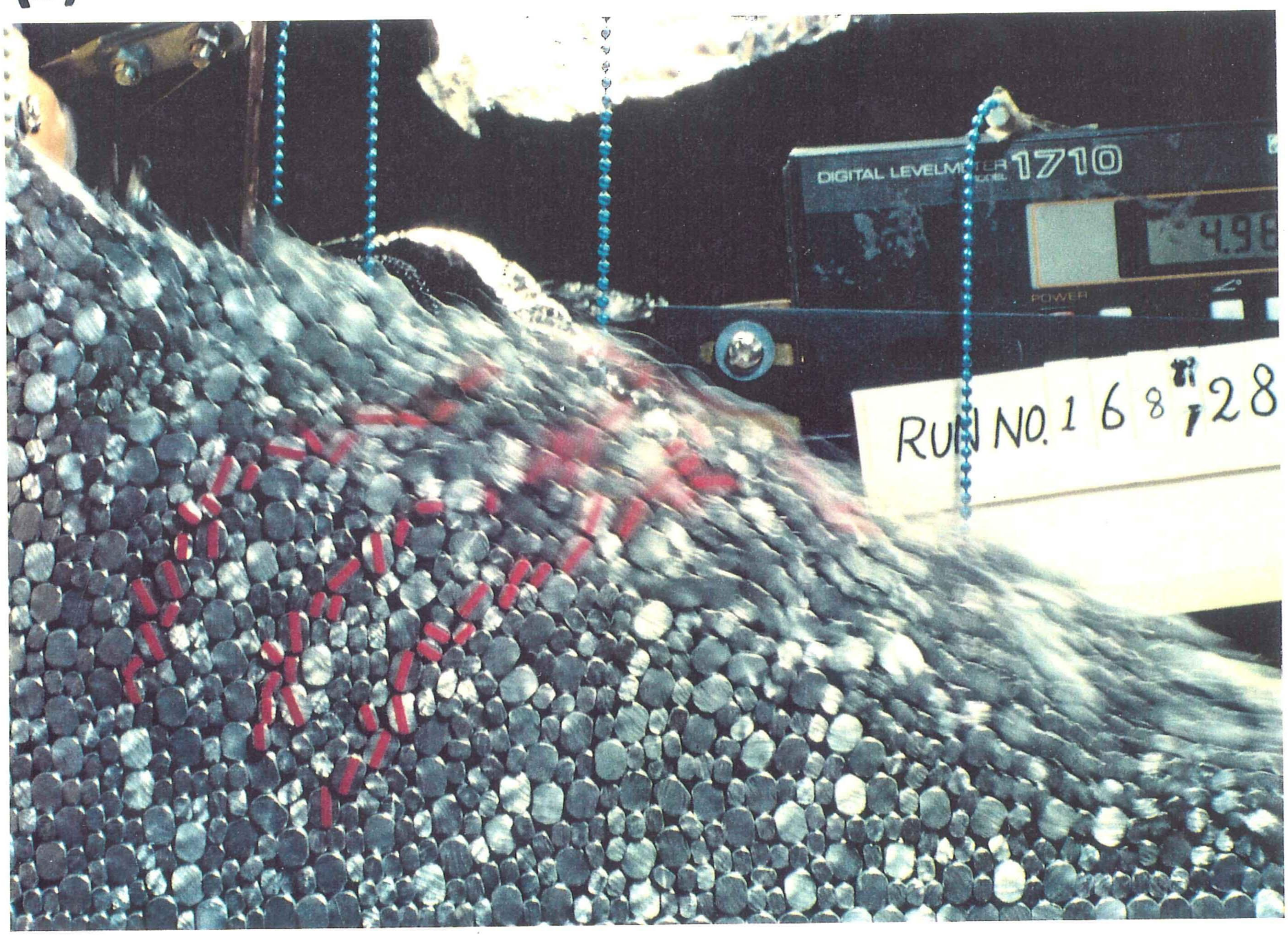

Fig.16 Nature of the avalanche of a mixture of oval rods with vertical packing (a; prior to avalanche and b; during avalanche)

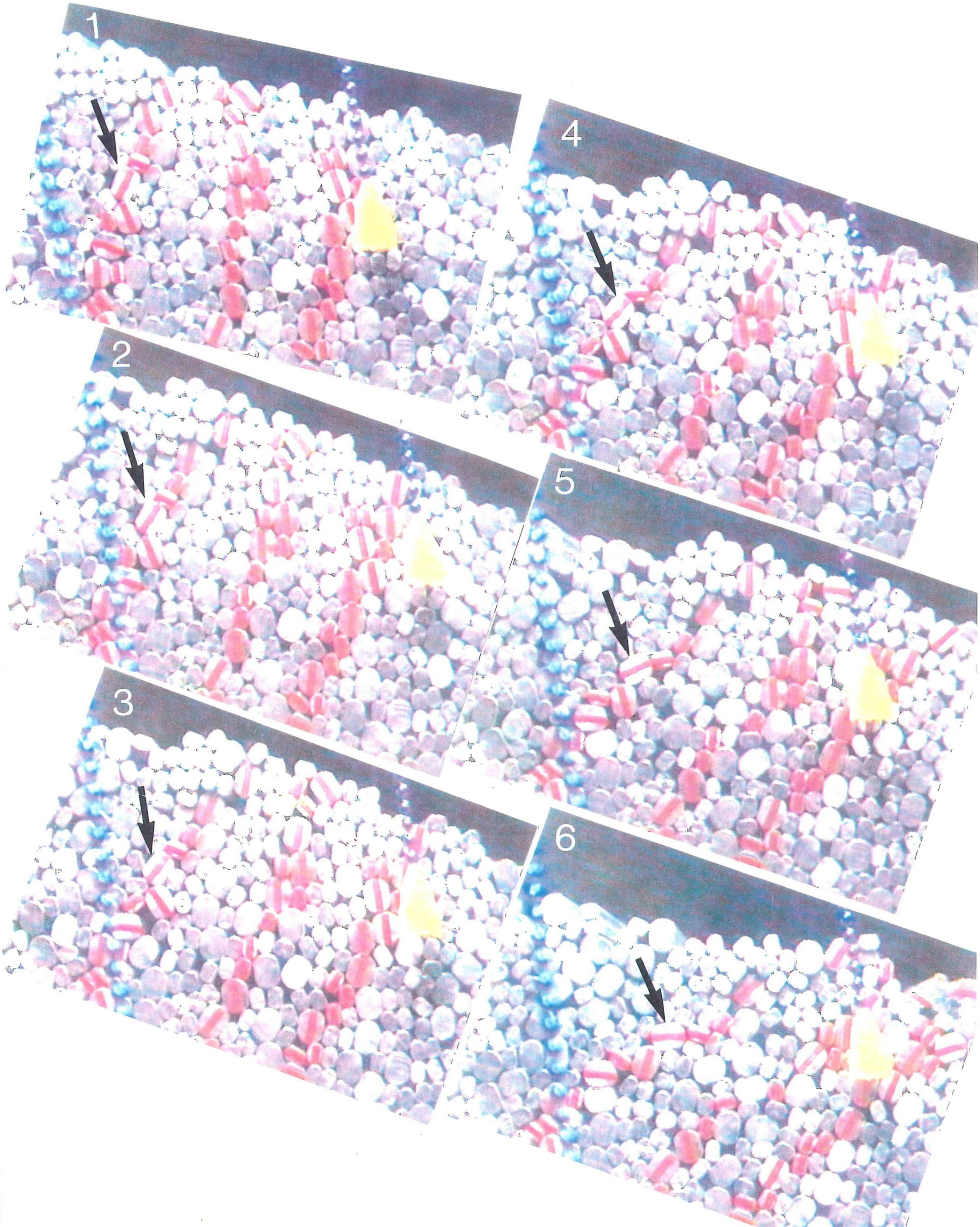

Fig.17 Sequential photos showing movements of the individual rod during the avalanche, which is the same one shown in Fig. 16

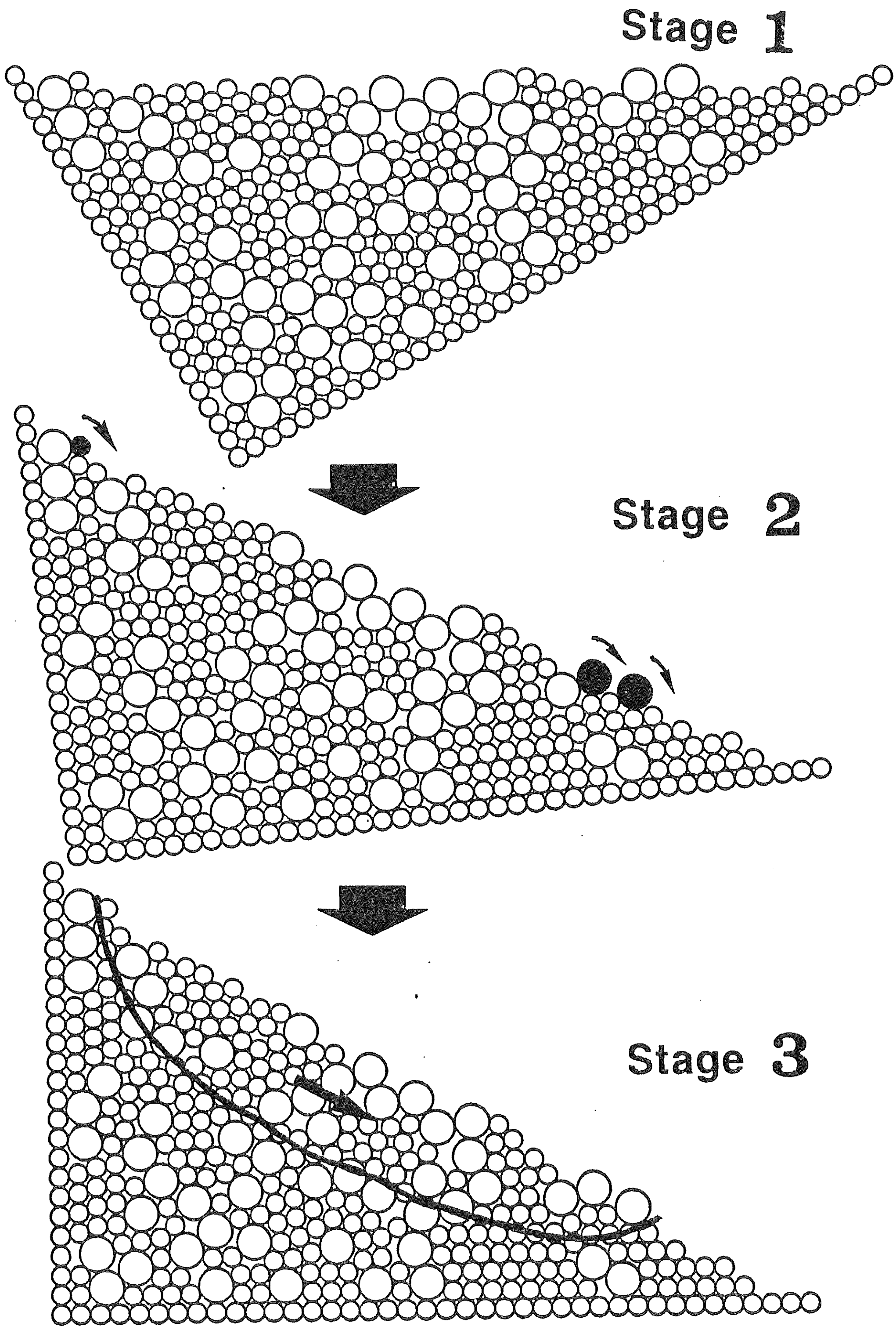

Fig.18 Schematic diagram of the commencement of the avalanche

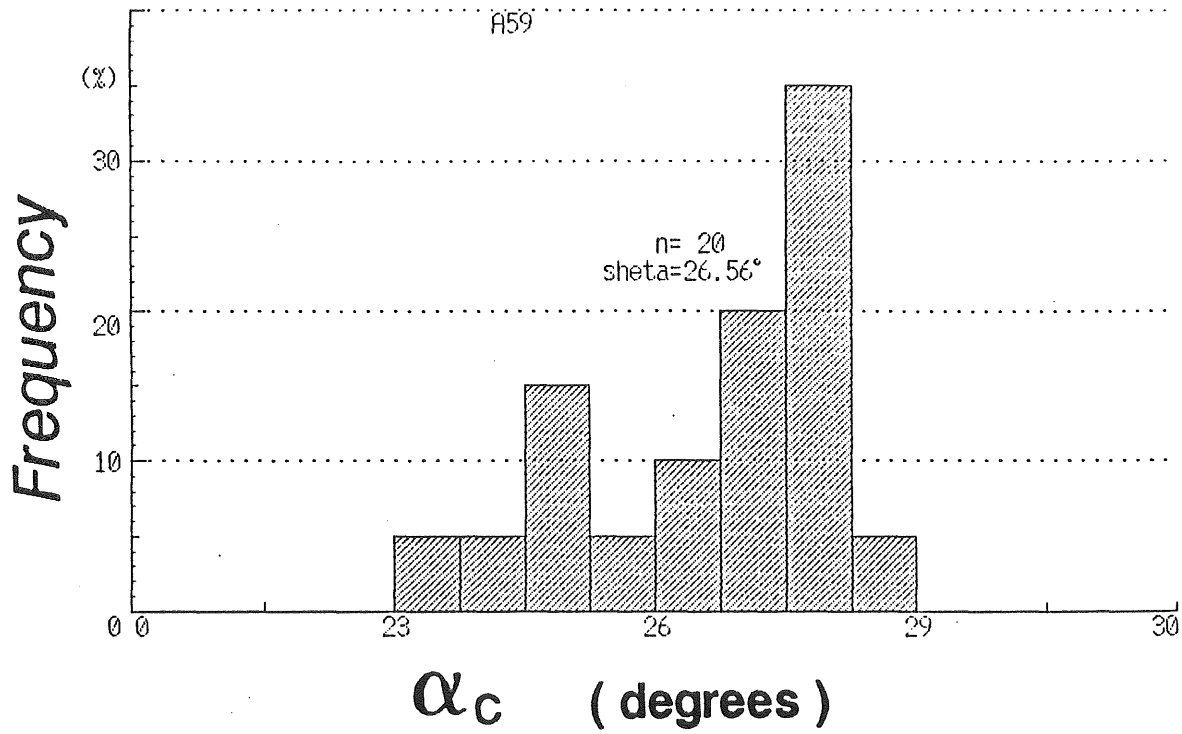

Fig.19 Frequency distribution of critical angle of repose, α_c, for 20 cases

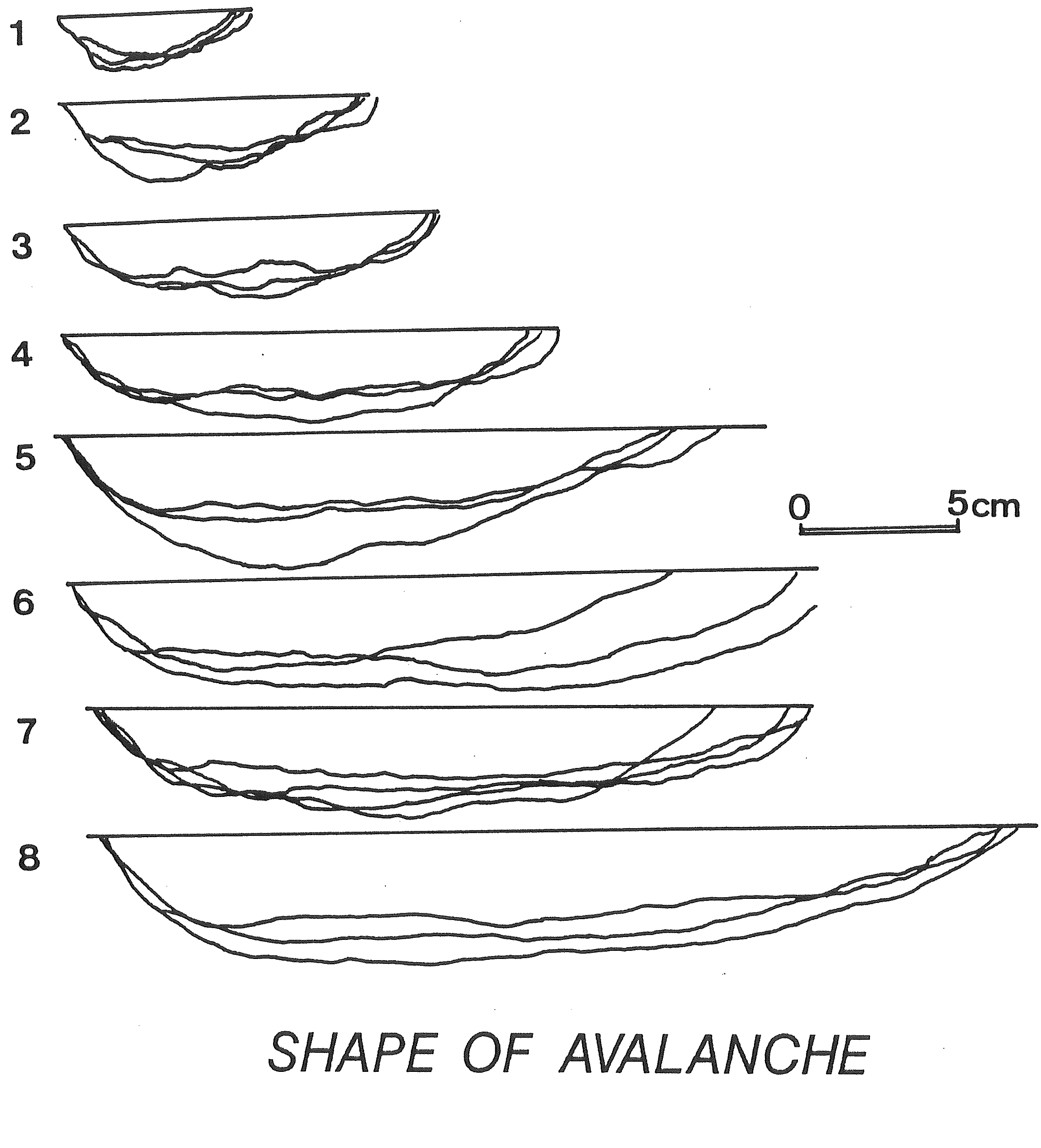

Fig.20 The longitudinal profile of the avalanche occurred on the slope with various lengths

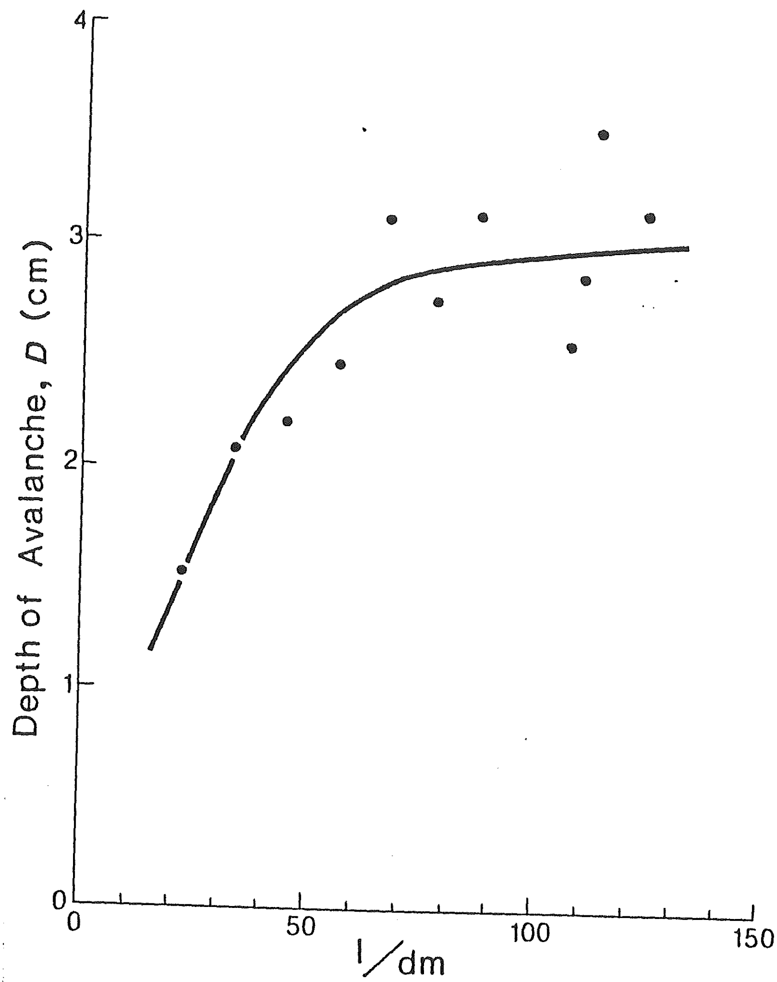

Fig.21 The relationship between l/d_m and the depth of the avalanche, D

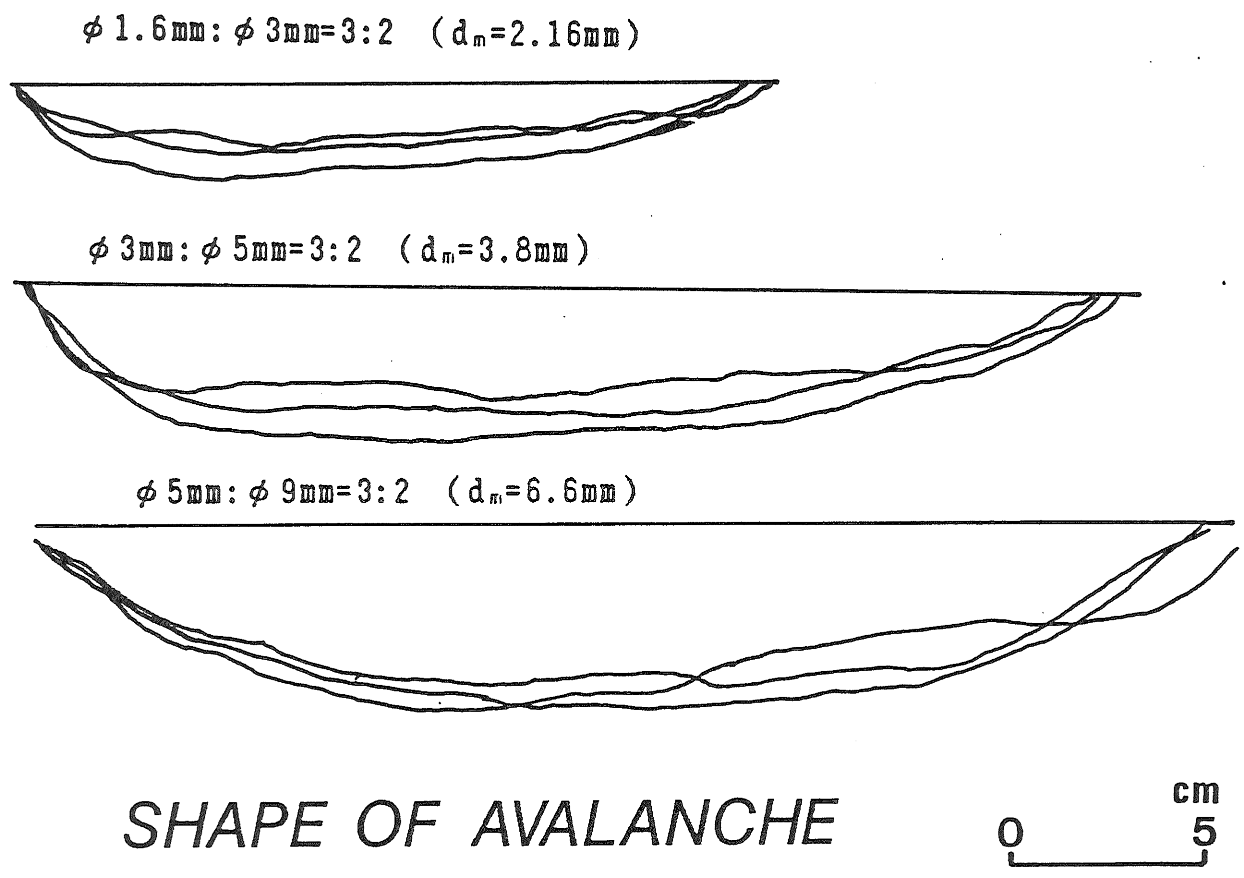

Fig.22 The longitudinal profile of the avalanche occurred on the mixed rods

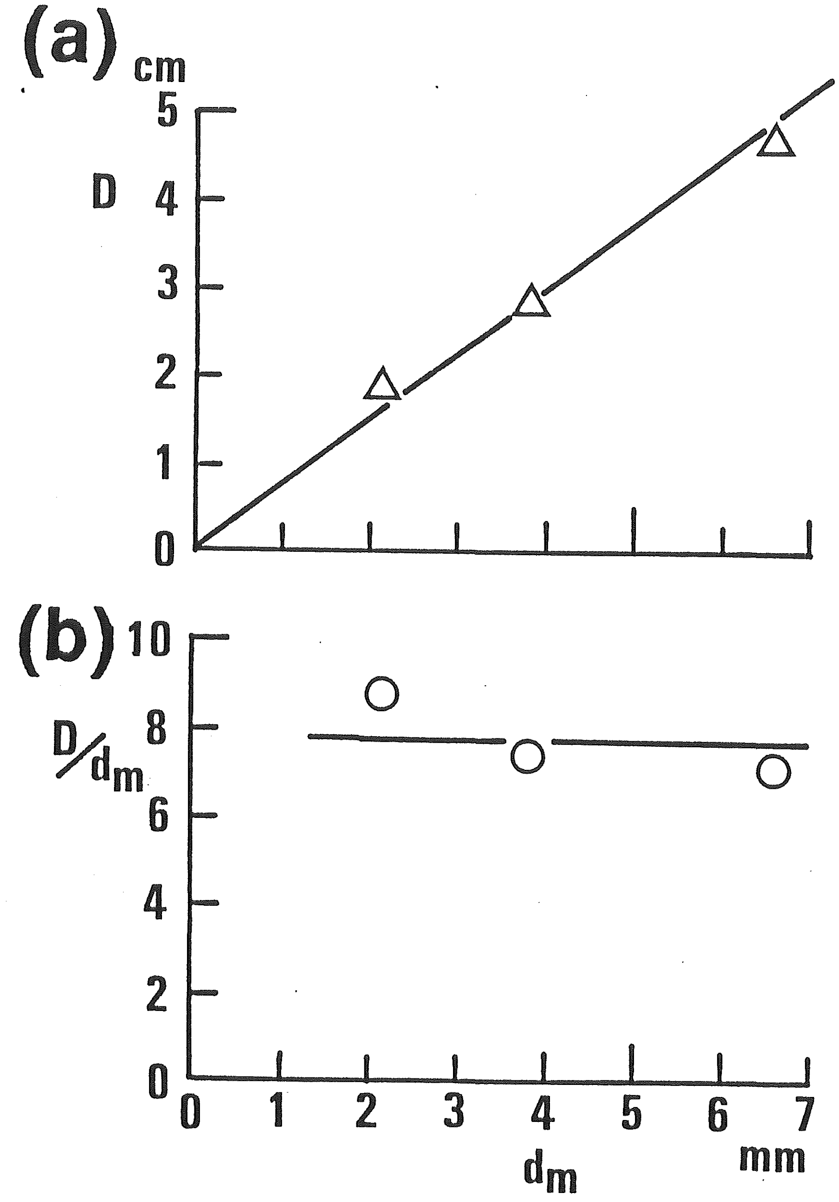

Fig.23 The relationship between mean diameter of rods, d_m , and the ratio of the depth of avalanches to mean diameter of rods, D/d_m

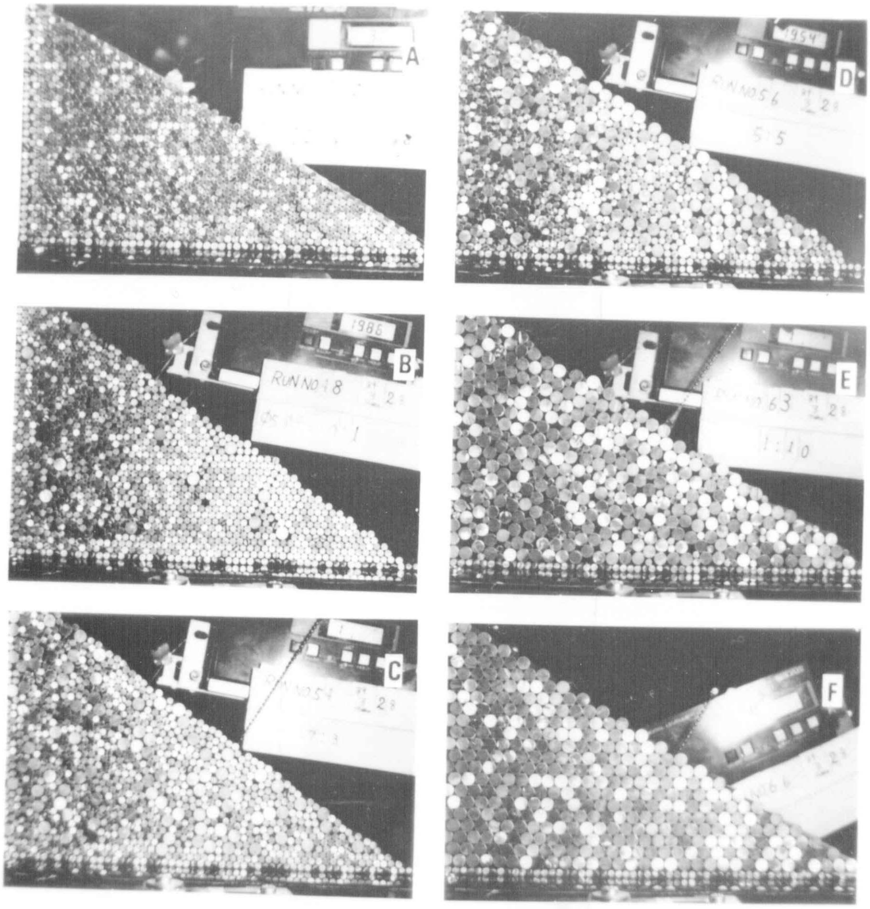

Fig.24 Difference in porosity due to the variance on mixture ratio. The test was conducted by changing the mixture ratio of 5-mm-diameter rods and 9-mm-diameter rods as 1 : 0 (A; uniform rods), 20 : 1, 10 : 1 (B), 8 : 2, 7 : 3 (C), 5 : 5 (D), 3 : 7, 2 : 8, 1:10 (Fig. 24E), and 0 : 1 (F; uniform rods)

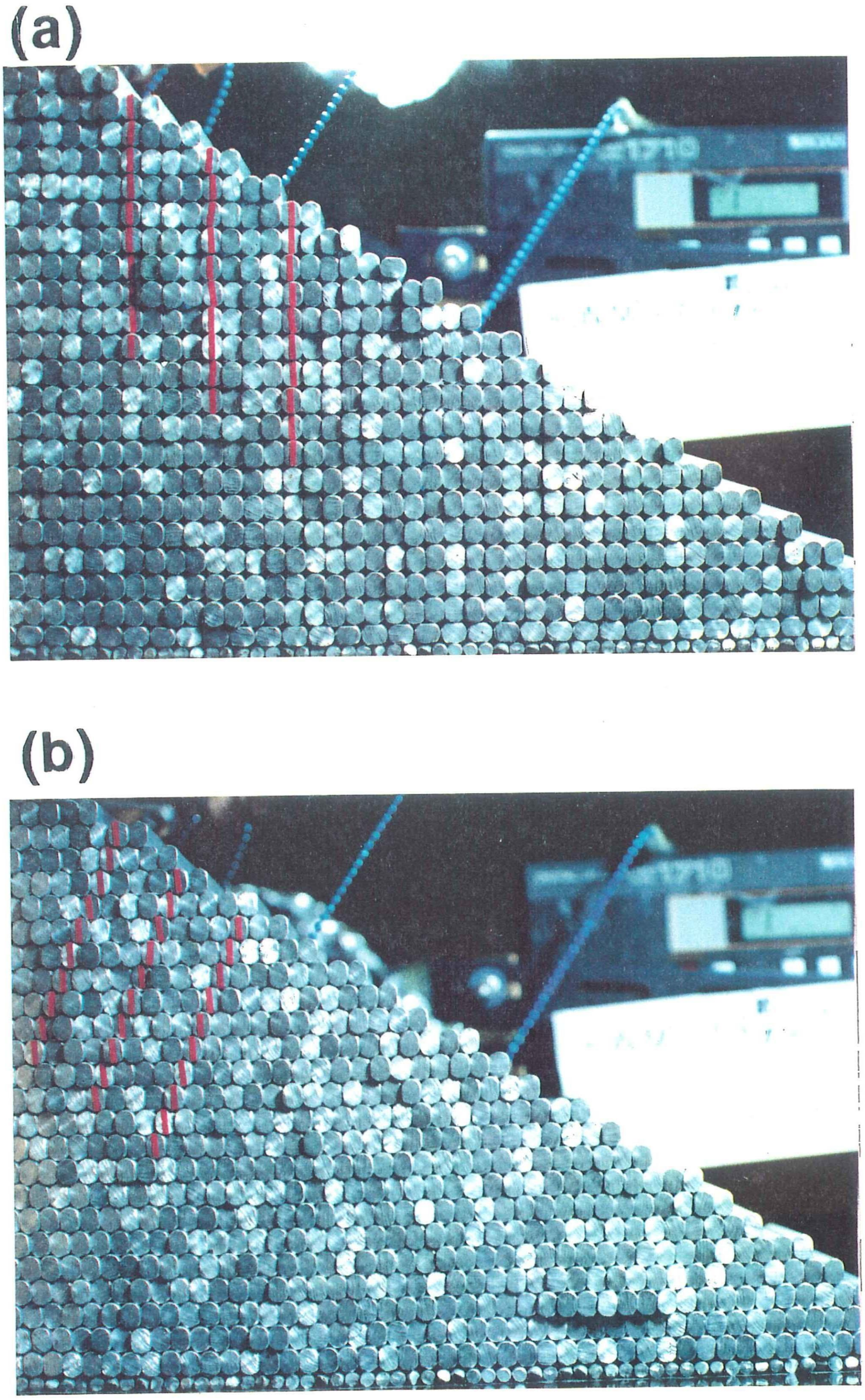

Fig.25 Two types of the vertical packing of the large oval rods with uniform diameter (a; open packing and b; dense packing)

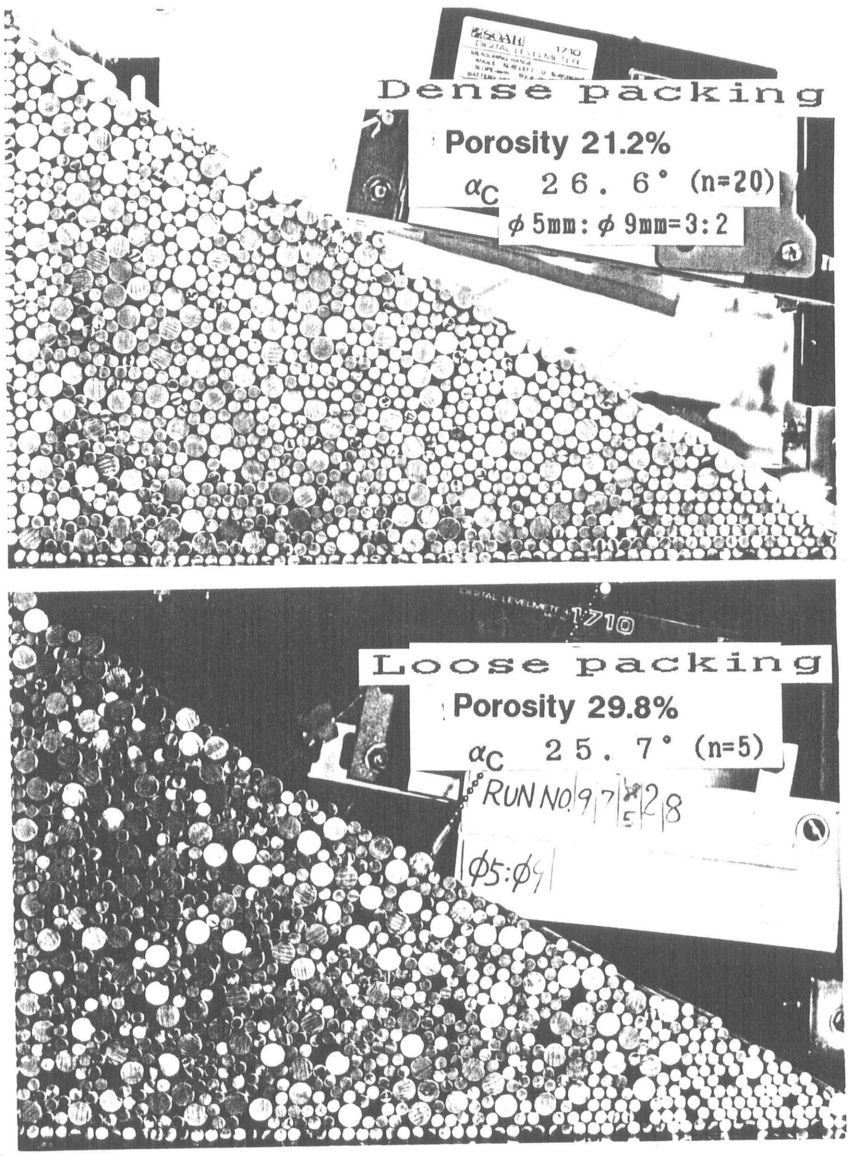

Fig.26 The effect of the porosity on critical angle of repose (upper; porosity = 21.2% and lower; porosity = 29.8%)

(a)

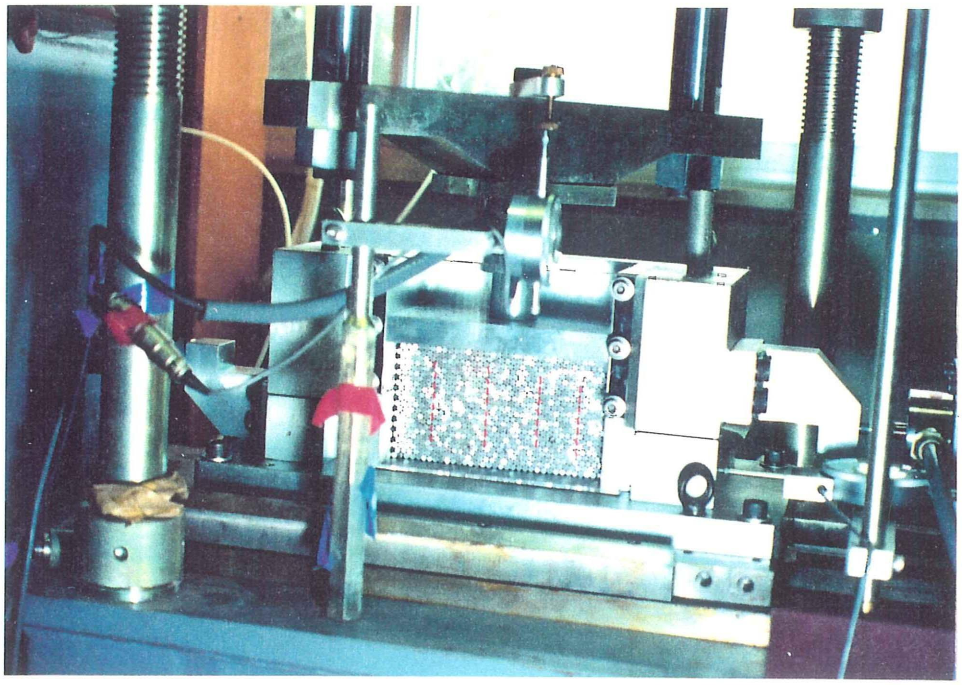

(b)

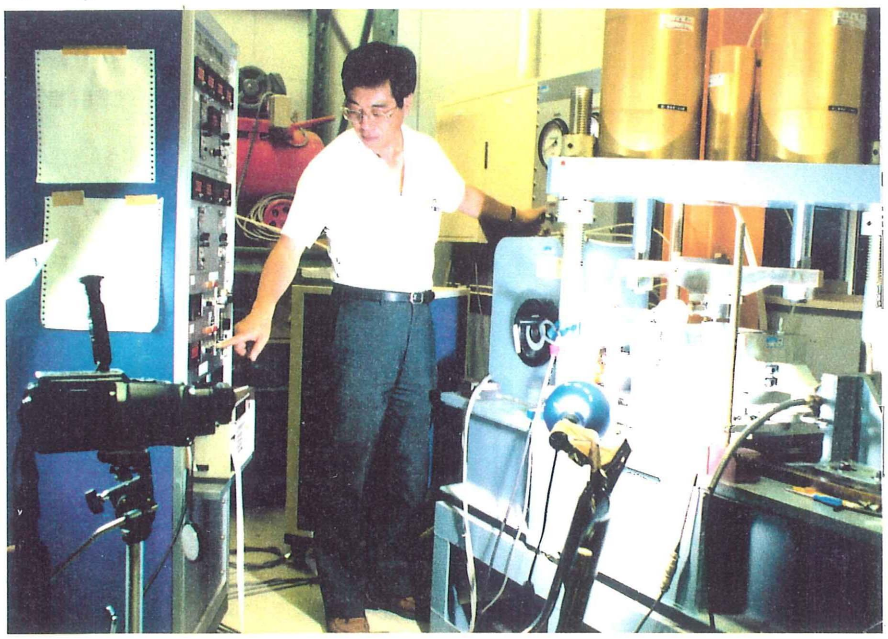

Fig.27 The shear box (a) and experimental system (b) of the direct shear test apparatus (18cm-type)

(a)

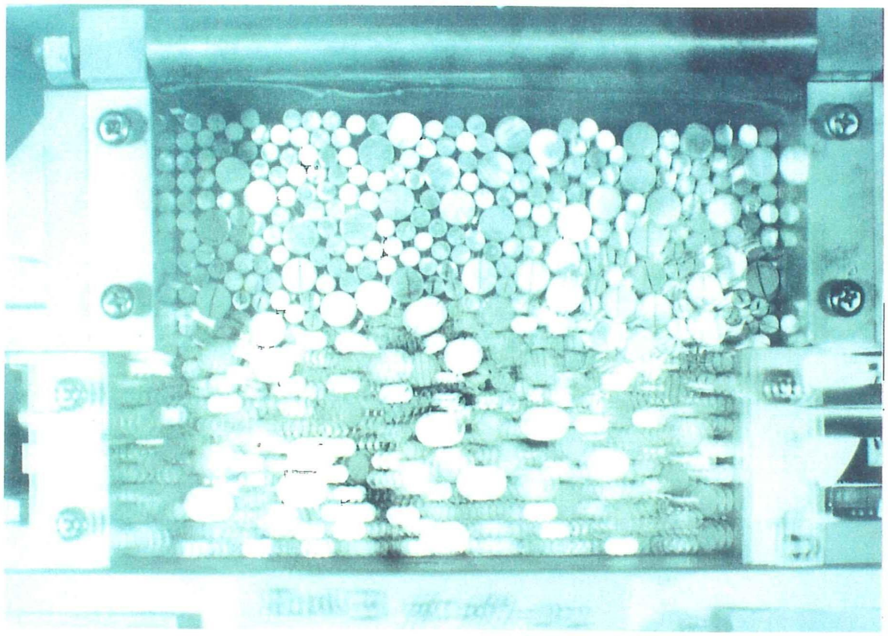

(b)

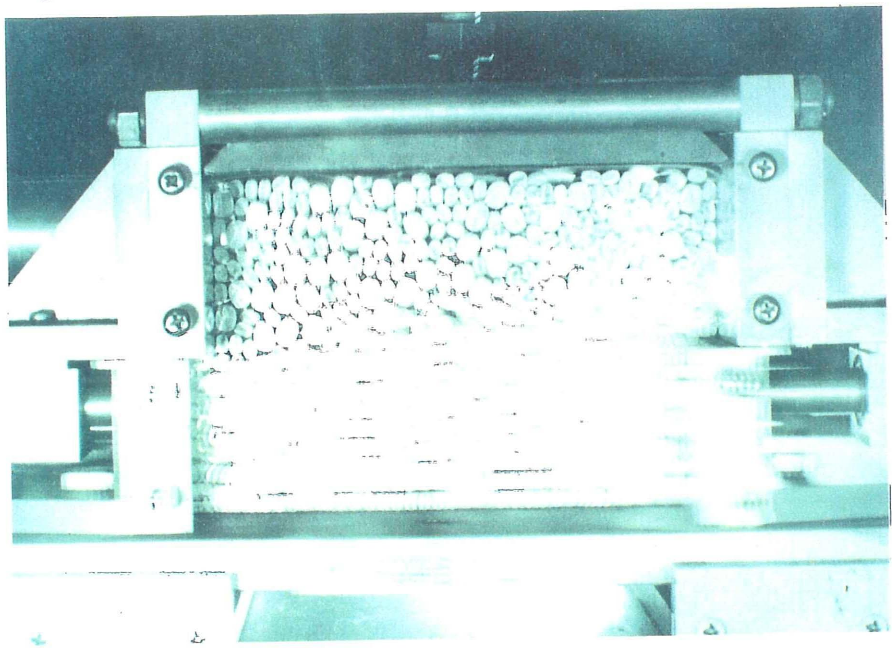

Fig.28 The nature of shearing for (a) mixed cylindrical rods (ϕ5mm : ϕ9mm = 3 : 2) during shearing (b) and mixed ellipsoidal rods

(a)

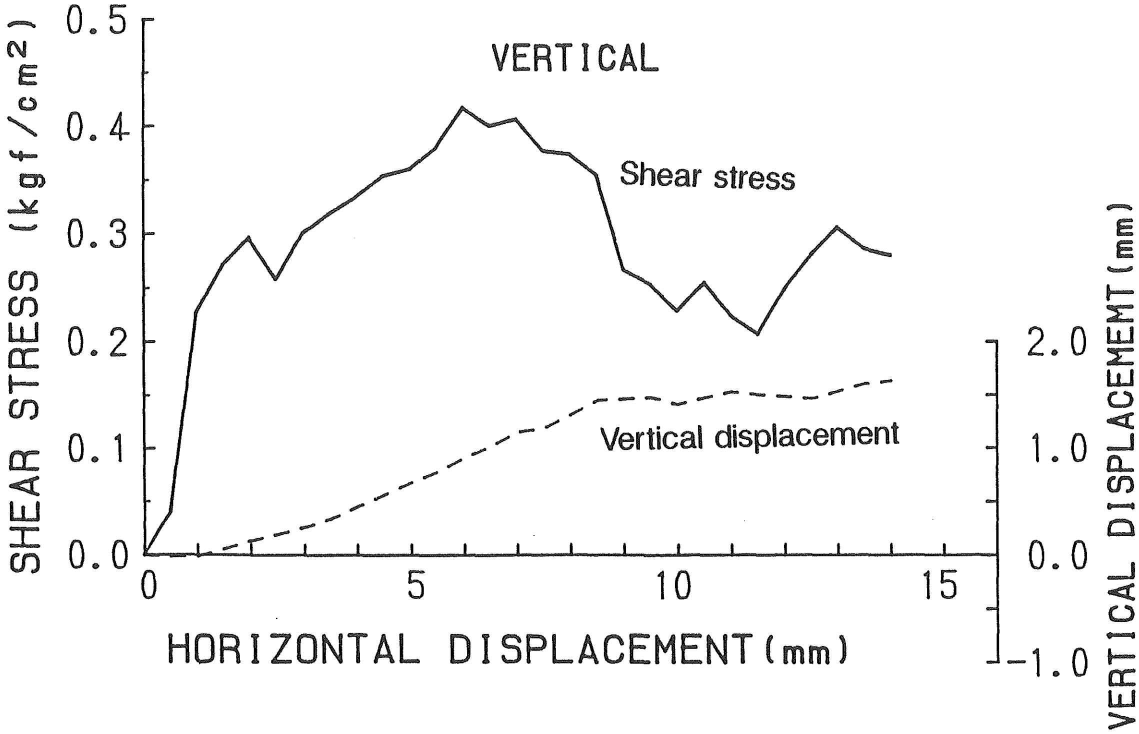

(b)

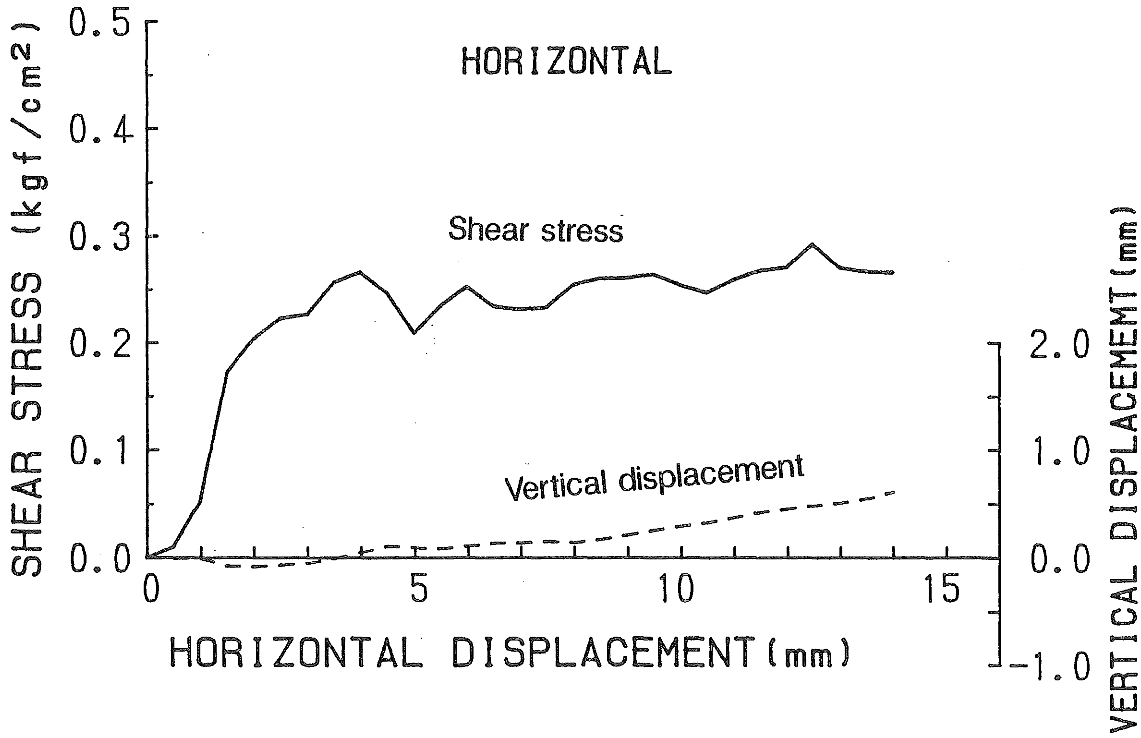

Fig.29 Stress-strain relationship on ellipsoidal aluminum-rod assemblies (a; vertical packing, b; horizontal packing)

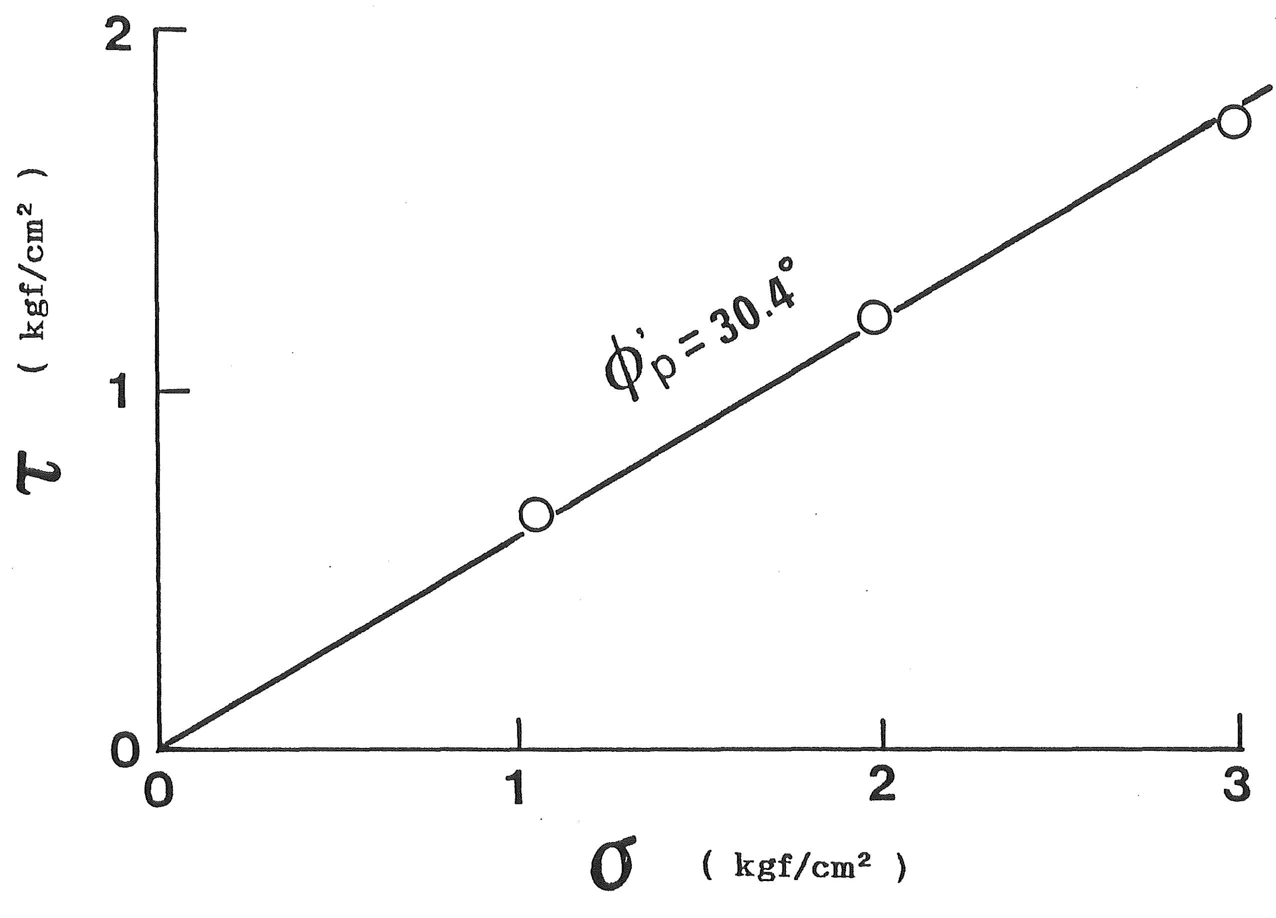

Fig.30 The relationship between normal stress, σ, and shearing strength, τ, on assemblies of 5-mm-cylindrical rods

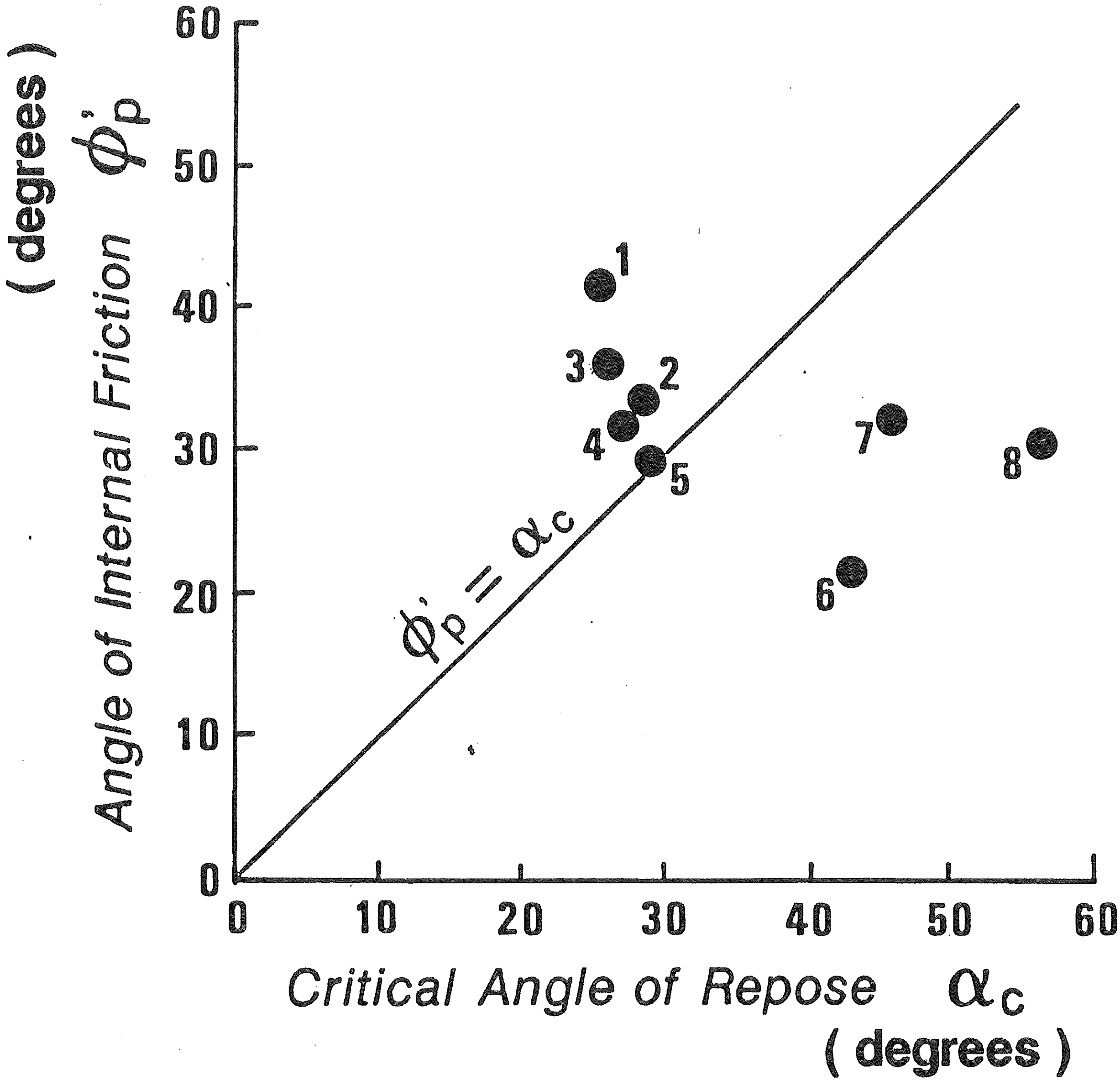

Fig.31 The critical angle of repose, α_c, vs. the angle of internal friction, ϕ'_p, on rods.

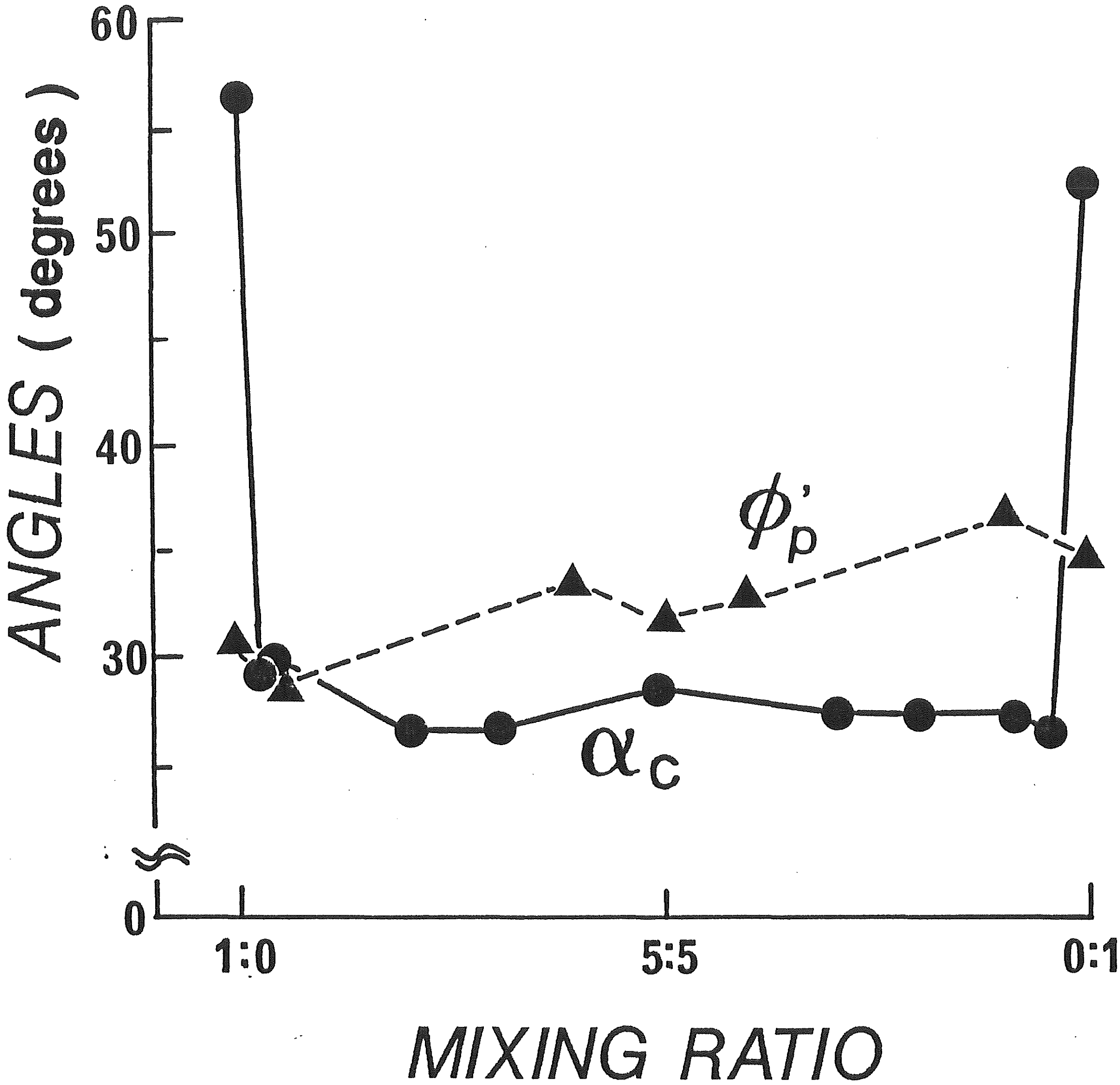

Fig.32 The relationship between mixing ratio vs. α_c or ϕ'_p on mixed cylindrical rods

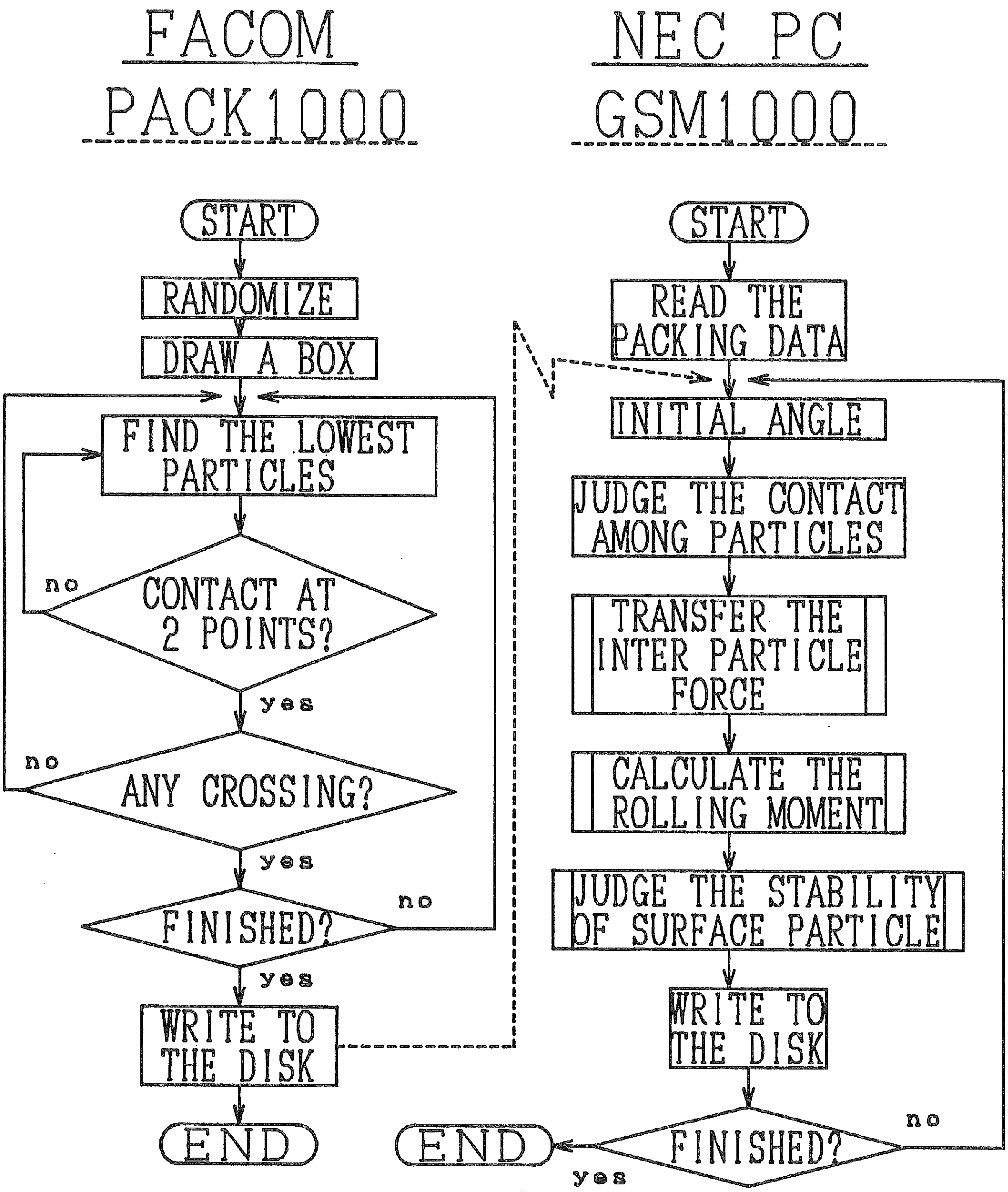

Fig.33 Flow chart of the programs of the GSM

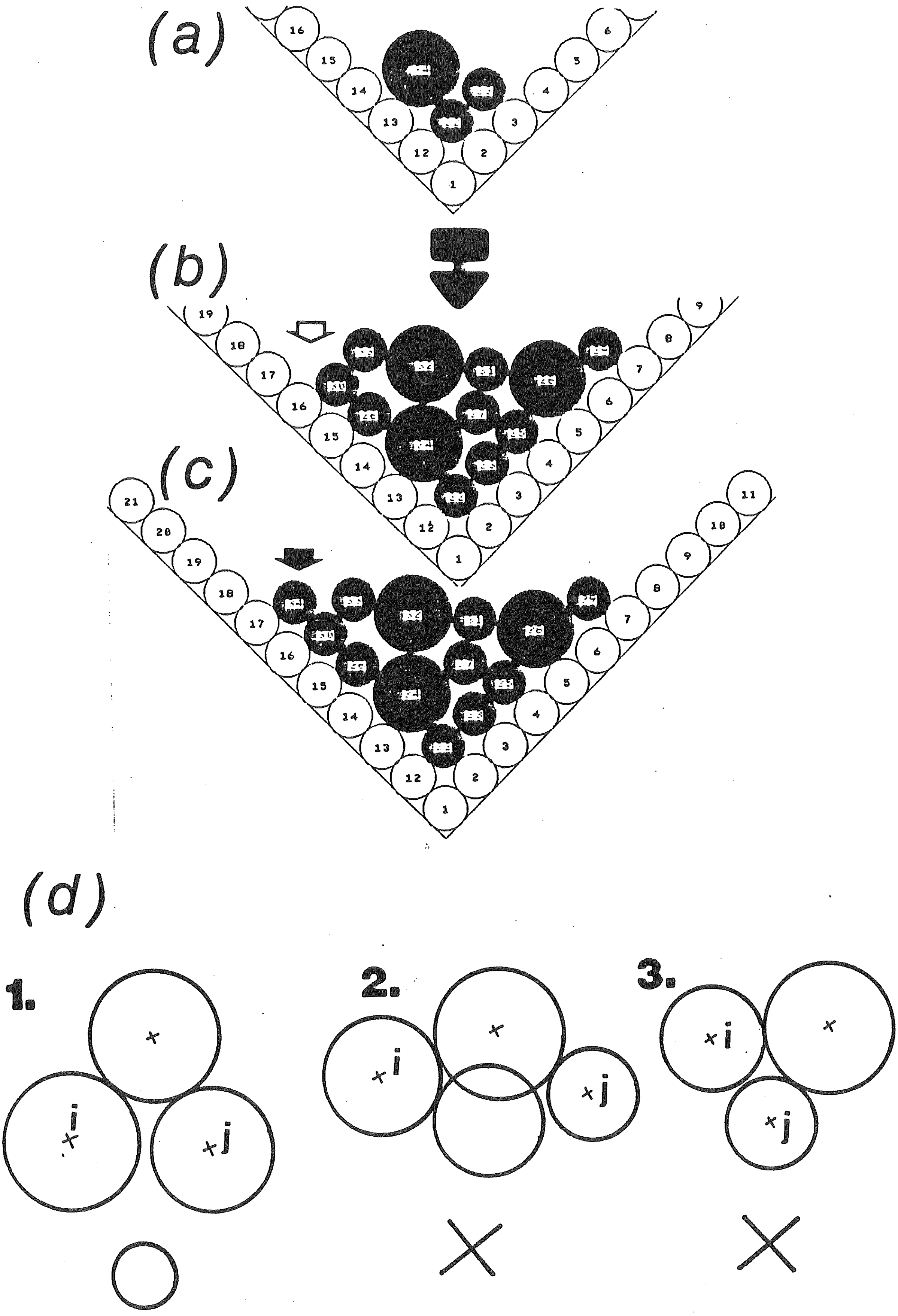

Fig.34 Method of random packing (intrusion method)

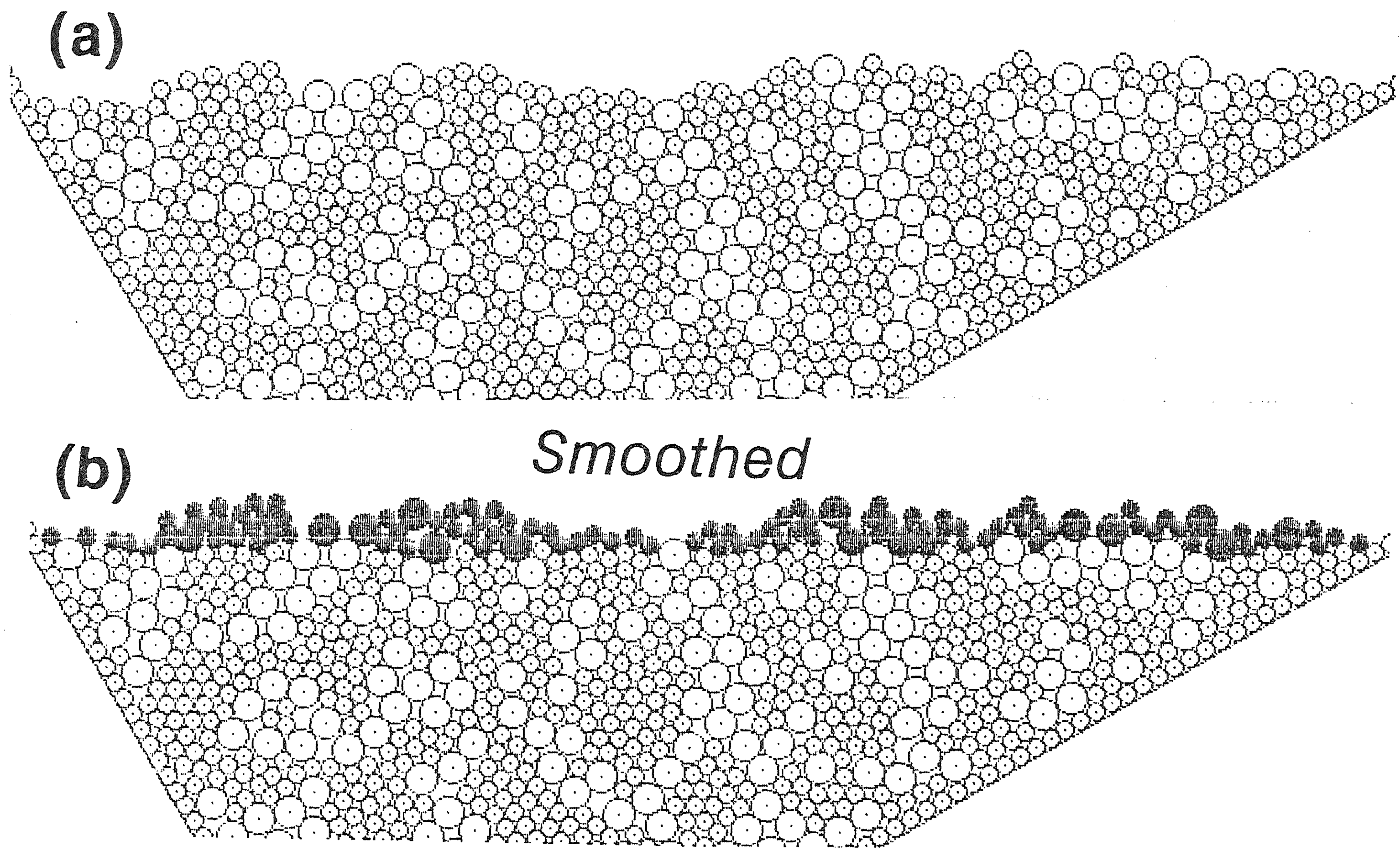

Fig.35 The method of smoothing the surface of granular-slope in the model

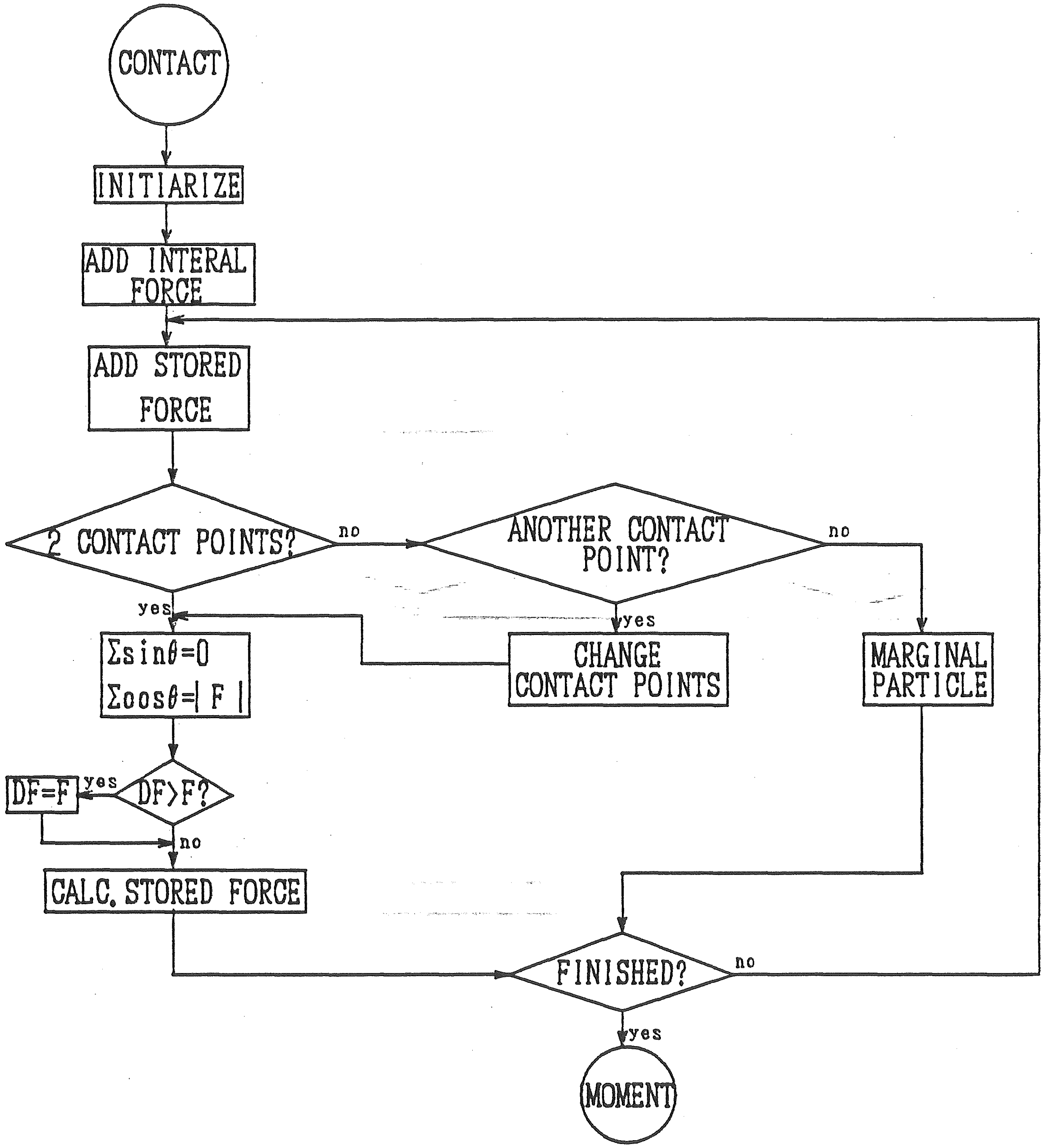

Fig.36 Flow chart of the main routine of *GSM1000*

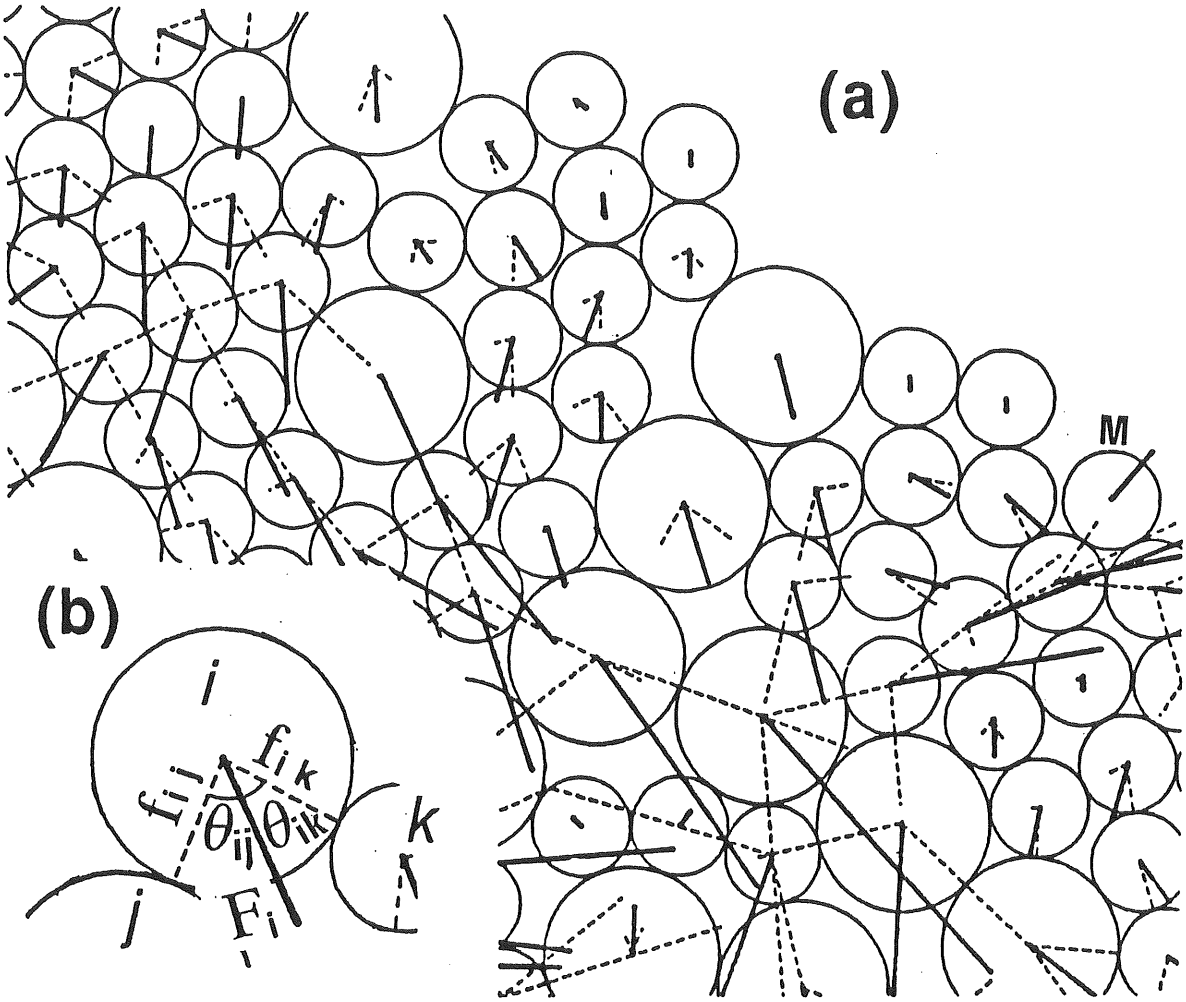

$$\theta_{ij} + \theta_{ik} < 170^\circ \quad (1)$$

$$f_{ij} \leqq F_i \quad \text{or} \quad f_{ik} \leqq F_i \quad (2)$$

$$\theta_{ij} < 110^\circ \quad \text{or} \quad \theta_{ik} < 110^\circ \quad (3)$$

Fig.37 The method for dividing the force and the example of the GSM calculation

ROLLING

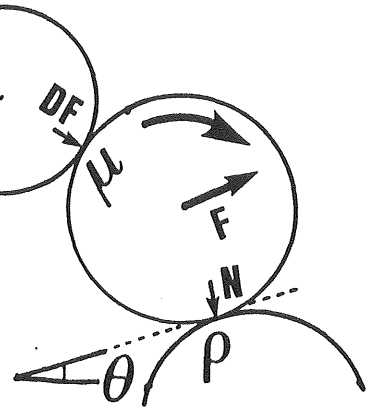

$$F = \mu \cdot DF + W \sin \theta + \rho \cdot N$$

SLIDING

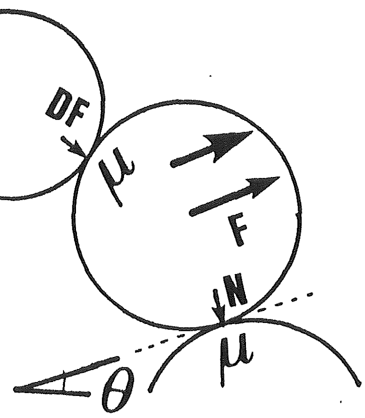

$$F = \mu \cdot DF + \frac{W \cdot (\sin \theta + \mu \cos \theta)}{1 + (\sin \theta + \mu \cos \theta) \cdot \sin \theta}$$

Fig.38 The critical condition for the stability of a rod derived from rolling friction and sliding friction

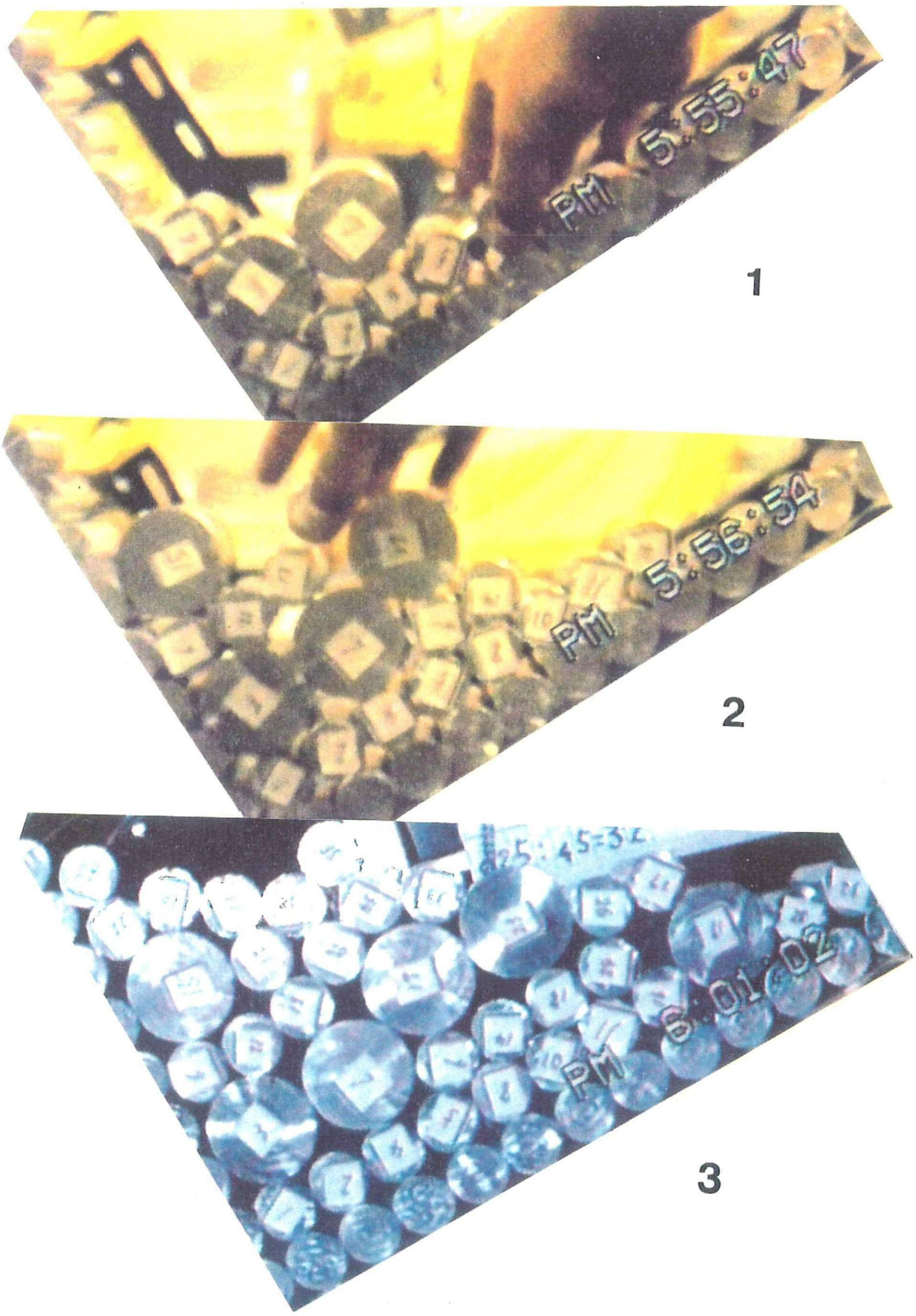

Fig.39 The method of packing 35-particle in tilting-box experiment

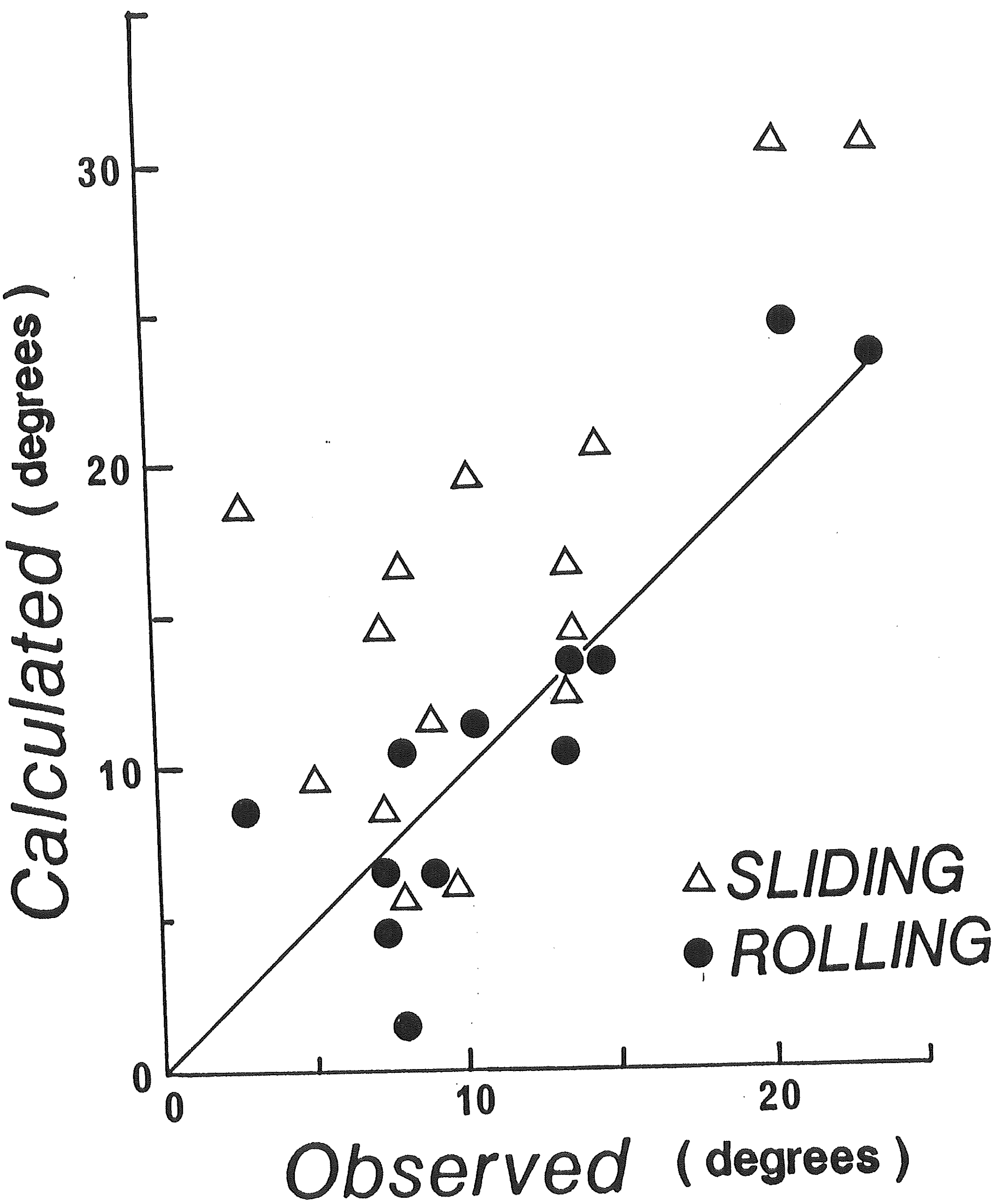

Fig.40 The relationship between experimental values and and calculated values for the initiation angle of movement in the 35-particle experiment

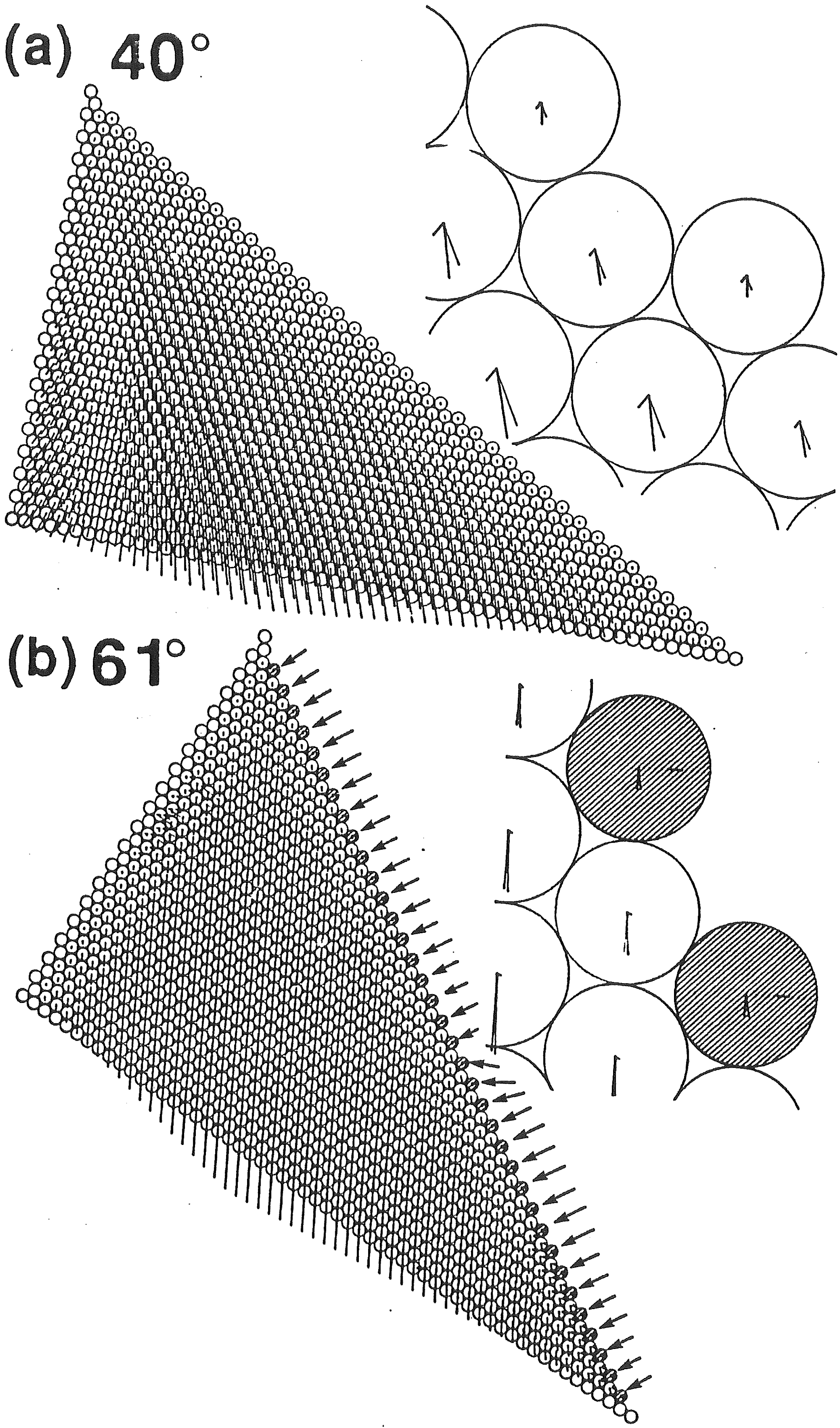

Fig.41 The calculation of the GSM in the case of uniform diameter

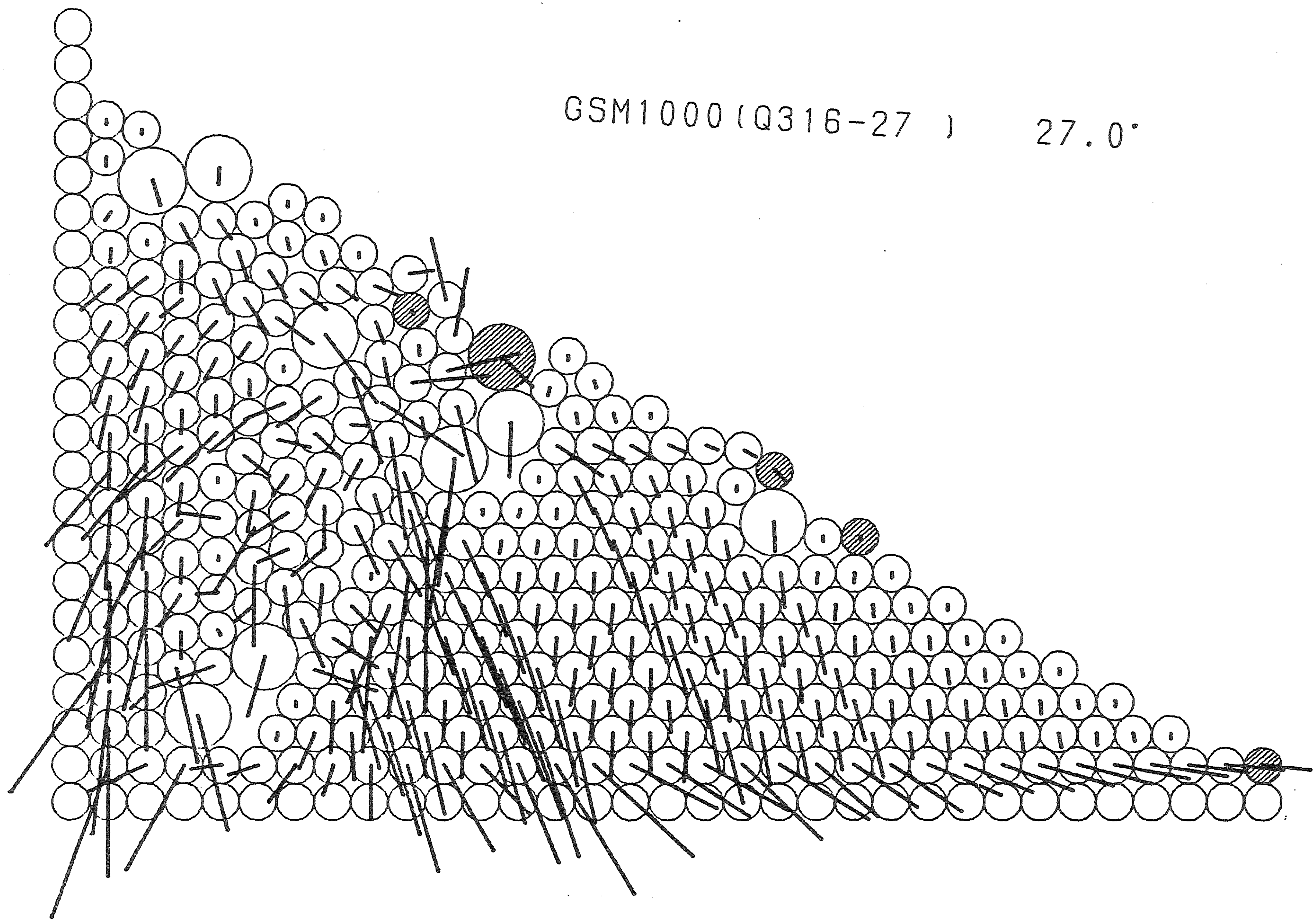

Fig.42 The calculation of the GSM in the case of mixed materials with small number of different-diameter particles

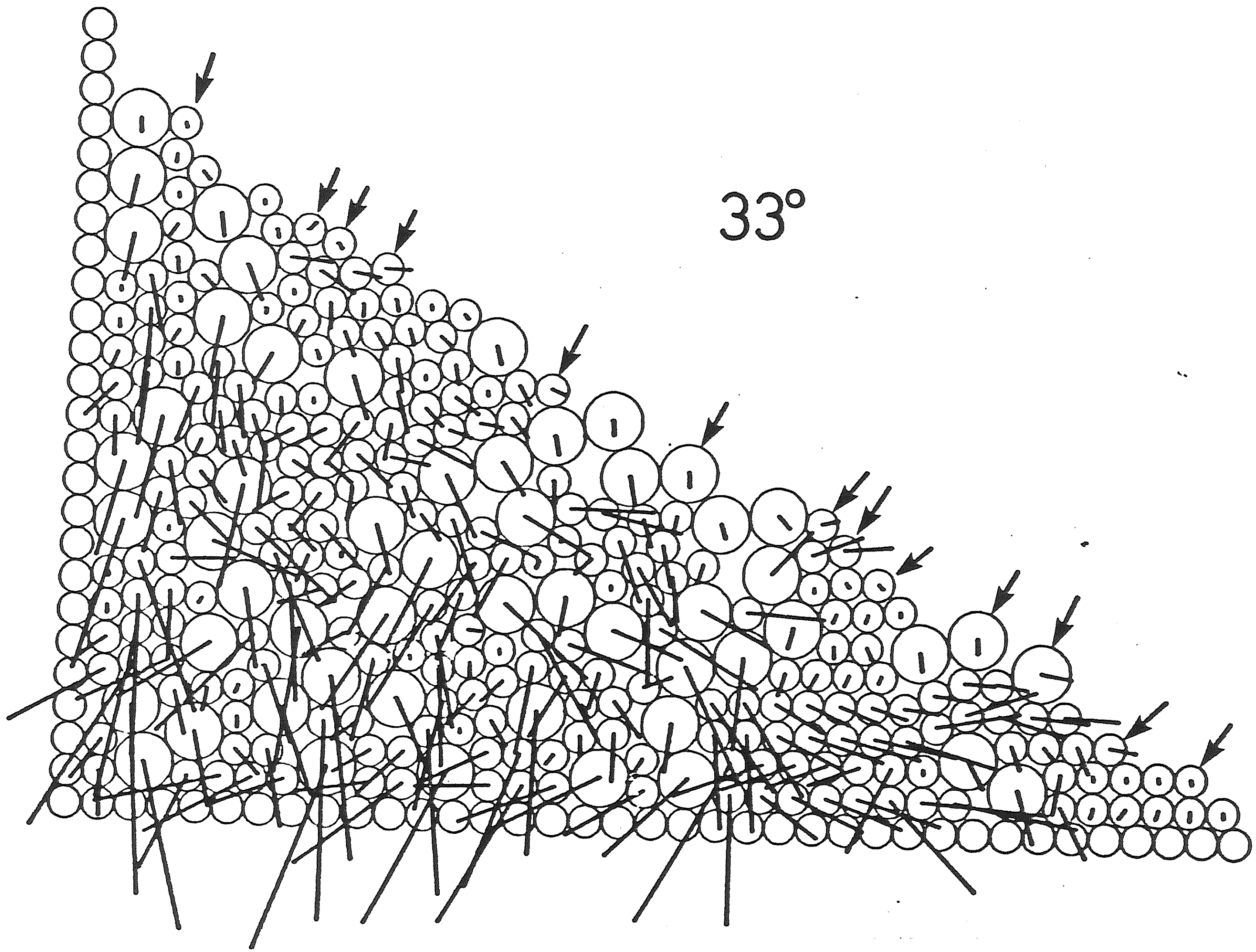

Fig.43 The calculation of the GSM in the case of the mixed particles;
ϕ5 mm : ϕ9mm = 3 : 2

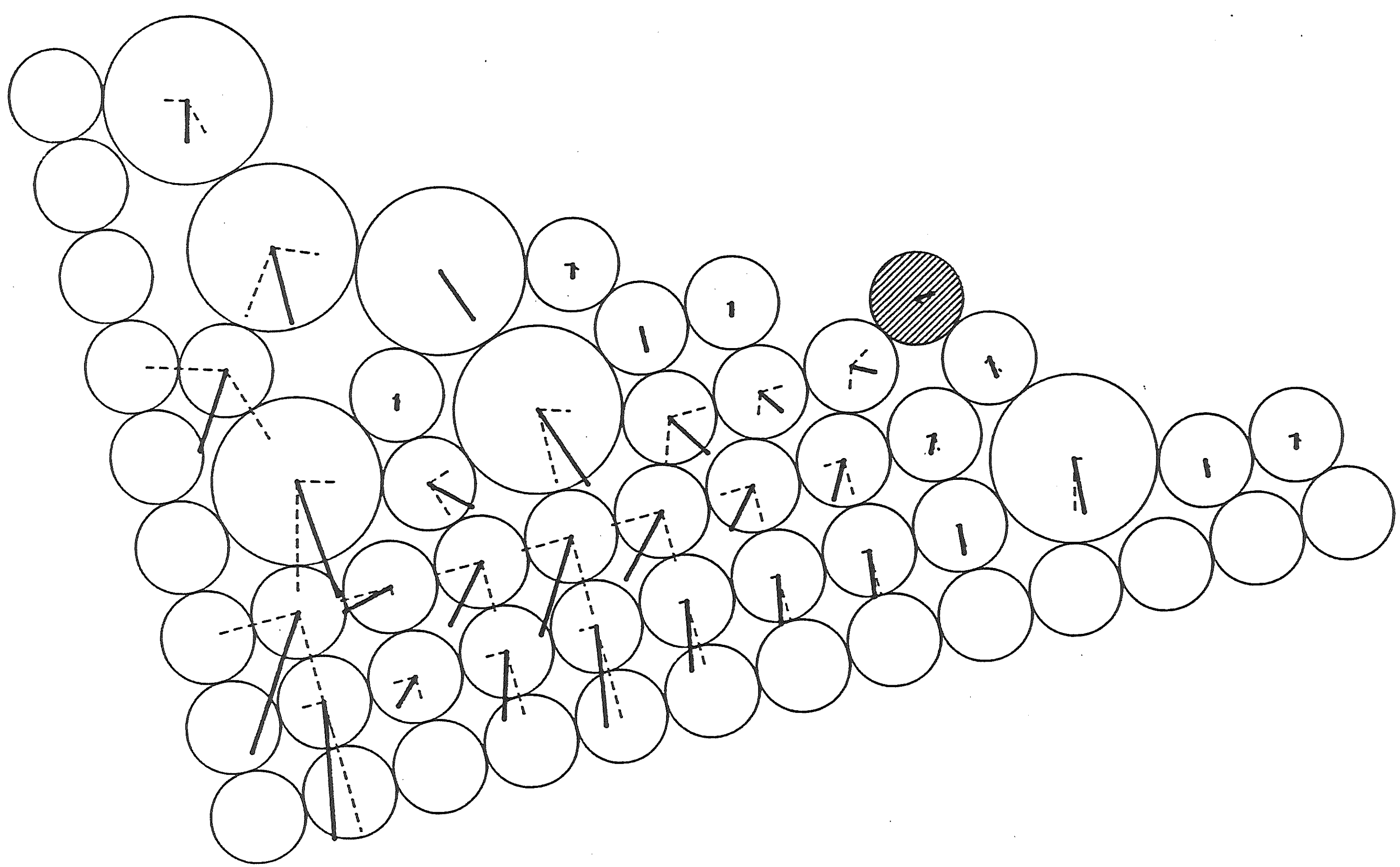

Fig.44 The GSM calculation of the 35 particles (14°)

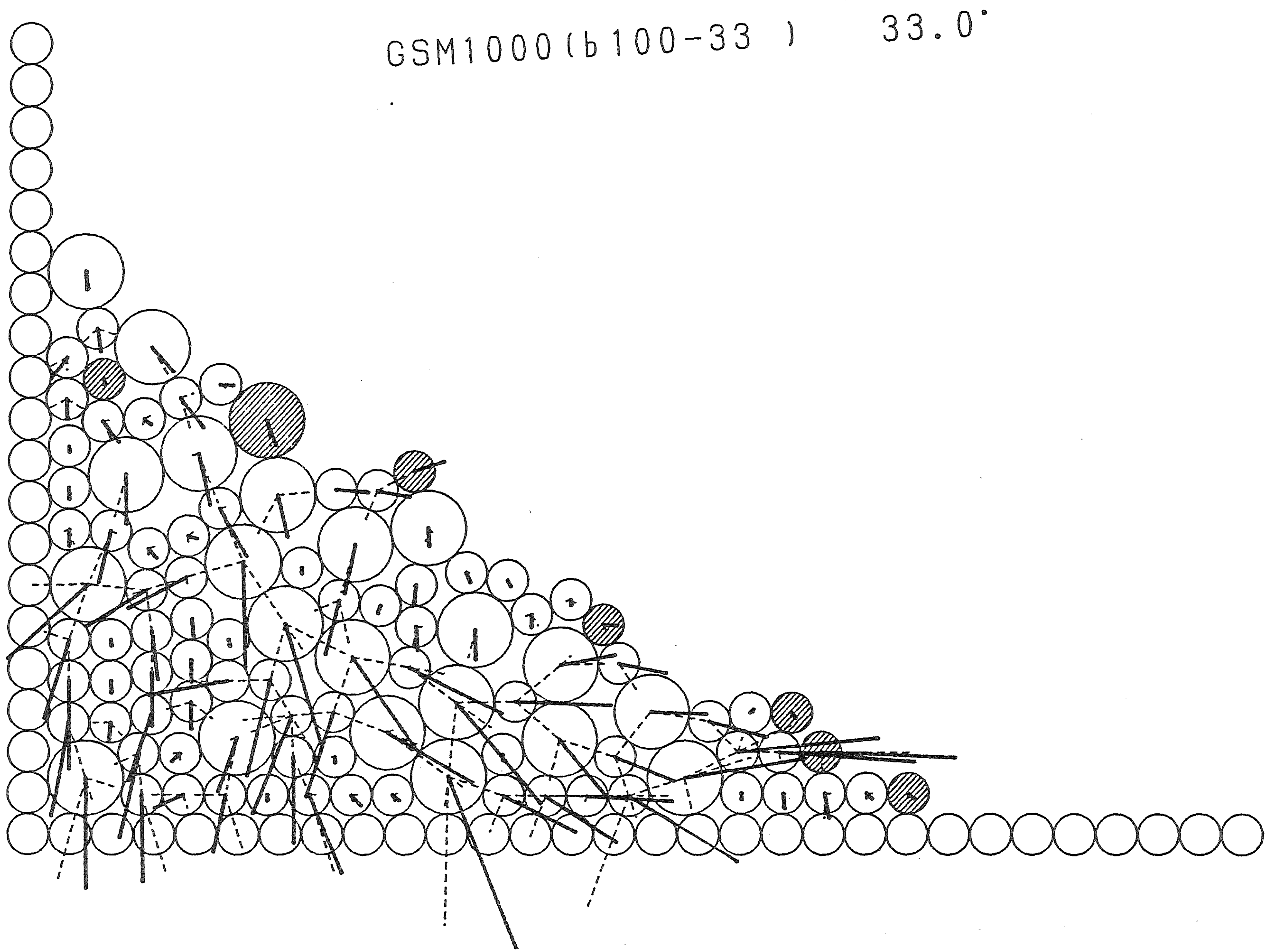

Fig.45 The GSM calculation of the 100 particles (33°)

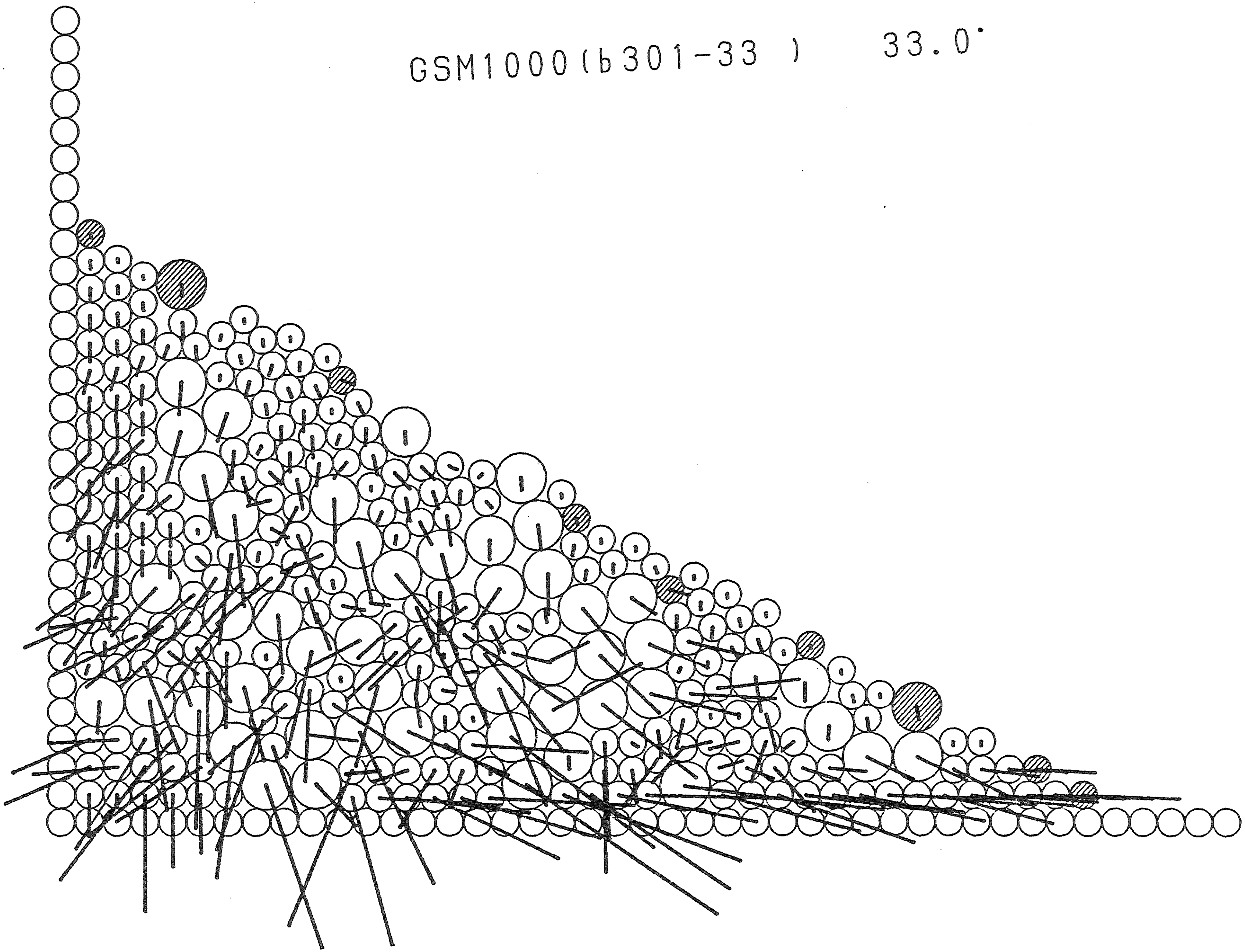

Fig.46 The GSM calculation of the 301 particles (33°)

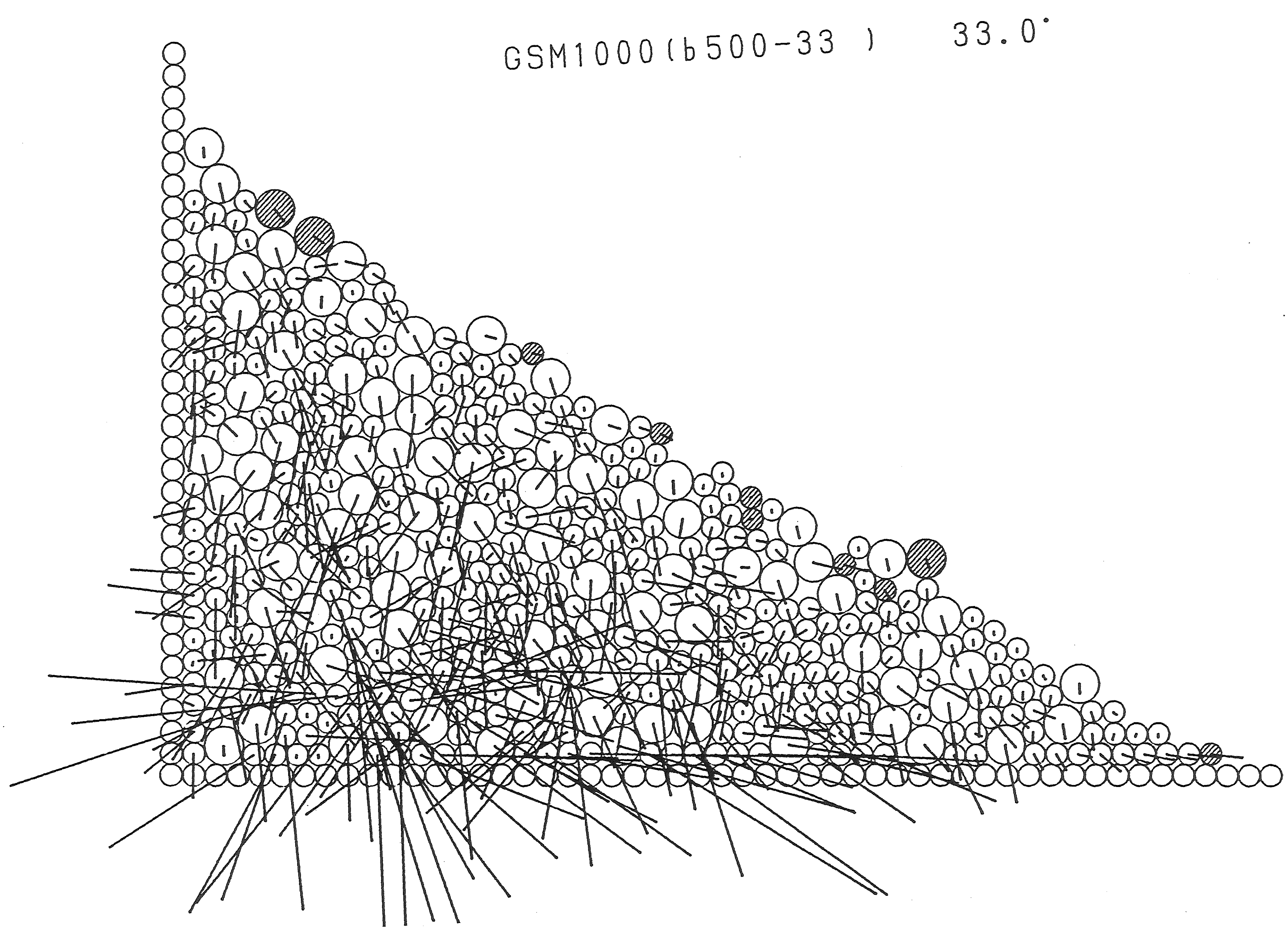

Fig.47 The GSM calculation of the 500 particles (33°)

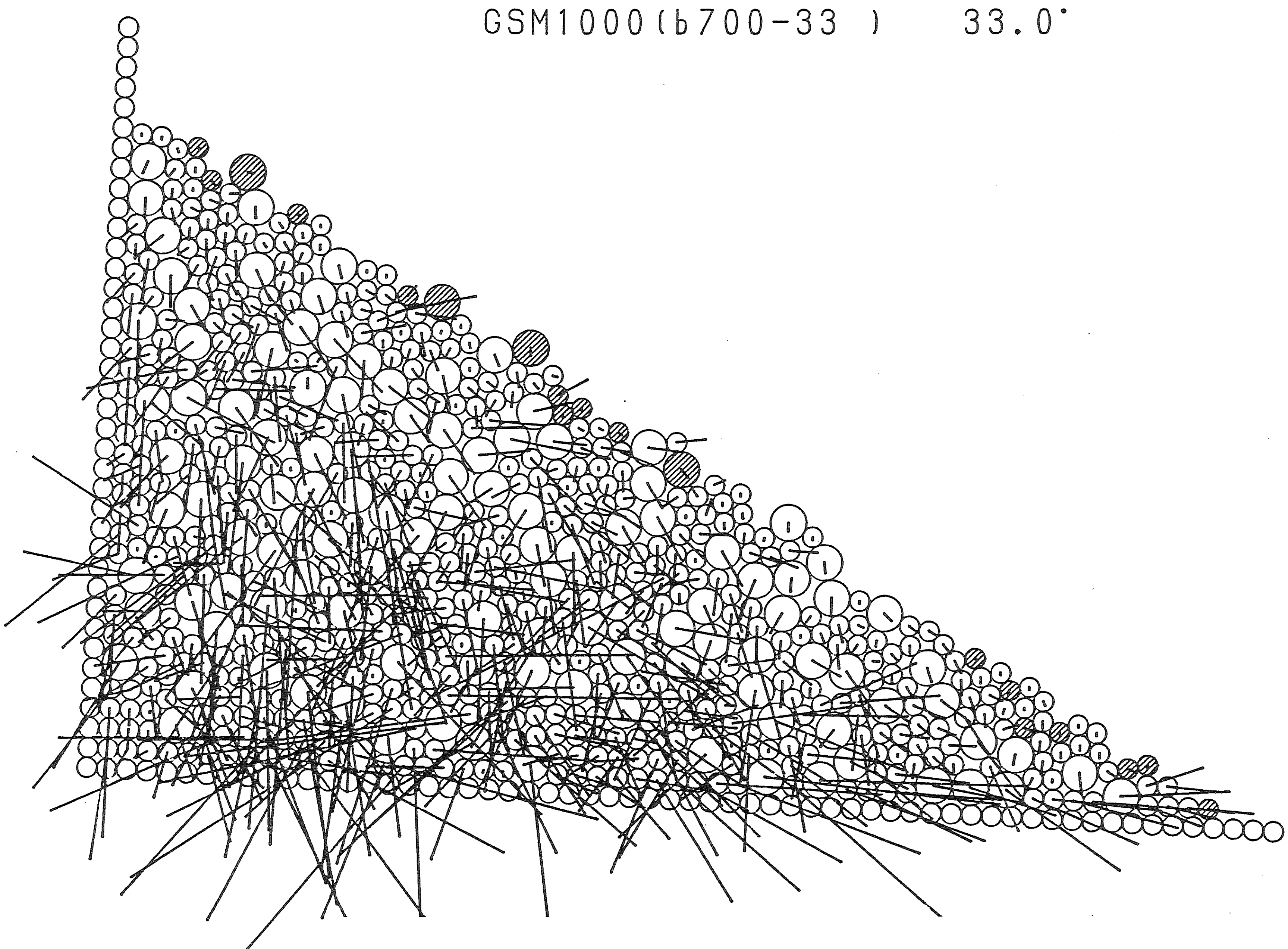

Fig.48 The GSM calculation of the 700 particles (33°)

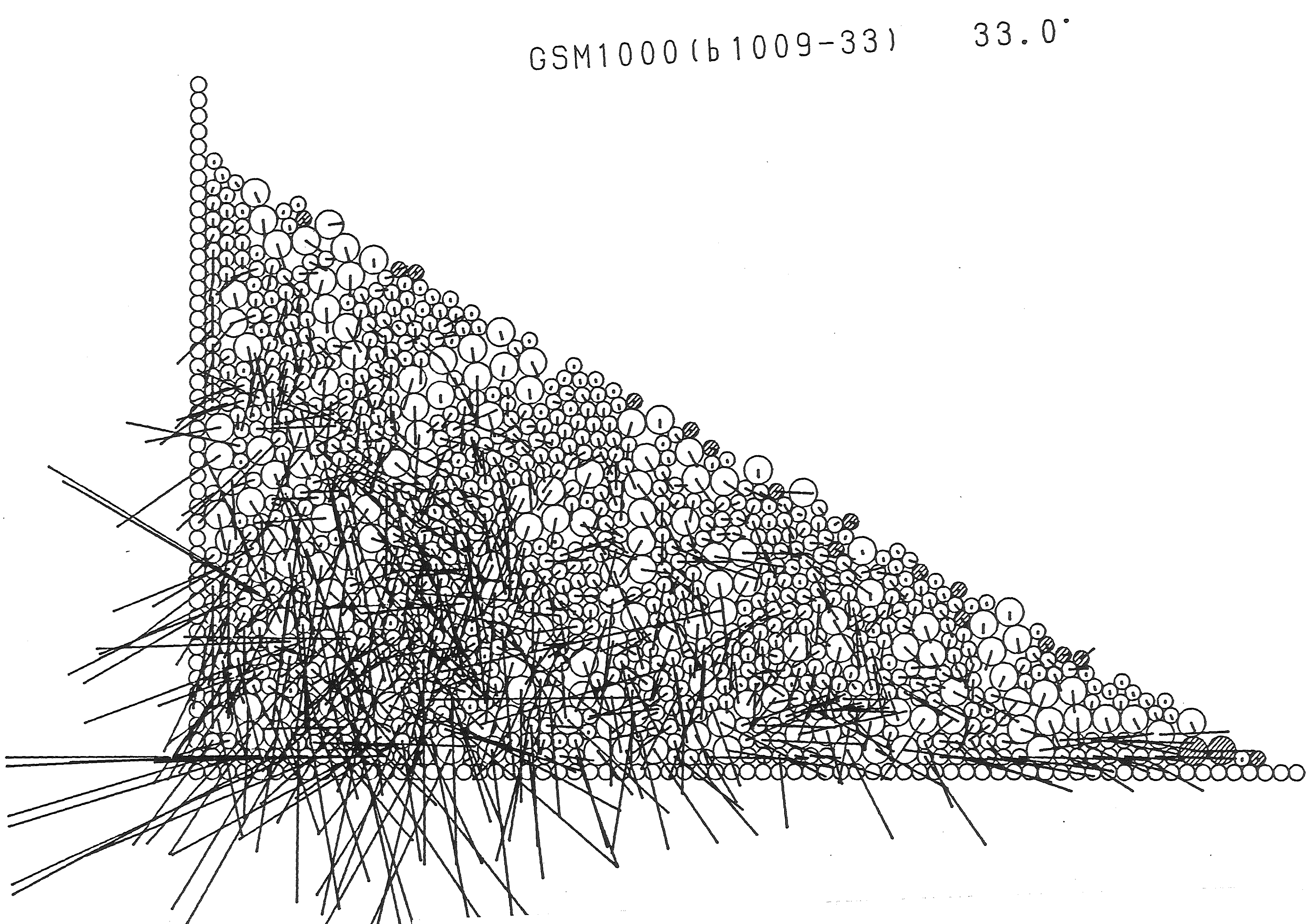

Fig.49 The GSM calculation of the 1009 particles (33˚)

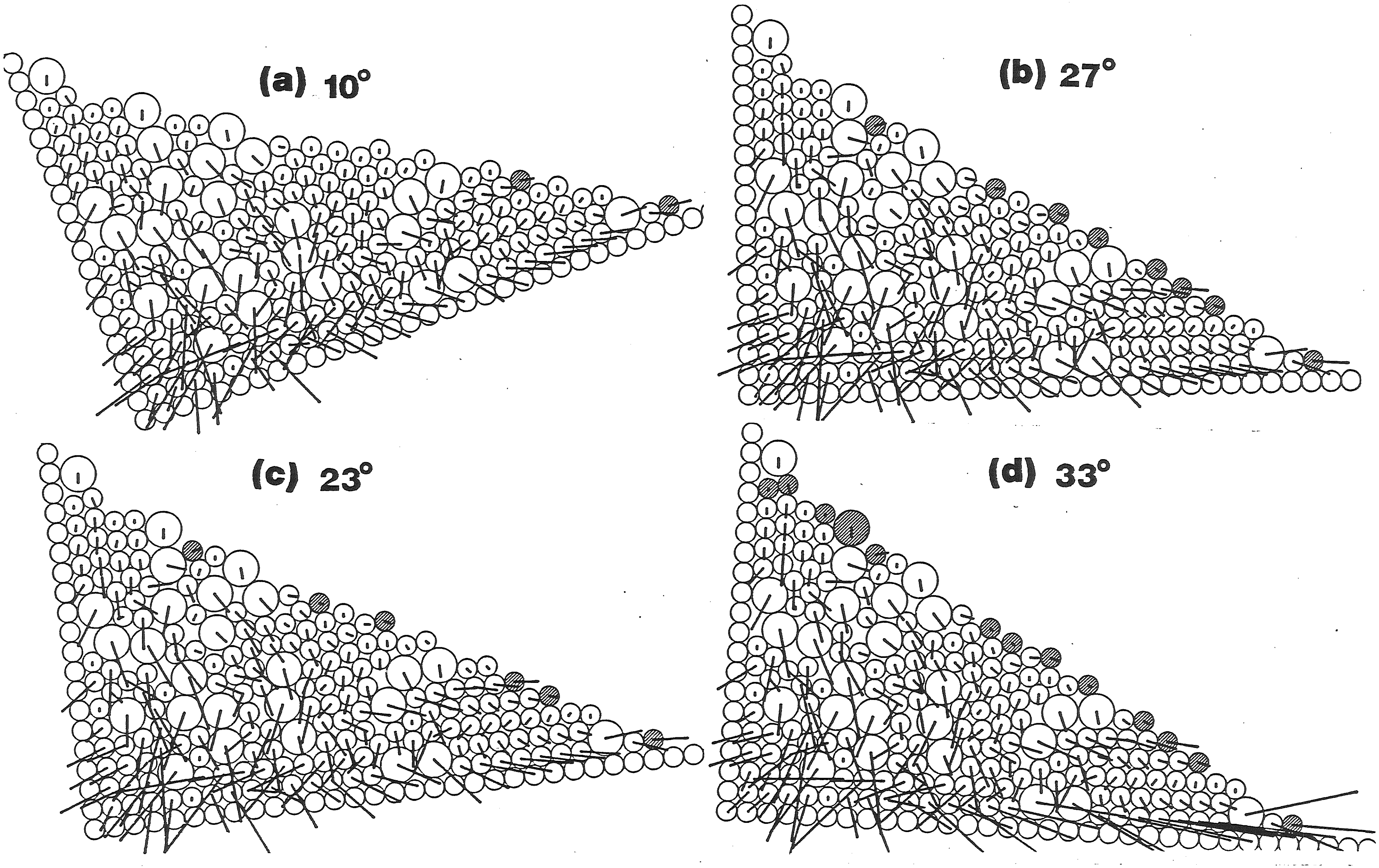

Fig.50 The GSM calculation of the 200 particles with various angles

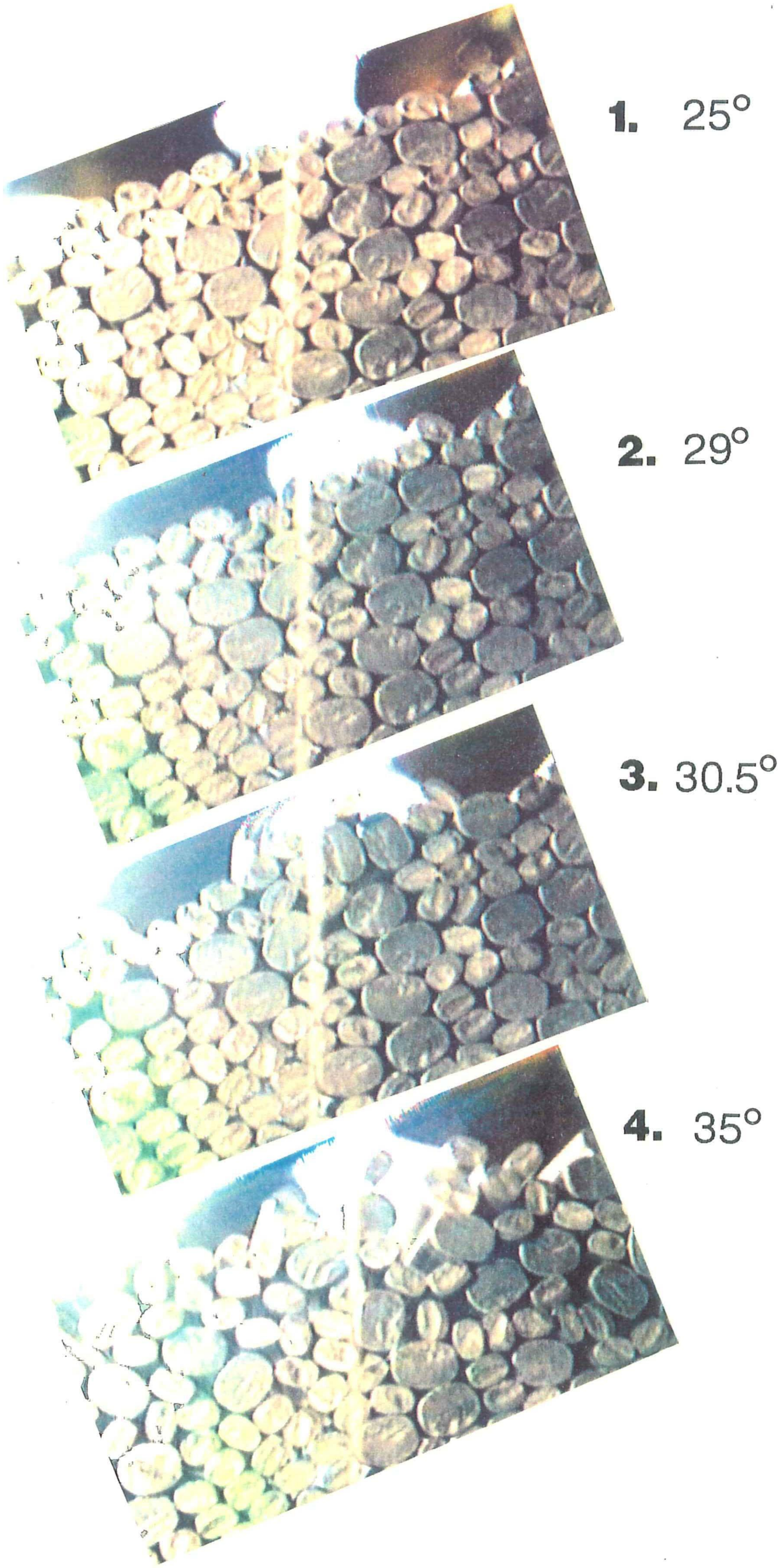

Fig.51 Avalanche of ellipsoidal rods with horizontal packing: 1 stable, 2 and 3 start to erect, and 4 avalanching

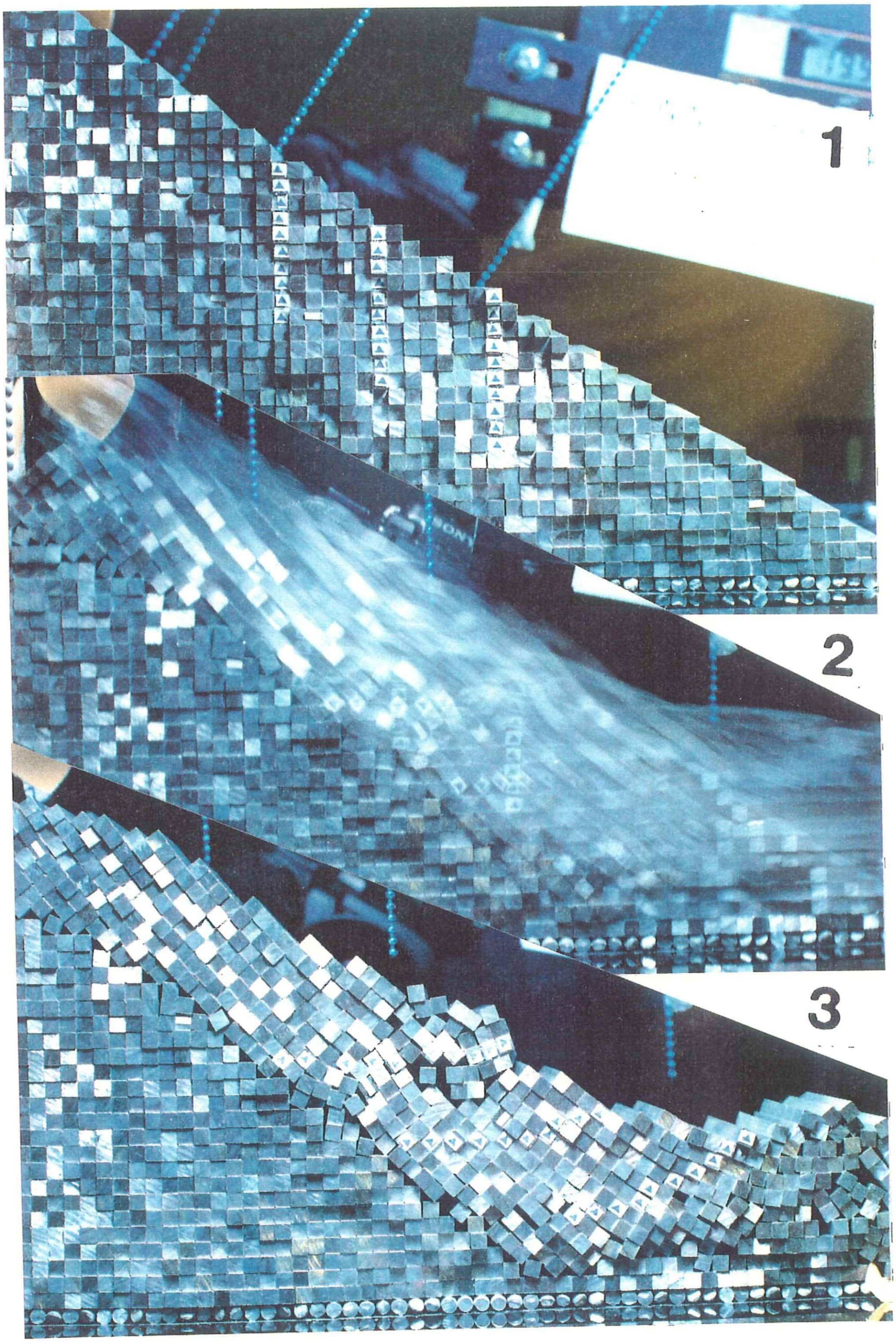

Fig.52 The avalanche of the square rods of uniform diameters: 1 before an avalanching, 2 during an avalanche, and 3 after the avalanche

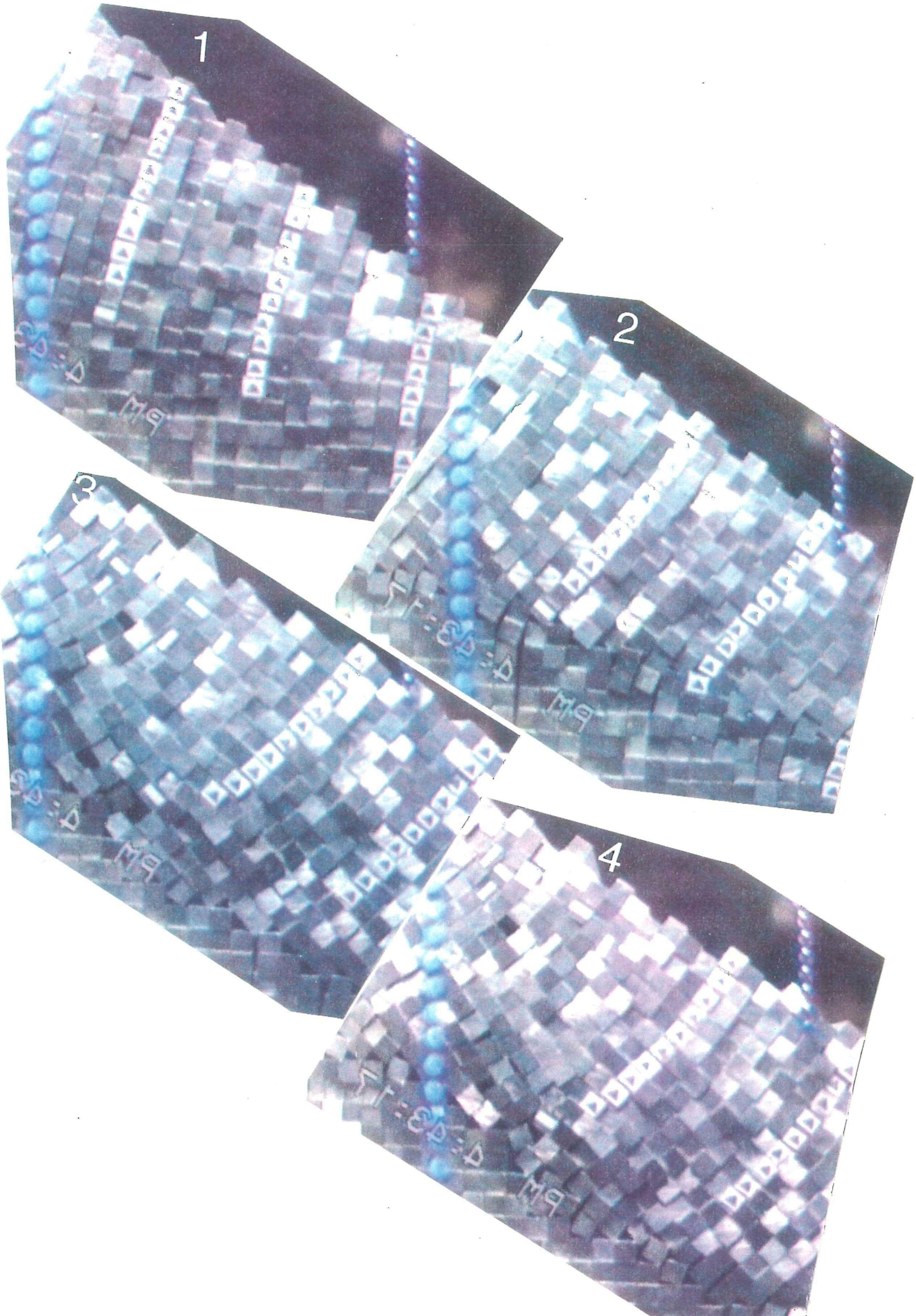

Fig.53 The avalanching of the square rods (slow speed): interval 0.1 sec

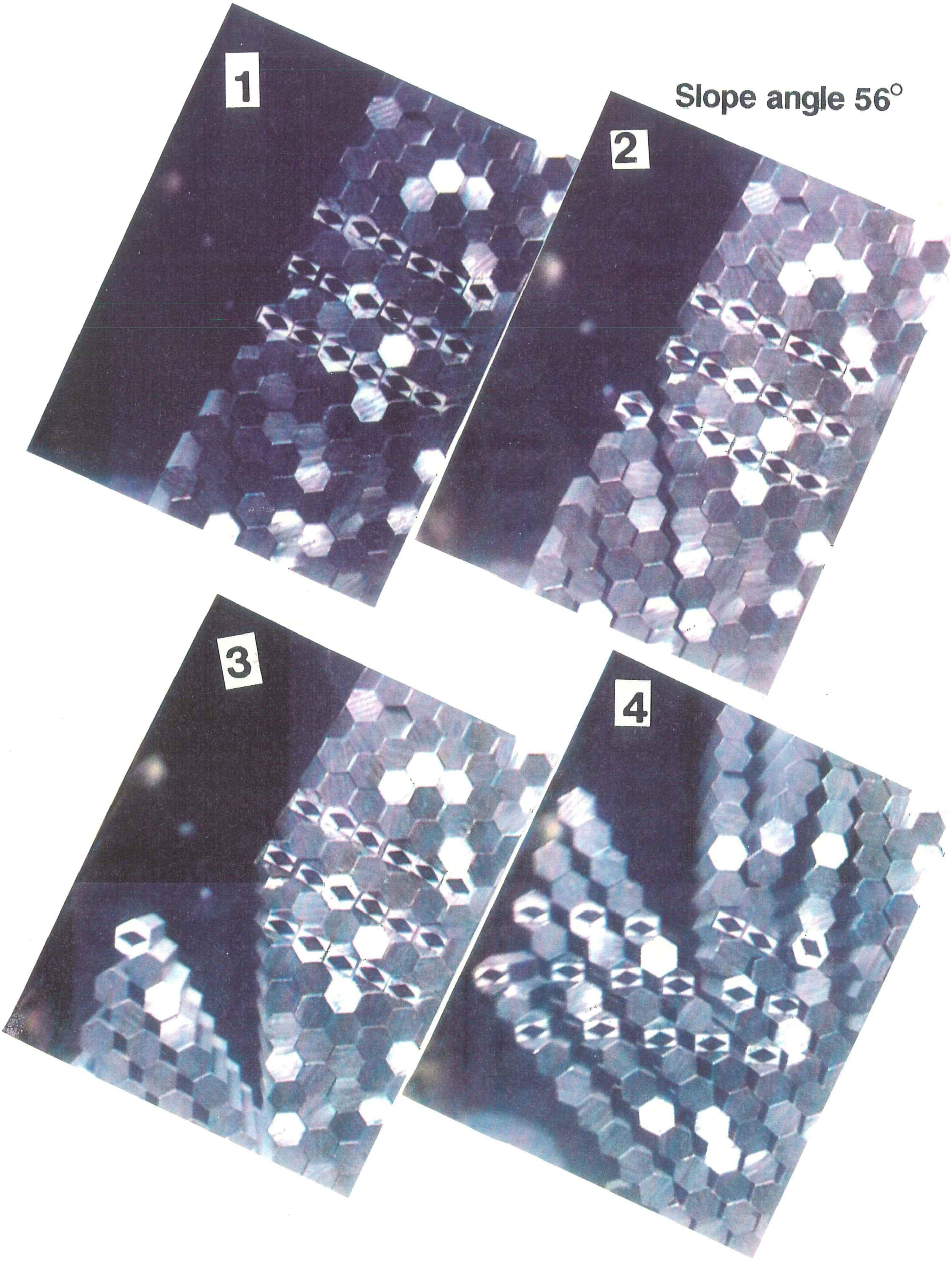

Fig.54 The pillar like avalanching of the octagonal rods (slow speed): interval 1/30 sec

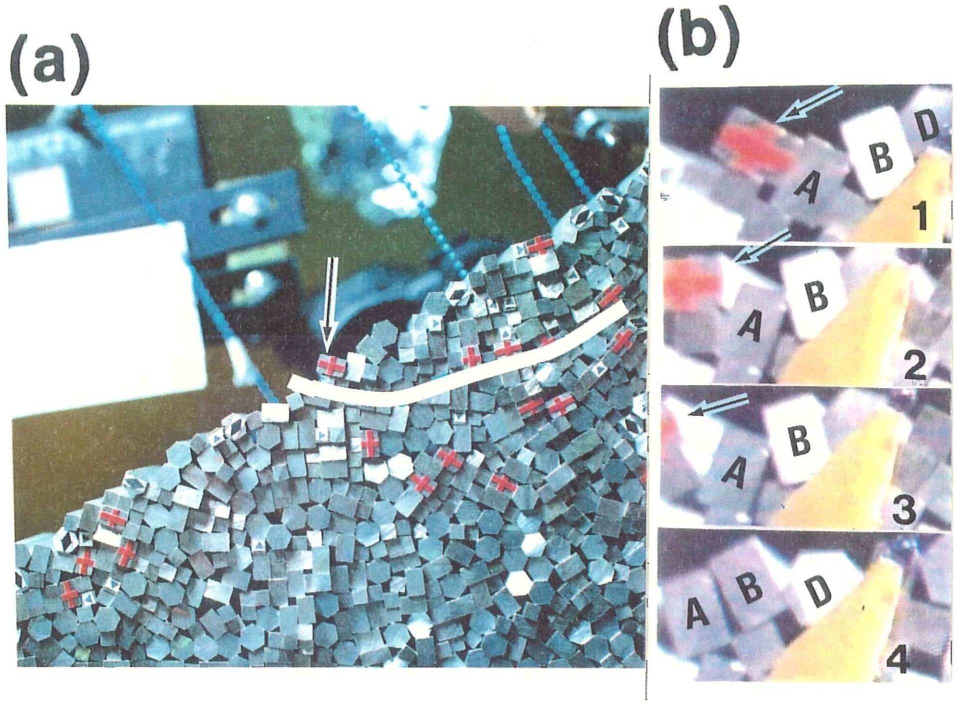

Fig.55 The commencement of the avalanche by rotation of a rod (a; an avalanche is triggered by rotation of the arrow marked particle, b; slow speed pictures of rotating the arrow marked rod, interval 1/30 sec)

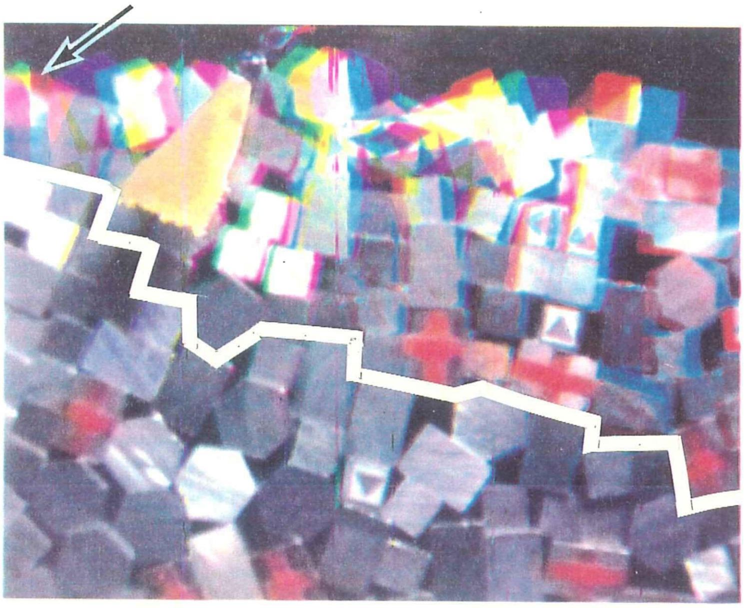

Fig.56 The movement of rods during the same avalanche as shown in Fig. 55. The boundary between the regions showing moving and still rods is depicted by a white line. Movement of the rods is easily seen from blur of the picture in the upper half region

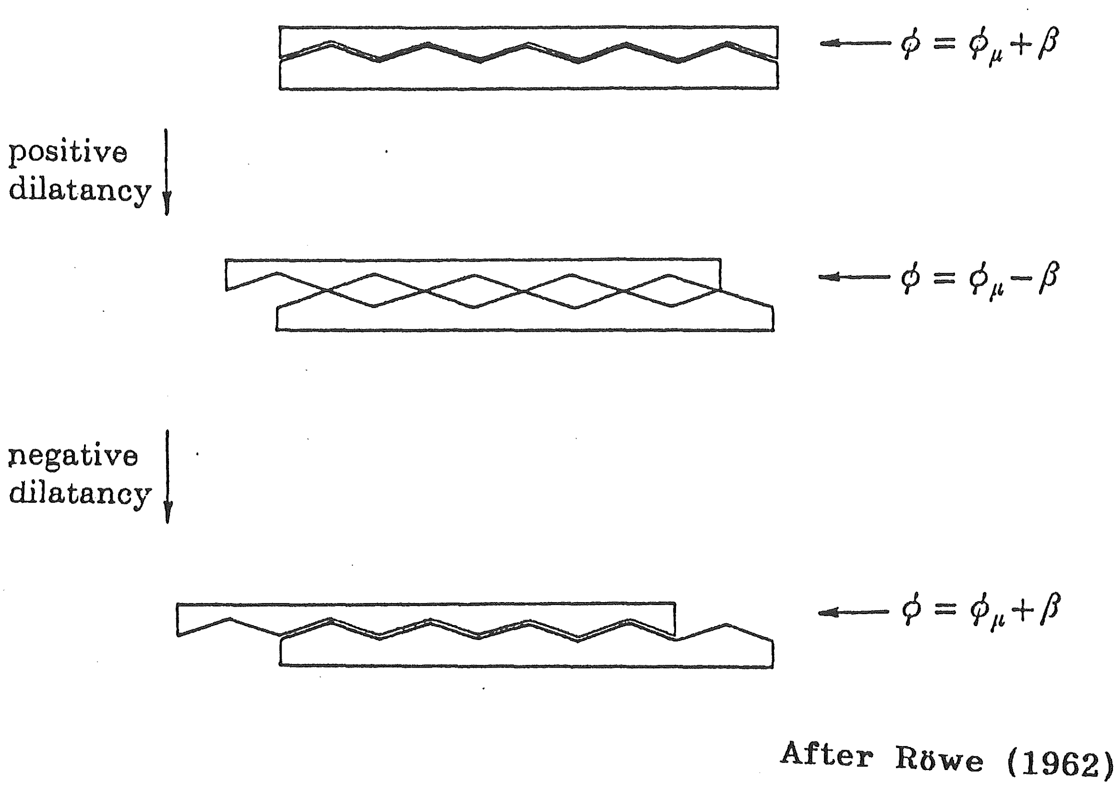

Fig.57 The model for the angle of internal friction (after Röwe, 1962)

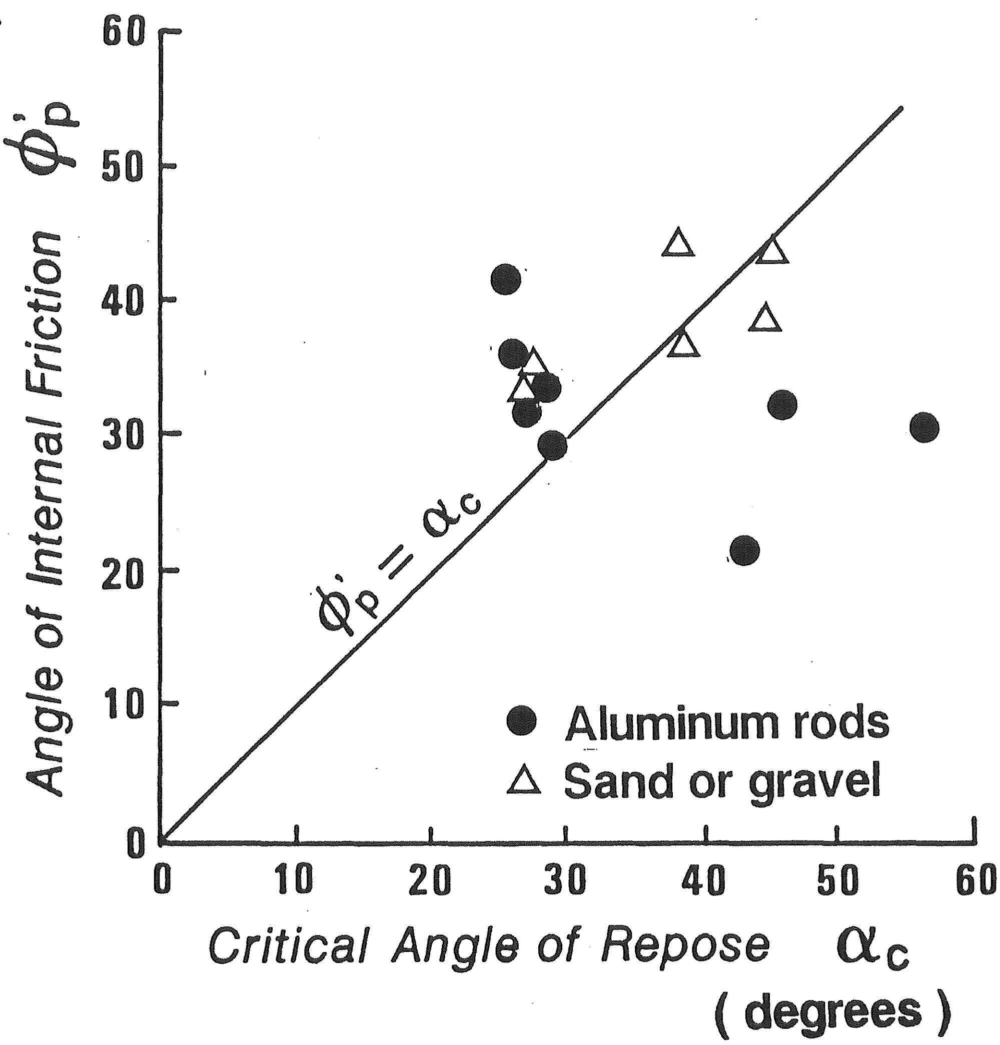

Fig.58 The critical angle of repose, α_c, vs. the angle of internal friction, ϕ'_p, on rods and sand or gravel.

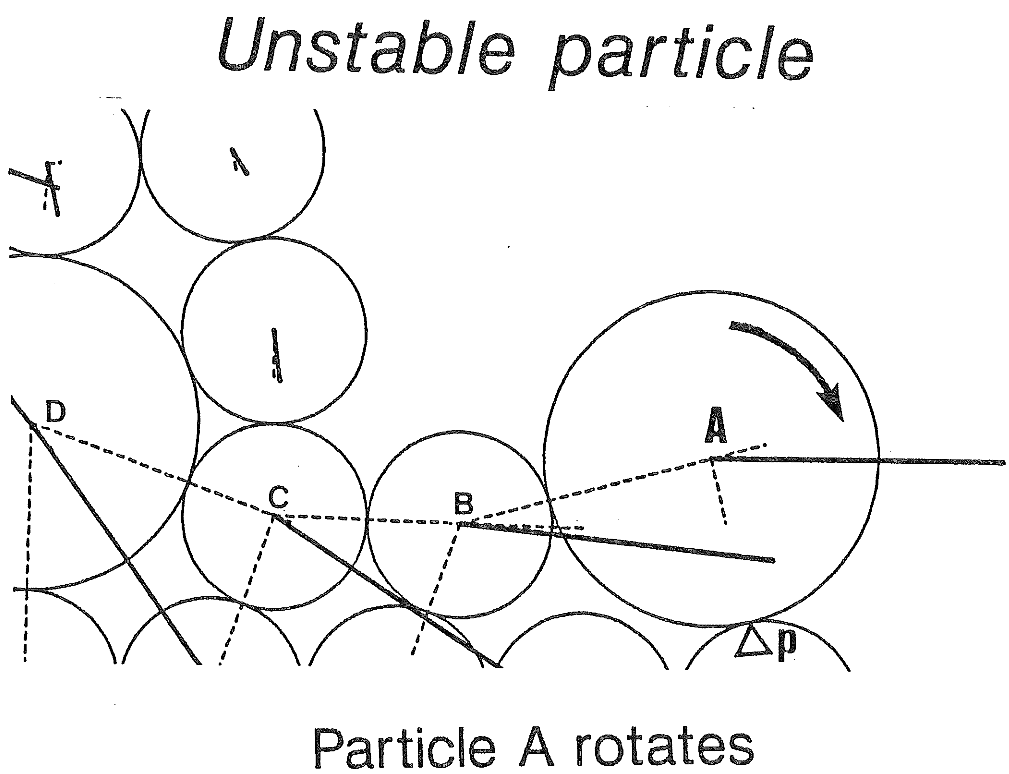

Fig.59 The schematic diagram of the critical condition for stability of the marginal particles

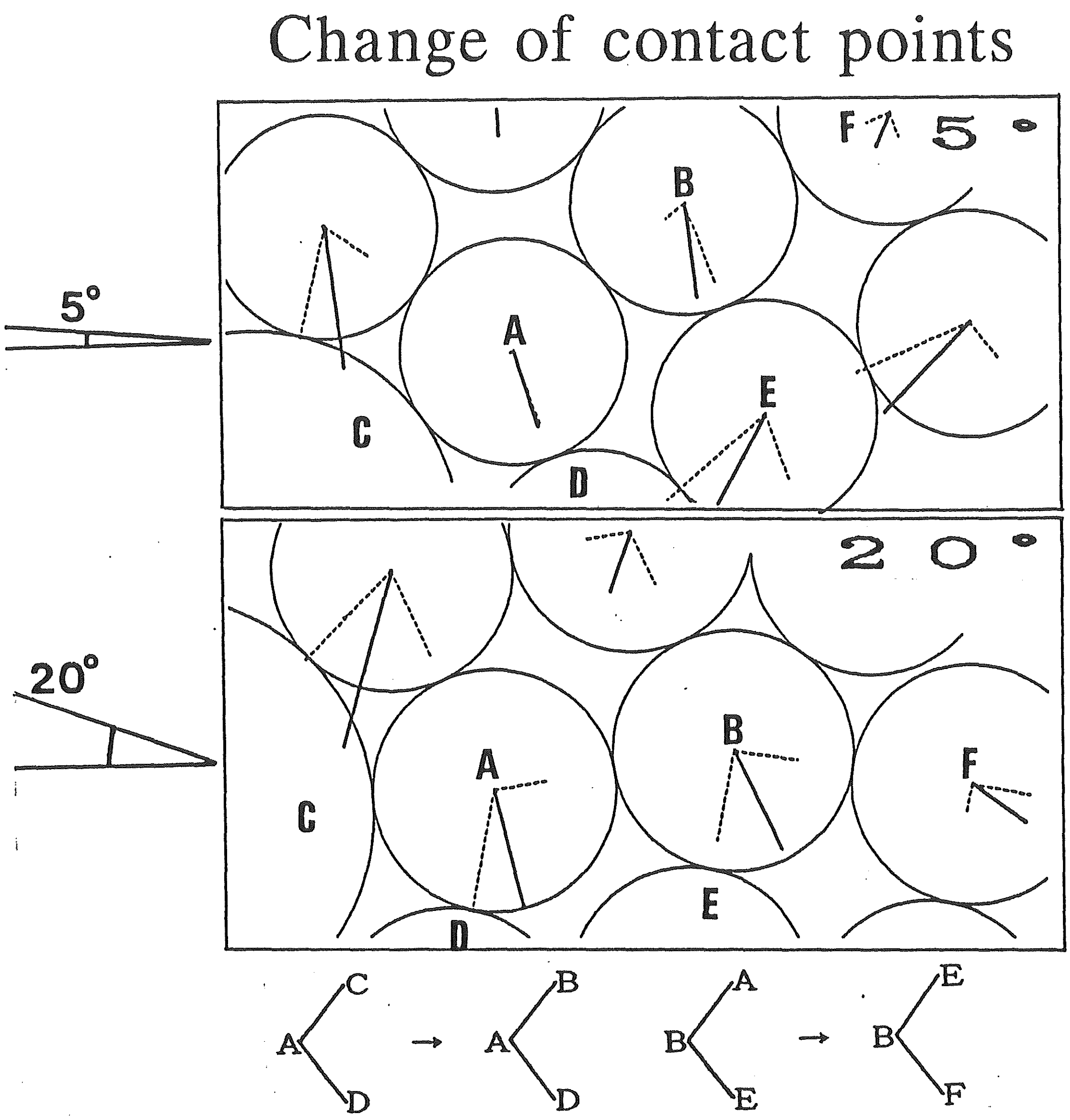

Fig.60 Schematic diagram showing the change in the contact points and the direction of both transmitted force and total force by tilting

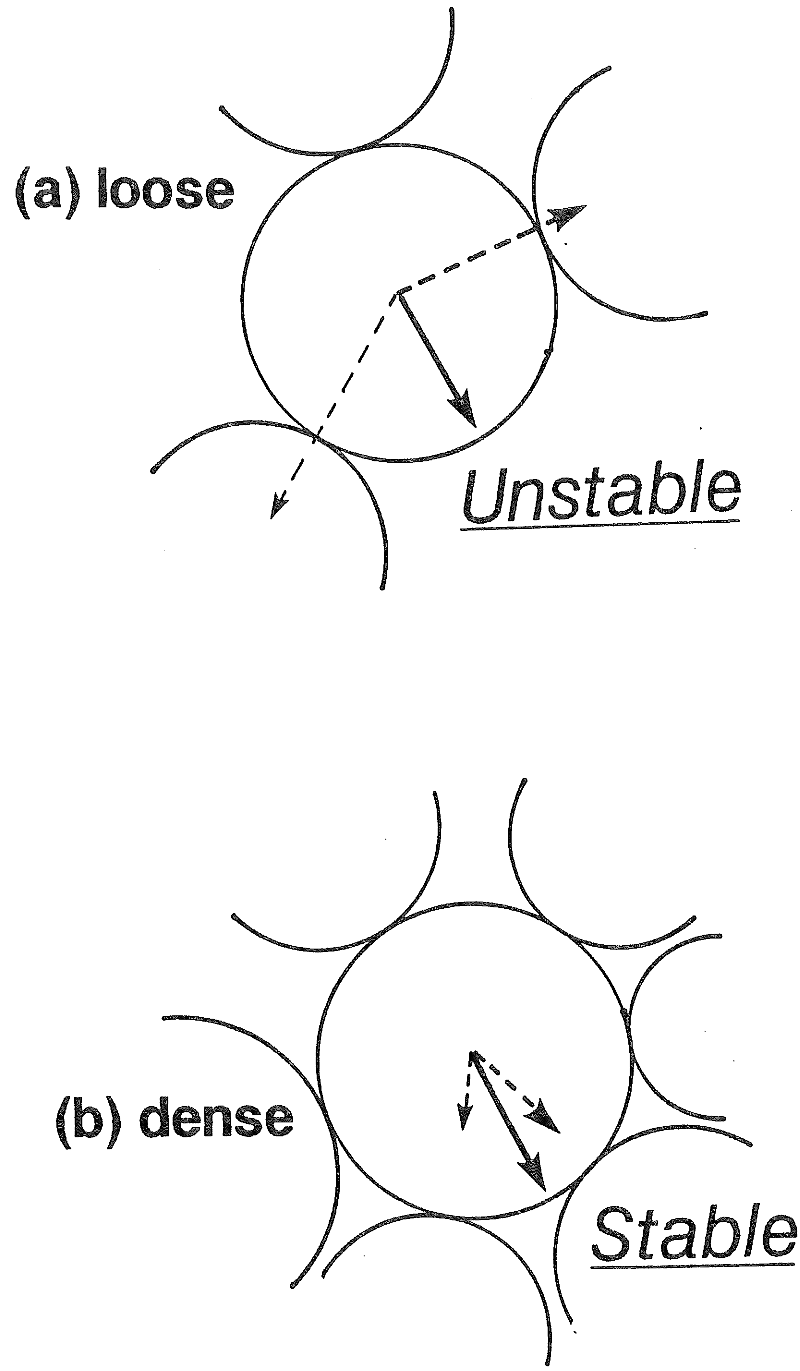

Fig.61 The effect of the number of contact points on the direction of the transmitted and total forces

35-particle experiment

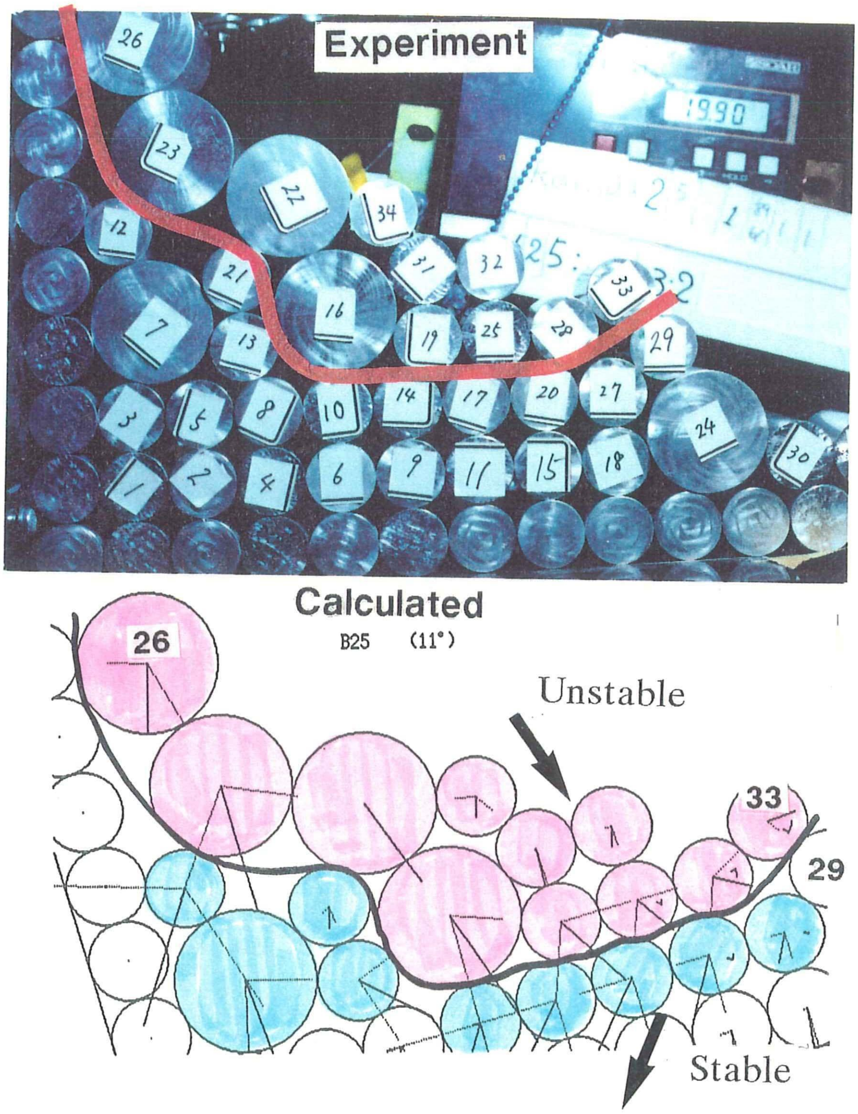

Fig.62 The avalanching zone in the tilting-box experiment and the result of GSM calculation using the 35-particle model

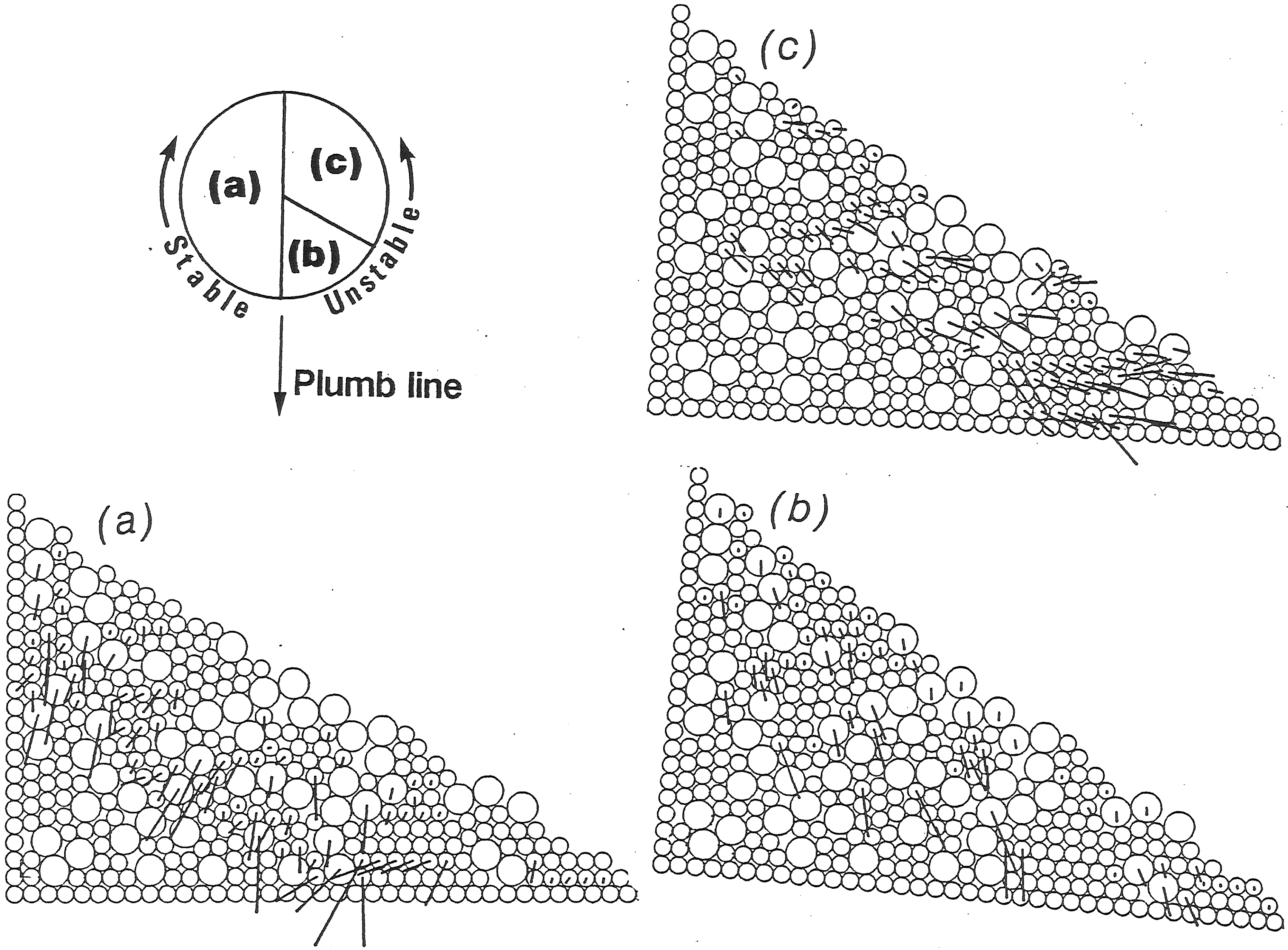

Fig.63 Direction of vectors classified into three categories shallower than 5cm (B300, 33°)

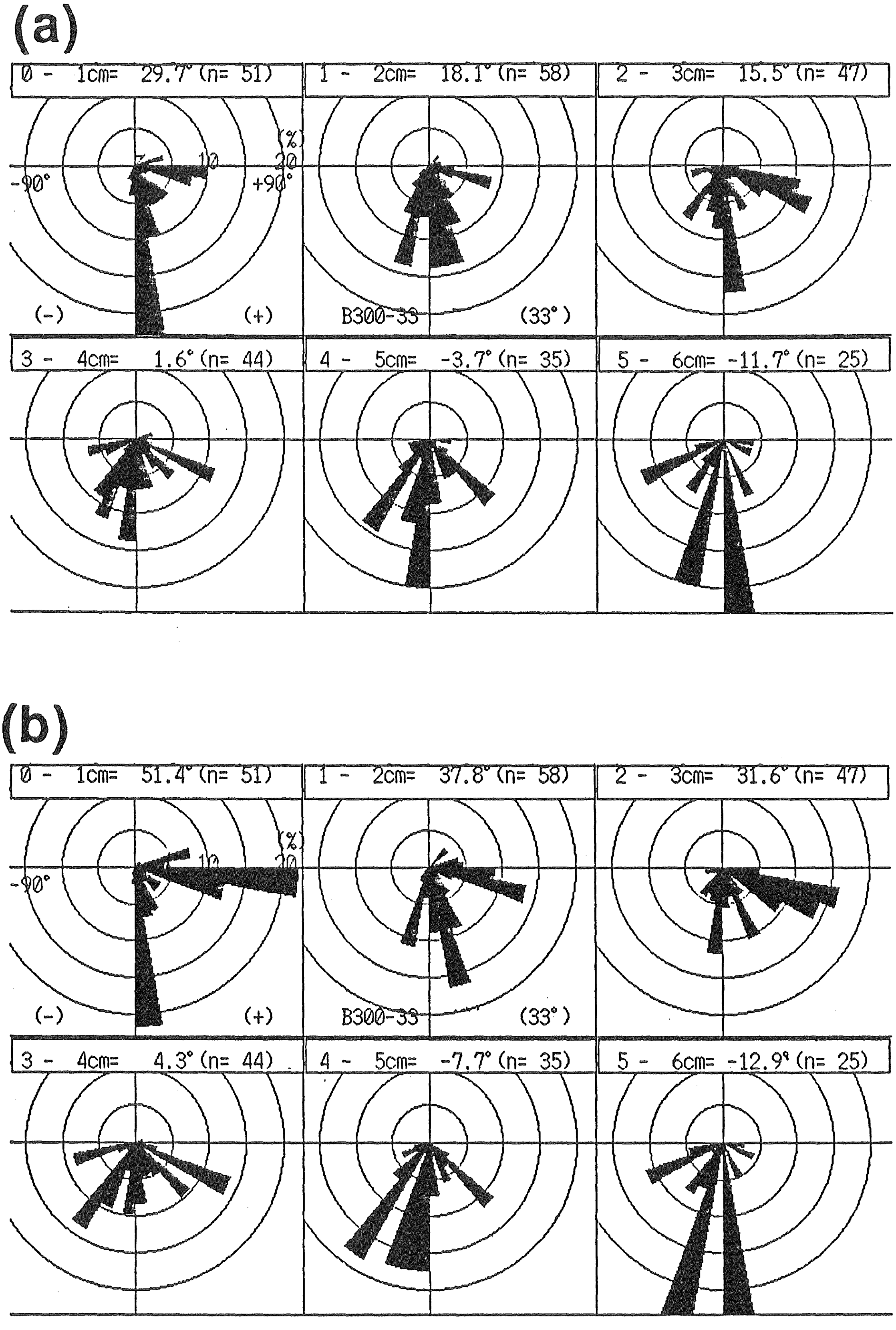

Fig.64 Frequency distribution of the total forces, the same result in Fig. 63, classified by 10 degrees in the rods with different depths: a; the number in direction of the vectors and b; the summation of their absolute value of the vectors.

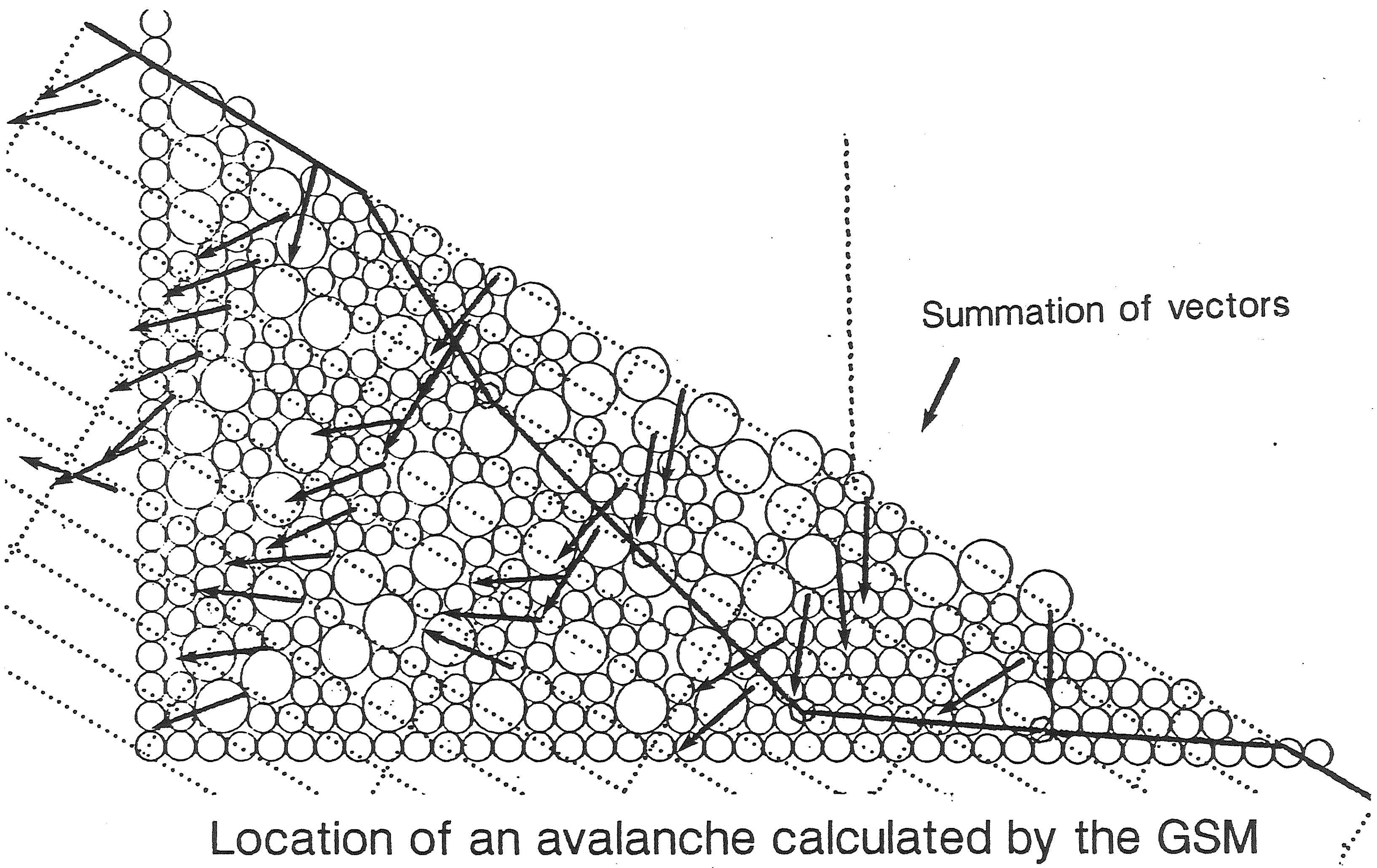

Fig.65 The summation of the total forces for a 1cm× 4cm area and the depth of the avalanche. Solid line indicates the basement of the avalanche

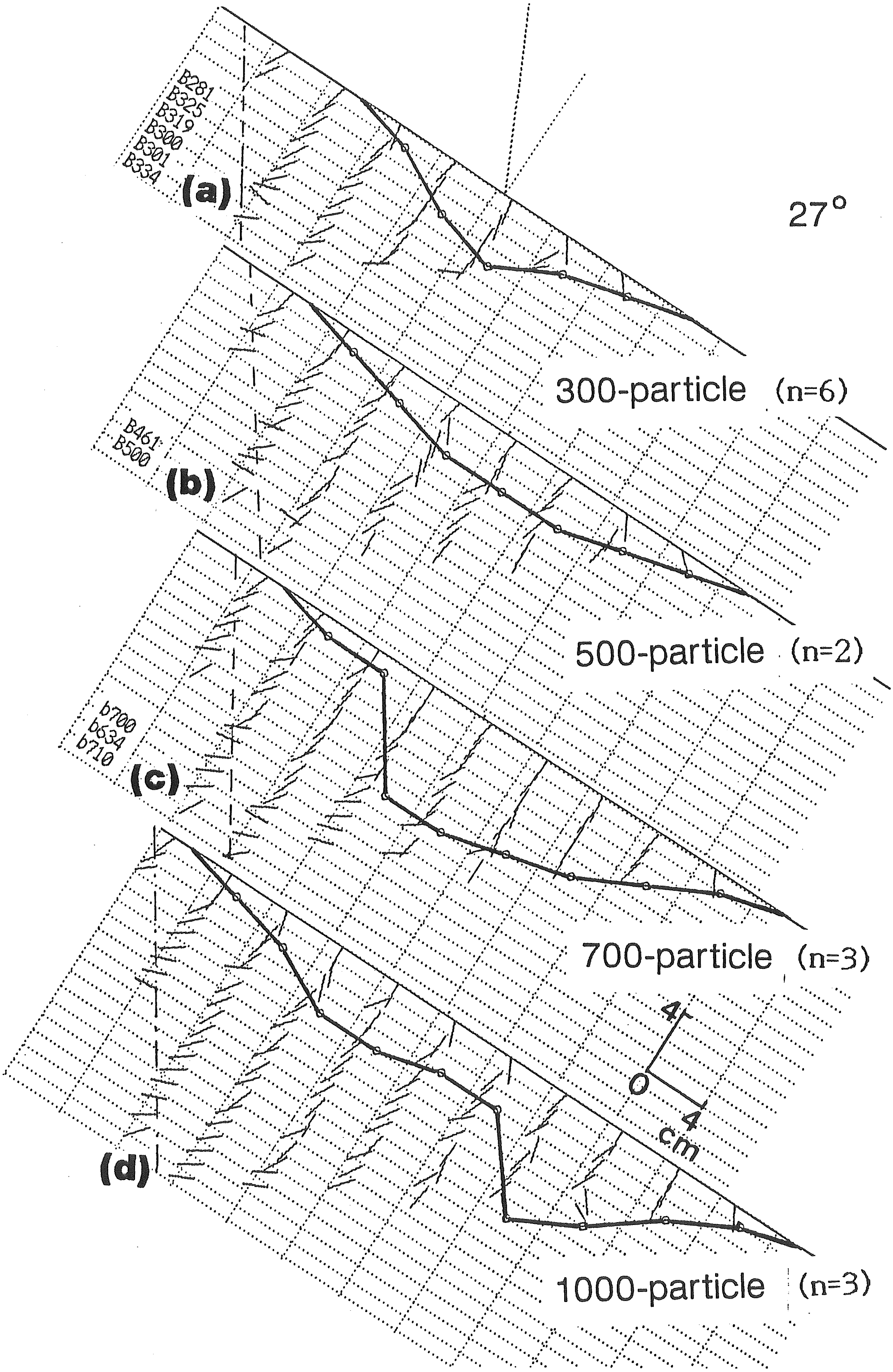

Fig.66 The prediction of the avalanching depth for several cases

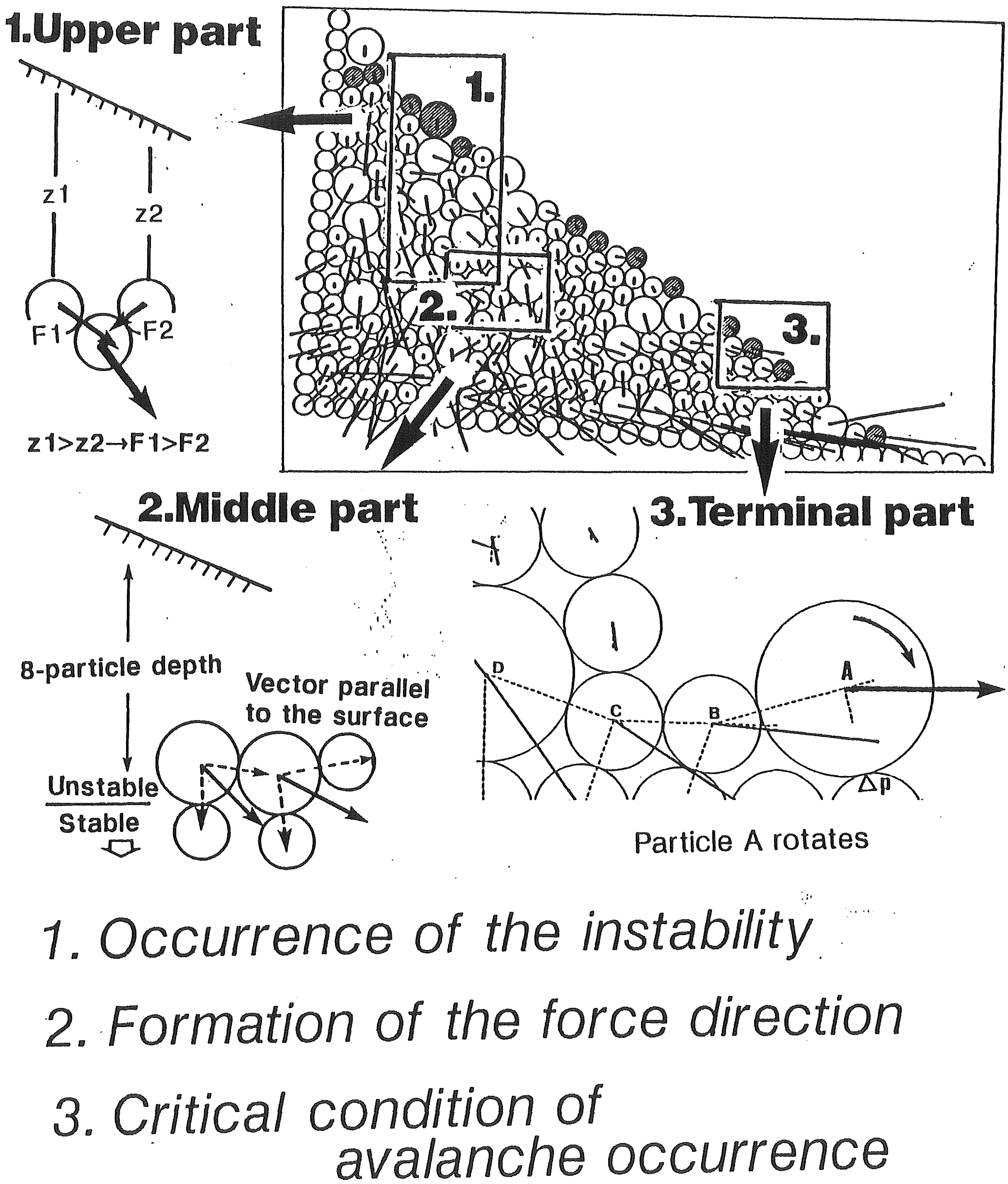

Fig.67 Schematic diagram of avalanching of granular materials

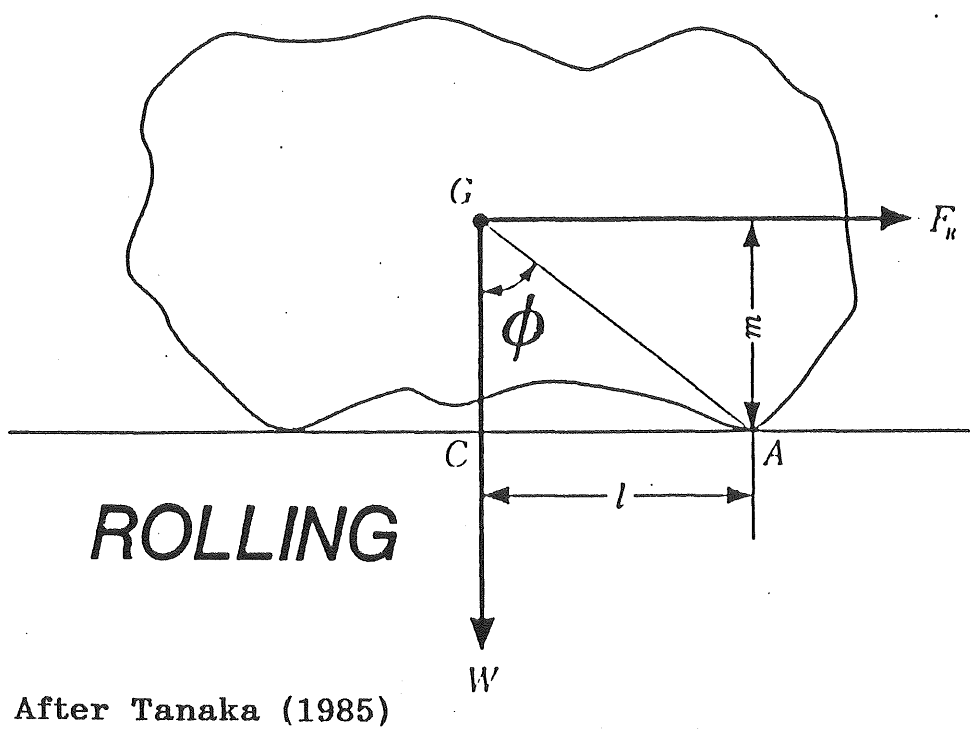

Fig.68 Model of rolling friction for an irregular-shaped material (after Tanaka, 1970)

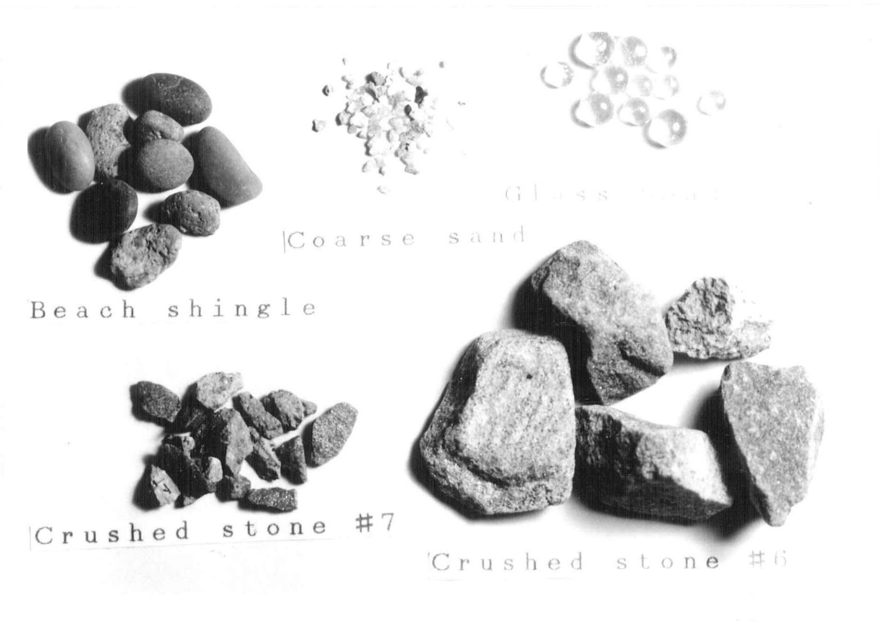

Fig.69 The materials used for the 3-dimensional rolling test

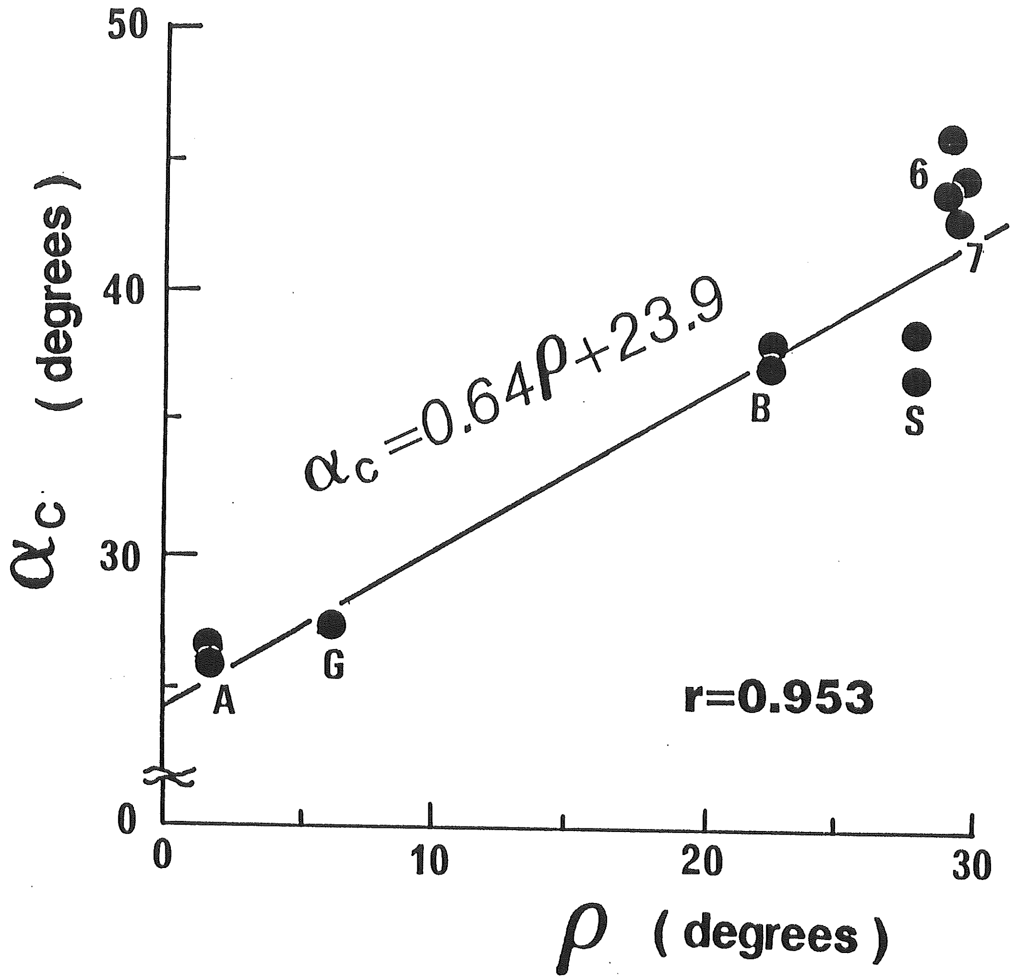

Fig.70 The relationship between angle of rolling friction, ρ, and critical angle of repose, α_c

A:*aluminum rods (φ5mm:φ9mm=3:2)*, G:*grass beads*, B:*beach shingle* 6:*crushed stone #6*, 7:*crushed stone #7*

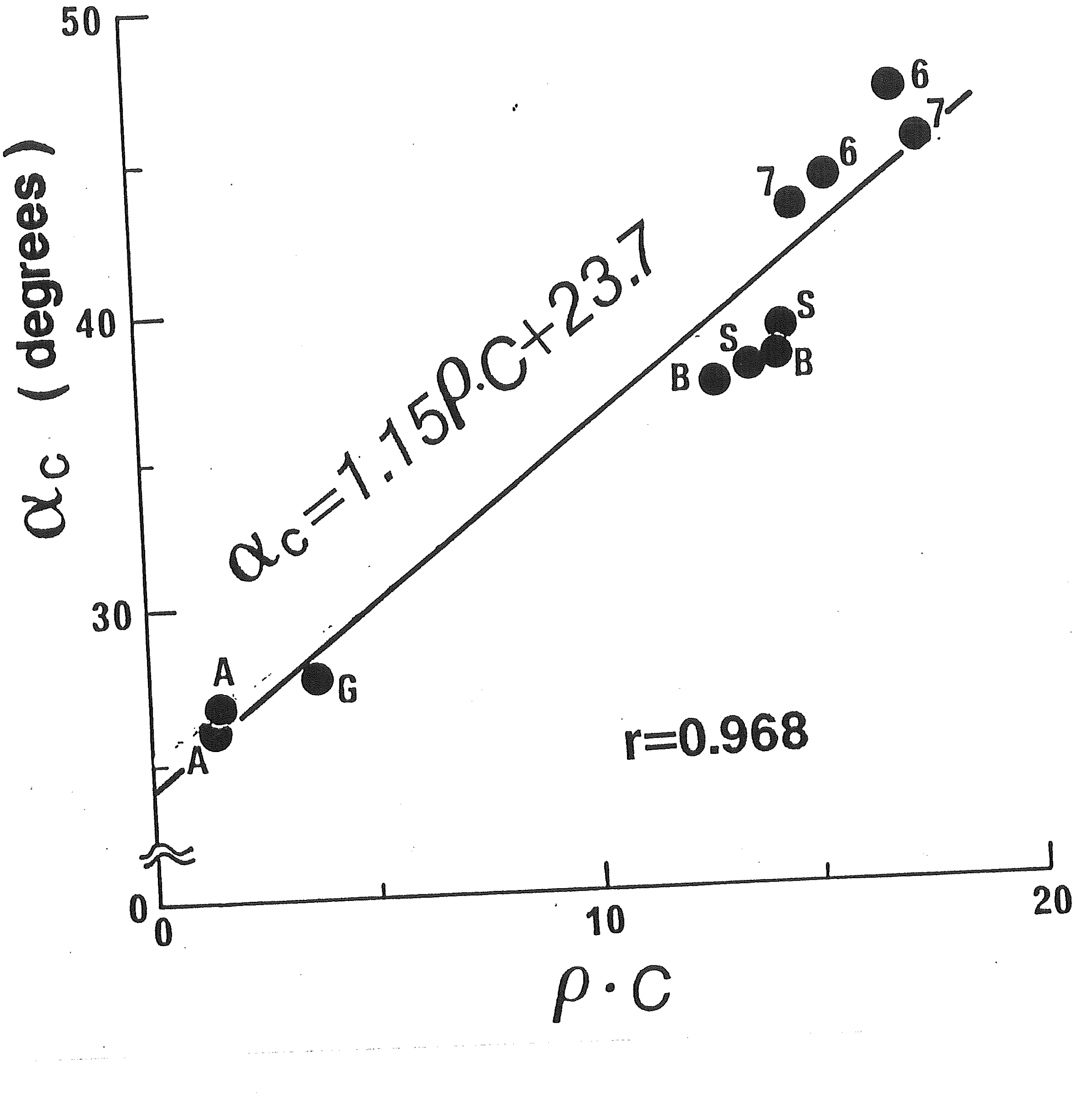

Fig.71 The relationship between $\rho \cdot C$ and critical angle of repose, α_c

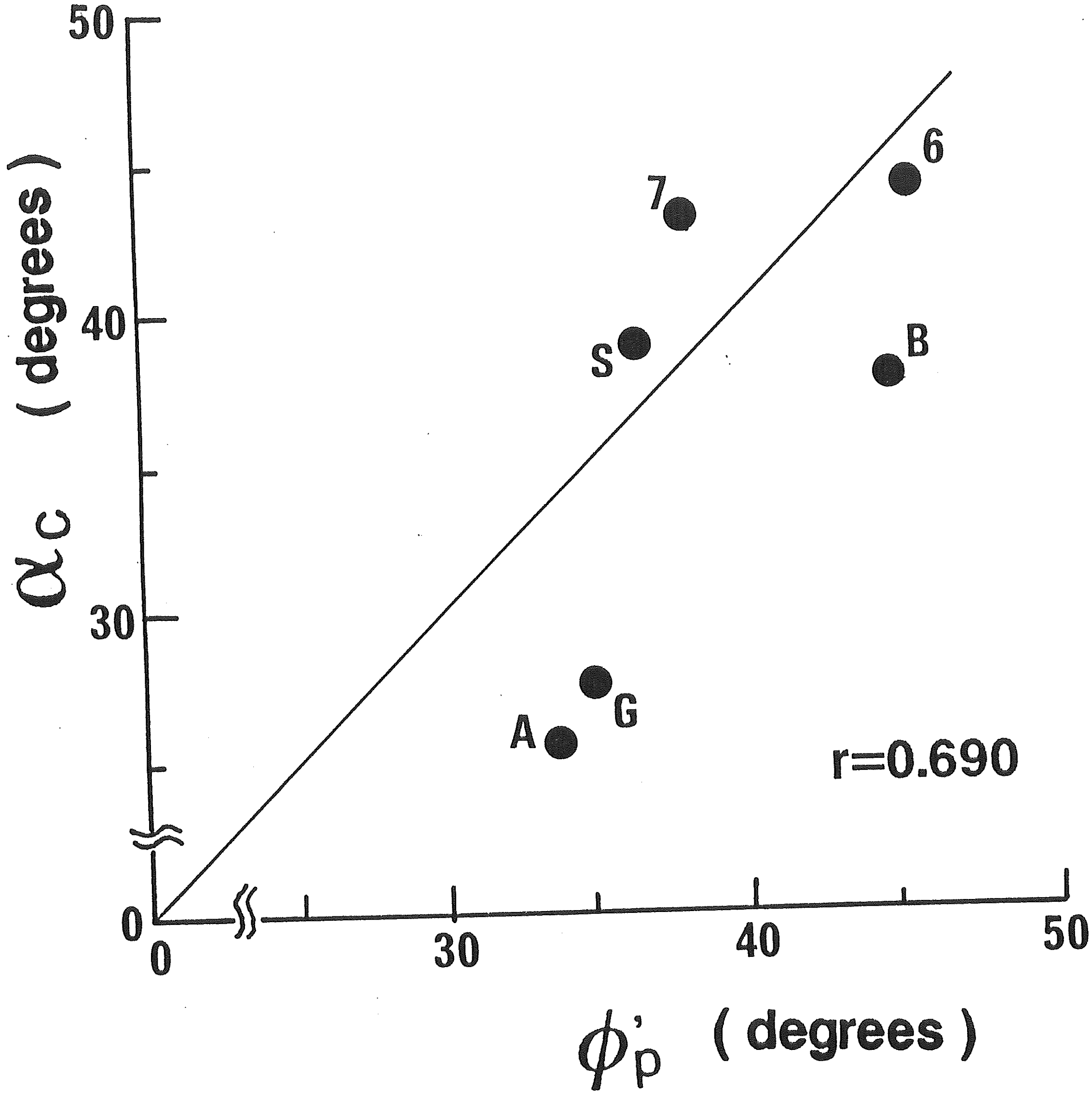

Fig.72 The relationship between angle of shearing resistance, ϕ'_p , and critical angle of repose, α_c , sand or gravel

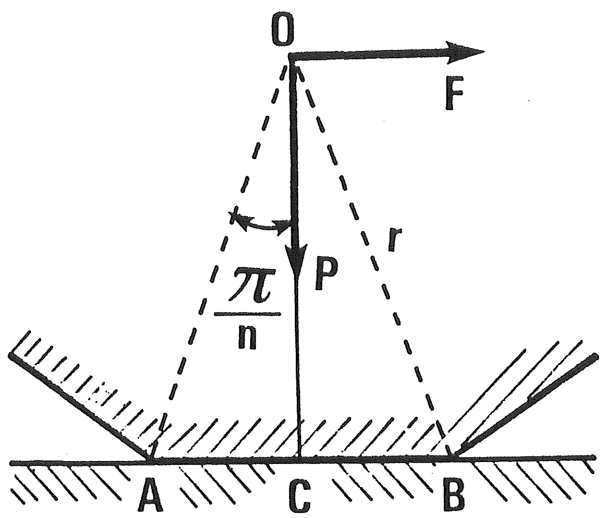

After Soda (1971)

Fig.A-1 The model of rolling friction (after Soda, 1971)

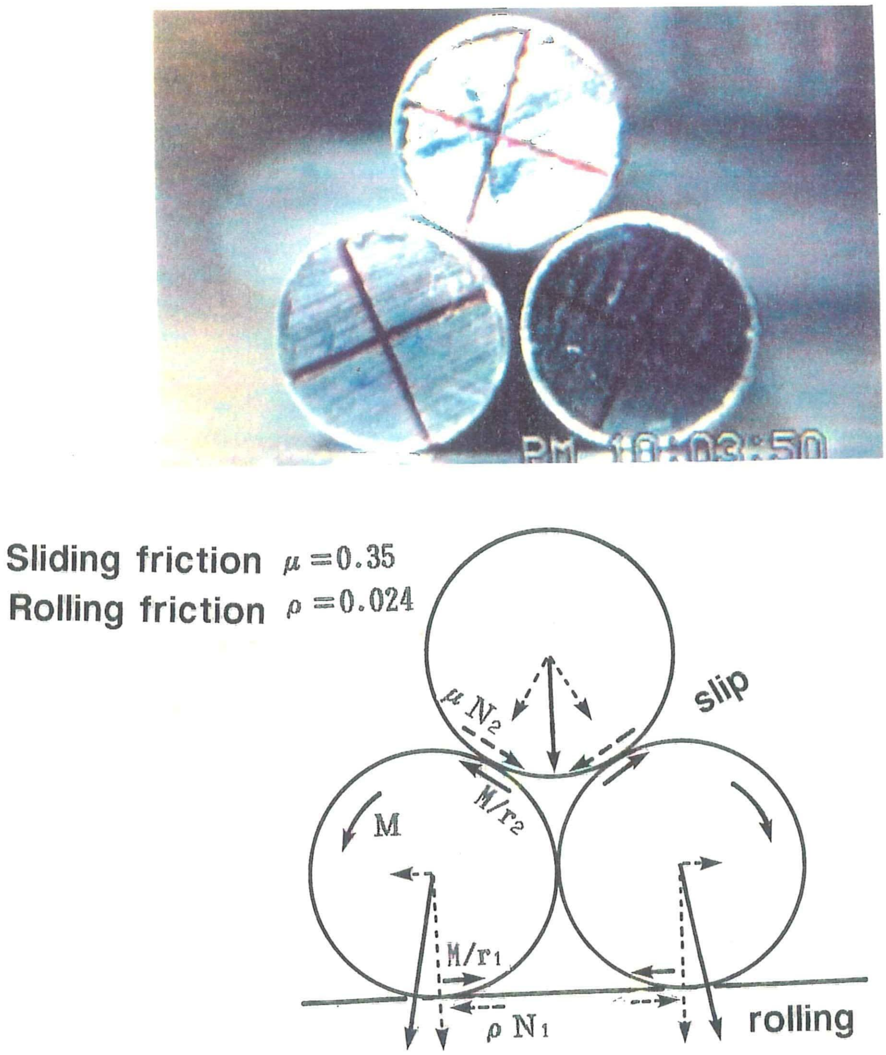

Fig.A-2 Comparison between the experimental result and the calculation of the GSM for the case of 3-rod piling

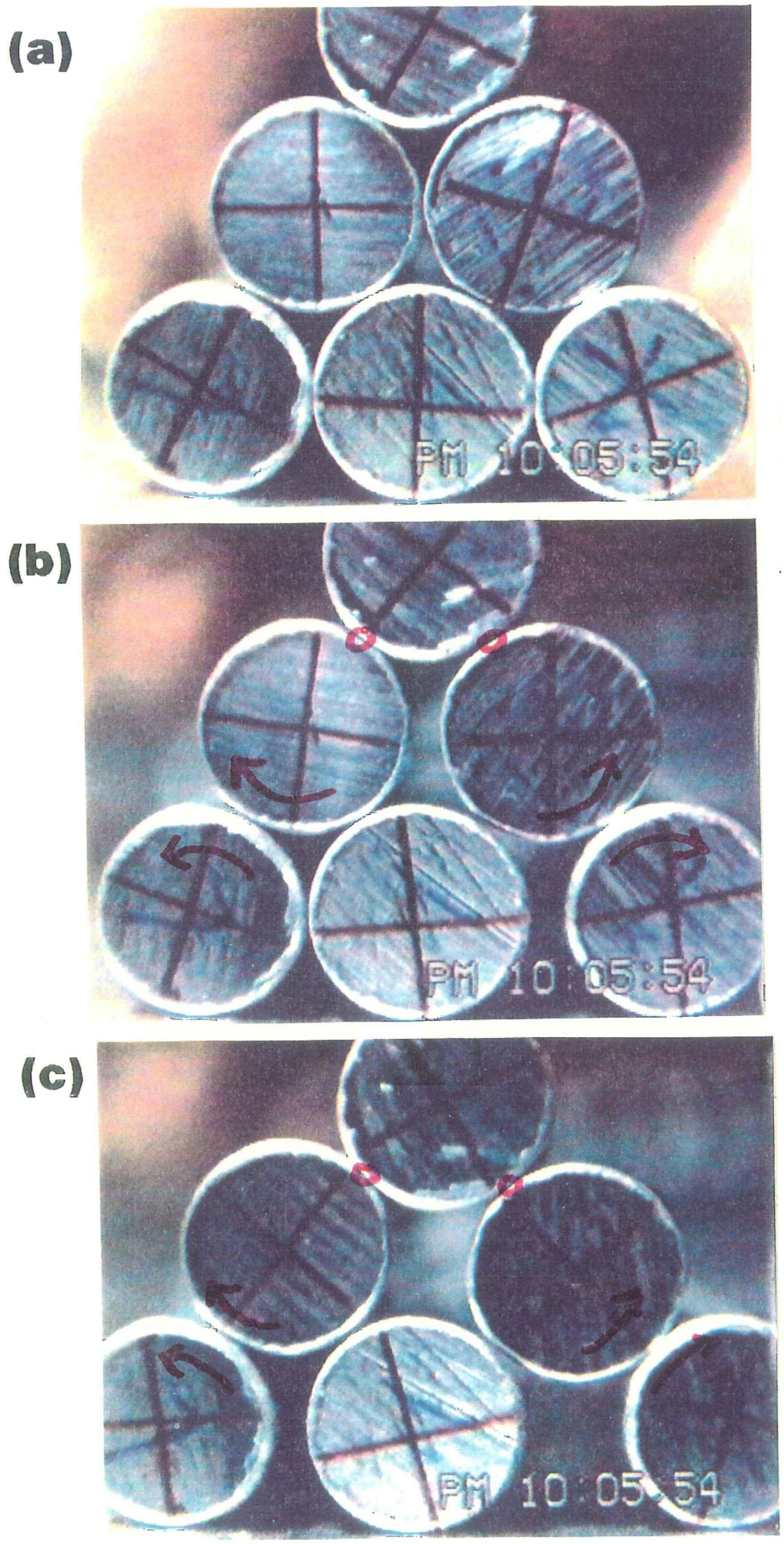

Fig.A-3 The collapse of the 6-rod piling (interval 1/30 sec)

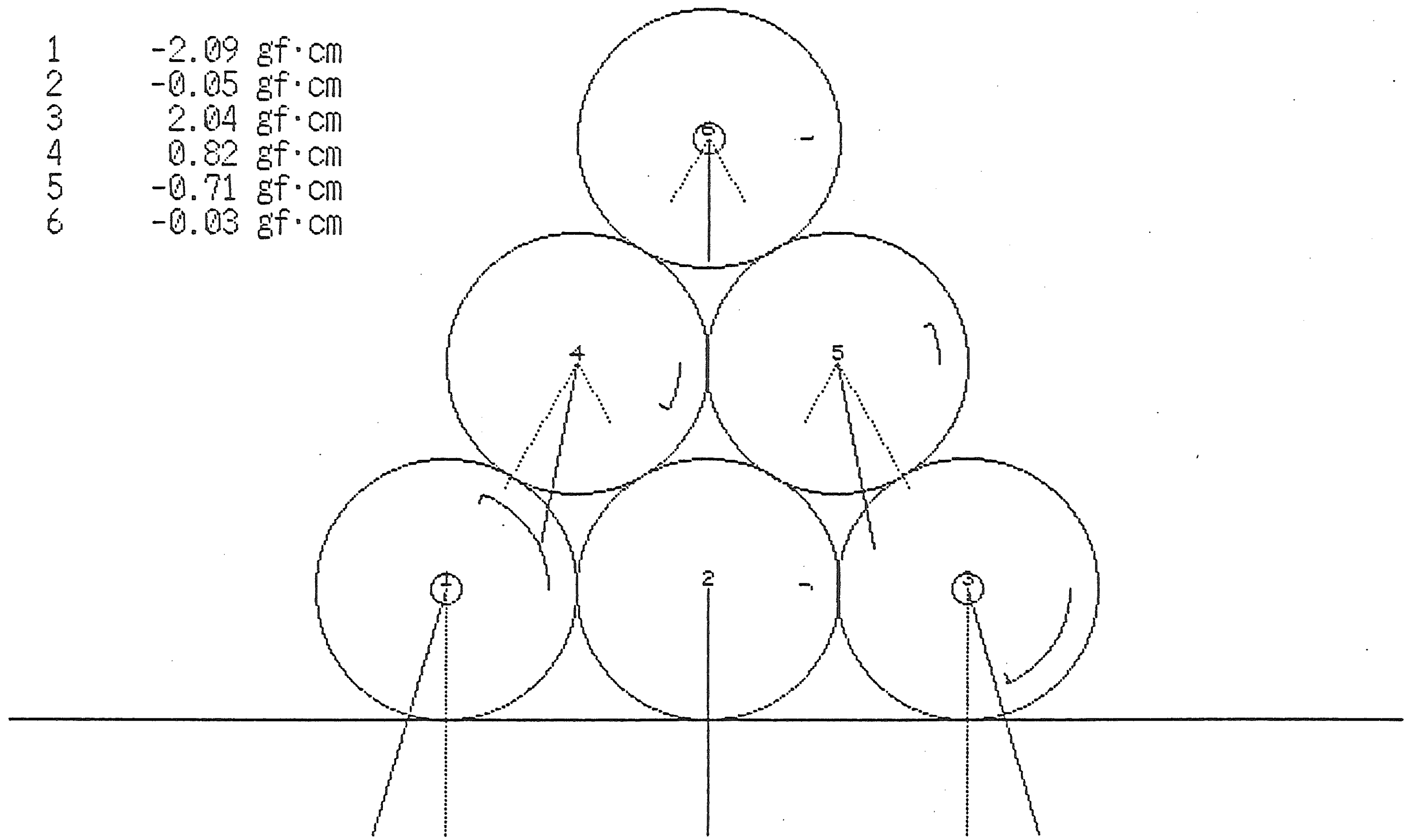

Fig.A-4 The result of the GSM calculation for 6-rod piling

(a)

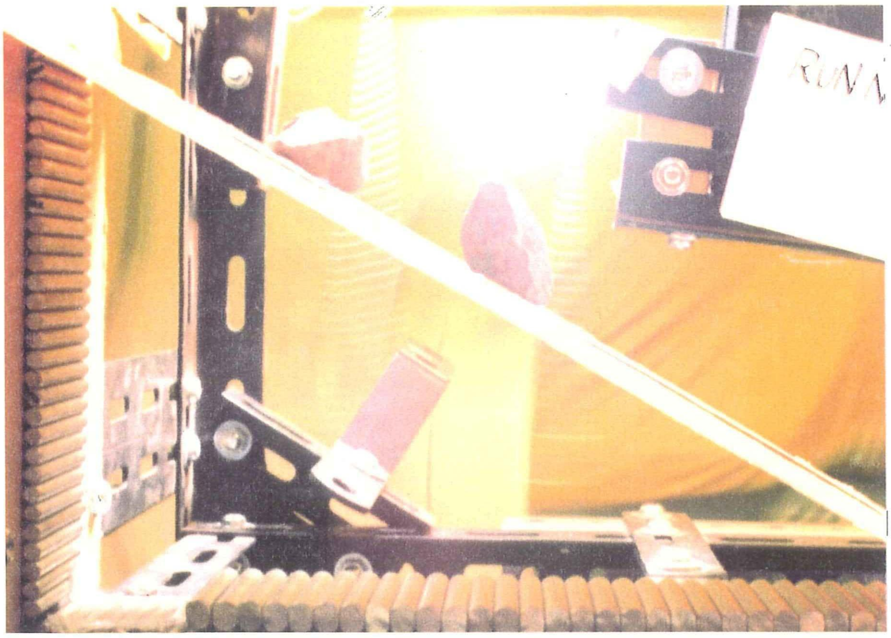

(b)

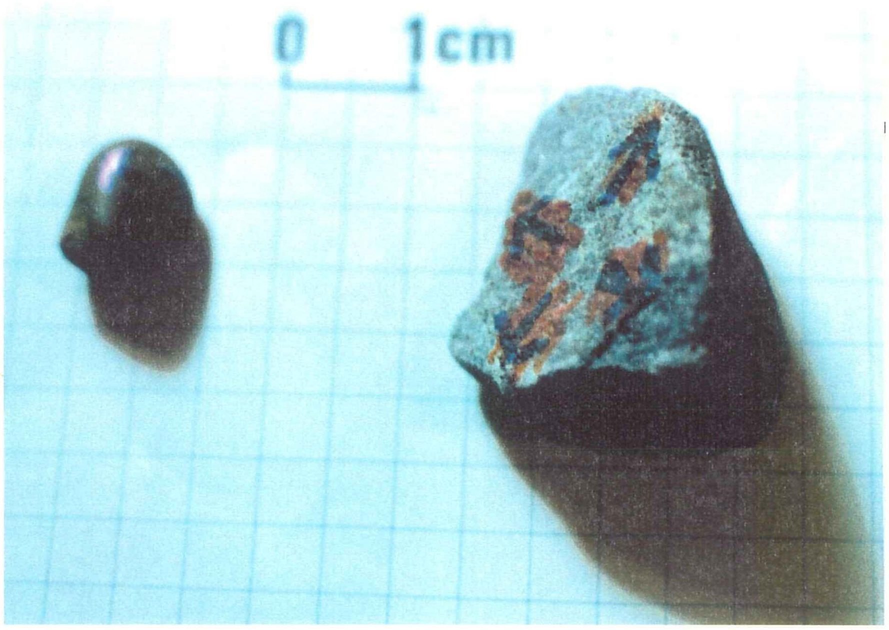

Fig.A-5 The measuring method for rolling friction of 3-dimensional materials (a; tilting apparatus, b; arrows on rock surface show the directions measuring the angle of rolling friction)

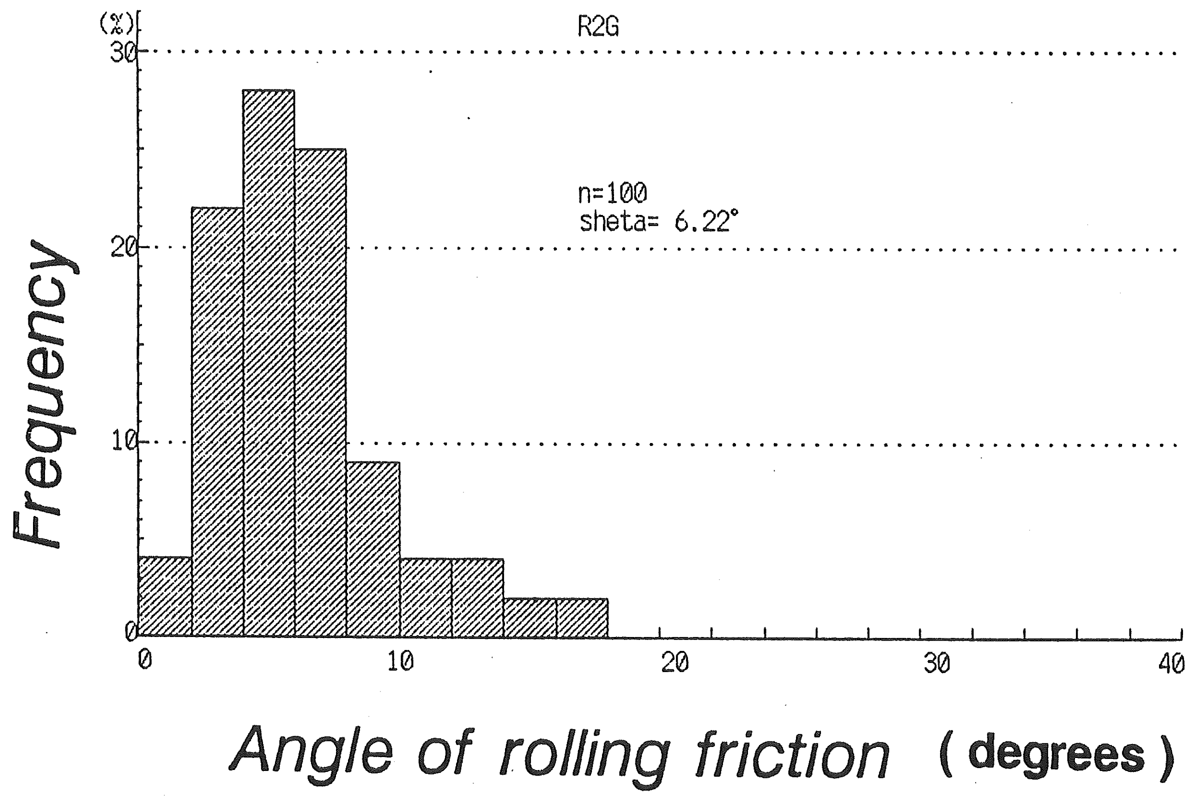

Fig.A-6 Histogram of the angle of rolling friction for glass beads

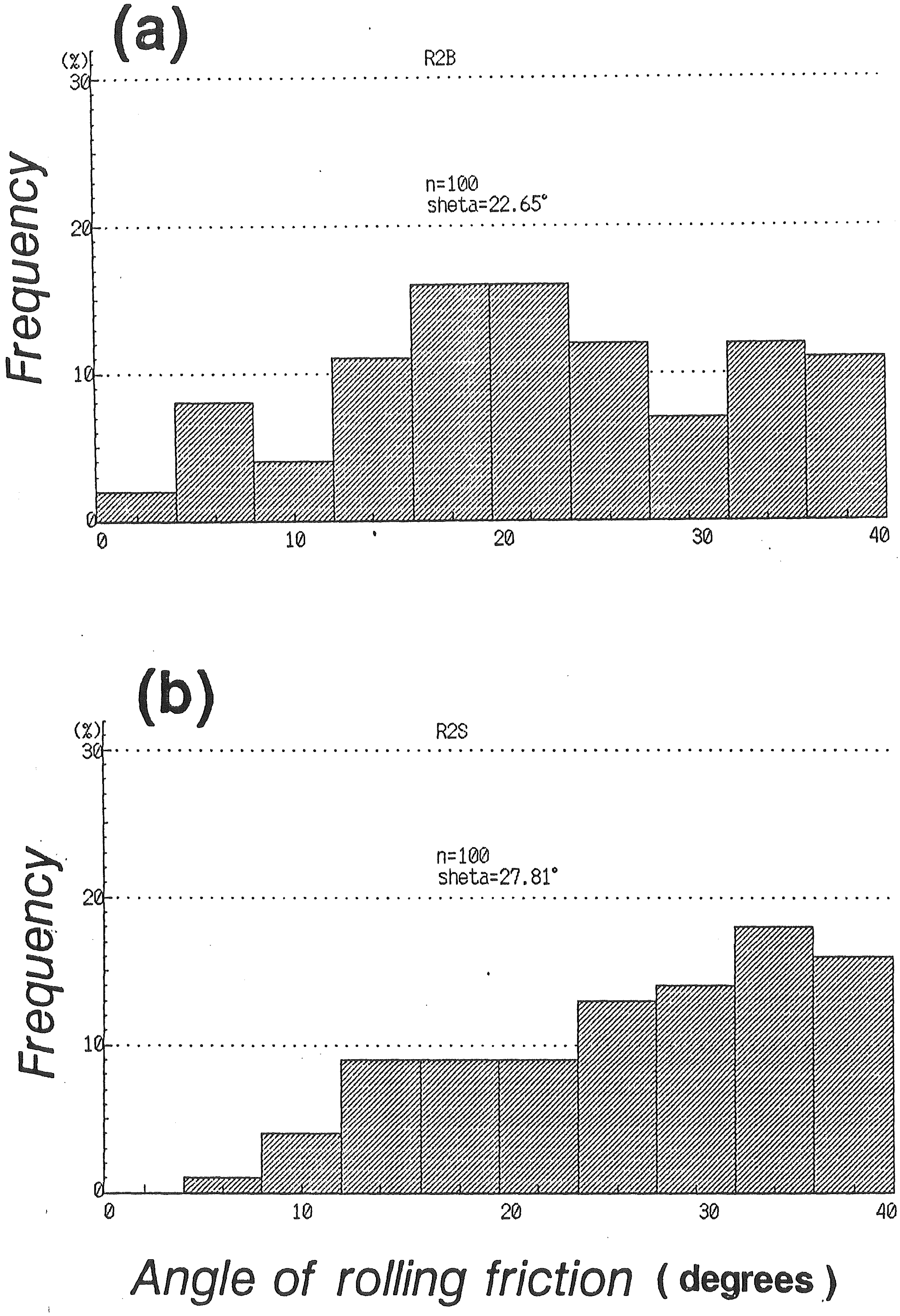

Fig.A-7 Histogram of the angle of rolling friction for two kinds of the 3-dimensional materials (a; beach shingle and b; coarse sand)

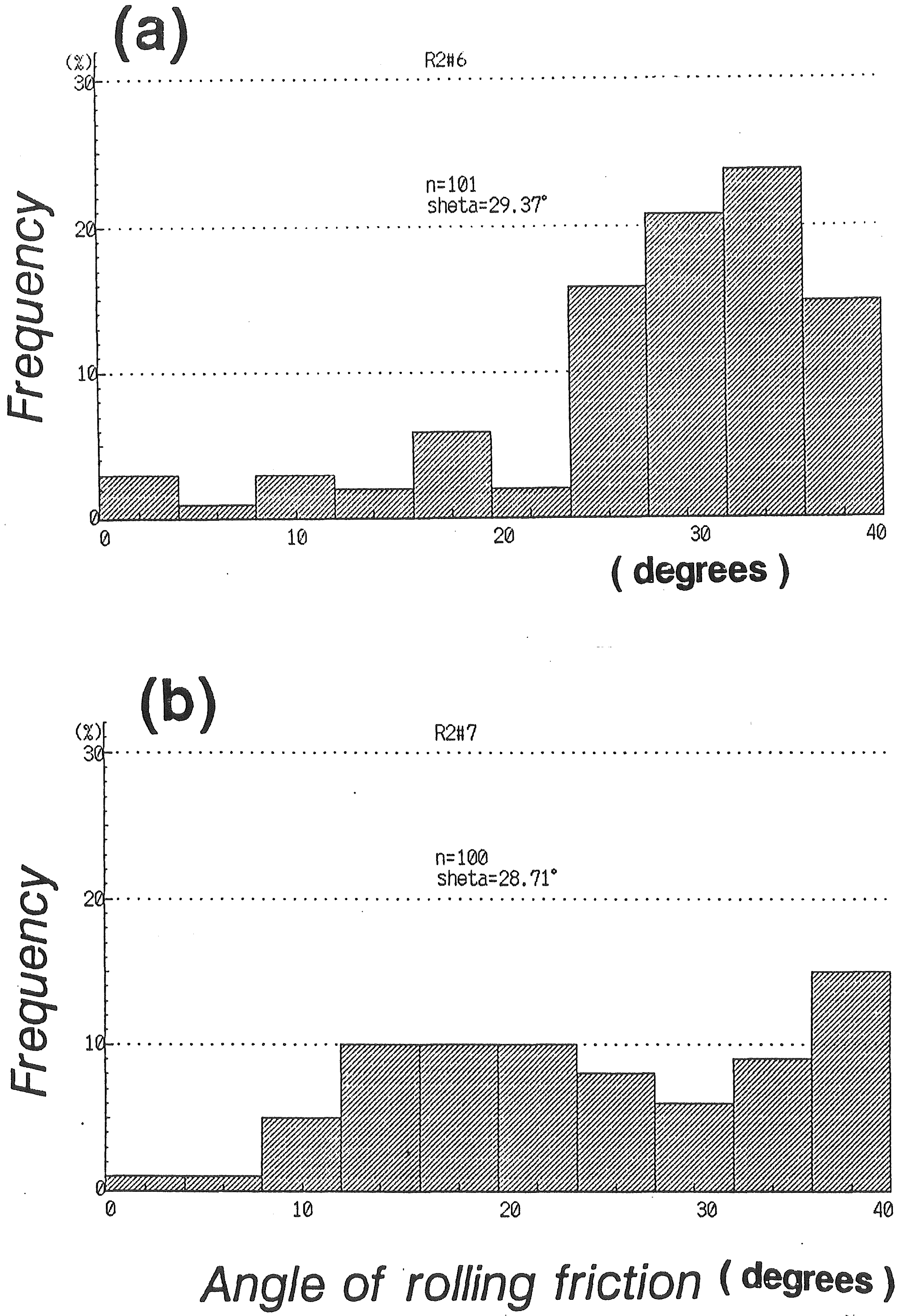

Fig.A-8 Histogram of the angle of rolling friction for two kinds of the 3-dimensional materials (a; crushed stone #6 and b; crushed stone #7)

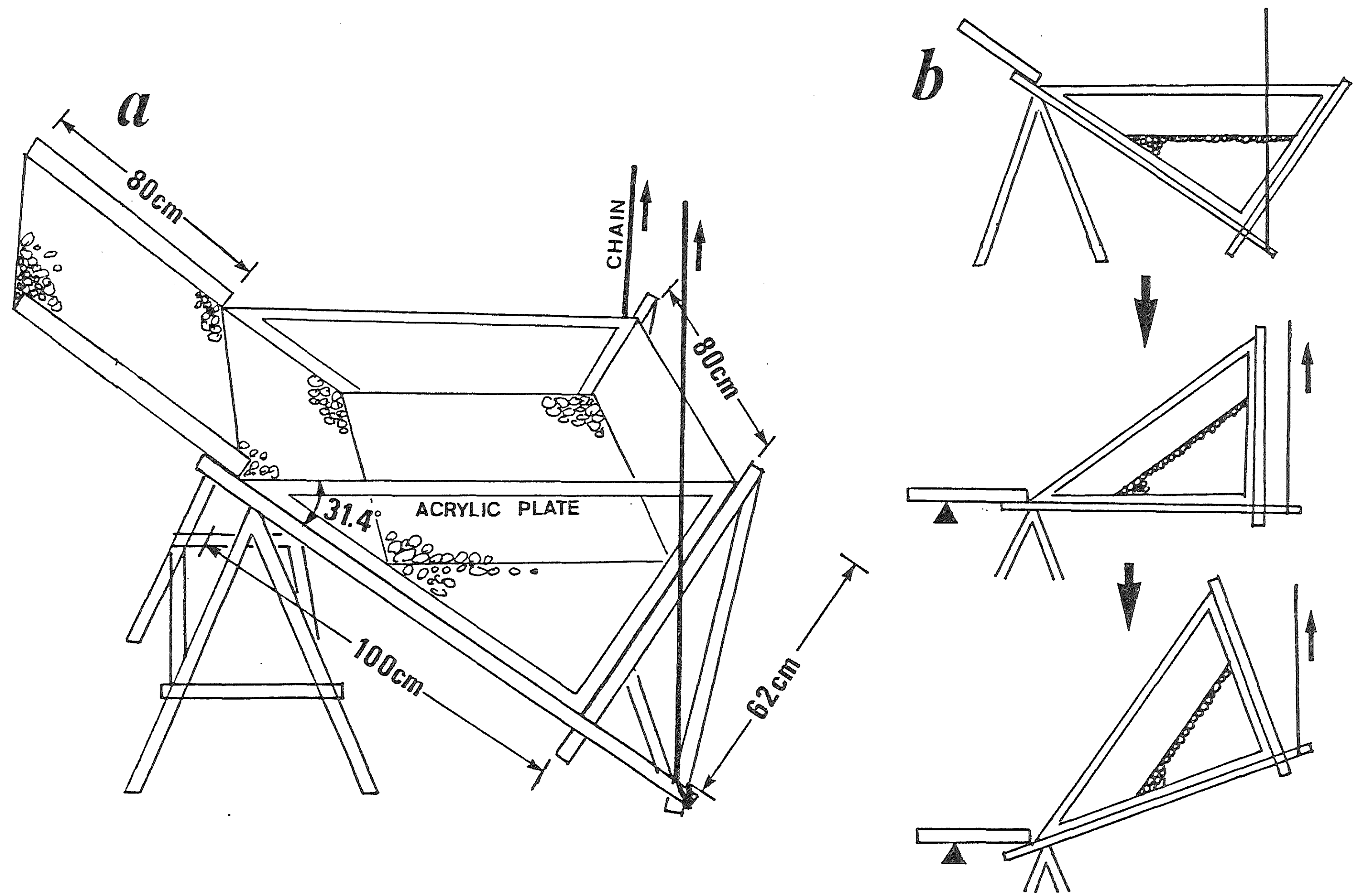

Fig.A-9 Large sized tilting-box for measuring the critical angle of repose for sand or gravel

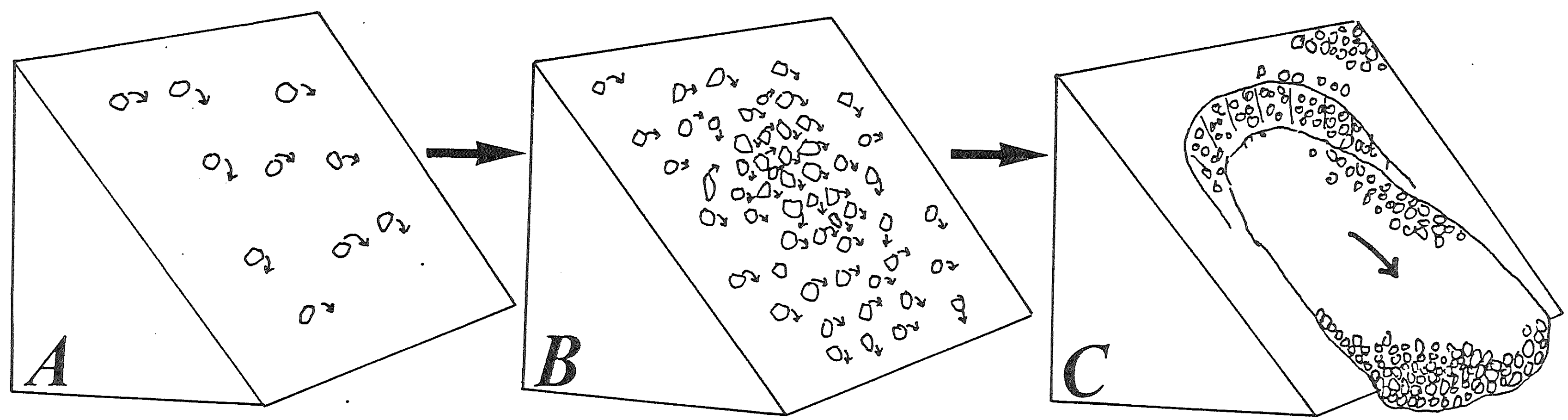

Fig.A-10 Idealized diagram of avalanching in the slope made of the 3-dimensional materials

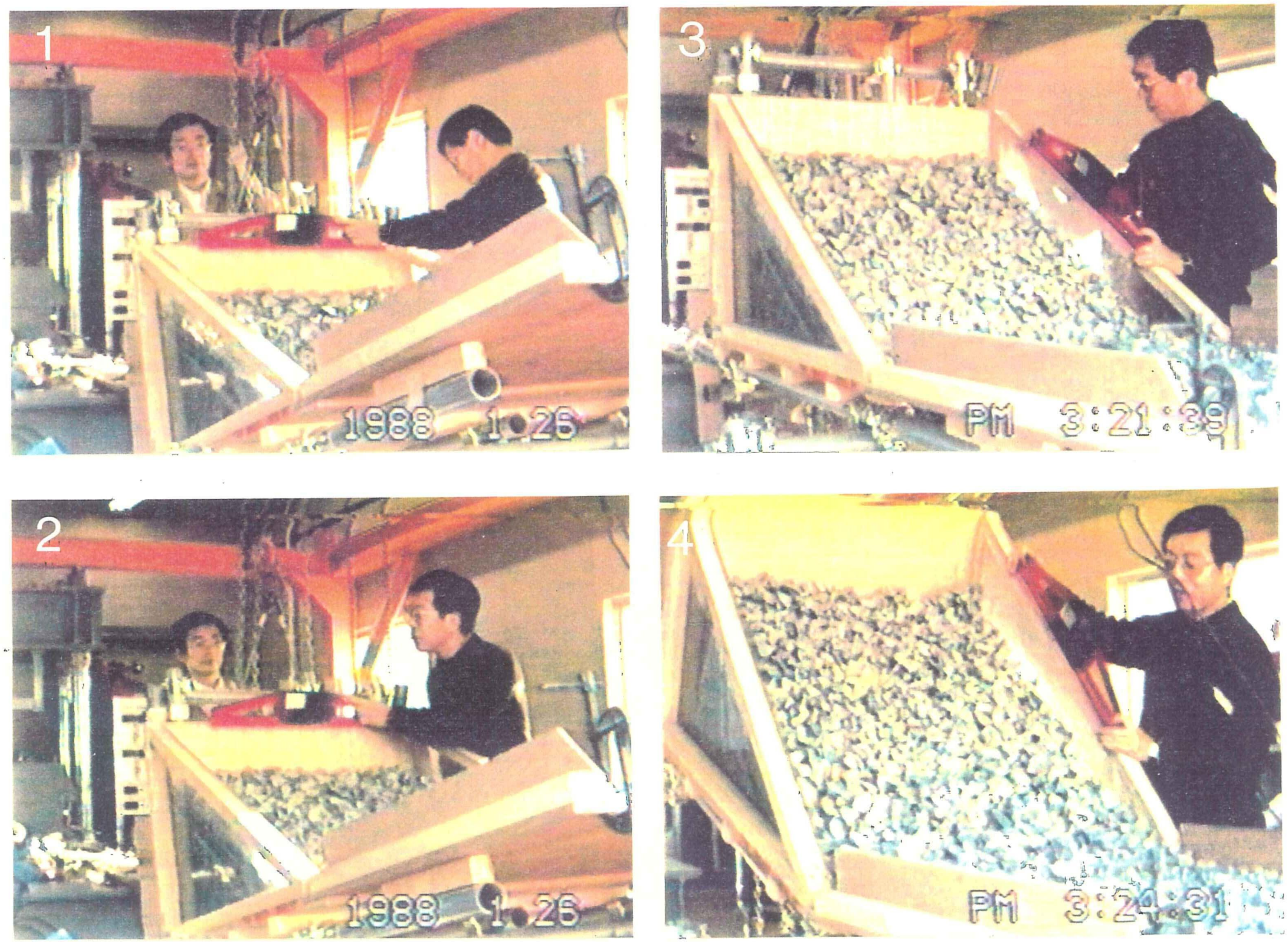

Fig.A-11 The change in slope angle during the tilting box experiment

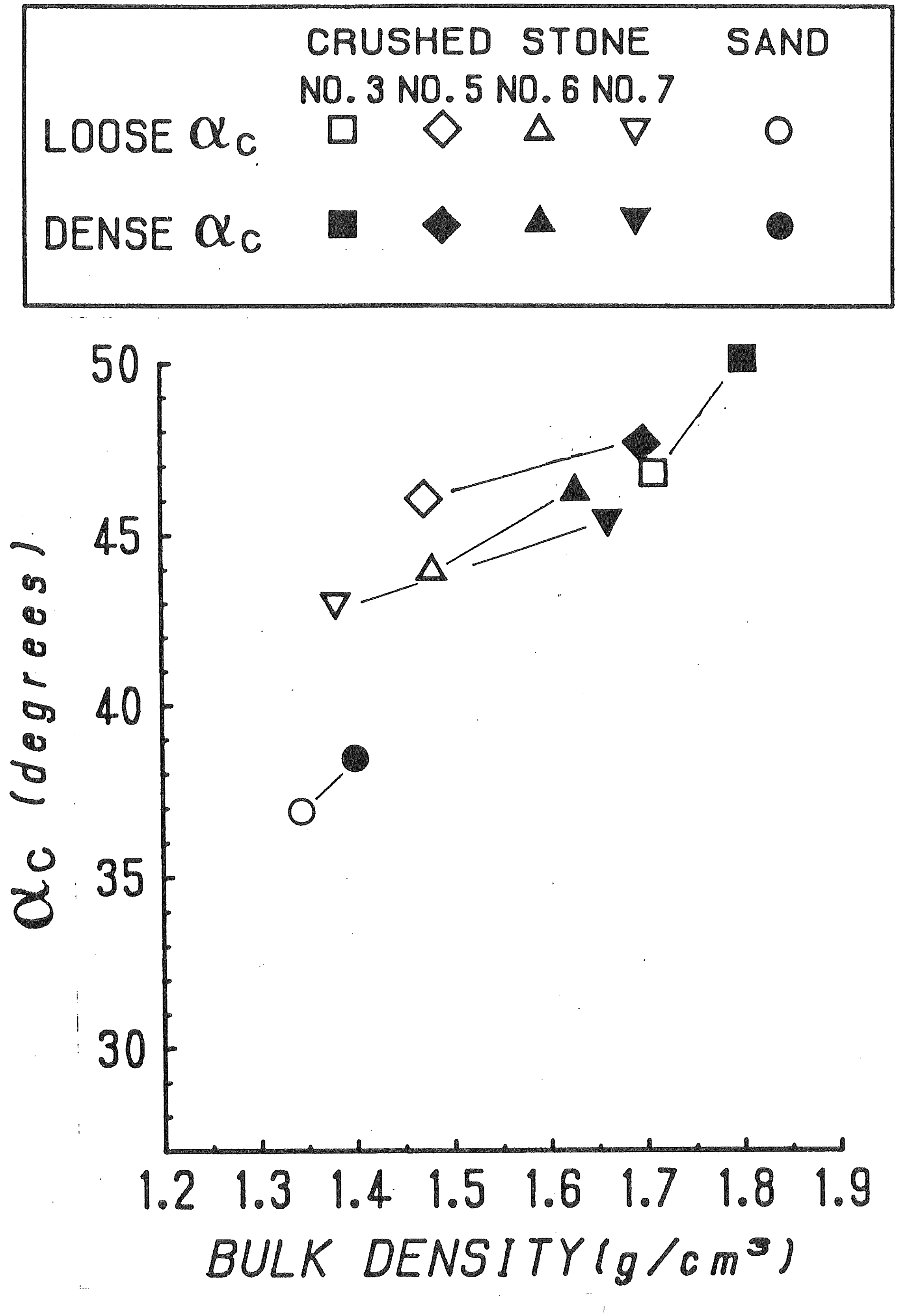

Fig.A-12 The relationship between bulk density and critical angle of repose, α_c, for the 3-dimensional materials

APPENDIX 1

RESULTS OF THE EXPERIMENTS

Table A-1.1 Results of the tilting box experiment

No.	Shape,diameter mixture ratio	porosity (g/cm^2)	slope length (l :cm)	α_c (degrees)
1	ϕ 5mm uniform	4.6	26.4	51.0
2	ϕ 5mm 1-layer	-----		28.0
3	ϕ 5mm 2-layer	-----		27.4
4	ϕ 5mm 1-layer	-----		28.0
5	*ditto*	-----		29.5
6	*ditto*	-----		29.4
7	*ditto*	-----		27.1
8	3 rods	-----		28.5
9	*ditto*	-----		26.9
10	*ditto*	-----		27.3
11	ϕ 5:ϕ 9=3:2	9.4	27.0	29.7
12	*ditto*	*ditto*	*ditto*	29.8
13	*ditto*	*ditto*	*ditto*	28.5
14	ϕ 5:ϕ 9=3:2	7.7	19.4	30.7
15	*ditto*	*ditto*	*ditto*	33.7
16	*ditto*	*ditto*	*ditto*	33.7
17	ϕ 1.6:ϕ 3=3:2	19.1	26.5	28.2
18	*ditto*	*ditto*	*ditto*	28.5
19	*ditto*	*ditto*	*ditto*	27.8
20	ellipsoidal mixed;random	6.5	26.7	33.3
21	*ditto* *ditto*	*ditto*	*ditto*	29.9
22	*ditto* *ditto*	*ditto*	*ditto*	30.8
23	*ditto* parallel to the bottom	8.0	26.8	33.0
24	*ditto* parallel to the slope	*ditto*	*ditto*	35.3
25	*ditto* vertical to the bottom	4.4	26.2	28.7

Table A-1.2 Results of the tilting-box experiment

No.	Shape, diameter mixture ratio		porosity (g/cm^2)	slope length $(l$:cm)	α_c (degrees)
26	square1 mixed*	random	6.8	26.4	37.5
28	ellipsoidal mixed	vertical	12.2	43.0	24.2
29	*ditto*	*ditto*	*ditto*	*ditto*	(26.9)
30	ϕ5mm:ϕ9mm=3:2	random	11.1	39.2	30.1
31	*ditto*	*ditto*	*ditto*	*ditto*	27.5
32	*ditto*	*ditto*	*ditto*	*ditto*	26.8
33	*ditto*	*ditto*	*ditto*	*ditto*	29.1 (24.7)
34	ellipsoidal mixed	vertical	12.3	41.0	24.7
35	ellipsoidal mixed	horizontal	*ditto*	*ditto*	28.5
36	*ditto*	*ditto*	10.1	39.2	26.3
37	ellipsoidal ϕ_m =8mm	vertical	11.8	35.6	24.3
38	*ditto*	horizontal2**	*ditto*	*ditto*	23.7
39	*ditto*	horizontal2 [dense]	2.6	34.2	(48.0) bottom?
40	*ditto*	vertical2***	14.3	40.3	30.7
41	*ditto*	horizontal2	15.1	40.9	33.5 (29.0)
47	ϕ5mm uniform	regular	9.5	34.0	56.5
48	ϕ5mm:ϕ9mm=20:1	random	13.7	34.7	30.5
49	*ditto*	*ditto*	*ditto*	*ditto*	27.5
50	ϕ5mm:ϕ9mm=10:1	*ditto*	13.7	35.1	28.0

* square rods mixed: 10*10,6*6,6*3,3*3 mixture ratio ; 1:1:1:1

** vertical2: vertical to the plumb line.

***horizontal2: horizontal to the bottom of the box.

Table A-1.3 Results of the tilting-box experiment

No.	Shape,diameter mixture ratio		porosity (g/cm^2)	slope length (l :cm)	α_c (degrees)
51	ϕ5mm:ϕ9mm=10:1	random	13.7	35.1	32.0
52	ϕ5mm:ϕ9mm=8:2	*ditto*	15.8	35.4	27.5
53	*ditto*	*ditto*	*ditto*	*ditto*	25.1
54	ϕ5mm:ϕ9mm=7:3	*ditto*	18.0	35.6	25.7
55	*ditto*	*ditto*	*ditto*	*ditto*	27.0
56	ϕ5mm:ϕ9mm=5:5	*ditto*	17.2	35.8	30.5
57	*ditto*	*ditto*	*ditto*	*ditto*	26.5
58	ϕ5mm:ϕ9mm=3:7	*ditto*	17.9	36.4	27.7
59	*ditto*	*ditto*	*ditto*	*ditto*	26.5
60	ϕ5mm:ϕ9mm=2:8	*ditto*	16.6	35.9	25.5
61	*ditto*	*ditto*	*ditto*	*ditto*	27.7
62	ϕ5mm:ϕ9mm=1:10	*ditto*	14.3	35.7	27.5
63	*ditto*	*ditto*	*ditto*	*ditto*	25.7
64	ϕ5mm:ϕ9mm=1:20	*ditto*	16.6	35.9	32.0
65	ϕ9mm	regular	12.2	35.0	36.0
66	ϕ9mm	regular	12.2	35.4	52.5
67	ϕ3mm:ϕ5mm=3:2	random	13.9	8.7	33.0
68	*ditto*	*ditto*	*ditto*	*ditto*	28.0
69	*ditto*	*ditto*	*ditto*	*ditto*	33.0
70	ϕ3mm:ϕ5mm=3:2	*ditto*	14.8	12.3	31.0
71	*ditto*	*ditto*	*ditto*	*ditto*	28.5
72	*ditto*	*ditto*	*ditto*	*ditto*	33.0
73	ϕ3mm:ϕ5mm=3:2	*ditto*	13.2	15.8	30.0
74	*ditto*	*ditto*	*ditto*	*ditto*	27.5
75	*ditto*	*ditto*	*ditto*	*ditto*	34.0

Table A-1.4 Results of the tilting-box experiment

No.	Shape, diameter mixture ratio		porosity (g/cm^2)	slope length (l :cm)	α_c (degrees)
76	φ3mm:φ5mm=3:2	*ditto*	17.9	19.6	29.0
77	*ditto*	*ditto*	*ditto*	*ditto*	25.5
78	*ditto*	*ditto*	*ditto*	*ditto*	28.0
79	φ3mm:φ5mm=3:2	*ditto*	19.6	23.4	25.0
80	*ditto*	*ditto*	*ditto*	*ditto*	28.5
81	*ditto*	*ditto*	*ditto*	*ditto*	27.1
82	φ3mm:φ5mm=3:2	*ditto*	21.9	27.7	30.0
83	*ditto*	*ditto*	*ditto*	*ditto*	27.5
84	*ditto*	*ditto*	*ditto*	*ditto*	24.0
85	*ditto*	*ditto*	21.4	27.7	28.0
86	φ3mm:φ5mm=3:2	*ditto*	17.4	30.3	23.5
87	*ditto*	*ditto*	*ditto*	*ditto*	28.0
88	*ditto*	*ditto*	*ditto*	*ditto*	26.0
89	φ3mm:φ5mm=3:2	random	18.2	37.9	27.0
90	*ditto*	*ditto*	*ditto*	*ditto*	23.1
91	*ditto*	*ditto*	*ditto*	*ditto*	24.4
93	φ5mm:φ9mm=3:2	*ditto*	21.7	37.4	27.0
94	*ditto*	*ditto*	*ditto*	*ditto*	22.0
95	*ditto*	*ditto*	*ditto*	*ditto*	24.5
96	*ditto*	*ditto*	*ditto*	*ditto*	26.8
97	*ditto*	*ditto*	*ditto*	*ditto*	28.1
98	φ5mm:φ9mm=3:2	random	18.2	39.3	27.3
99	*ditto*	*ditto*	*ditto*	*ditto*	27.5
100	*ditto*	*ditto*	*ditto*	*ditto*	28.0

Table A-1.5 Results of the tilting-box experiment

No.	Shape, diameter mixture ratio		porosity (g/cm^2)	slope length (l :cm)	α_c (degrees)
101	φ5mm:φ9mm=3:2	random	18.2	39.3	28.0
102	*ditto*	*ditto*	*ditto*	*ditto*	27.0
103	*ditto*	*ditto*	*ditto*	*ditto*	27.5
104	*ditto*	*ditto*	*ditto*	*ditto*	26.6
105	*ditto*	*ditto*	*ditto*	*ditto*	27.5
106	*ditto*	*ditto*	*ditto*	*ditto*	28.5
107	*ditto*	*ditto*	*ditto*	*ditto*	24.8
108	*ditto*	*ditto*	*ditto*	*ditto*	27.0
109	*ditto*	*ditto*	*ditto*	*ditto*	25.3
110	*ditto*	*ditto*	*ditto*	*ditto*	27.0
111	φ5mm:φ9mm=3:2	random	18.2	39.3	27.8
112	*ditto*	*ditto*	*ditto*	*ditto*	23.3
113	*ditto*	*ditto*	*ditto*	*ditto*	25.2
114	*ditto*	*ditto*	*ditto*	*ditto*	24.6
115	*ditto*	*ditto*	*ditto*	*ditto*	23.9
116	*ditto*	*ditto*	*ditto*	*ditto*	28.2
117	*ditto*	*ditto*	*ditto*	*ditto*	26.2
118	φ3mm:φ5mm=3:2	*ditto*	19.2	44.1	22.6
119	*ditto*	*ditto*	*ditto*	*ditto*	23.0
120	*ditto*	*ditto*	*ditto*	*ditto*	22.0
121	*ditto*	*ditto*	*ditto*	*ditto*	22.5
122	φ3mm:φ5mm=3:2	*ditto*	21.0	47.7	22.8
123	*ditto*	*ditto*	*ditto*	*ditto*	21.7
124	*ditto*	*ditto*	*ditto*	*ditto*	24.0
125	*ditto*	*ditto*	*ditto*	*ditto*	22.0

Table A-1.6 Results of the tilting-box experiment

No.	Shape, diameter mixture ratio		porosity (g/cm²)	slope length (l :cm)	α_c (degrees)
126	ϕ3mm:ϕ5mm=3:2	*ditto*	18.1	40.7	25.4
127	*ditto*	*ditto*	*ditto*	*ditto*	22.6
128	*ditto*	*ditto*	*ditto*	*ditto*	22.4
129	*ditto*	*ditto*	*ditto*	*ditto*	24.4
130	*ditto*	*ditto*	*ditto*	*ditto*	21.8
131	octagonal ϕ_m =8mm	dense	0.0	24.3	56.1
132	*ditto* (*A*)	*ditto*	*ditto*	*ditto*	56.2
133	*ditto*	*ditto*	*ditto*	*ditto*	56.2
134	*ditto*	*ditto*	*ditto*	*ditto*	54.2
135	*ditto*	*ditto*	*ditto*	*ditto*	56.6
136	square ϕ_m =5mm	open	0.0	33.3	30.0
137	*ditto* (*B*)	*ditto*	*ditto*	*ditto*	29.5
138	*ditto*	*ditto*	*ditto*	*ditto*	30.0
141	rectangle 6*9mm	horizontal	0.0	27.5	33.0
142	*ditto* (*C*)	*ditto*	*ditto*	*ditto*	33.8
145	*ditto*	*ditto*	*ditto*	*ditto*	31.8
146	rectangle 6*9mm	vertical	0.0	27.5	32.0
147	*ditto*	*ditto*	*ditto*	*ditto*	32.0
148	*ditto*	*ditto*	*ditto*	*ditto*	31.7

Table A-1.7 Results of the tilting-box experiment

No.	Shape, diameter mixture ratio		porosity (%)	slope length (l :cm)	α_c (degrees)
151	*A,B,C* mixed 1:1:1	random	14.9	38.1	30.0
152	*ditto*	*ditto*	*ditto*	*ditto*	30.5
156	*ditto*	*ditto*	*ditto*	*ditto*	37.0
157	*el2* ϕ_m =8mm(dense)	horizontal	6.7	38.0	46.0
158	*el2* ϕ_m =8mm	horizontal	17.0	41.3	28.5
159	*ditto*	*ditto*	*ditto*	*ditto*	27.5
160	*ditto*	*ditto*	*ditto*	*ditto*	27.5
161	*el2* ϕ_m =8mm(dense)	horizontal	6.7	38.0	40.5
162	*el2* ϕ_m =8mm	vertical	7.9	39.8	25.0
163	*ditto*	*ditto*	*ditto*	*ditto*	25.5
164	*el2* ϕ_m =8mm(dense)	vertical	1.1	38.6	45.0
165	*ditto*	*ditto*	*ditto*	*ditto*	46.0
166	*ditto*	*ditto*	*ditto*	*ditto*	46.0
167	*el2* ϕ_m =8mm	vertical	7.9	39.8	22.0
168	*el2* mixed random	vertical	18.8	39.1	23.8
169	*ditto*	*ditto*	*ditto*	*ditto*	27.0
170	*ditto*	*ditto*	*ditto*	*ditto*	27.0
171	*el2* mixed random	horizontal	13.9	37.4	34.0
172	*ditto*	*ditto*	*ditto*	*ditto*	26.0
173	*ditto*	*ditto*	*ditto*	*ditto*	28.0

Table A-2.1 Results of the direct shear test.

No.	shear-box	material and packing		normal stress (kgf/cm²)	porosity (%)	ϕ'_p (degrees)
N 1	15	φ5mm	regular	0.43	12.6	41.2
N 2	15	*ditto*	*ditto*	1.02	12.6	37.8
N 4	15	*ell* mixed	vertical	0.47	14.2	41.6
N 5	15	*ell* mixed	horizontal	0.47	14.2	31.9
N 6	15	φ5mm:φ9mm=3:2	random	0.47	18.6	35.4
N 7	15	*ditto*	*ditto*	0.47	18.6	37.4
T 1	18	φ5mm	regular	3.00	12.6	30.1
T 2	18	*ditto*	*ditto*	2.00	12.6	30.9
T 3	18	*ditto*	*ditto*	1.05	12.6	31.3
T 4	18	φ5mm:φ9mm=10:1	random	2.06	15.3	28.4
T 5	18	φ5mm:φ9mm=3:2	*ditto*	2.08	19.8	35.8
T 6	18	*ditto*	*ditto*	2.23	20.4	31.7
T 7	18	φ5mm:φ9mm=5:5	*ditto*	1.80	20.9	31.7
T 8	18	*ditto*	*ditto*	1.90	20.0	32.0
T 9	18	φ5mm:φ9mm=2:3	*ditto*	2.09	21.3	33.6
T10	18	*ditto*	*ditto*	1.92	20.8	31.1
T11	18	φ5mm:φ9mm=1:10	*ditto*	1.83	20.4	39.2
T12	18	*ditto*	*ditto*	2.24	19.3	33.7
T13	18	φ9mm	regular	2.12	11.5	33.2
T14	18	*ditto*	*ditto*	2.26	14.5	35.8

Table A-2.2 Results of the direct shear test.

No.	shear-box	material and packing		normal stress (kgf/cm^2)	porosity (%)	ϕ'_p (degrees)
T15	18	*el2* mixed	horizontal	2.06	15.6	30.0
T16	18	*ditto*	*ditto*	2.12	16.2	28.1
T17	18	*el2* mixed	vertical	2.00	16.4	34.5
T18	18	*ditto*	*ditto*	2.03	16.4	37.5
T19	18	*el2* ϕ_m=8mm	horizontal	2.13	18.2	20.1
T20	18	*ditto*	*ditto*	2.10	18.2	23.7
T21	18	*el2* ϕ_m=8mm	vertical	2.48	14.7	30.7
T22	18	*ditto*	*ditto*	1.10	15.6	34.7

APPENDIX 2

ROLLING FRICTION OF THE MATERIALS

2.1 Mechanism for Rolling Friction of the 2-Dimensional Materials

One of the simplest model for the rolling friction is the *polygon model* (Soda, 1971; Fig. A-1), in which the cross section of a cylindrical rod is regarded as a polygon. The number of the sides of the polygon (S) was obtained by following equation:

$$S = \rho \ / \ 360 \qquad (18)$$

Let us suppose that the polygon is a equilateral polygon, a mean lengths of the sides (l_s) of the polygon was also can be calculated as:

$$l_s = 2 \cdot r \cdot \sin \ (\rho/2) \qquad (19)$$

The values for ρ and l_s for cylindrical rods are summarized in Table 16. The value for l_s, in other words, the length of particle contact, should change when the weight of the rod changes. The width of the contact length which is undergone the elastic deformation by the load (W). The length of the elastic deformation of the rods (a) can be calculated by the Herzian analysis (Sarkar, 1980);

$$a = \frac{2}{\sqrt{\pi}}\left[W \cdot r \frac{(1-\nu^2)}{E}\right]^{1/2} \tag{20}$$

where ν and E are the Poisson's ratio and the Young's modulus, respectively. If we assume W = 100gf for the maximum value when a particle is loaded in it in the tilting-box experiment, then the value of contact length, a, is calculated at 0.0024mm. Thus, the effect of the elastic deformation between the rods are negligible.

The histograms of these experiments are shown in Figs. 13 and 14. The values for rolling friction (ρ) become smaller as the diameter increase. This suggests that the value for rolling friction of the rods depends upon the accuracy due to manufacturer's work.

2.2 Application to the Problem of 2-Dimensional Piling

To understand the mechanism of piling, some physical analysis is required in addition to the value of rolling friction and the value of the sliding friction. An interesting example of the mechanism of piling is shown for the case of piling of 3 or 6 rods. The rods can be stable when 3 rods are piled as shown in Fig. A-2. For the 6-rod case, however, the pile cannot stand by itself (Fig. A-3). The problem can be easily solved by the static model, the GSM. The result of the calculation is shown in Fig. A-2 (3-rod case) and Fig. A-4 (6-rod case).

2.3 Rolling Friction in 3-Dimensional Material

The value for rolling friction for materials such as sand and gravel can be determined by the method illustrated in Fig. 68. The values for rolling friction in sand and gravel (Fig. 69) were also gained by the tilting method. The measurement is conducted as follows: A sand paper, which roughness is proportional to the grain size, was underlain in the tilting box. Next, a sample, which was selected at random from a number of samples, was placed on the sand paper. The direction of the sample was also determined at random. Then, the tilting box was tilted until the rolling of the specimen was started. Sometimes the specimen did not move beyond the angle of slope exceeded 40°. In this case the value of rolling friction was decided at 40°.

The measurement was repeated for four different directions and the procedure was performed at four faces which can stand by itself in each sample (Fig. A-5b). The method of the experiment is shown in Fig. A-5. Less than 16 measurements were made for the case that the diameters of the specimens were small, since they are too small to stand at four side. For this instance the measurements were made as many as possible. The results were summarized in Table 16 and the histograms of the values of rolling friction are shown in Figs. A-6 to A-8.

APPENDIX 3

TILTING-BOX EXPERIMENT USING SAND OR GRAVEL

The tilting-box experiments for sand or gravel (three dimensional materials) were performed to study the behavior of 3-dimensional materials and to know the effect of density on the critical angle of repose (α_c). The apparatus used for the experiment is the large-sized tilting-box (Fig. A-9). The tilting-box has a triangular-prizm-like box, which has a width of 80 cm, a height of 62 cm and a length of 100cm. The slope was steepened by pulling up the chains as shown in Fig. A-9b. Four types of crushed stones and coarse sand with a mean diameter of 1.7 mm were used.

The schematic diagram of the avalanching of the 3-dimensional materials is shown in Fig. A-10 (Onda *et al.*, 1988). Some unstable particles began to rotate at the stage A, many unstable particles moved at the stage B, and finally the mass movement of an avalanche occurred at the stage C. The processes were considerably similar to the 2-dimensional avalanche. The method of the experiment is shown in Fig. A-11.

The result of experiment is shown in Fig. A-12 and data are summarized in Table 15. The plot of the bulk density against the critical angle of repose (α_c) clearly defines a linear relationship. This means that the α_c-value increases as the bulk density increases.

APPENDIX 4

PROGRAM LISTS

4.1 *PACK1000*

(FACOM OS IV BASIC)

```
KEQ52800I  A805240.PACK1000.BASIC
0100  REM RANDOM PACK 1000 ------
0110  REM programmed by Yuichi ONDA
0120  REM  19-Apr. 1989----------
0140  PROGRAM PACKF4
0145  OPTION BASE 1
0146  DIM X(2000)
0202  DIM Y(2000),D2(2000),R(2000),ENG(50),H(50),N(50)
0210  DIM XS(2000),XL(2000),YS(2000),YL(2000)
0212  DIM SO%(2000),SE%(2000),NNA(2000)
0214  DEF FNACS(X)=-ATN(X/SQR(-X*X+1))+1.5708
0216  DEF FNASN(X)=-ATN(X/SQR(-X*X+1))
0220  REM
0230  H(1)=4.5
0240  H(2)=2.5
0250  N(1)=2
0255  N(2)=9
0256  WAKI=109
0260   FOR I%=1 TO WAKI
0270       R(I%)=2.5
0280  NEXT
0290  KOSU=1000+WAKI
0320  RANDOMIZE
0330  A%=0
0335  C%=0
0340  FOR I%=WAKI+1 TO KOSU
0350     K=RND*5.86
0360     REM K=RND*65
0370     IF K<1 THEN
0371       R(I%)=H(1)
0372       ELSE
0373       R(I%)=H(2)
0375     END IF
0379     IF K<1 THEN
0380        ZZ=1
0381        C%=C%+1
0383        END IF
0390  NEXT I%
0410  FOR I%=WAKI+1 TO KOSU
0420    PRINT INT(R(I%));
0430  NEXT I%
0435  REM INPUT PROMPT "ok? yes=1":YN
0440  REM IF YN=1 THEN 480 ELSE 320
0480  S2=SQR(2)/2
0481  X(1)=0
0490  Y(1)=SQR(2)*R(1)
0510  FOR I%=2 TO 68
0520    X(I%)=X(I%-1)+R(I%)*2*S2
0530    Y(I%)=Y(I%-1)+R(I%)*2*S2
0540  NEXT
0560   X(69)=X(1)-R(69)*2*S2
0565   Y(69)=Y(1)+R(69)*2*S2
0570  FOR I%=70 TO 109
0580    X(I%)=X(I%-1)-R(I%)*2*S2
0590    Y(I%)=Y(I%-1)+R(I%)*2*S2
0600  NEXT I%
```

```
0610 REM -------------------------------------------------
0630   SHIRAD=-15*3.14159/180
0640   AAA=TAN(45*3.14159/180+SHIRAD)
0650   BBB=-1/AAA
0720 REM
0730 FOR I%=1 TO WAKI
0740   XX=X(I%)
0742   YY=Y(I%)
0750   X(I%)=XX*COS(SHIRAD)-YY*SIN(SHIRAD)
0760   Y(I%)=XX*SIN(SHIRAD)+YY*COS(SHIRAD)
0770 NEXT I%
0780 REM
0790 REM ***********************************************
0800 FOR I%=1 TO WAKI
0820   XS(I%)=X(I%)-R(I%)
0821   XL(I%)=X(I%)+R(I%)
0830   YS(I%)=Y(I%)-R(I%)
0832   YL(I%)=Y(I%)+R(I%)
0910 NEXT I%
0930 NU=WAKI
0920 REM loop   **************************************************
0940  LOOP:
0950  IF NU>=KOSU THEN  ENDDO
0960 REM PRINT KX;X(NU),KY;Y(NU)
0970 REM --------------------------------------------------------
0980 I%=NU
1000   XS(I%)=X(I%)-R(I%)
1010   YS(I%)=Y(I%)-R(I%)
1011   XL(I%)=X(I%)+R(I%)
1012   YL(I%)=Y(I%)+R(I%)
1090 YMAX=-1
1100 FOR I%=1 TO NU
1110    IF YMAX<YL(I%) THEN
1111        NN=I%
1113    END IF
1114    IF YMAX<YL(I%) THEN
1116         YMAX=YL(I%)
1118    END IF
1120 NEXT I%
1130 REM PRINT NN,YMAX
1150 FOR I%=1 TO NU
1160  REM PRINT XS(I%),XL(I%),YL(I%)
1170 NEXT I%
1180 REM
1190 FOR I%=1 TO NU
1195   REM I%=SO(Q%)
1200   FOR J%=1 TO NU
1205     REM J%=SO(R%)
1210     IF I%=J% THEN 1250
1220     IF XS(I%)<=XS(J%) AND XL(I%)=>XS(J%) THEN 1240 ELSE 1250
1230     REM  JUD1
1240       IF YL(I%)>YL(J%) THEN
1242          XS(J%)=XL(I%)
1244       ELSE
1246          XL(I%)=XS(J%)
1248       END IF
1250   NEXT J%
1260 NEXT I%
1270 REM ----------------------------
1280 REM
1290 FOR I%=1 TO NU
1300   IF  XS(I%)>XL(I%) THEN
```

```
1301        XS(I%)=0
1305        XL(I%)=0
1308     END IF
1310  NEXT I%
1320  REM
1330  XMIN=500
1331  XMAX=0
1332  YMIN=500
1340  FOR I%=1 TO NU
1350     IF XS(I%)<XMIN THEN
MIN=XS(I%)
1355        SSN%=I%
1257     END IF
1360     IF XL(I%)>XMAX THEN
1362        XMAX=XL(I%)
1365        LLN%=I%
1367     END IF
1370      IF XS(I%)<>0 AND YL(I%)<YMIN THEN
1372        YMIN=YL(I%)
1376        YYN%=I%
1377      END IF
1380  NEXT I%
1390  DS=YL(SSN%)-(YL(SSN%)+XMIN)*0.7
1395  DL=YL(LLN%)-(YL(LLN%)-XMAX)*0.7
1400  REM
1410  REM PRINT
1420  REM PRINT DS,DL
1430  FOR I%=1 TO NU
1440      IF XS(I%)=0 THEN 1470
1460   REM PRINT USING "###   ###.#   ###.#   ###.#";I,XS(I),XL(I),YL(I)
1470  NEXT
1480  DEEP=YYN%
1540  REM PRINT DEEP
1550  KX=(XS(YYN%)+XL(YYN%))/2-.01
1560  KY=YMIN+R(NU+1)*1.35
1570  REM PRINT KX,KY
1580  REM ***********************************************************    ***
1590  REM
1610  ENN=0
1620  FOR I%=1 TO NU
1630   D2(I%)=(KX-X(I%))*(KX-X(I%))+(KY-Y(I%))*(KY-Y(I%))-R(I%)*R(I%)
1640  NEXT
1650     N1=500
1655     N2=500
1660  REM
1670  NN2%=YYN%
1680  REM
1690  FOR I%=1 TO NU
1700      IF D2(I%)<N1 AND I%<>YYN% THEN
1701          N1=D2(I%)
1702          NN1%=I%
1705      END IF
1710   NEXT
1720  REM
1730  REM PRINT NN1%,NN2%
1740  GOSUB  CALC
1750  REM
1770   HANTEI:
1780  S%=0
1782  N%=NU
1790  FOR I%=1 TO NU
1800     DD2=(X(N%+1)-X(I%))*(X(N%+1)-X(I%))+(Y(N%+1)-Y(I%))*(Y(N%+1)-Y(I%))
```

```
1810     IF (R(N%+1)+R(I%))*(R(N%+1)+R(I%))-.0001>DD2 THEN
1811         OTN=I%
1812         ENN=ENN+1
1816    GOTO 1830
1818    END IF
1820    IF RRR>DD2-.001 AND RRR<DD2+.001 THEN
1822        S%=S%+1
1823        SE%(S%)=I%
1825    END IF
1830 NEXT I%
1840  IF S%<2 THEN  AGE
1850   IF X(SE%(1))<X(N%+1)  AND X(SE%(2))<X(N%+1) THEN  AGE
1860   IF X(SE%(1))>X(N%+1)  AND X(SE%(2))>X(N%+1) THEN  AGE
1880 NU=NU+1
1882 GOTO  LOOP
1890 REM ***************************************************************
1900  AGE:
1920  REM SORTING ---------------------------------------
1930  FOR I%=1 TO NU
1933   SO%(I%)=I%
1934  NEXT I%
1940  B=0
1950  FOR I%=1 TO NU-1
1960    IF D2(SO%(I%))>D2(SO%(I%+1)) THEN
1961         Q%=SO%(I%)
1963         SO%(I%)=SO%(I%+1)
1965         SO%(I%+1)=Q%
1966         B=B+1
1967     END IF
1970  NEXT I%
1980   IF B>0 THEN 1940
1990  REM  -----------------
2000  FOR I%=1 TO NU
2020   NNA(I%)=SO%(I%)
2030 NEXT I%
2040 KK=NU
2051  CCCC=0
2252  REM =======================
2060 FOR Q%=1 TO KK
2070   FOR W%=1 TO KK
2080     IF Q%<=W% THEN 2250
2090     NN1%=NNA(Q%)
2091     NN2%=NNA(W%)
2092     NNU%=NU+1
2093       IF ABS(X(NN1%)-X(NN2%))>4*R(NNU%) THEN 2250
2094       IF ABS(Y(NN1%)-Y(NN2%))>3*R(NNU%) THEN 2250
2099     REM
2100     GOSUB  CALC
2120      HANTEI2:
2130      S%=0
2135      N2%=NU+1
2140      FOR Z%=1 TO NU
2145        I%=SO%(Z%)
2150        DD2=(X(N2%)-X(I%))*(X(N2%)-X(I%))+(Y(N2%)-Y(I%))*(Y(N2%)-Y(I%))
2160         RRR=(R(N2%)+R(I%))*(R(N2%)+R(I%))
2170          IF RRR-.001>DD2 THEN
2171             OTN=I%
2173             ENN=ENN+1
2174             GOTO 2250
2176          END IF
2180          IF RRR>DD2-.001 AND RRR<DD2+.001 THEN
2182             S%=S%+1
```

```
2183              SE%(S%)=I%
2185           END IF
2190       NEXT Z%
2191       REM-----------------------------------------
2192       IF S%<2 THEN 2250
2193       REM-----------------------------------------
2194       OKM=0
2195       OKP=0
2196        IF NU/KOSU<0.7 THEN
2197           CRIT=0
2198        ELSE
2199           CRIT=-0.267
2200        END IF
2201        FOR I%=1 TO S%
2202           ANGG=ATN((X(NNU%)-X(SE%(I%)))/ABS(Y(NNU%)-Y(SE%(I%))))
2203           IF ANGG<CRIT THEN
2204              OKM=1
2205           END IF
2206           IF ANGG>=-0.017 THEN
2207              OKP=1
2208           END IF
2209        NEXT I%
2210        REM
2211        IF OKM=1 AND OKP=1 THEN
2212          CCCC=1
2213          GOTO 2265
2214        END IF
2220        REM
2250    NEXT W%
2260 NEXT Q%
2261  REM -----------------------------------------
2265  IF CCCC=0 THEN
2266    PRINT "failure"
2267    PRINT Q%
2268    GOTO 2600
2269  END IF
2270 NU=NU+1
2280  GOTO  LOOP
2290 REM  ---------------------------------------------------------
2300   CALC:
2302  N2%=NU+1
2310 IF X(NN1%)>X(NN2%) THEN
2312     A%=NN2%
2313     NN2%=NN1%
2315     NN1%=A%
2317  END IF
2320   IF NN1%<1 OR NN2%<1 THEN
2321      PRINT NN1%,NN2%
2323   END IF
2325   IF   X(NN2%)-X(NN1%)=0 THEN
2326      SHI1=0
2327      GOTO 2340
2329   END IF
2330 SHI1=ATN((Y(NN2%)-Y(NN1%))/(X(NN2%)-X(NN1%)))
2340 KD=((X(NN1%)-X(NN2%))*(X(NN1%)-X(NN2%))+(Y(NN1%)-Y(NN2%))*(Y(NN1%)-Y(NN2%))
)
2345 D=SQR(KD)
2350 A=R(NN2%)+R(N2%)
2360 B=R(NN1%)+R(N2%)
2361  IF (2*B*D)=0 THEN
2362    COSA=0
2363    SHI2=1.5708
```

```
2364     GOTO 2380
2365   END IF
2366   REM 2361 KARA 2365 MADE ADD AT 9 MAY
2370   COSA=(B*B+D*D-A*A)/(2*B*D)
2380    IF COSA=1 THEN
2381         SHI2=0
2385         GOTO 2420
2386    END IF
2390    IF COSA>1 THEN
2392         SHI=3.14159/2
2395         GOTO 2420
2397    END IF
2398   IF COSA>=1 OR COSA<=-1 THEN
2399   PRINT COSA;
2400   END IF
2405 SHI2=FNACS(COSA)
2410 REM
2420 SHITA=SHI1+SHI2
2430 X(N2%)=(R(NN1%)+R(N2%))*COS(SHITA)+X(NN1%)
2440 Y(N2%)=(R(NN1%)+R(N2%))*SIN(SHITA)+Y(NN1%)
2450 RETURN
2460 REM *************************************************************
2470   ENDDO:
2475   FOR I%=WAKI+1 TO KOSU
2477     PRINT I%-WAKI,X(I%),Y(I%)
2479   NEXT I%
2520 OPEN #1,OUTPUT,STREAM,DISPLAY
2530 PRINT #1:KOSU
2540 PRINT #1:WAKI
2550 FOR I%=1 TO KOSU
2570     PRINT #1:X(I%),Y(I%),R(I%)
2580 NEXT I%
2590 CLOSE #1
2600   STOP
2610 END
```

4.2 GSM1000

(NEC N88BASIC Ver.4.0)

```
100 'GSM1000------------------------
110 '1000ｹ ﾉ ﾘｭｳｼﾞｮｳﾀｲ ﾉ ｱﾝﾃｲ ﾓﾃﾞﾙ
120 '   basic
130 '  programmed by Yuichi ONDA
140 ' 11-Mar., 1990 ---------------
150 '//////////////////////////////////////////////////////////////////////////
160 CONSOLE 0,25,0,1:SCREEN 3,0:WIDTH 80,25:'d
170 OPTION BASE 1
180 KEY 7,"cls 2"+CHR$(13):'d
190 KEY 9,"L? CHR$(12)"+CHR$(13):'d
200 DEF FNACS(X)=-ATN(X/SQR(-X*X+1))+1.5708
210 DEF FNASN(X)=ATN(X/SQR(-X*X+1))
220 DIM X(1000),Y(1000),R(1000),SO%(1000),CH%(1000,6),SDAME%(10),CUF%(105)
230 DIM XMO(1000),YMO(1000),RMO(1000),UPP%(1000),DRN(1000),DRF(1000),WE(1000)
240 DIM XS(1000),XL(1000),YS(1000),YL(1000),F(1000),SHI(1000),ROT(1000)
250 DIM IX(1000),IY(1000),SAFX(1000,6),SAFY(1000,6),SASHI(1000),SAF(1000)
260 DIM FORB(1000,2),MOME(1000),NET%(1000,6),UNET%(1000,6),SNET%(1000,6)
270 DIM ANGLE(1000,6),KOSF(1000,6),SH(10),KSH(10),KESH(10),SKOSF(1000)
280 DIM AAA(4,4),BBB(10),CCC(10),DF(1000,6),KEI%(10),SLR(1000),HCON%(1000)
290  DIM RBAN%(1000),TREE1%(7),TREE2%(7,7),KQN%(1000),KKNET%(10),ANDA(40)
300 DIM DRFX(1000),DRFY(1000),DRANG(1000),HAJ%(1000),NETT%(1000),RDF(1000)
310 '@@@  main routine @@@@@@@@@@@@@@@@@@@@@@@@@@@@@@@@@@@@@@@@@@@@@@@@
320 PRINT"   @@@@@@@@@@@@@@@@  GSM 1000  @@@@@@@@@@@@@@@@@@@@"
335 PRINT"                         Ver. 4.30  at   0:27 15-MAR, 1990  "
340 COLOR 6
350 'INPUT "PACK DATA DRIVE A-D ";IDRV$
360 'IDRV$=IDRV$+":"
362  IDRV$="b:"
370 'INPUT "WRITE DRIVE A-D ";WDRV$
380 'WDRV$=WDRV$+":"
383  WDRV$="b:"
390  GOSUB *ANREAD
400  GOSUB *DATAREAD1
410  GOSUB *DATAWRITEOPEN
411 LPRINT"   @@@@@@@@@@@@@@@  GSM 1000  @@@@@@@@@@@@@@@@@@@@"
412  LPRINT FILE$;"  Started at  ";DATE$;TIME$,SHITA
420 SMIU=.345575
430 RM(1)=.92*3.14159/180
440 RM(2)=.5*3.14159/180
450 'HITA=4.9
460 KAIKAI=0
463 EEEE=0
470 '+++++++++++++++++++++++++++++++++++++++++++++++++++++++++++++++
480 *NEWONE
483 'IF EEEE=1 THEN *ENDDO
490 KAIKAI=KAIKAI+1
500 IF KAIKAI>ANNUM THEN *ENDDO
510 QQ%=0
520 UGO%=0
530 CKC%=4
540 SHITA=ANDA(KAIKAI)
550 GOSUB *KAITEN
560  ' --------------------------
570  WQZ%=0
580  *LOOP
590 'LPRINT FILE$;"  Started at  ";DATE$;TIME$,SHITA
592  LPRINT USING "###'  ";SHITA
600  WQZ%=WQZ%+1
```

```
610  GOSUB *DATAINT
620  GOSUB *GRAPHICS
630  GOSUB *DATAINT2
640   GOSUB *CONTACT
650 'LPRINT "Contact had finished at ";DATE$,TIME$
660  GOSUB *FORCE
670  GOSUB *ROTATE
680  GOSUB *CRITERION
690  GOSUB *DRAWING
700  GOSUB *DATAWRITE
710  'CLS:PRINT  USING  "GSM-1000III(&         &)       ###' ";FILE$,-SHITA  :PRINT
      TIME$
720   'OPY 3:LPRINT CHR$(&HC);
730 'INPUT A$
740 GOTO *NEWONE
750 '=============================================================
760 *ANREAD
770 INPUT "ｼｮｳ--1  ﾁｭｳ--2  ﾀﾞｲ--3";SIZ
771 IF SIZ=1 THEN PPP=1
772 IF SIZ=2 THEN PPP=7
773 IF SIZ=3 THEN PPP=14
775 ANNUM=18
790 FOR I=1 TO ANNUM
794  'READ AA
800   ANDA(I)=-I-PPP
810 NEXT
820 RETURN
830 *ANGLEDATA
870  DATA  2,3,4,5,6,7,8,9,10,11,12,13,14,15,16,17,18,19,20,21
880 '============================================================
890 *ENDDO
900 CLOSE
902 COPY 3
903 LPRINT CHR$(12)
910 'HDIR WDRV$+".."
920 END
930  '*******************************************************************
940 *KAITEN
950  SHIRAD=SHITA*3.14159/180
960   PRINT SHITA
970  FOR I%=1 TO KOSU
980    X(I%)=IX(I%)*COS(SHIRAD)-IY(I%)*SIN(SHIRAD)
990    Y(I%)=IX(I%)*SIN(SHIRAD)+IY(I%)*COS(SHIRAD)
1000  NEXT I%
1010  RETURN
1020 '*******************************************************************
1030 *DATAINT
1040  FOR I%=1 TO NU%
1050    SAF(I%)=0
1060    DRF(I%)=0
1070    DRN(I%)=0
1080    DRFX(I%)=0
1090    DRFY(I%)=0
1100    ROT(I%)=0
1110    DRANG(I%)=0
1120    HAJ%(I%)=0
1130    UPP%(I%)=0
1140    RBAN%(I%)=0
1150    MOME(I%)=0
1160    SLR(I%)=0
1165    HCON%(I%)=0
1170    FOR J%=1 TO 2
```

```
1180       FORB(I%,J%)=0
1190     NEXT
1200     FOR J%=1 TO 6
1210       UNET%(I%,J%)=0
1220       SNET%(I%,J%)=0
1230       ANGLE(I%,J%)=0
1240      NET%(I%,J%)=0
1250      CH%(I%,J%)=0
1260      DF(I%,J%)=0
1270      KOSF(I%,J%)=0
1280      SAFY(I%,J%)=0
1290     SAFX(I%,J%)=0
1300     NEXT J%
1310 NEXT I%
1320  NU%=KOSU
1330 RETURN
1340 '************************************************************
1350 *GRAPHICS
1360 'CLS 3
1362  CLS 2
1370  'ｶﾀﾑｷ ｷﾒ
1380  SHIRAD=SHITA*3.14159/180
1390  SHIRA2=(SHITA-15)*3.14159/180
1400  AAA=TAN(45*3.14159/180+SHIRA2)
1410  IF AAA<>0 THEN BBB=-1/AAA  ELSE BBB=0 :'ｶﾀﾑｷ
1420  PRINT SHITA
1430 'WX=INT(6*SQR(50  ))
1440  WX=INT(5.88*SQR(KOSUKE))
1443 'WX=INT(25*SQR(KOSUKE))        :'35ｹ ﾉﾐ
1450   DS=-(WX*SIN(SHIRAD))
1460 WY=WX*1.25
1470  WINDOW (-WX+DS/2+WX/2,-WY+DS/4 )-(WX+DS/2+WX/2,0+DS/4)
1480 'WINDOW (-WX+DS/2+45,-WY+DS/3 )-(WX+DS/2+45,0+DS/3)
1490   K=200/BBB
1500 IF AAA>0 THEN LINE (0,0)-(200,-200*AAA),7:LINE (0,0)-(K,-K*BBB),7
1510 IF AAA<0 THEN LINE (0,0)-(200,-200*AAA),7:LINE (K,-K*BBB)-(0,0),7
1520 IF AAA=0 THEN LINE (0,0)-(200,-200*AAA),7:LINE (0,-200)-(0,0),7
1530 '
1540 '
1550 FOR I%=1 TO KOSU
1560   CIRCLE (X(I%),-Y(I%)),R(I%)
1570   PSET (X(I%),-Y(I%)),1
1580   XS(I%)=X(I%)-R(I%):XL(I%)=X(I%)+R(I%)
1590   YS(I%)=Y(I%)-R(I%):YL(I%)=Y(I%)+R(I%)
1600    SX=MAP(X(I%),0):SY=MAP(-Y(I%),1)
1610    Q%=I%-WAKI:IF Q%<1 THEN 1690
1620  ' PAINT (X(I%),-Y(I%)),5,7
1630   IF KOSU>150 THEN 1690
1640      IF Q%<10 THEN 1650 ELSE J=Q%¥10:K=Q% MOD 10:GOTO 1660
1650     PUT (SX-4,SY-8),KANJI(VAL("&H130")+Q%),PSET :GOTO 1680
1660      PUT (SX-8,SY-8),KANJI(VAL("&H130")+J),PSET
1670      PUT (SX,SY-8),KANJI(VAL("&H130")+K),PSET :GOTO 1680
1680  'LINE (XS(I%),-YS(I%))-(XL(I%),-YL(I%)),6,B
1690 NEXT
1700 RETURN
1710 '************************************************************
1720 *DATAINT2
1730 FOR I%=WAKI+1 TO NU%
1740   FOR J%=WAKI+1 TO NU%
1750      IF I%=J% THEN 1790
1760      IF XS(I%)<=XS(J%) AND XL(I%)=>XS(J%) THEN *JUD1 ELSE 1790
1770      *JUD1
```

```
1780       IF YL(I%)>YL(J%) THEN XS(J%)=XL(I%) ELSE XL(I%)=XS(J%)
1790   NEXT J%
1800 NEXT I%
1810 '
1820 FOR I%=WAKI+1 TO NU%
1830   IF  XS(I%)>XL(I%) THEN XS(I%)=0
1840   IF  XS(I%)>XL(I%) THEN XL(I%)=0
1850 NEXT I%
1860 'sort-----------------
1870 FOR I%=WAKI+1 TO NU%
1880   SO%(I%)=I%
1890 NEXT I%
1900 B%=0
1910 FOR I%=WAKI+1 TO NU%-1
1920   IF Y(SO%(I%))<Y(SO%(I%+1)) THEN SWAP SO%(I%),SO%(I%+1):B%=B%+1
1930 NEXT I%
1940  IF B%>0 THEN 1900
1950 '
1960 RETURN
1970 '************contact calculation********************************
1980 *CONTACT :'---------------------------------------------
1990 FOR I%=WAKI+1 TO NU%
2000   T%=0
2010   FOR J%=1 TO NU%
2020      IF T%=6 THEN 2140  :'6 ﾂ ﾆ ｾｲｹﾞﾝ
2030     IF I%=J% THEN 2130
2040     IF ABS(X(I%)-X(J%))>9 THEN 2130
2050     IF ABS(Y(I%)-Y(J%))>9 THEN 2130
2060     RRR=(R(I%)+R(J%))*(R(I%)+R(J%))
2070     D2=(X(I%)-X(J%))*(X(I%)-X(J%))+(Y(I%)-Y(J%))*(Y(I%)-Y(J%))
2080     IF Y(I%)<=Y(J%) THEN 2100 ELSE 2120
2090 '    ' upper ------
2100            IF        RRR>D2-.01        AND        RRR<D2+.01        THEN
     T%=T%+1:NET%(I%,T%)=J%:UNET%(I%,T%)=J% :GOTO 2130
2110 '    ' under ------
2120            IF        RRR>D2-.01        AND        RRR<D2+.01        THEN
     T%=T%+1:NET%(I%,T%)=J%:SNET%(I%,T%)=J%
2130   NEXT J%
2140   NETT%(I%)=T%
2150 NEXT I%
2160 'PRINT
2170 FOR I%=WAKI+1 TO NU%
2180   FOR J%=1 TO NETT%(I%)
2190     K%=NET%(I%,J%)
2200     IF Y(I%)<Y(K%) THEN 2210 ELSE 2260
2210     'ｳｴ-------------------------
2220       IF   X(K%)-X(I%)>0   THEN   ANGLE(I%,J%)=ATN((Y(K%)-Y(I%))/(X(K%)-
     X(I%)))+1.5708 ELSE ANGLE(I%,J%)=ATN((Y(K%)-Y(I%))/(X(K%)-X(I%)))-1.5709
2230   ' IF  X(K%)-X(I%)<=0  THEN  ANGLE(I%,J%)=ATN((Y(K%)-Y(I%))/(X(K%)-X(I%)))-
     1.5708
2240    GOTO 2270
2250      'ｼﾀ ------------------------
2260    ANGLE(I%,J%)=ATN((X(K%)-X(I%))/(Y(I%)-Y(K%)))
2270   NEXT
2280 NEXT
2290 '
2300 FOR I%=WAKI+1 TO NU%
2310    MI%=0:PL%=0
2320    MAX=-500:MIN=500
2330   FOR J%=1 TO NETT%(I%)
2340     IF ANGLE(I%,J%)<0 AND ANGLE(I%,J%)>MAX THEN MAX=ANGLE(I%,J%):MI%=J%
2350     IF ANGLE(I%,J%)>0 AND ANGLE(I%,J%)<MIN THEN MIN=ANGLE(I%,J%):PL%=J%
```

```
2360   NEXT
2370   FOR J%=1 TO NETT%(I%)
2380     IF J%=MI% OR J%=PL% THEN 2410
2390      IF SNET%(I%,J%)=0 THEN 2410
2400     UNET%(I%,J%)=NET%(I%,J%):SNET%(I%,J%)=0
2410   NEXT
2420   'PRINT
2430 NEXT
2440 '
2450 FOR I%=WAKI+1 TO NU%
2460 ' PRINT I%-WAKI;
2470   FOR J%=1 TO NETT%(I%)
2480  '   PRINT USING "### ";NET%(I%,J%)-WAKI;
2490  '   PRINT USING "### ";SNET%(I%,J%);
2500   NEXT
2510 '   PRINT
2520 NEXT
2530 RETURN
2540 '*****force calculate*******************************************************
2550 '@@@@@@@@@@@@@@@@@@@@@@@@@@@@@@@@@@@@@@@@@@@@@@@@@@@@@@@@@@@@@@@@@@@@@@@@@@@
2560 *FORCE
2570  EEQ=EEQ+1
2580 PRINT:PRINT "ｳｴｶﾗ ｹｲｻﾝｦ ﾊｼﾞﾒﾏｽ!!"
2590  IF KAKI=1 THEN 2610 ELSE GOTO 2760
2600   '*************karii---------------------------------
2610 FOR Q%=1 TO W%
2620   I%=SO%(Q%)
2630   IF I%<=WAKI THEN 2730
2640    XXK=X(I%)+F(I%)*SIN(SHI(I%))/4
2650    YYK=Y(I%)-F(I%)*COS(SHI(I%))/4
2660    LINE (X(I%),-Y(I%))-(XXK,-YYK),0
2670    FOR J%=1 TO NETT%(I%)
2680       IF DF(I%,J%)=0 THEN 2720
2690      XXK=X(I%)+DF(I%,J%)*SIN(ANGLE(I%,J%))/4
2700      YYK=Y(I%)-DF(I%,J%)*COS(ANGLE(I%,J%))/4
2710       LINE (X(I%),-Y(I%))-(XXK,-YYK),0,,&H5555
2720    NEXT
2730 NEXT Q%
2740   ' karii ***********************----------------------
2750    ' ++++++++++++++++++++++++++++++++++++++++++++++++++
2760 FOR J%=1 TO NU%
2770   FOR K%=1 TO NETT%(J%)
2780     DF(J%,K%)=0
2790   NEXT K%
2800   FOR K%=1 TO 2
2810     FORB(J%,K%)=0
2820   NEXT K%
2830 NEXT J%
2840 '*****************************************************************
2850 FOR W%=1 TO NU%
2860   CHECK=0
2870   '----from upper part
2880   I%=SO%(W%)
2890   IF I%<=WAKI THEN 4170
2900 '  Upper force/////////////////////////////////////////////
2910 '  add the  SAF!!---------------------
2920  SAX=0
2930  SAY=0
2940  FOR J%=1 TO NETT%(I%)
2950    SAX=SAX+SAFX(I%,J%)
2960    SAY=SAY+SAFY(I%,J%)
2970  NEXT
```

```
2980 '
2990 IF SAX=0 AND SAY=0 THEN 3050
3000 ' --saf plus ---------------------------
3010    FORB(I%,1)=FORB(I%,1)+SAX
3020    FORB(I%,2)=FORB(I%,2)+SAY
3030  '  PRINT USING "###   sX=####.##gf   sY=####.##gf";I%-WAKI,SAX,SAY
3040 ' --------------------------------------
3050   FOR J%=1 TO NETT%(I%)
3060                  IF                 SNET%(I%,J%)=0                  THEN
     FORB(I%,2)=FORB(I%,2)+R(I%)*R(I%)/100*3.14159*5*2.69
3070     IF SNET%(I%,J%)=0 THEN *UNDERFORCE
3080   NEXT J%
3090    '--most upper particle
3100    FORB(I%,2)=R(I%)*R(I%)/100*3.14159*5*2.69
3110 '  Under force //////////////////////////////////////////////////
3120 *UNDERFORCE
3130   C%=0
3140   FOR J%=1 TO NETT%(I%)
3150      IF UNET%(I%,J%)=0 THEN 3160 ELSE 3180
3160      C%=C%+1
3170      SH(C%)=ANGLE(I%,J%)
3180   NEXT J%
3190   CNUM%=C%
3200     ' CALC. Shi and F ----------------------
3210     SHIDA=ATN(FORB(I%,1)/FORB(I%,2))
3220     IF FORB(I%,1)<0 AND FORB(I%,2)<0 THEN SHI(I%)=-3.14159+SHIDA:GOTO 3250
3230     IF FORB(I%,1)>0 AND FORB(I%,2)<0 THEN SHI(I%)=3.14159+SHIDA:GOTO 3250
3240    SHI(I%)=SHIDA
3250    F(I%)=SQR(FORB(I%,1)*FORB(I%,1)+FORB(I%,2)*FORB(I%,2))
3260    '  ----------------------------------
3270   C%=0
3280   FOR J%=1 TO NETT%(I%)
3290    IF UNET%(I%,J%)=0 THEN 3300 ELSE 3350
3300    C%=C%+1
3310     KSH(C%)=SH(C%)-SHI(I%)
3320     IF KSH(C%)>3.14159 THEN KSH(C%)=KSH(C%)-6.28318
3330     IF KSH(C%)<-3.14159 THEN KSH(C%)=KSH(C%)+6.28318
3340    'PRINT  KSH(C%)
3350   NEXT  J%
3360 '  ----------------------------------------------
3370    IF CNUM%=1 THEN 3380 ELSE 3420
3380  '    IF HAJ%(I%)>=1 THEN *IKKEHAJI ELSE *IKKE
3390      IF HCON%(I%)>3 OR HAJ%(I%)=2 THEN *IKKEHAJI
3400      GOTO *IKKE
3410    '
3420    IF CNUM%>=2 THEN KESH(1)=SH(1):KESH(2)=SH(2):GOTO *DIVIDEFORCE
3430   '/////DIVIDE FORCE//////////////////////////////////////
3440   *DIVIDEFORCE
3450   N%=2
3460   AAA(1,1)=COS(KSH(1))
3470   AAA(1,2)=COS(KSH(2))
3480   AAA(2,1)=SIN(KSH(1))
3490   AAA(2,2)=SIN(KSH(2))
3500   BBB(1)=F(I%)
3510   BBB(2)=0
3520    GOSUB *GAUSS
3530   ' +++++++++++++++++  +++++++++++++++++++++++++++
3540   FOR J%=1 TO 2
3545     '  IF CCC(J%)>F(I%) THEN CCC(J%)=F(I%)
3550       IF CCC(J%)>F(I%)*1.2 THEN CCC(J%)=F(I%)*1.2
3560   NEXT
3570   ' ++++++++++++++++++++++++++++++++++++++++++++++
```

```
3580   FOR J%=1 TO 2
3590     KX(J%)=CCC(J%)*SIN(KESH(J%))
3600     KY(J%)=CCC(J%)*COS(KESH(J%))
3610   NEXT J%
3620   K%=0
3630   FOR J%=1 TO NETT%(I%)
3640     IF SNET%(I%,J%)=0 THEN 3680
3650        K%=K%+1
3660       DF(I%,J%)=CCC(K%)
3670     '---------
3680     IF DF(I%,J%)<0 THEN 3690 ELSE 3740
3690       PRINT USING "### -> ### ####.#gf";I%-WAKI,NET%(I%,J%)-WAKI,DF(I%,J%)
3700    '  DAME%=NET%(I%,J%)
3710      SDAME%(1)=NET%(I%,J%)
3720       GOTO *RETRY
3730     '---------
3740     IF SNET%(I%,J%)=0 THEN 3770
3750      FORB(NET%(I%,J%),1)=FORB(NET%(I%,J%),1)+KX(K%)
3760      FORB(NET%(I%,J%),2)=FORB(NET%(I%,J%),2)+KY(K%)
3770   NEXT
3780   '------------------
3790   *SAFPLUS
3800   K%=0
3810   FOR J%=1 TO NETT%(I%)
3820     IF UNET%(I%,J%)=0 THEN 3830 ELSE 4000
3830     K%=K%+1
3840      IF ABS(ANGLE(I%,J%))<1.5708 THEN 4000
3850     Z%=NET%(I%,J%)
3860     IF Z%<=WAKI THEN 4000
3870    'FOR L%=1 TO NETT%(J%)
3880     FOR L%=1 TO NETT%(Z%)
3890       SAFX(Z%,L%)=0
3900       SAFY(Z%,L%)=0
3910     NEXT L%
3920     '
3930      FOR L%=1 TO NETT%(Z%)
3940        IF NET%(Z%,L%)=I% THEN EE%=L%
3950     NEXT L%
3960     '
3970     SAFX(Z%,EE%)=KX(K%)
3980     SAFY(Z%,EE%)=KY(K%)
3990      PRINT USING "### -> ### sx=###.##gf sy=###.#gf";I%-WAKI,NET%(I%,J%)-
  WAKI,SAFX(Z%,EE%),SAFY(Z%,EE%)
4000   NEXT J%
4010   '-------------karii--------------------------------
4020   *KARIDRAW
4030    IF EEQ MOD 10=0 THEN KAKI=1 ELSE KAKI=0
4040    IF KAKI=0 THEN 4170
4050    XXK=X(I%)+F(I%)*SIN(SHI(I%))/4
4060    YYK=Y(I%)-F(I%)*COS(SHI(I%))/4
4070    LINE (X(I%),-Y(I%))-(XXK,-YYK),6
4080    FOR J%=1 TO NETT%(I%)
4090      IF DF(I%,J%)=0 THEN 4130
4100      XXK=X(I%)+DF(I%,J%)*SIN(ANGLE(I%,J%))/4
4110      YYK=Y(I%)-DF(I%,J%)*COS(ANGLE(I%,J%))/4
4120       LINE (X(I%),-Y(I%))-(XXK,-YYK),1,,&H5555
4130    NEXT J%
4140  ' karii ***********************----------------------
4150   ' +++++++++++++++++++++++++++++++++++++++++++++++++++
4160   PRINT USING "###  ###.#'  ###.##gf";I%-WAKI,SHI(I%)*180/3.14159,F(I%)
4170 NEXT W%
4180 '=====================================================
```

```
4190 PRINT
4200 FOR I%=WAKI+1 TO NU%
4210    SAX=0
4220    SAY=0
4230    SSKOSF=0
4240    FOR J%=1 TO NETT%(I%)
4250    'kosoku Force
4260     KOSF(I%,J%)=DF(I%,J%)
4270     Z%=NET%(I%,J%)
4280     IF Z%<=WAKI THEN 4370
4290      FOR L%=1 TO NETT%(Z%)
4300        IF NET%(Z%,L%)=I% THEN EE%=L%
4310     NEXT L%
4311      ' SKOSF ｦ ﾁｶﾗ ｦ ｳｹﾙﾎｳﾆ ﾉﾐ ﾆ ｽﾙ!!---------
4320     KOSF(I%,J%)=KOSF(I%,J%)+DF(Z%,EE%)
4330     SSKOSF=SSKOSF+DF(Z%,EE%)
4340    '  KOSF(NET%(I%,J%),J%)=KOSF(NET%(I%,J%),J%)+DF(NET%(I%,J%),J%)
4350      SAX=SAX+SAFX(I%,J%)
4360      SAY=SAY+SAFY(I%,J%)
4370    NEXT J%
4380    SKOSF(I%)=SSKOSF
4390    IF SAX=0 AND SAY=0 THEN 4470
4400    '  SAF =================================
4410    SHIDA=ATN(SAX/SAY)
4420    IF SAX<0 AND SAY<0 THEN SASHI(I%)=-3.14159+SHIDA :GOTO 4450
4430    IF SAX>0 AND SAY<0 THEN SASHI(I%)=3.14159+SHIDA:GOTO 4450
4440    SASHI(I%)=SHIDA
4450    SAF(I%)=SQR(SAX*SAX+SAY*SAY)
4460   '  ======================================
4470   'PRINT  USING  "###   ####.#'   ###.##gf   (sa####.#'   ###.##gf)";I%-
     WAKI,SHI(I%)*180/3.14159,F(I%),SASHI(I%)*180/3.14159,SAF(I%)
4480   '  LPRINT  USING  "###   ####.#'   ###.##gf   (sa####.#'   ###.##gf)";I%-
     WAKI,SHI(I%)*180/3.14159,F(I%),SASHI(I%)*180/3.14159,SAF(I%)
4490 '
4500 NEXT I%
4510 RETURN
4520 '@@@@@@@@@@@@@@@@@@@@@@@@@@@@@@@@@@@@@@@@@@@@@@@@@@@@@@@@@@@@@@@@@@@@@@@@@@@@@@
4530   *RETRY
4540   FOR J%=1 TO NETT%(I%)
4550     CH%(I%,J%)=0
4560   NEXT
4570   CHECK=CHECK+1
4580   FOR J%=1 TO NETT%(I%)
4590      IF SNET%(I%,J%)=0 THEN PRINT "  0";:GOTO 4610
4600      PRINT USING "###";SNET%(I%,J%)-WAKI;
4610   NEXT
4620 '///df<0  and  *2*>=2 then return ////////////////////
4630   '-----2 >=2 -> return and HAJI^^^^^
4640   IF CHECK<NETT%(I%) THEN 4690
4650      HAJ%(I%)=1
4660      PRINT "1ｹ ﾊｼﾞ --";I%-WAKI
4670      GOTO *IKKEDECIDE
4680   '  HAJ CHECK2--------------------
4690   D%=0
4700   FOR J%=1 TO NETT%(I%)
4710      IF SNET%(I%,J%)=0 THEN D%=D%+1
4720   NEXT
4730   IF D%=0 THEN *IKKEDECIDE
4740  '--------------------------------
4750   SE=0
4760   FOR J%=1 TO NETT%(I%)
4770      IF DF(I%,J%)<0 THEN UNET%(I%,J%)=SNET%(I%,J%):C%=1
```

```
4780      IF DF(I%,J%)<0 THEN SNET%(I%,J%)=0:DF(I%,J%)=0
4790      IF UNET%(I%,J%)=0 THEN Q%=J% :SE=SE+1
4800   NEXT
4810    IF SE=>2 THEN *UNDERFORCE:'CCCCCCCCCCC
4820  '
4830  ' calc KSH////////////////////////////////////////////////
4840   C%=0
4850   FOR J%=1 TO NETT%(I%)
4860     FOR K%=1 TO CHECK
4870       IF NET%(I%,J%)=SDAME%(K%) THEN 4940
4880     NEXT
4890     C%=C%+1
4900      SH(C%)=ANGLE(I%,J%)
4910      KQN%(C%)=J%
4920     '
4930    IF UNET%(I%,J%)=0 THEN IIKO%=J%
4940   NEXT J%
4950   CNUM%=C%
4960    '
4970  IISHI=ANGLE(I%,IIKO%)-SHI(I%)
4980   IF IISHI>3.14159 THEN IISHI=IISHI-6.28318
4990   IF IISHI<-3.14159 THEN IISHI=IISHI+6.28318
5000  'PRINT IISHI              :'CCCCCCCCCCC
5010   MIN=500                   :'CCCCCCCCC
5020   FOR J%=1 TO CNUM%
5030     KSH(J%)=SH(J%)-SHI(I%)
5040     IF KSH(J%)>3.14159 THEN KSH(J%)=KSH(J%)-6.28318
5050     IF KSH(J%)<-3.14159 THEN KSH(J%)=KSH(J%)+6.28318
5060     III=ABS(KSH(J%))
5070     IF III<MIN THEN MIN=III:IIKO%=J%
5080   ' PRINT J%,KQN%(J%)-WAKI,KSH(J%)
5090   NEXT  J%
5100  'IISHI=ANGLE(I%,IIKO%)-SHI(I%)  :'CCCCCC
5110  '// another contact point ////////////////////////////
5120   IF CNUM%=0 THEN HAJ%(I%)=1:GOTO *IKKEDECIDE
5130   IF IISHI<0 THEN 5290
5140  '----------IISHI(PLUS)-----------------------------
5150   KYO=2.967-IISHI
5160   IF KYO>1.92 THEN KYO=1.92
5170  ' IF KYO>2.44 THEN KYO=2.44
5180   C%=0
5190   MAX=-500
5200   FOR J%=1 TO CNUM%
5210     IF KSH(J%)>0 OR KSH(J%)<-KYO THEN 5250
5220   ' IF KSH(J%)>0   THEN 5140
5230     C%=C%+1
5240      IF KSH(J%)>MAX THEN MAX=KSH(J%):AN%=KQN%(J%)
5250   NEXT J%
5260   IF C%=0 THEN HAJ%(J%)=1:GOTO *IKKEDECIDE
5270   GOTO *CHANGE
5280  '----------IISHI(MINUS)----------------------------
5290   MIN=500
5300   KYO=2.967+IISHI
5310   IF KYO>1.92 THEN KYO=1.92
5320  ' IF KYO>2.44 THEN KYO=2.44
5330   C%=0
5340   FOR J%=1 TO CNUM%
5350     IF KSH(J%)<0 OR KSH(J%)>KYO THEN 5390
5360  '  IF KSH(J%)<0  THEN 5240
5370     C%=C%+1
5380      IF KSH(J%)<MIN THEN MIN=KSH(J%):AN%=KQN%(J%)
5390   NEXT J%
```

```
5400   IF C%=0 THEN HAJ%(J%)=1:GOTO *IKKEDECIDE
5410  '///////////////////////////////////////////////////////////
5420 *CHANGE
5430    SNET%(I%,AN%)=NET%(I%,AN%)
5440    UNET%(I%,AN%)=0
5450    CH%(I%,AN%)=1
5460    PRINT "ｱﾀﾗｼｲﾉﾊ ";NET%(I%,AN%)-WAKI
5470  '
5480   FOR J%=1 TO NETT%(I%)
5490      IF SNET%(I%,J%)=0 THEN PRINT "  0";:GOTO 5510
5500      PRINT USING "###";SNET%(I%,J%)-WAKI;
5510   NEXT
5520   ' ----------------------------------------
5530   PRINT"AN=";AN%
5540   GOTO *CALCAGAIN
5550   '///////////////////////////////////////////////////////////
5560 *IKKEDECIDE
5570  HAJ%(I%)=2
5580  HCON%(I%)=HCON%(I%)+1
5590   FOR J%=1 TO NETT%(I%)
5600      SH(J%)=ANGLE(I%,J%)
5610      KQN%(J%)=J%
5620   NEXT J%
5630   CNUM%=NETT%(I%)
5640   '
5650   FOR J%=1 TO CNUM%
5660     KSH(J%)=ABS(SH(J%)-SHI(I%))
5670   ' IF KSH(J%)>3.14159 THEN KSH(J%)=6.28318-KSH(J%)
5680   NEXT J%
5690   '
5700   MIN=1000 :NNN%=1
5710   FOR J%=1 TO CNUM%
5720     IF KSH(J%)<MIN THEN NNN%=KQN%(J%)
5730     IF KSH(J%)<MIN THEN MIN=KSH(J%)
5740   NEXT  J%
5750   '
5760   FOR J%=1 TO NETT%(I%)
5770      IF UNET%(I%,J%)=0 THEN UNET%(I%,J%)=SNET%(I%,J%):SNET%(I%,J%)=0
5780      IF J%=NNN% THEN SNET%(I%,J%)=UNET%(I%,J%):UNET%(I%,J%)=0
5790      'END IF
5800      IF SNET%(I%,J%)=0 THEN PRINT "  0";:GOTO 5820
5810      PRINT USING "###";SNET%(I%,J%)-WAKI;
5820   NEXT
5830   PRINT
5840   FOR J%=1 TO NETT%(I%)
5850      IF UNET%(I%,J%)=0 THEN PRINT "ｼﾀﾊ !";SNET%(I%,J%)-WAKI:GOTO 5870:'q
5860   NEXT
5870   PRINT
5880   GOTO *FORCE
5890 '@@@@@@@@@@@@@@@@@@@@@@@@@@@@@@@@@@@@@@@@@@@@@@@@@@@@@@@@@@@@@@@@@@@@
5900 *IKKE
5910   ' calc KSH////////////////////////////////////////////////
5920   C%=0
5930   FOR J%=1 TO NETT%(I%)
5940     IF SNET%(I%,J%)=0 THEN C%=C%+1:SH(C%)=ANGLE(I%,J%):KQN%(C%)=J%
5950     '
5960     IF UNET%(I%,J%)=0 THEN IIKO%=J%
5970   NEXT J%
5980   CNUM%=C%
5990   '
6000   IISHI=ANGLE(I%,IIKO%)-SHI(I%)
6010   IF IISHI>3.14159 THEN IISHI=IISHI-6.28318
```

```
6020   IF IISHI<-3.14159 THEN IISHI=IISHI+6.28318
6030   FOR J%=1 TO CNUM%
6040     KSH(J%)=SH(J%)-SHI(I%)
6050       IF KSH(J%)>3.14159 THEN KSH(J%)=KSH(J%)-6.28318
6060       IF KSH(J%)<-3.14159 THEN KSH(J%)=KSH(J%)+6.28318
6070   NEXT  J%
6080  '// another contact point ////////////////////////////
6090   IF CNUM%=0 THEN *IKKEHAJI
6100   IF IISHI<0 THEN 6270
6110  '----------IISHI(PLUS)------------------------------
6120 '
6130   KYO=2.967-IISHI
6140    IF KYO>1.92 THEN KYO=1.92
6150 '  IF KYO>2.44  THEN KYO=2.44
6160   MAX=-500
6170   C%=0
6180   FOR J%=1 TO CNUM%
6190     IF KSH(J%)>0 OR KSH(J%)<-KYO THEN 6230
6200 '   IF KSH(J%)>0  THEN 6040
6210      C%=C%+1
6220      IF KSH(J%)>MAX THEN MAX=KSH(J%):AN%=KQN%(J%)
6230   NEXT
6240   IF C%=0 THEN *IKKEHAJI
6250   GOTO *CHANGE2
6260  '----------IISHI(MINUS)-----------------------------
6270   MIN=500
6280   KYO=2.967+IISHI
6290    IF KYO>1.92 THEN KYO=1.92
6300  ' IF KYO>2.44  THEN KYO=2.44
6310   C%=0
6320   FOR J%=1 TO CNUM%
6330     IF KSH(J%)<0 OR KSH(J%)>KYO THEN 6370
6340   ' IF KSH(J%)<0 THEN 6140
6350      C%=C%+1
6360      IF KSH(J%)<MIN THEN MIN=KSH(J%):AN%=KQN%(J%)
6370   NEXT
6380    IF C%=0 THEN *IKKEHAJI
6390  '//////////////////////////////////////////////////////
6400 *CHANGE2
6410    SNET%(I%,AN%)=NET%(I%,AN%)
6420    UNET%(I%,AN%)=0
6430    CH%(I%,AN%)=1
6440    PRINT "ｱﾀﾗｼｲﾉﾊ ";NET%(I%,AN%)-WAKI;
6450   FOR J%=1 TO NETT%(I%)
6460      IF SNET%(I%,J%)=0 THEN PRINT "  0";:GOTO 6480
6470      PRINT USING "###";SNET%(I%,J%)-WAKI;
6480   NEXT
6490   PRINT "AN=";AN%
6500    ' ---------------
6510    GOTO *CALCAGAIN
6520    ' ---------------
6530 ' @@@@@@@@@@@@@@@@@@@@@@@@@@@@@@@@@@@@@@@@@@@@@@@@@@@@@@@@@@@@@@@@@@@
6540 *IKKEHAJI
6550  HAJ%(I%)=1
6560   FOR J%=1 TO NETT%(I%)
6570     DF(I%,J%)=0
6580     IF UNET%(I%,J%)=0 THEN Q%=J%
6590   NEXT
6600  '
6610   FOR J%=1 TO NETT%(I%)
6620     IF J%=Q% THEN 6650
6630     UNET%(I%,J%)=NET%(I%,J%)
```

```
6640     SNET%(I%,J%)=0
6650   NEXT
6660    '
6670   PRINT USING "1ｹ ﾊｼﾞ  no-###";I%-WAKI
6680   KS=SHI(I%)-ANGLE(I%,Q%)
6690     IF KS>3.14159 THEN KS=KS-6.28318
6700     IF KS<-3.14159 THEN KS=KS+6.28318
6710   DF(I%,Q%)=F(I%)*COS(KS)
6720   IF DF(I%,Q%)<0 THEN DF(I%,Q%)=0
6730 ' --- ROT -rotating moment  ---ks ｶﾞ  SIN ｶ?--sliding force --------
6740   ROT(I%)=F(I%)*SIN(KS)*R(I%)/10
6750   RDF(I%)=F(I%)*SIN(KS)
6760    '
6770   KX=DF(I%,Q%)*SIN(ANGLE(I%,Q%))
6780   KY=DF(I%,Q%)*COS(ANGLE(I%,Q%))
6790 ' BEEP 1:BEEP 0:'PRINT Q%,KX,KY
6800                               FORB(NET%(I%,Q%),1)=FORB(NET%(I%,Q%),1)+KX :FORB(NET%(I%,Q%),2)=FORB(NET%(I%,Q%),2)+KY
6810 '  ----------SAF OR NOT-------------------------------------
6820 'OTO 6770
6830       IF NET%(I%,Q%)<=WAKI THEN 6990
6840       IF Y(NET%(I%,Q%))<Y(I%) THEN 6990
6850      '
6860       FOR K%=1 TO NETT%(NET%(I%,Q%))
6870         IF NET%(NET%(I%,Q%),K%)=I% THEN EE%=K%
6880       NEXT K%
6890      '
6900       FOR K%=1 TO NETT%(NET%(I%,Q%))
6910         SAFX(NET%(I%,Q%),K%)=0
6920         SAFY(NET%(I%,Q%),K%)=0
6930      NEXT K%
6940      '
6950        SAFX(NET%(I%,Q%),EE%)=KX
6960        SAFY(NET%(I%,Q%),EE%)=KY
6970         PRINT  USING  "h###  ->  ###  SAF=###.##g  (####' )";I%-WAKI,NET%(I%,Q%)-WAKI ,DF(I%,Q%),ANGLE(I%,Q%)*180/3.14159
6980    '
6990   GOTO *KARIDRAW
7000 '@@@@@@@@@@@@@@@@@@@@@@@@@@@@@@@@@@@@@@@@@@@@@@@@@@@@@@@@@@@@@@@@@
7010 *CALCAGAIN
7020 'ﾑｹﾞﾝ loop ｷﾘ  -------------------------
7030 ' ﾚﾝｿﾞｸｼﾃ 5ｶｲ ｲｼﾞｮｳｸﾙ-- ﾑｹﾞﾝ loopﾄﾐﾅｼ
7040 '1ｹ ﾊｼﾞ ﾉ ｹｲ ﾆ ｼｮｽ
7050  CKC%=CKC%+1
7060                  IF                  CKC%=100                  THEN CUF%(1)=CUF%(96):CUF%(2)=CUF%(97):CUF%(3)=CUF%(98):CUF%(4)=CUF%(99) :CKC%=5
7070  CUF%(CKC%)=I%
7080  C%=0
7090  '
7092  PRINT USING "i=####   ";I%
7100  FOR J%=CKC%-4 TO CKC%-1
7110    C%=C%+1
7120     PRINT USING "C ##  ####  ";C%,CUF%(J%);
7130  NEXT
7140  PRINT
7150  C%=0
7160  '
7170  FOR J%=CKC%-4 TO CKC%-1
7180    IF I%=CUF%(J%) THEN C%=1:LCO%=LCO%+1
7190  NEXT
7200  IF C%=0 THEN LCO%=0
```

```
7210  PRINT USING "LCO=###";LCO%
7220  IF LCO%=>3 THEN HAJ%(I%)=1:GOTO *IKKEHAJI
7230 '-------------------------------------
7240 C%=0
7250   FOR J%=1 TO NETT%(I%)
7260     IF UNET%(I%,J%)=0 THEN C%=C%+1:SH(C%)=ANGLE(I%,J%)
7270   NEXT J%
7280   CNUM%=C%
7290   ' --------------------------------------
7300   FOR J%=1 TO CNUM%
7310     KSH(J%)=SH(J%)-SHI(I%)
7320     IF KSH(J%)>3.14159 THEN KSH(J%)=KSH(J%)-6.28318
7330     IF KSH(J%)<-3.14159 THEN KSH(J%)=KSH(J%)+6.28318
7340   NEXT  J%
7350   ' ++++DIVIDE FORCE+++++++++++++++++++++++++++++++
7360   N%=2
7370   AAA(1,1)=COS(KSH(1))
7380   AAA(1,2)=COS(KSH(2))
7390   AAA(2,1)=SIN(KSH(1))
7400   AAA(2,2)=SIN(KSH(2))
7410   BBB(1)=F(I%)
7420   BBB(2)=0
7430    GOSUB *GAUSS
7440   ' ++++++++++++f ++++++++++++++++++++++++++++++++++++
7450   FOR J%=1 TO 2
7455    '  IF CCC(J%)>F(I%) THEN CCC(J%)=F(I%)
7460      IF CCC(J%)>F(I%)*1.2  THEN CCC(J%)=F(I%)*1.2
7470   NEXT
7480   ' ++++++++++++++++++++++++++++++++++++++++++++++
7490    FOR J%=1 TO 2
7500      KX(J%)=CCC(J%)*SIN(SH(J%))
7510      KY(J%)=CCC(J%)*COS(SH(J%))
7520    NEXT J%
7530   K%=0
7540   FOR J%=1 TO NETT%(I%)
7550     IF UNET%(I%,J%)=0 THEN K%=K%+1:DF(I%,J%)=CCC(K%)
7560       '
7570       IF  DF(I%,J%)<0  THEN  PRINT  USING  "###  ->  ###   ###.#gf";I%-
      WAKI,NET%(I%,J%)-WAKI,DF(I%,J%)
7580     '---------
7590      IF DF(I%,J%)=0 THEN 7810
7600     '---------
7610 '   IF DF(I%,J%)<0 THEN DAME%=NET%(I%,J%)
7620     IF DF(I%,J%)<0 THEN SDAME%(CHECK+1)=NET%(I%,J%)
7630     IF DF(I%,J%)<0 THEN *RETRY
7640     '---------
7650     IF CH%(I%,J%)<>1 THEN 7810
7660      IF NET%(I%,J%)<=WAKI THEN 7810
7670      IF Y(NET%(I%,J%))<Y(I%) THEN 7810
7680     '
7690      FOR K%=1 TO NETT%(NET%(I%,J%))
7700        IF NET%(NET%(I%,J%),K%)=I% THEN EE%=K%
7710     NEXT K%
7720     '
7730       FOR K%=1 TO NETT%(NET%(I%,J%))
7740         SAFX(NET%(I%,J%),K%)=0
7750         SAFY(NET%(I%,J%),K%)=0
7760       NEXT K%
7770     '
7780       SAFX(NET%(I%,J%),EE%)=DF(I%,J%)*SIN(ANGLE(I%,J%))
7790       SAFY(NET%(I%,J%),EE%)=DF(I%,J%)*COS(ANGLE(I%,J%))
7800       PRINT USING "r ### -> ### SAF=###.##g (####' )";I%-WAKI,NET%(I%,J%)-
```

```
     WAKI ,DF(I%,J%),ANGLE(I%,J%)*180/3.14159
7810  NEXT J%
7820  '
7830 PRINT
7840  GOTO *FORCE
7850 '****************************************************************
7860 '+++++++++++++++++ ROTATE +++++++++++++++++++++++++++++++++++++++++++
7870 *ROTATE
7880 FOR I%=WAKI+1 TO NU%
7890   'clockwise=+
7900   MOME(I%)=ROT(I%)
7910 NEXT I%
7920  FOR I%=1 TO NU%:ROT(I%)=0:NEXT
7930 '------------------------
7940 *FRICTION
7950 C%=0
7960 FOR I%=WAKI+1 TO NU%
7970   IF ABS(MOME(I%))>.5  THEN C%=C%+1:RBAN%(C%)=I%
7980 NEXT I%
7990 RNUM%=C%
8000 ' TREE SYSTEMS  =  to GRANDCHILD ========================
8010 FOR QQ%=1 TO RNUM%
8020  FOR I%=1 TO 7
8030    TREE1%(I%)=0
8040    FOR J%=1 TO 7
8050      TREE2%(I%,J%)=0
8060    NEXT J%
8070  NEXT I%
8080  C%=0
8090  '  1(SON)-------------
8100  FOR J%=1 TO NETT%(RBAN%(QQ%))
8110      TREE1%(J%)=NET%(RBAN%(QQ%),J%)
8120  NEXT J%
8130  TRNUM%=NETT%(RBAN%(QQ%))
8140  '  2(GRANDSON)--------
8150  FOR I%=1 TO TRNUM%
8160    IF TREE1%(I%)<=WAKI THEN 8210
8170    FOR J%=1 TO NETT%(TREE1%(I%))
8180      IF NET%(TREE1%(I%),J%)=RBAN%(QQ%) THEN 8200
8190       TREE2%(I%,J%)=NET%(TREE1%(I%),J%)
8200    NEXT J%
8210  NEXT I%
8220  'tree ﾋｮｳｼﾞ //////////////////////////////////
8230  PRINT USING "ｹﾞｲｲﾝ-> (###)";RBAN%(QQ%)-WAKI
8240  CIRCLE (X(RBAN%(QQ%)),-Y(RBAN%(QQ%))),.5
8250  FOR I%=1 TO TRNUM%
8260    PRINT TREE1%(I%)-WAKI;
8270    FOR J%=1 TO 7
8280      IF TREE2%(I%,J%)=0 THEN 8300
8290      PRINT USING "    #### -> ";TREE2%(I%,J%)-WAKI;
8300    NEXT J%
8310    PRINT
8320   NEXT I%
8330 '+++TORQUE ++++++++++++++++++++++++++++++++++++++++++
8340 '-- 1ｹ ﾒ----  ｺ ------------
8350 FOR I%=1 TO TRNUM%
8360  FOR J%=1 TO NETT%(RBAN%(QQ%))
8370    IF NET%(RBAN%(QQ%),J%)=TREE1%(I%) THEN KEI%(I%)=J%
8380  NEXT J%
8390 NEXT I%
8400 TF=0
8410  FOR I%=1 TO TRNUM%
```

```
8420    TF=TF+KOSF(RBAN%(QQ%),KEI%(I%))
8430  NEXT I%
8440  'ﾓｰﾒﾝﾄ ﾉ ﾌﾞﾝｶﾂ  (ｺｳｿｸﾘｮｸ ﾆ ﾋﾚｲ)
8450  FOR I%=1 TO TRNUM%
8460    '[F R(TREE1%(I%))=2.5 THEN RFRI=RM(1)*KOSF(RBAN%(QQ%),KEI%(I%))
8470    'IF R(TREE1%(I%))=4.5 THEN RFRI=RM(2)*KOSF(RBAN%(QQ%),KEI%(I%))
8480     RRR=MOME(RBAN%(QQ%))/TF*KOSF(RBAN%(QQ%),KEI%(I%))
8490     RRF=RRR/(R(RBAN%(QQ%))/10)
8500     ROT(TREE1%(I%))=ROT(TREE1%(I%))-RRR
8510     PRINT  USING  "###  ->  ###      F=###.##gf";RBAN%(QQ%)-WAKI,TREE1%(I%)-
      WAKI,RRF
8520  NEXT I%
8530  '--2 ｹﾒ -   ﾏｺﾞ -----------
8540  FOR I%=1 TO TRNUM%
8550    TF=0 :C%=0
8560 '
8570    FOR J%=1 TO NETT%(TREE1%(I%))
8580    ' IF KEI%(J%)=0 THEN 8380
8590     'TF=TF+KOSF(TREE1%(I%),KEI%(J%))
8600      IF NET%(TREE1%(I%),J%)=RBAN%(QQ%) THEN 8620
8610      TF=TF+KOSF(TREE1%(I%),J%)
8620    NEXT J%
8630 '
8640    FOR J%=1 TO NETT%(TREE1%(I%))
8650       IF TREE2%(I%,J%)=0 THEN 8740
8660       'IF R(TREE2%(j%,k%))=2.5 THEN RFRI=RM(1)*KOSF(TREE1%(I%),KEI%(k%))
8670       'IF R(TREE2%(I%,J%))=4.5 THEN RFRI=RM(2)*KOSF(TREE1%(I%),KEI%(J%))
8680       ' RRR=ROT(TREE1%(I%))/TF*KOSF(TREE1%(I%),KEI%(J%))
8690         RRR=ROT(TREE1%(I%))/TF*KOSF(TREE1%(I%),J%)
8700         RRF=RRR/(R(TREE1%(I%))/10)
8710  '
8720        ROT(TREE2%(I%,J%))=ROT(TREE2%(I%,J%))-RRR
8730           PRINT   USING   "###   ->   ###        F=###.##gf";TREE1%(I%)-
      WAKI,TREE2%(I%,J%)-WAKI,RRF
8740    NEXT J%
8750  NEXT I%
8760 ' -----------------------------
8770 'LPRINT RBAN%(QQ%)
8780  FOR I%=WAKI+1 TO NU%
8790    IF  ROT(I%)<>0  THEN  PRINT  USING  "###   MOME=###.#   ROT  ###.##";I%-
      WAKI,MOME(I%),ROT(I%)
8800    MOME(I%)=MOME(I%)+ROT(I%)
8810  NEXT I%
8820 NEXT QQ%
8830 RETURN
8840 '*****************************************************************
8850 '-++STABILITY CRITERION++++++++++++++++++++++++++++++++++++++++++++
8860 *CRITERION
8870 CLS
8880 PRINT -SHITA-.5;"'  ";
8882 LPRINT -SHITA-.5;"'  ";
8890 C%=0
8900 KONKAI%=0
8910 FOR I%=WAKI+1 TO NU%
8920    IF HAJ%(I%)=1 THEN C%=C%+1
8930    IF HAJ%(I%)=1 THEN KQN%(C%)=I%
8940 NEXT I%
8950 '
8960 CNUM%=C%
8970 FOR QQ%=1 TO CNUM%
8980   I%=KQN%(QQ%)
8990   C%=0
```

```
9000   ' searching the SHITA to UE ----------------
9010   FOR J%=1 TO NETT%(I%)
9020     IF UNET%(I%,J%)=0 THEN UNDER%=J%
9030     IF SNET%(I%,J%)=0 THEN C%=C%+1:UPP%(C%)=J%
9032     WE(I%)=2.69*R(I%)*R(I%)/100*3.14159*5
9040   NEXT J%
9050   '
9060   UPNUM=C%
9070   ' //////SLIDING BOUNDARY (net%=1)////////////////////
9080   SHEARF=RDF(I%)
9090  'SHEARF=MOME(I%)/(R(I%)/10)
9100   ROTR=0
9110   NN=DF(I%,UNDER%)
9120     ' normal force NN ----
9130     'ｽﾍﾞﾘｷｮｳｶｲﾃﾞﾉ ｽﾍﾞﾘﾏｻﾂ
9134     NS=SKOSF(I%)
9140     ' resistance RR  ----
9150     RR=NS*SMIU
9160     'PRINT USING "### kOSFﾊ ####  ###.#gf miu=##.##gf";I%-WAKI,UPP%(J%)-
    WAKI,NN,RR
9162     LPRINT USING "### kOSF ###.#gf NN ###.#gf miu=##.##gf";I%-WAKI,NS,NN,RR
9180     ROTR=ROTR+RR  :'ｽﾍﾞﾘｷｮｳｶｲﾃﾞﾉｽﾍﾞﾘ  (ｺﾛｶﾞﾘ ﾉ ﾊﾞｱｲ)
9200  '
9210  KOBAI=ANGLE(I%,UNDER%)
9220   '//////// SLIDING ///////////////////////////////////////////
9230   ' normal force NN ----
9233   EEEE=0
9240   NN=DF(I%,UNDER%)
9250   FFF=RDF(I%)-ROTR :'ｳｺﾞｶｽﾁｶﾗ ｳｺﾞｸﾀﾒﾆﾊ ｽﾘｯﾌﾟ'
9260   ' resistance RR  ----
9270   RR=NN*SMIU+WE(I%)*SIN(KOBAI)
9271     ' criterion ------------------
9272     IF FFF>RR  THEN PRINT "sliding !!";I%-WAKI
9273     IF FFF>RR  THEN LPRINT "sliding !! ";I%-WAKI
9274     IF FFF>RR  THEN EEEE=1 :BEEP :FOR EE=1 TO 1000:NEXT:BEEP
9275  '
9276 ' PRINT USING "### KOBAI=###.#' NN=###.##gf";I%-WAKI,KOBAI*180/3.14159,NN
9277 'LPRINT USING "### KOBAI=###.#' NN=###.##gf";I%-WAKI,KOBAI*180/3.14159,NN
9279  '/////// ROTATING ///////////////////////////////////////////
9300 '
9350     IF R(I%)=2.5 THEN RFRI=RM(1)
9360     IF R(I%)=4.5 THEN RFRI=RM(2)
9364     ' ﾍｲｼﾝﾘｮｸ ---------------------
9365     RRRF=SHEARF-ROTR
9368     HE=WE(I%)*(SIN(KOBAI))
9370     ' rolling friction RFRI ------
9380     RRRR=NN*RFRI+HE
9420     ' criterion ------------------
9470     IF RRRF>RRRR THEN SLR(I%)=1
9474      IF EEEE=1 THEN SLR(I%)=2
9480     IF RRRF>RRRR THEN PRINT USING "rotate NO##";I%-WAKI
9490     IF RRRF>RRRR THEN LPRINT USING "rotate NO##";I%-WAKI
9493     IF RRRF>RRRR THEN BEEP
9500     IF RRRF<=RRRR THEN PRINT USING "NO## did not move.";I%-WAKI
9510 '   IF rrrF<=rrrr THEN LPRINT USING "NO## did not move.";I%-WAKI
9511       PRINT  USING  "###   sf=###.##  sr=###.##    rf=###.##  rr=###.##";I%-
    WAKI,FFF,RR,RRRF,RRRR
9512   '   LPRINT  USING  "###   sf=###.##  sr=###.##    rf=###.##  rr=###.##";I%-
    WAKI,FFF,RR,RRRF,RRRR
9520 NEXT QQ%
9530 '
9540 RETURN
```

```
9550 '**********************************************************************
9560 '@@@@@@@@@@@@@@@@@@@@@@@@@@@@@@@@@@@@@@@@@@@@@@@@@@@@@@@@@@@@@@@@@@@@@@
9570 *DRAWING
9580 'UGOITA MONO
9590 FOR I%=1 TO UGO%
9600   CIRCLE (XMO(I%),-YMO(I%)),RMO(I%)
9610   PAINT(XMO(I%),-YMO(I%)),7
9620 NEXT I%
9630 '---------
9640 FOR I%=WAKI+1 TO NU%
9650    XXK=X(I%)+F(I%)*SIN(SHI(I%))/4
9660    YYK=Y(I%)-F(I%)*COS(SHI(I%))/4
9670    LINE (X(I%),-Y(I%))-(XXK,-YYK),6
9680  ' PRINT I%;
9690   '
9700    FOR J%=1 TO NETT%(I%)
9710       IF DF(I%,J%)=0 THEN 9750
9720      XXK=X(I%)+DF(I%,J%)*SIN(ANGLE(I%,J%))/4
9730      YYK=Y(I%)-DF(I%,J%)*COS(ANGLE(I%,J%))/4
9740       LINE (X(I%),-Y(I%))-(XXK,-YYK),1,,&H5555
9750    NEXT
9755   GOTO 9830
9760   'SAF-------
9770       IF SAF(I%)=0 THEN 9810
9780      XXK=X(I%)+SAF(I%)*SIN(SASHI(I%))/4
9790      YYK=Y(I%)-SAF(I%)*COS(SASHI(I%))/4
9800      LINE (X(I%),-Y(I%))-(XXK,-YYK),1,,&H3333
9810  '  PRINT I%-WAKI,SAF(I%),SASHI(I%)*180/3.14159
9820 'PRINT
9830 NEXT
9840 'ﾓｰﾒﾝﾄ ｦ ｶｸ -------------------------
9850 FOR I%=WAKI+1 TO NU%
9860   'PRINT  USING  "###    ###.#'   F=###.##gf          M=  ###.##gf  ";I%-
      WAKI,SHI(I%)*180/3.14159,F(I%),MOME(I%)
9870 '
9880   CS=MOME(I%)/(R(I%)-1)
9890   IF CS>6.28317 THEN CS=6
9900   IF CS<-6.28317 THEN CS=-6
9910   A=6.28317
9920   IF MOME(I%)>0 THEN CIRCLE (X(I%),-Y(I%)),R(I%)-1,1,A-CS,A
9930   IF MOME(I%)<0 THEN CIRCLE (X(I%),-Y(I%)),R(I%)-1,1,0,-CS
9940 'PRINT A,CS
9950   X1=X(I%)+(R(I%)-1)*COS(A-CS):Y1=Y(I%)+(R(I%)-1)*SIN(A-CS)
9960   X2=X(I%)+(R(I%)-1.3)*COS(A-CS):Y2=Y(I%)+(R(I%)-1.3)*SIN(A-CS)
9970   X3=X(I%)+(R(I%)-1)*COS(CS):Y3=Y(I%)-(R(I%)-1)*SIN(CS)
9980   X4=X(I%)+(R(I%)-1.3)*COS(CS):Y4=Y(I%)-(R(I%)-1.3)*SIN(CS)
9990    IF MOME(I%)>.01 THEN LINE (X1,-Y1)-(X2,-Y2),7 :'ﾔｼﾞﾙｼ---
10000    IF MOME(I%)<-.01 THEN LINE (X3,-Y3)-(X4,-Y4),7 :'ﾔｼﾞﾙｼ---
10010 NEXT I%
10020 RETURN
10030 '-------------------------------------------------------
10040 '************************************************************
10050 *GAUSS :'****************************************************
10060 'FOR I%=1 TO N%
10070 '  FOR J%=1 TO N%
10080 '     READ AAA(I%,J%)
10090 '  NEXT
10100 '   READ BBB(I%)
10110 'NEXT
10120 GOSUB *CALC
10130 FOR M%=1 TO N%
10140 '  PRINT CCC(M%)
```

```
10150 NEXT
10160 RETURN
10170  '
10180 *CALC  :'------------------------------------------------
10190 NM1=N%-1
10200 FOR K%=1 TO NM1
10210   KP1=K%+1
10220   FOR J%=KP1 TO N%
10230     AAA(K%,J%)=AAA(K%,J%)/AAA(K%,K%)
10240   NEXT
10250   BBB(K%)=BBB(K%)/AAA(K%,K%)
10260   FOR M%=KP1 TO N%
10270     FOR J%=KP1 TO N%
10280       AAA(M%,J%)=AAA(M%,J%)-AAA(M%,K%)*AAA(K%,J%)
10290     NEXT
10300     BBB(M%)=BBB(M%)-AAA(M%,K%)*BBB(K%)
10310   NEXT
10320 NEXT
10330 CCC(N%)=BBB(N%)/AAA(N%,N%)
10340 '
10350 FOR L=1 TO NM1
10360    K%=N%-L
10370    KP1=K%+1
10380    S=0
10390    FOR J%=KP1 TO N%
10400      S=S+AAA(K%,J%)*CCC(J%)
10410    NEXT
10420    CCC(K%)=BBB(K%)-S
10430 NEXT
10440 RETURN
10450 '^^^^^^^^^^^^^^^^^^^^^^^^^^^^^^^^^^^^^^^^^^^^^^^^
10460 *GADATA
10470 DATA 2
10480 DATA 5,1,2
10490 DATA 1,3,-8
10500 DATA 1,3,-8
10510 DATA -1,2,-2,-1
10520 '************************************************************
10530 *DATAREAD1
10540 'FILES IDRV$
10550 'INPUT "DIRECTRY";DRC$
10553  DRC$="¥n88data¥gsm¥data35"
10560  'HDIR IDRV$+DRC$
10563  RDRV$=IDRV$+DRC$
10570  FILES RDRV$ :INPUT "filename";FFF$ :FILE$=RDRV$+"¥B35-"+FFF$
10580 'FILE$="R35-5"
10590 OPEN  FILE$ FOR INPUT AS #1
10600 INPUT #1,KOSU
10610 INPUT #1,WAKI
10620 FOR I%=1 TO KOSU
10630    INPUT #1,IX(I%),IY(I%),R(I%)
10640 NEXT
10650 CLOSE
10660 'CHDIR IDRV$+".."
10670 'CHDIR ".."
10680 KOSUKE=KOSU :'delete ｵｵｶﾞﾀ
10690 RETURN
10700 '*****************************************************************
10710 *DATAWRITEOPEN
10720 ' CHDIR DRV$+"CALCDATA"
10730   FILES RDRV$
10740 'INPUT "OUTPUT FILE DIRECTRY NAME ";WFILE$
```

```
10743  WFILE$="D-"+FFF$
10750  DIREC$="¥"+WFILE$
10760   MKDIR RDRV$+DIREC$
10770 'INPUT "OUTPUT FILE NAME ";WFILE$
10780 RETURN
10790 '*****************************************************************
10800 *DATAWRITE
10810 OPEN RDRV$+DIREC$+DIREC$+STR$(SHITA) FOR OUTPUT AS #2
10820 WRITE #2,KOSU,WAKI,SHITA
10830 FOR I%=1 TO KOSU
10840   WRITE #2,X(I%),Y(I%),R(I%)
10850 NEXT
10860 FOR I%=WAKI+1 TO KOSU
10870   WRITE #2,F(I%),SHI(I%),MOME(I%)
10880   WRITE #2,SKOSF(I%),SLR(I%)
10890 NEXT
10900 FOR I%=WAKI+1 TO KOSU
10910   WRITE #2,NETT%(I%)
10920   FOR J%=1 TO NETT%(I%)
10930      WRITE #2,NET%(I%,J%),ANGLE(I%,J%),DF(I%,J%)
10940   NEXT
10950 NEXT
10960 CLOSE
10970 RETURN
10980 '*****************************************************************
```

4.3 *GSMPRT*

(NEC N88BASIC Ver.4.0)

```
100 'GSM PRT 3 ----------------------
110 '1000 ﾉ ﾘｭｳｼﾞｮｳﾀｲ ﾉ ｱﾝﾃｲ ﾓﾃﾞﾙ
120 '   basic
130 '  programmed by Yuichi ONDA
140 ' 15-MAY,  1989 ----------------
150 '
160 CONSOLE 0,25,0,1:SCREEN 3,0:WIDTH 80,25:'d
170 OPTION BASE 1
180 KEY 7,"cls 2"+CHR$(13):'d
190 KEY 8,"CHDIR "
200 KEY 9,"L? CHR$(12)"+CHR$(13):'d
210 DEF FNACS(X)=-ATN(X/SQR(-X*X+1))+1.5708
220 DEF FNASN(X)=ATN(X/SQR(-X*X+1))
230 DIM X(1110),Y(1110),R(1110),SO%(1110),CH%(1110,6),UGOKU%(1110)
240 DIM XS(1110),XL(1110),YS(1110),YL(1110),F(1110),SHI(1110),ROT(1110)
250 DIM IX(1110),IY(1110) ,SAF(1110)
260 DIM FORB(1110,2),MOME(1110),NET%(1110,6)
270 DIM ANGLE(1110,6),KOSF(1110),SH(10),KSH(10),KESH(10),ROTFORCE(1110)
280  DIM AAA(4,4),BBB(10),CCC(10),DF(1110,6),KEI%(10),SLR(1110),ROR(1110)
290  DIM RBAN%(1110),TREE1%(7),TREE2%(7,7),KQN%(50),KKNET%(10),ANDA(29)
300 DIM DRFX(1110),DRFY(1110),DRANG(1110),HAJ%(1110),NETT%(1110)
310 '@@@  main routine @@@@@@@@@@@@@@@@@@@@@@@@@@@@@@@@@@@@@@@@@@@@@@@
311 PRINT "         @@@@@@@@@@@@ GSM PRT III @@@@@@@@@@@@@@@@@"
313 PRINT "                                        at  23:45 21-MAY, 1989"
319 INPUT "DATA DRIVE  A-D";DRV$
320 DRV$=DRV$+":"
321 COUNT=0
324 *LOOP
330  GOSUB *DATAREADOPEN
370 '++++++++++++++++++++++++++++++++++++++++++++++++++++++++++++
371 COUNT=0
380 *NEWONE
420  COUNT=COUNT+1
430  GOSUB *DATAREAD
440 'IF COUNT>=7 THEN 442 ELSE *LOOP
442  GOSUB *MKWINDOW
450  GOSUB *GRAPHICS
460 ' GOSUB *DRAWING
470  INPUT "PLOT ｽﾙ  YES=1";PLT :IF PLT=1 THEN 480 ELSE 490
480  GOSUB *PLOT
490  CLS:PRINT USING "GSM-PRT3(&         &)      ###' ";WFILE$,-SHITA :PRINT TIME$
500  'COPY 3:LPRINT CHR$(&HC);
501  INPUT "ﾓｰｲﾁﾄﾞ ﾐﾙ  yes=1";UN: IF UN=1 THEN 442
510  INPUT "ﾎｶ ﾉ ﾌｧｲﾙ ｦ ﾐﾙ  YES=1";YN: IF YN=1 THEN *LOOP
520  IF ENDD=1 THEN *ENDDO
530 GOTO *NEWONE
540 '=============================================================
550 *ENDDO
560 CLOSE
570 END
580  '*******************************************************************
590 *DATAINT
600  FOR I%=1 TO NU%
610    SAF(I%)=0
620    DRF(I%)=0
630    DRN(I%)=0
640    DRFX(I%)=0
```

```
650     DRFY(I%)=0
660     ROT(I%)=0
670     DRANG(I%)=0
680     HAJ%(I%)=0
690     UPP%(I%)=0
700     RBAN%(I%)=0
710     MOME(I%)=0
720     ROR(I%)=0
730     SLR(I%)=0
740     ROTFORCE(I%)=0
750     FOR J%=1 TO 2
760       FORB(I%,J%)=0
770     NEXT
780     FOR J%=1 TO 6
790       UNET%(I%,J%)=0
800       SNET%(I%,J%)=0
810       ANGLE(I%,J%)=0
820      NET%(I%,J%)=0
830      CH%(I%,J%)=0
840      DF(I%,J%)=0
850      KOSF(I%,J%)=0
860      SAFY(I%,J%)=0
870     SAFX(I%,J%)=0
880     NEXT J%
890 NEXT I%
900  NU%=KOSU
910 RETURN
920 '****************************************************************
930 *MKWINDOW
1010 'WX=INT(6*SQR(50  ))
1020 ' WX=INT(5.88*SQR(KOSU))
1030  WX=INT(6*SQR(KOSU))
1035  SHIRAD=SHITA*3.14159/180
1040   DS=-(WX*SIN(SHIRAD))
1050 WY=WX*1.25
1060  WINDOW (-WX+DS/2+WX/2,-WY+DS/4 )-(WX+DS/2+WX/2,0+DS/4)
1070  'ﾌﾂｳ
1080   DX1=-WX+DS/2+WX/2:DY1=WY-DS/4
1090   DX2=WX+DS/2+WX/2:DY2=-DS/4
1100  '
1110 'ｷﾝｲﾂ
1120 'DX1=-WX+DS/2+WX/2:DY1=WY-DS/1.5
1130 'DX2=WX+DS/2+WX/2:DY2=-DS/1.5
1140  '
1150  WINDOW (DX1,-DY1)-(DX2,-DY2)
1160 RETURN
1170 '****************************************************************
1180 *GRAPHICS
1188  CLS 3
1190 'ｶﾀﾑｷ ｷﾒ
1191 SHIRAD=SHITA*3.14159/180
1192 SHIRA2=(SHITA-15)*3.14159/180
1193 AAA=TAN(45*3.14159/180+SHIRA2)
1194 IF AAA<>0 THEN BBB=-1/AAA  ELSE BBB=0 :'ｶﾀﾑｷ
1195  PRINT SHITA
1200   K=200/BBB
1210 IF AAA>0 THEN LINE (0,0)-(200,-200*AAA),7:LINE (0,0)-(K,-K*BBB),7
1220 IF AAA<0 THEN LINE (0,0)-(200,-200*AAA),7:LINE (K,-K*BBB)-(0,0),7
1230 IF AAA=0 THEN LINE (0,0)-(200,-200*AAA),7:LINE (0,-200)-(0,0),7
1240 '
1260 FOR I%=1 TO KOSU
1270   CIRCLE (X(I%),-Y(I%)),R(I%)
```

```
1280   PSET (X(I%),-Y(I%)),1
1290   XS(I%)=X(I%)-R(I%):XL(I%)=X(I%)+R(I%)
1300   YS(I%)=Y(I%)-R(I%):YL(I%)=Y(I%)+R(I%)
1310    SX=MAP(X(I%),0):SY=MAP(-Y(I%),1)
1320    Q%=I%-WAKI:IF Q%<1 THEN 1400
1330  ' PAINT (X(I%),-Y(I%)),5,7
1340   IF KOSU>150 THEN 1400
1350     IF Q%<10 THEN 1360 ELSE J=Q%¥10:K=Q% MOD 10:GOTO 1370
1360  ' PUT (SX-4,SY-8),KANJI(VAL("&H130")+Q%),PSET :GOTO 1390
1370  '  PUT (SX-8,SY-8),KANJI(VAL("&H130")+J),PSET
1380  '  PUT (SX,SY-8),KANJI(VAL("&H130")+K),PSET :GOTO 1390
1390 'LINE (XS(I%),-YS(I%))-(XL(I%),-YL(I%)),6,B
1400 NEXT
1410 'ETURN
1420 '************************************************************
1430 '@@@@@@@@@@@@@@@@@@@@@@@@@@@@@@@@@@@@@@@@@@@@@@@@@@@@@@@@@@@@@@@@@@
1440 *DRAWING
1450  'GOITA MONO
1460 FOR I%=WAKI+1 TO NU%
1480   IF SLR(I%)=1 THEN LINE (X(I%)-.7,-Y(I%)-.7)-(X(I%)+.7,-Y(I%)+.7),2,BF
1490 NEXT I%
1500 '---------
1510 FOR I%=WAKI+1 TO NU%
1520    XXK=X(I%)+F(I%)*SIN(SHI(I%))/4
1530    YYK=Y(I%)-F(I%)*COS(SHI(I%))/4
1540    LINE (X(I%),-Y(I%))-(XXK,-YYK),6
1550  ' PRINT I%;
1560 ' GOTO 9050
1570    FOR J%=1 TO NETT%(I%)
1580       IF DF(I%,J%)=0 THEN 1620
1590      XXK=X(I%)+DF(I%,J%)*SIN(ANGLE(I%,J%))/4
1600      YYK=Y(I%)-DF(I%,J%)*COS(ANGLE(I%,J%))/4
1610       LINE (X(I%),-Y(I%))-(XXK,-YYK),5,,&H5555
1620    NEXT
1700 NEXT
1710 'ﾓｰﾒﾝﾄ ｦ ｶｸ -------------------------
1720 FOR I%=WAKI+1 TO NU%
1730   'PRINT USING "###   ###.#'   F=###.##gf        M=  ###.##gf  ";I%-
      WAKI,SHI(I%)*180/3.14159,F(I%),MOME(I%)
1740 '
1750 ' CS=MOME(I%)/(R(I%)-1)/2
1751   CS=MOME(I%)/(R(I%)-1)/KOSF(I%)*4
1760   IF CS>6.28317 THEN CS=6
1770   IF CS<-6.28317 THEN CS=-6
1780   A=6.28317
1790   IF MOME(I%)>0 THEN CIRCLE (X(I%),-Y(I%)),R(I%)-1,3,A-CS,A
1800   IF MOME(I%)<0 THEN CIRCLE (X(I%),-Y(I%)),R(I%)-1,3,0,-CS
1810 'PRINT A,CS
1820   X1=X(I%)+(R(I%)-1)*COS(A-CS):Y1=Y(I%)+(R(I%)-1)*SIN(A-CS)
1830   X2=X(I%)+(R(I%)-1.3)*COS(A-CS):Y2=Y(I%)+(R(I%)-1.3)*SIN(A-CS)
1840   X3=X(I%)+(R(I%)-1)*COS(CS):Y3=Y(I%)-(R(I%)-1)*SIN(CS)
1850   X4=X(I%)+(R(I%)-1.3)*COS(CS):Y4=Y(I%)-(R(I%)-1.3)*SIN(CS)
1860    IF MOME(I%)>.01 THEN LINE (X1,-Y1)-(X2,-Y2),3 :'ﾔｼﾞﾙｼ---
1870    IF MOME(I%)<-.01 THEN LINE (X3,-Y3)-(X4,-Y4),3 :'ﾔｼﾞﾙｼ---
1880 NEXT I%
1882 INPUT "ｶｸﾀﾞｲｽﾙ  YES=1 ";KAKU
1883  IF KAKU=1 THEN *KAKU
1890 RETURN
1900 '/////////////////////////////////////////////////////////
1902 *KAKU
1910 PRINT "ﾋﾀﾞﾘｳｪ "
1920 GOSUB *KAKUDAI1
```

```
1930 PRINT "ｼﾀ      "
1940 GOSUB *KAKUDAI2
1941  WINDOW (DX1,-DY1)-(DX2,-DY2)
1942 DX1=MAP(X0,2):DX2=MAP(X1,2)
1943 DY1=-MAP(Y0,3):DY2=-MAP(Y1,3)
1946 WINDOW (DX1,-DY1)-(DX2,-DY2)
1950 GOTO *GRAPHICS
1960 '//////////////////////////////////////////////////////////////
1970 *KAKUDAI1
1980 PRINT "ｹｯﾃｲ -5"
1990 WINDOW (0,0)-(639,399)
2000 X0=320:Y0=200
2010 LINE (X0-5,Y0)-(X0+5,Y0),2:LINE (X0,Y0-5)-(X0,Y0+5),2
2020  A$=""
2030 WHILE A$=""
2040   A$=INKEY$
2050 WEND
2060 LINE (X0-5,Y0)-(X0+5,Y0),0:LINE (X0,Y0-5)-(X0,Y0+5),0
2070 IF A$="5" THEN RETURN
2080 IF A$="8" THEN Y0=Y0-2
2090 IF A$="4" THEN X0=X0-2
2100 IF A$="6" THEN X0=X0+2
2110 IF A$="2" THEN Y0=Y0+2
2120 'RINT PRINT A$,X0,Y0
2130 LINE (X0-5,Y0)-(X0+5,Y0),2:LINE (X0,Y0-5)-(X0,Y0+5),2
2140 GOTO 2020
2150 '//////////////////////////////////////////////////////////////
2160 *KAKUDAI2
2170 PRINT "ｹｯﾃｲ -5"
2180 WINDOW (0,0)-(639,399)
2190 X1=320:Y1=200
2200 LINE (X0-5,Y0)-(X0+5,Y0),2:LINE (X0,Y0-5)-(X0,Y0+5),2
2210  A$=""
2220 WHILE A$=""
2230   A$=INKEY$
2240 WEND
2250 LINE (X1-5,Y1)-(X1+5,Y1),0:LINE (X1,Y1-5)-(X1,Y1+5),0
2260 LINE (X0,Y0)-(X1,Y1),0,B
2270 IF A$="5" THEN RETURN
2280 IF A$="8" THEN Y1=Y1-2
2290 IF A$="2" THEN Y1=Y1+2
2300 X1=(Y1-Y0)*640/400+X0
2310 LINE (X1-5,Y1)-(X1+5,Y1),2:LINE (X1,Y1-5)-(X1,Y1+5),2
2320 LINE (X0,Y0)-(X1,Y1),7,B
2330 GOTO 2210
2340 '//////////////////////////////////////////////////////////////////////
2350 *PLOT､
2351 INPUT "MOMENT ｶｸ  YES=1";MMMM
2352 INPUT "DF  ｶｸ  YES=1";DDDF
2360 E$=CHR$(3)
2370 LPRINT "J1";E$
2380 FOR I%=1 TO KOSU
2390   X(I%)=X(I%)-DX1
2400   Y(I%)=Y(I%)-DY2
2410 NEXT
2420 '
2430 E=1
2440 BAI=3400/(-DX1+DX2)
2450 PRINT BAI
2460 FOR I%=1 TO NU%
2470   X(I%)=X(I%)*BAI+100
2480   Y(I%)=Y(I%)*BAI+200
```

```
2490   R(I%)=R(I%)*BAI
2500 NEXT
2510 ' GOTO 2572
2520 '-------------
2530 FOR I%=1 TO NU%
2540   IF X(I%)<10 OR X(I%)>3500 THEN 2580
2550   IF Y(I%)<10 OR Y(I%)>2500 THEN 2580
2560   LPRINT "W";X(I%),Y(I%),R(I%),R(I%),0,3600;E$
2570     IF SLR(I%)=1 THEN LPRINT "M";X(I%),Y(I%);E$:LPRINT "%12,0",R(I%),0,3600,10,450;E$
2580 NEXT I%
2590 '----F
2600 LPRINT "J2";E$
2610 FOR I%=WAKI+1 TO NU%
2620    LPRINT "M";X(I%),Y(I%);E$
2630  ' XXK=X(I%)+F(I%)*SIN(SHI(I%))/6*BAI
2640    XXK=X(I%)+F(I%)*SIN(SHI(I%))/4*BAI
2650  ' YYK=Y(I%)-F(I%)*COS(SHI(I%))/6*BAI
2660    YYK=Y(I%)-F(I%)*COS(SHI(I%))/4*BAI
2670    LPRINT "D";XXK,YYK;E$
2680 NEXT I%
2690 IF DDDF=1 THEN 2710 ELSE 2810
2700 '---DF
2710 LPRINT "J3";E$
2720 FOR I%=WAKI+1 TO NU%
2730    FOR J%=1 TO NETT%(I%)
2740       IF DF(I%,J%)=0 THEN 2790
2750      LPRINT "M";X(I%),Y(I%);E$
2760      XXK=X(I%)+DF(I%,J%)*SIN(ANGLE(I%,J%))/4*BAI
2770      YYK=Y(I%)-DF(I%,J%)*COS(ANGLE(I%,J%))/4*BAI
2780       LPRINT "D";XXK,YYK;E$
2790    NEXT
2800 NEXT
2810 IF MMMM=1 THEN 2820 ELSE 3030
2820 LPRINT "J3";E$
2830 'ﾓｰﾒﾝﾄ ｦ ｶｸ ------------------------
2840 FOR I%=WAKI+1 TO NU%
2850  'RS=MOME(I%)/(R(I%)-1)/5
2851   RS=MOME(I%)/(R(I%)-1)/KOSF(I%)*4
2860   IF RS>6.28317 THEN RS=6
2870   IF RS<-6.28317 THEN RS=-6
2880 ' CS=RS*180/3.14159*100
2890   CS=RS*180/3.14159*100
2900  PRINT CS,RS
2910   A=6.28317
2920   IF MOME(I%)>0 THEN LPRINT "W";X(I%),Y(I%),R(I%)-BAI,R(I%)-BAI,CS,0;E$
2930   IF MOME(I%)<0 THEN LPRINT "W";X(I%),Y(I%),R(I%)-BAI,R(I%)-BAI,0,-CS;E$
2940 'PRINT A,CS
2950   X1=X(I%)+(R(I%)-1*BAI)*COS(0):Y1=Y(I%)+(R(I%)-1*BAI)*SIN(0)
2960   X2=X(I%)+(R(I%)-1.4*BAI)*COS(0):Y2=Y(I%)+(R(I%)-1.4*BAI)*SIN(0)
2970   X3=X(I%)+(R(I%)-1*BAI)*COS(RS):Y3=Y(I%)-(R(I%)-1*BAI)*SIN(RS)
2980   X4=X(I%)+(R(I%)-1.4*BAI)*COS(RS):Y4=Y(I%)-(R(I%)-1.4*BAI)*SIN(RS)
2990   IF MOME(I%)>.1  THEN LPRINT "M";X1,Y1;E$:LPRINT "D";X2,Y2;E$ :'ﾔｼﾞﾙｼ---
3000   IF MOME(I%)<-.1 THEN LPRINT "M";X3,Y3;E$:LPRINT "D";X4,Y4;E$:'ﾔｼﾞﾙｼ---
3010 NEXT I%
3020 '
3030 LPRINT "J1";E$
3040 '-------------------------
3050 LPRINT "M1500,2300";E$
3060 LPRINT "S60,60,Q60";E$
3070 LPRINT USING "PGSM1000(&      &)   ##.#' ";WFILE$,-SHITA
3080 LPRINT E$
```

```
3090 RETURN
3100 '*******************************************************************
3110 *DATAREADOPEN
3111 FILES DRV$
3112 INPUT "DIRECTORY ";DIREC$
3120 'CHDIR DRV$+DIREC$
3121 '
3130  FILES DRV$+"¥"+DIREC$
3140 INPUT "INPUT FILENAME ";WFILE$
3150 OPEN DRV$+"¥"+DIREC$+"¥"+WFILE$ FOR INPUT AS #1
3160 RETURN
3170 '*******************************************************************
3180 *DATAREAD
3190 INPUT #1,KOSU,WAKI,SHITA
3200 NU%=KOSU
3210 FOR I%=1 TO KOSU
3220   INPUT #1,X(I%),Y(I%),R(I%)
3230 NEXT
3240 FOR I%=WAKI+1 TO KOSU
3250   INPUT #1,F(I%),SHI(I%),MOME(I%)
3260   INPUT #1,KOSF(I%),SLR(I%)
3270 NEXT
3280 FOR I%=WAKI+1 TO KOSU
3290   INPUT #1,NETT%(I%)
3300   FOR J%=1 TO NETT%(I%)
3310      INPUT #1,NET%(I%,J%),ANGLE(I%,J%),DF(I%,J%)
3320   NEXT
3330 NEXT
3340 IF EOF(1) THEN CLOSE
3341 ENDD=1
3350 RETURN
3360 '*******************************************************************
```